AN ADVANCED ANALYTICAL PROGRAM FOR CHARRING ABLATORS

FINAL REPORT

Volume I

Analytical Formulation, Data Interpretation and Flight Simulation

AVSSD-0172-67-RR

Prepared by

AVCO Space Systems Division
Lowell, Massachusetts

Principal Contributors

T. R. Munson
R. E. Mascola
J. D. Brown
R. J. Spindler
J. Klugerman

[redacted]

Prepared for

National Aeronautics and Space Administration
Manned Spacecraft Center

Houston, Texas

NASA Contract No. NAS 9-4329

[redacted]

N91-70012

PREFACE

This document constitutes the final report on a study whose goal has been to provide (1) a physico-mathematical model of the coupled energy and mass transfer processes in char forming thermal protection systems, (2) a digital computer program based on this model and compatible with the NASA/MSC computational facilities, and (3) a critical selection of input parameters for use in describing the performance of the Apollo heat shield material. The final report consists of three volumes with supplementary material such as source and binary decks for the several computer programs together with punch cards and magnetic tape containing the Test Data Library described in Volume III. The three volumes are as follows:

Volume I .....Analytical Formulation, Data Interpretation and Flight Simulation

Volume II .....Numerical Analysis, Program Description, Test Cases and Program Listing

Volume III .....Test Data and Data Library Program Description

No single individual can be said to have developed the theoretical concepts, the numerical implementation techniques, or the programming for machine computations involved in the advanced analytical program for the thermal analysis of charring ablators described in this document. This package, subsequently referred to as Program 1600, represents the results of a team effort on the part of various personnel of the Thermodynamics Section and Mathematics Department of the Avco Missiles Systems Division. Although the following breakdown by disciplines is not mutually exclusive, it is thought to be fairly representative of the contributions of the individuals named. The bulk of the theoretical concepts were developed by Mr. T. R. Munson, Mr. R. E. Mascola, and Mr. R. J. Spindler of the Thermodynamics Section. The analysis and numerical implementation techniques were developed primarily by Mr. J. D. Brown of the Thermodynamics Section. The programming concepts were developed primarily by Mr. M. L. Waters and Mr. J. Klugerman of the Mathematics Department. The structural analyses were performed by Dr. C. Martin of the Space Systems Division. The Data Library was prepared by Mr. C. Lermond of the Space Systems Division Material Property Office; the data retrieval programs were prepared by Mr. W. Spendiff, Mr. V. Fantasia and Mr. E. Nickerson of the Mathematics Department. The wholehearted support and cooperation of Dr. J. Warga, Manager of the Mathematics Department, and Dr. H. Hurwicz of the Space Systems Division is gratefully acknowledged. The authors also wish to express their gratitude to Mr. J. Picone and Mrs. Freda Demers of the Thermodynamics Section for their painstaking efforts in the preparation of the final manuscript.

The effort reported here was under the general technical direction of T. R. Munson, Section Chief, Thermodynamics Section, Avco Missiles Systems Division and the Program Manager was H. Hurwicz. The Technical Monitor for the National Aeronautics and Space Administration, Manned Spacecraft Center located in Houston, Texas was Donald M. Curry of the Structures and Mechanics Division, Thermal Technology Branch.

VOLUME I TABLE OF CONTENTS

VOLUME I TABLE OF CONTENTS (Cont'd)

VOLUME I TABLE OF CONTENTS (Cont'd)

LIST OF TABLES

LIST OF SYMBOLS FOR VOLUME I IN ORDER OF APPEARANCE IN THE TEXT

ρ_s	density of the solid heat shield material defined as the mass of solid per unit volume
ρ_c	mass of char matrix per unit volume
ρ_a	mass of active (decomposable) material per unit volume
ρ_o	mass of solid heat shield per unit volume before any decomposition, i.e. virgin density
$\dot{s}$	rate of surface recession
A	cross section area of a central volume, perpendicular to heat and mass flow
x	distance measured from the original position of the heated surface of the heat shield
$\dot{\rho}_a$	rate of decomposition of the mass of active material per unit volume
s	position of the receding surface at time, t.
ℓ_1	distance from the original position of the heated surface to the charring material-bond interface
ℓ_2	distance from the original position of the heated surface to the bond-structure interface
L	distance from the original position of the heated surface to the rear surface of structure
w	mass of gaseous products of decomposition flowing through unit cross sectional area in unit time.
dM	total change of the mass of gas in control volume Adx in unit time increment dt.
dM_d	change of the mass of gas in the control volume Adx due to the decomposition of the solid to gaseous products
dM_c	change of the mass of gas in the control volume, Adx due to the compressibility of the gas.
$\dot{\rho}_s$	rate of decomposition of the mass of solid material per unit volume.
ρ_g	mass of gas per unit volume

$\dot{\rho}_g$	rate of change of the mass of gas per unit volume due to the compressibility of the gas.
dQ	total heat added to the control volume Adx in time increment dt
dQ_K	heat added to the control volume, Adx by thermal conduction in time increment dt
dQ_g	heat added to the control volume, Adx by gas flow in time increment dt
dQ_c	heat added to the control volume, Adx by chemical reaction in time increment dt
dQ_r	heat added to the control volume, Adx by radiation
k	thermal conductivity of the solid
h_g	specific enthalpy of the gas
ΔH_c	heat of decomposition per unit mass of gas formed
F	the radiant heat flux at any position in the solid
C_{pg}	specific heat of the gaseous products of decomposition
ρ	density of the control volume, i.e. the mass of solid and gas per unit volume
h	specific enthalpy of the control volume
h_a	specific enthalpy of the active component
h_c	specific enthalpy of the fully charred solid
C_{pc}	specific heat of the fully charred solid
C_{pa}	specific heat of the active component of the solid
k_o	thermal conductivity of the virgin solid
k_c	thermal conductivity of the fully charred solid
C_{ps}	specific heat of the solid
A, B, n	reaction rate constants for a single reaction zone.
$\rho_{o1}, \rho_{o2}, \rho_{o3}, \rho_{o4}$	limiting densities of the solid for multiple zone reactions
A_1, A_2, A_3 B_1, B_2, B_3 n_1, n_2, n_3	reaction rate constants for a multiple zone reaction.

F_o	radiation flux incident on the solid surface
R_o	reflectance of the heated surface of the solid
R_l	reflectance of the interface of the charring material and bonding agent
a	absorption coefficient of the charring material
R_A	apparent reflectivity of a semi-transparent material of thickness l_1-S
τ_a	apparent transmissivity of a semi-transparent material of thickness l_1-S
P	pressure
α	viscous resistance coefficient for gas flow through the porous heat shield
β	inertial resistance coefficient for gas flow through the porous heat shield
μ	viscosity of the gaseous products of decomposition
v_q	average velocity of the gas at a given position in the porous solid: also, referred to as the "filter" or "seepage" velocity.
R	specific gas constant for decomposition products
P_S	pressure at the heated surface, assume to be equal to the local static pressure at the outer edge of the boundary layer, P_e.
α_c	viscous resistance coefficient for gas flow through the porous fully charred heat shield.
α_v	viscous resistance coefficient for gas flow through the porous virgin heat shield
β_c	inertial resistance coefficient for gas flow through the porous fully charred heat shield
β_v	inertial resistance coefficient for gas flow through the porous virgin heat shield
S_i $i = 1, 2, \ldots$	a subscript denoting the thermal properting of the bond layer (i=1) and substructure (i=2).
ϵ	emissivity of the heated surface
H_v	heat of vaporization of the fully charred solid
σ	Stephan-Boltzman radiation constant
q	convective heat transfer rate to a "hot wall" in the presence of mass injection and chemical reactions with ablation products

q_o	convective heat transfer rate to a "hot wall" with no mass injection
q_c	convective heat transfer rate to a "cold wall"
H_r	local recovery enthalpy
H_s	stagnation enthalpy
H_w	enthalpy of the environmental gas (air) at the temperature and pressure of the heated surface
ρ_w	density of the environment gas (air) at the temperature and pressure of the heated surface
μ_w	viscosity of the environmental gas (air) at the temperature and pressure of the heated surface
T_w	temperature of the heated surface
T_{wr}	temperature of the heated surface assumed for the a priori computing of a cold wall heat transfer rate
H_{wr}	enthalpy of the heated surface at temperature T_{wr} and local static pressure
$(q_c)_r$	convective heat transfer rate to a "cold wall" using transport and thermodynamic properties of the environmental gas evaluated at H_{wr} or H_r^*
H^*	Eckert reference enthalpy.
H_e	local free stream static enthalpy
μ^*	viscosity of the environmental gas evaluated at the Eckert reference enthalpy, H* and local static pressure
ρ^*	density of the environmental gas evaluated at the Eckert reference enthalpy, H* and local static pressure
r	recovery factor
H_r^*	Eckert reference enthalpy based on surface temperature, T_{wr}
ϕ	ratio of heat transfer to a "hot wall" with mass injection to heat transfer to a "hot wall" with no mass injection
u_e	local velocity at the edge of the boundary layer
z	distance along the outside contour of the vehicle surface measured from the stagnation point
ρ_e	density of the environmental gas at the edge of the boundary layer

μ_e	viscosity of the environmental gas at the edge of the boundary layer
R_{e_z}	Reynolds number based on boundary layer edge conditions and distance along the vehicle contour
$\dot{m}_w$	total mass loss rate per unit area leaving the heating surface
f	boundary layer mass transfer parameter.
η	transpiration coefficient
M_a	molecular weight of air
M_i	molecular weight of the ablated or injected species
η_s	transpiration coefficient for the injection of vaporized species of the surface
η_g	transpiration coefficient for the injection of the subsurface gaseous products of decomposition
δ_1	gram moles of molecular nitrogen per unit mass of "cold" gas mixtures of molecular nitrogen and molecular oxygen
δ_2	gram moles of molecular oxygen per unit mass of "cold" gas mixture of molecular nitrogen and molecular oxygen
X	gram moles of molecular oxygen at temperature T, and pressure P which have dissociation to form atomic oxygen
K	equilibrium constant for oxygen dissociation
A_e, B_e	constants appearing in the equation for the equilibrium constant for oxygen dissociation
H_1	specific enthalpy of molecular nitrogen
H_2	specific enthalpy of molecular oxygen
H_3	specific enthalpy of atomic oxygen
$\gamma_{i1}, \gamma_{i2}, \gamma_{i3}$	empirical constant appearing in wall enthalpy equations
$\Gamma_1, \Gamma_2, \Gamma_3$	coefficients appearing in the equation which expresses the enthalpy of the mainstream as at heated wall conditions
$\dot{m}_r$	rate of carbon mass loss from the heated surface due to rate limited oxidation
A_r, B_r, n_r	constants appearing in equation which determines the rate controlled mass loss of carbon from the heated surface

P_e	the local static pressure
w_s	weight fraction of oxygen at the reacting surface
μ_1	molecular weight ratio which converts W_s from a weight fraction to a mole fraction
$\dot{m}_l$	limiting rate of carbon mass loss from the heated surface due to the rate at which oxygen can diffuse across the boundary layer
μ_2	molecular weight ratio which describes the ratio in which oxygen and carbon enter into the heated surface reaction
w_e	weight fraction of oxygen in the mainstream
$\bar{h}$	heat transfer coefficient with mass transfer and using enthalpy as the driving potential
$\dot{m}_v$	vaporization rate
γ	condensation accomodation coefficient
μ_v	molecular weight of the vaporizing species
P_v	equilibrium vapor pressure
$\dot{m}_e$	condensation rate
P_a	partial pressure associated with the condensing species
$\bar{\mu}$	mean molecular weight of all species entering into the vaporization-condensation phenomena of the heated carbon surface
N_c	mole fraction of carbon vapor in the gas phase at the vaporizing surface
W_{es}	weight fraction of injected gas at the heated surface
μ_o	molecular weight of nitrogen and/or carbon monoxide
Q_1	energy associated with mass removal including combustion effects
$\dot{m}_o$	the mass flow rate of oxygen diffusing to the surface

AN ADVANCED ANALYTICAL PROGRAM FOR CHARRING ABLATORS

FINAL REPORT

Volume I

Analytical Formulation, Data Interpretation and Flight Simulation

AVSSD-0172-67-RR, Vol. I

Prepared by

AVCO Space Systems Division
Lowell, Massachusetts

Principal Contributors

T. R. Munson
R. E. Mascola
J. D. Brown
R. J. Spindler
J. Klugerman

Prepared for

National Aeronautics and Space Administration
Manned Spacecraft Center

Houston, Texas

NASA Contract No. NAS 9-4329

[redacted]

1.0 Summary, Conclusions and Recommendations

This report describes an analytical treatment of the problem of calculating heat and mass transfer in char forming ablation materials with particular reference to the thermal analysis of the heat shield material as used in the Apollo application. To accomplish this task, a mathematical model describing the physical processes occurring in this material when exposed to the extreme temperatures encountered during hypersonic re-entry was formulated, and a digital computer program was developed to implement numerical calculations based on this model. A careful search was made of all available thermal and ablation test data pertinent to this material and the results were coded on punch cards and transferred to a master library on magnetic tape. A retrieval system, consisting of three digital computer programs was developed to permit recall of selected portions of these data on demand. The data in this library were used to obtain the thermophysical and ablation parameters necessary to characterize the performance of the material under re-entry conditions pertinent to the Apollo mission. Tests of the computational accuracy of the numerical program were performed, and the validity of the mathematical model was demonstrated by numerical simulation of ground test ablation data. A complete description of the numerical program is given, including nomenclature, equations, input format, and Fortran listing.

Although flight test data were not available in time to be included in the numerical validation of the analytical and numerical methods developed in this study, the results of the ground test simulations indicate that these procedures can be employed with confidence in the design of the heat shield of the Apollo vehicle. As a logical extension of the studies reported herein, it is recommended, that the procedures developed be employed in post-flight analyses of the Apollo vehicle, when these data are available.

In the course of these studies considerable effort was expended in the investigation of possible ablation mechanisms due to structural failure of the weakened char material under the combined influence of internal pressure buildup, external aerodynamic loads and thermal stresses. Provisions for calculating, the internal temperature, density and pressure distributions were incorporated into the numerical procedures. Implementation of these procedures require experimental data on the pressure drop parameters for the flow of gas through the porous char material, and the structural parameters necessary for calculating the state of stress of the weakened char material. From a knowledge of these it would be possible to complete the structural analysis studies started in this study, postulate suitable failure criteria and develop a quantitative method for predicting ablation phenomena due to mechanical spallation effects. Although the experimental data on the ablation of the Apollo material do not indicate that mechanical spallation plays any significant role in the Apollo application, it is thought that these studies are of general enough interest to warrant further investigation. Accordingly, it is recommended that consideration be given to further studies along these lines.

2.0 Theory of Heat and Mass Transfer in Char-Forming Ablation Materials

2.1 Introduction

The successful design of manned space vehicles and high performance ballistic missiles is to a large extent dependent upon the adequacy of the heat shielding provided for the protection of such vehicles from the extreme tremperatures associated with the hypersonic environment encountered during atmospheric re-entry. The materials selected for this purpose vary considerably with mission requirements and vehicle configuration, but the dominant factor behind the selection of a material for a particular application is the requirement of minimizing total vehicle weight. This constraint has led to the choice of materials deliberately designed to undergo internal endothermic chemical reactions leading to the formation of a carbonaceous char when heated and to vaporize at the surface exposed to the hypersonic environment. The energy absorption associated with such processes, together with the reduction of the heat transfer coefficient as a result of injection of the products of degradation and the vaporized species into the boundary layer, have proved to be extremely effective in providing reliable lightweighted thermal protection systems for these applications.

To fully exploit the potential of this class of materials for heat shielding applications, the designer must have available an accurate mathematical description of the complex heat and mass transfer phenomena associated with such processes and an efficient numerical procedure for implementing calculations based on the mathematical model. In addition, adequate experimental data must be available from which the necessary parameters required by the mathematical model can be extracted. Before utilizing the model in particular design applications, its validity must be demonstrated through adequate numerical simulation of the observed performance of the material in ground and flight tests. For brevity in the following discussion, the materials considered shall be referred to as charring ablators, and the combined processes of vaporization of the material at the surface exposed to the hypersonic environment and injection of the products of thermal degradation into the boundary layer shall be loosely referred to as ablation. Throughout this report it is to be understood that the reference material is considered to be that used on the Apollo vehicle.

In practice ablation phenomena are most often encountered in situations where the environmental parameters are rapidly varying functions of time. This fact coupled with the necessity for working with heat shields of finite thickness and usually within rather tight limits on allowable strucutral temperatures makes it necessary to perform transient rather than steady state calculations. Modern high speed computers bring these calculations into the realm of practicality for even quite complex systems. In this chapter a mathematical theory is developed for the transient behaviour of charring ablators.

FIGURE 1

Geometry and Coordinate System

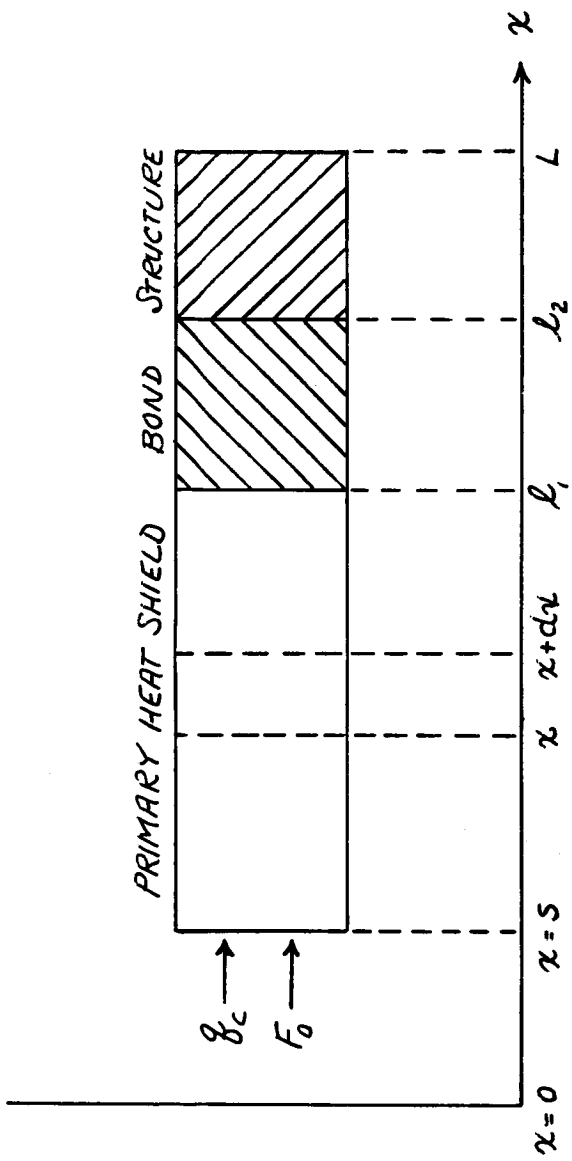

2.2 Internal Heat and Mass Transfer

Any attempt at a mathematical description of nature involves a series of compromises. In the theory presented here, an attempt has been made to strike a balance between physical rigor on one hand and the practical necessity for obtaining numerical results for engineering application in terms of physically measurable material properties.

Qualitative descriptions of the ablation process in polymeric materials are available in many sources (Ref. 1) and will not be detailed here. In brief, however, when subjected to environmental conditions severe enough to cause mass transfer in addition to energy transfer by conduction and radiation, certain materials, such as polytetraflouroethylene, undergo a thermal degradation which yields only gaseous products. Other materials, such as the silica fiber reinforced plastics yield a set of gaseous products and in addition produce a more or less complex porous condensed phase. In either case the flow of gaseous decomposition products toward the heated surface leads to additional energy transfer process besides conduction. In the present theory, energy transfer within the decomposable material is considered to occur by conduction, convection and radiation.

Conceptually the virgin material is considered as a hypothetical mixture consisting of an irreducible "char matrix" (denoted by the subscript c) and an "active material" (subscript a) which undergoes thermal decomposition yielding only gaseous products. Then at any state of decomposition the mass of solid per unit volume may be expressed as

$$\rho_s = \rho_c + \rho_a \tag{1}$$

where ρ_c is the mass of inactive char matrix per unit volume and ρ_a is the mass of active (decomposable) material per unit volume. Before any decomposition occurs, the mass of solid per unit volume is designated as ρ_o and is referred to as the virgin density. The decomposition reaction is assumed to be a sum of "n'th" order rate laws with the rate constants being a simple Arrhenius function of temperature. The material is assumed to have continuously variable properties throughout and as a result it is neither necessary nor desirable to define a "charring temperature" as in Barriault and Yos (Ref. 2) or a "reaction zone thickness" as in Scala and Gilbert (Ref. 3). This feature of the present model provides definite advantages, both conceptual and computational, over a model requiring charring temperatures as a basic input.

2.2.1 Energy Balance for Control Volume

Consider a cross-section through a typical heat shield of the ablative type. In general the material affording the thermal protection will be backed up by one or more materials which act as structural members, as bonding materials, etc. Figure 1 illustrates such a cross-section for a shield consisting of the primary

material with two back-up materials acting as a bonding agent and a structural material, respectively. For the present purposes these secondary materials are considered to be non-porous, non-decomposable and opaque. The heat transfer process in these materials is by simple conduction.

Consider a control volume within the primary material whose surface is receding at an unsteady rate S(t). Choosing cross-sectional area A for the bar the volume between the planes x and (x + dx) is then Adx. Gaseous decomposition products are produced in unit volume at a rate $(-\dot{\rho}_a)$, this being the rate at which the active component of the primary material undergoes thermal decomposition. It is assumed that the gases produced in the decomposition are free to move in the direction of negative x-i.e., toward the heated surface, and that thermal equilibrium exists between the gaseous and condensed phases at all points in the material. Letting w denote the mass of gas flowing across unit cross-sectional area in the direction of the heated surface in unit time, and dM denote the total change of the mass of gas in control volume Adx in time increment dt then,

$$dM = -\frac{\partial w}{\partial x} A\, dx\, dt \tag{2}$$

This change in mass is due to the mass of gaseous products of decomposition added to the control volume, dM_g, and the change in mass because of the compressibility of the gas as a function of temperature and pressure, dM_c.

The mass added to the control volume in time dt by decomposition may be written as

$$dM_g = -\dot{\rho}_a A\, dx\, dt = -\dot{\rho}_s A\, dx\, dt \tag{3}$$

where $\dot{\rho}_a = \dot{\rho}_s$ is the rate at which solid mass decomposes per unit volume.

The change in the mass of gas in the control volume in time dt due to the compressibility of the gas is

$$dM_c = -\dot{\rho}_g A\, dx\, dt \tag{4}$$

where $\dot{\rho}_g$ is the rate of change of the mass of gas per unit volume due to the compressibility of the gas. Writing a mass balance employing equations 2, 3, and 4 yields the continuity equation for the gas, i.e.

$$\frac{\partial w}{\partial x} = \dot{\rho}_s + \dot{\rho}_g \tag{5}$$

It can be shown that for the application of interest, the Apollo heat shield, the gas flow, w, depends almost entirely of $\dot{\rho}_s$ and is essentially independent of the compressibility of the gas*. With this consideration the continuity equation is reduced to

$$\frac{\partial w}{\partial x} = \dot{\rho}_s = \dot{\rho}_a \tag{6}$$

The total heat, dQ, added to the control volume in time dt is the sum of the contributions due to thermal conduction, dQ_k, by gas flow, dQ_g, by chemical reaction, dQ_c, and by the absorption of radiant energy, dQ_r.

$$dQ = dQ_k + dQ_g + dQ_c + dQ_r \tag{7}$$

Considering the one-dimensional case these contributions are given by equations (8) through (11).

$$dQ_k = \frac{\partial}{\partial x}\left(k \frac{\partial T}{\partial x}\right) A\, dx\, dt \tag{8}$$

$$dQ_g = \frac{\partial}{\partial x}(w h_g) A\, dx\, dt \tag{9}$$

$$dQ_c = \dot{\rho}_a \Delta H_c A\, dx\, dt = \dot{\rho}_s \Delta H_c A\, dx\, dt \tag{10}$$

$$dQ_r = -\frac{\partial F}{\partial x} A\, dx\, dt \tag{11}$$

*Considering the case of a charring ablator of semi infinite extent and in steady state, the integrated continuity equation gives the gas flow as

$$w(g) = \dot{s}(\rho_o - \rho_c)\left[1 - \frac{\rho_a}{\rho_o - \rho_a} - \frac{\rho_g}{\rho_o - \rho_c}\right]$$

Certainly the last term in the bracket, $\rho_g / (\rho_o - \rho_c) \ll 1$ at all times for the applications of interest to the Apollo heat shield material.

In these equations k is the thermal conductivity of the solid material and thermal conduction through the gas has been neglected. Also, h_g denotes the specific enthalpy of the gaseous products, ΔH_c is the heat absorbed per unit mass of gases produced, and F is the radiant heat flux at any point in the material. Assuming a constant specific heat for the gaseous decomposition products and making use of the thermal equilibrium assumption dQ_g can be written in the form of equation (12).

$$dQ_g = C_{pg}\left(w\frac{\partial T}{\partial x} + \dot{\rho}_a T\right) A\, dx\, dt \tag{12}$$

The heat added to the control volume is then given by equation (13).

$$dQ = \left\{\frac{\partial}{\partial x}\left(k\frac{\partial T}{\partial x}\right) + C_{pg}\, w\frac{\partial T}{\partial x} + \dot{\rho}_a\left(C_{pg}T + \Delta H_c\right) - \frac{\partial F}{\partial x}\right\} A\, dx\, dt \tag{13}$$

The heat equation is found by equating dQ to the change in enthalpy of the control volume and neglecting higher order differential products.

$$\frac{d}{dt}(\rho h) = \frac{\partial}{\partial x}\left(k\frac{\partial T}{\partial x}\right) + C_{pg}\, w\frac{\partial T}{\partial x} + \dot{\rho}_a\left(\Delta H_c + C_{pg}T\right) - \frac{\partial F}{\partial x} \tag{14}$$

2.2.2 Restrictions on Property Values

In equation (14) ρ and h are the density and specific enthalpy of the control volume.

The density and enthalpy are considered to be additive functions of the contributions due to the solid and gas. Making use of equation (1) the following relationships are obtained.

$$\rho = \rho_s + \rho_g = \rho_a + \rho_c + \rho_g \tag{15}$$

$$h = \frac{\rho_a}{\rho} h_a + \frac{\rho_c}{\rho} h_c + \frac{\rho_g}{\rho} h_g \tag{16}$$

The energy per unit volume is the product ρh, which is obtained by combining equations (15) and (16).

$$\rho h = \rho_a h_a + \rho_c h_c + \rho_g h_g \tag{17}$$

Since ρ_g, the mass of gas in the control volume, is very much less than the solid density, ρ_s, then to a very good approximation, equation (15) may be written as:

$$\rho = \rho_s = \rho_a + \rho_c \tag{18}$$

Equation (16) may also be simplified by noting that the specific enthalpies h_g, h_a, h_c are all of the same order of magnitude so that the following relations are valid.

$$\rho_g h_g \ll \rho h \tag{19}$$

and

$$\rho h = \rho_a h_a + \rho_c h_c \tag{20}$$

Taking the time derivation of equation (20) results in

$$\frac{\partial}{\partial t}(\rho h) = \frac{\partial}{\partial t}(\rho_a h_a) + \frac{\partial}{\partial t}(\rho_c h_c)$$

$$= \rho_a \frac{\partial h_a}{\partial t} + h_a \frac{\partial \rho_a}{\partial t} + \rho_c \frac{\partial h_c}{\partial t} + h_c \frac{\partial \rho_c}{\partial t} \tag{21}$$

Recalling the assumption that the char matrix is irreducible, employing constant specific heats, and using equation (18) results in the following.

$$\frac{\partial}{\partial t}(\rho h) = \left\{(\rho_s - \rho_c) C_{p_a} + \rho_c C_{p_c}\right\} \frac{\partial T}{\partial t} + \dot{\rho}_a C_{p_a} T$$

$$= \rho_s \left\{C_{p_a} + \left(\frac{\rho_c}{\rho_s}\right)\left(C_{p_c} - C_{p_a}\right)\right\} \frac{\partial T}{\partial t} + \dot{\rho}_s C_{p_a} T \tag{22}$$

A similar line of reasoning may be used to develop an expression for thermal conductivity which depends on the decomposition of the solid material. Denoting the thermal conductivity of the virgin material as k_o, and that of the fully charred state as k_c, the following linear dependence of thermal conductivity on density is assumed.

$$k = k_c - \left(\frac{k_o - k_c}{\rho_o - \rho_c}\right)(\rho_o - \rho_s) \tag{23}$$

The thermal conductivity given by equation (23) is not temperature dependent in the usual sense, but rather is a function of the temperature history through the density. This is also true of the specific heat of the solid, C_{ps}, which from inspection of equation (22) is readily seen to be as follows.

$$C_{p_s} = C_{p_a}\left(\frac{\rho_s - \rho_c}{\rho_s}\right) + C_{p_c}\left(\frac{\rho_c}{\rho_s}\right) \tag{24}$$

2.2.3 Internal Decomposition

The quantity ρ_c is considered to be a constant and the quantity ρ_a is assumed to vary in accordance with a "n'th" order decomposition law. For a single reaction zone $\dot{\rho}_a$ is given by equation (25).

$$\dot{\rho}_a = -\rho_a^n A_c \exp\left\{-\frac{B}{T}\right\} \tag{25}$$

Combining equations (18) and (25) we then obtain equation (26).

$$\dot{\rho}_s = -(\rho_s - \rho_c)^n A_c \exp\left\{-\frac{B}{T}\right\} \tag{26}$$

Equation (26) can be generalized to account for decomposition in multiple reaction zones. Let the variation of density with temperature be assumed to be of the form displayed in Figure (2). As shown in this figure, it is assumed that the material is characterized by decomposition reactions occurring in three more or less distinct temperature zones. The density, ρ_o, of the virgin material is designated equivalently by ρ_{01}, and the limiting densities, of the three reaction zones are designated equivalently by ρ_{02}, ρ_{03} and ρ_{04}, respectively, where the fully charred density is understood to be ρ_{04}. The rate expressions assumed for each of the three regions are given by equations (27) through (29).

FIGURE 2

ILLUSTRATIVE CHAR DENSITY HISTORY

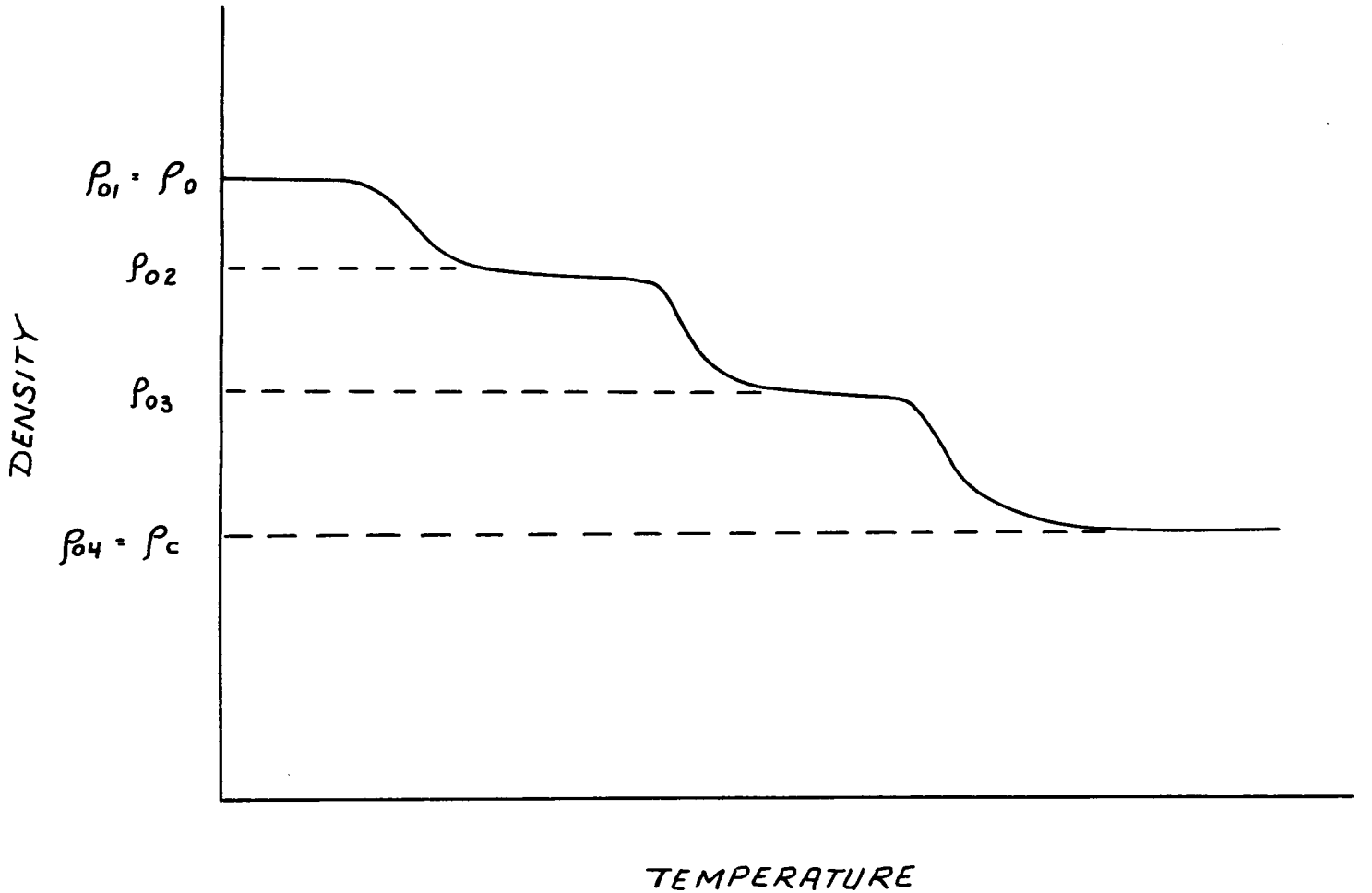

$$\frac{d}{dt}\left(\frac{\rho_s}{\rho_{o1}}\right) = -A_1\left(\frac{\rho_s - \rho_{o2}}{\rho_{o1}}\right)^{n_1} \exp\left\{-\frac{B_1}{T}\right\} \tag{27}$$

$$\frac{d}{dt}\left(\frac{\rho_s}{\rho_{o2}}\right) = -A_2\left(\frac{\rho_s - \rho_{o3}}{\rho_{o2}}\right)^{n_2} \exp\left\{-\frac{B_2}{T}\right\} \tag{28}$$

$$\frac{d}{dt}\left(\frac{\rho_s}{\rho_{o3}}\right) = -A_3\left(\frac{\rho_s - \rho_{o4}}{\rho_{o3}}\right)^{n_3} \exp\left\{-\frac{B_3}{T}\right\} \tag{29}$$

Hence, in the first zone:

$$\dot{\rho}_{s1} = -A_1 \rho_{o1}\left(\frac{\rho_s - \rho_{o2}}{\rho_{o1}}\right)^{n_1} \exp\left\{-\frac{B_1}{T}\right\} \tag{30}$$

and in the second and third zones:

$$\dot{\rho}_{s2} = -A_2 \rho_{o2}\left(\frac{\rho_s - \rho_{o3}}{\rho_{o2}}\right)^{n_2} \exp\left\{-\frac{B_2}{T}\right\} \tag{31}$$

$$\dot{\rho}_{s3} = -A_3 \rho_{o3}\left(\frac{\rho_s - \rho_{o4}}{\rho_{o3}}\right)^{n_3} \exp\left\{-\frac{B_3}{T}\right\} \tag{32}$$

The total reaction rate is then obtained by summation of equations (30) through (32). The result is given by equation (33).

$$\dot{\rho}_s = -\sum_{i=1}^{3} A_i \rho_{oi}\left(\frac{\rho - \rho_{oi+1}}{\rho_{oi}}\right)^{n_i} \exp\left\{-\frac{B_i}{T}\right\} \tag{33}$$

2.2.4 Radiant Heating

The formulation of the term for the radiant flux F is based on an exponential absorption law. For constant optical properties, an incident

flux F_o is attenuated in accordance with equation (34) where R_o is the relectance of the interface x = S, (x - S) is the distance traversed by the ray in the primary material and a is the absorption coefficient of the solid.

$$F = F_o (1 - R_o) \exp \left\{ -a(x-S) \right\} \tag{34}$$

Designating the reflectance of the interface at $x = \ell_1$ as R_ℓ and assuming the reflectance of the interface at x = s is the same from either direction, it can easily be shown that consideration of multiple internal reflections results in the following relationships. The apparent reflectivity and apparent transmissivity are given respectively by equations (35) and (36).

$$R_A = \left\{ R_o + \frac{(1-R_o)^2 R_\ell \exp\left[-2a(\ell_1 - S)\right]}{1 - R_o R_\ell \exp\left[-2a(\ell_1 - S)\right]} \right\} \tag{35}$$

$$\tau_A = \left\{ \frac{(1-R_o)(1-R_\ell) \exp\left[-a(\ell_1 - S)\right]}{1 - R_o R_\ell \exp\left[-2a(\ell_1 - S)\right]} \right\} \tag{36}$$

The radiant flux leaving the interface at x = S and travelling in the direction of positive x is then given by equation (37).

$$F(S) = \left\{ \frac{(1-R_o)}{1 - R_o R_\ell \exp\left[-2a(\ell_1 - S)\right]} \right\} \tag{37}$$

The radiant flux leaving the $x = \ell_1$ interface and travelling in the direction of negative x is given by equation (38).

$$F(\ell_1) = \left\{ \frac{(1-R_o) R_\ell \exp\left[-a(\ell_1 - S)\right]}{1 - R_o R_\ell \exp\left[-2a(\ell_1 - S)\right]} \right\} \tag{38}$$

The total radiant flux at any point x within the primary material is then given by equation (39).

$$F(x) = (1-R_o) F_o \left\{ \frac{\exp\left[-a(x-S)\right] - R_\ell \exp\left[-a(2\ell_1 - x - S)\right]}{1 - R_o R_\ell \exp\left[-2a(\ell_1 - S)\right]} \right\} \tag{39}$$

The term in F for inclusion in equation (14) is then obtained from equation (39) by differentiation.

$$-\frac{\partial F}{\partial x} = \alpha(1-R_o)F_o\left\{\frac{\exp[-\alpha(x-s)]+R_\ell\exp[-\alpha(2\ell_i-x-s)]}{1-R_o R_\ell \exp[-2\alpha(\ell_i-s)]}\right\} \quad (40)$$

This formulation considers only the problem of the in-depth absorption of radiation from a source external to the thermal protection system. This treatment is generally adequate for most problems involving charring ablators since the transport of energy by "self-glowing" of the heated material is quite small due to the relatively large absorption coefficients associated with these materials. A formulation of the equations necessary to describe this additional transport mechanism is available and is given in Appendix I to this volume.

2.2.5 Internal Pressure

In the material for which the model was developed, available evidence does not indicate that internal pressure forces played a major role in the ablation process. However, it was considered unwise to totally disregard the pressure in the mathematical model, since other materials may be more strongly affected. In particular, the internal pressure buildup resulting from the formation of products of decomposition may lead to sudden abrupt rupture of the weakened char material near the surface thereby increasing the ablation rate in a timewise discontinuous manner. A detailed structural analysis is necessary in order to establish possible failure modes associated with this process. The progress made to date on solution of this complicated problem is described in Appendix II. Pending completion of these studies no attempt has been made to include mechanical spallation phenomena in the mathematical model for charring ablators.

On the other hand, it is relatively simple to incorporate provisions for calculating the internal pressure distribution resulting from the formation of decomposition products in the charring process. This may be done by uncoupling the momentum equation for the flow of decomposition products from the energy equation such that a post-facto calculation of the pressure distributions may be performed from a knowledge of the temperature and mass flow rate distributions. A non-linear extension of Darcy's law together with an equation of state of a perfect gas is used for this purpose.

$$\frac{dP}{dx} = \alpha\mu v_g + \beta v_g^2 \quad (41)$$

$$P = \rho_g R T \quad (42)$$

In these P, ρ_g and T represent the gas pressure, density and temperature, μ represents gas viscosity, α and β represent the viscous and inertial resistance coefficients to the flow, and R is the specific gas constant. The quantity v_g is the so called "filter" or "seepage" velocity.

Solutions are sought subject to the condition that $P = P_s(t)$ at the ablating surface, where $P_s(t)$ is the time dependent local static pressure.

The quantities α and β are characteristics of the porous char and will therefore depend on the state of the material, i.e., they will vary as the material is only partially or fully charred. Combining equations (41) and (42) and calling $\rho_g v_g = w$ gives:

$$\frac{1}{RT}\frac{dP^2}{dy} = 2\alpha\mu w + 2\beta w^2 \tag{43}$$

To obtain values for α and β, mass flow experiments must be performed using small specimen thicknesses, and controlled pressures. The derivation of values for the coefficients α and β are discussed in Section 3.

To obtain a form suitable for calculating the pressure distribution through the heat shield, equation (43) may be written as

$$\int_{P_s}^{P} dP^2 = 2R\int_{s}^{x}\alpha\mu T w\, dx + 2R\int_{s}^{x}\beta T w^2 dx$$

or

$$P = \left\{ P_s^2 + 2R\int_{s}^{x}\alpha\mu T w\, dx + 2R\int_{s}^{x}\beta T w^2 dx \right\}^{1/2} \tag{44}$$

where the temperature, T is obtained for the solution of the energy equation, and the mass flow of gas, w is obtained from the integration of equation (6). The resistance coefficients are assumed to be linear functions of the density, i.e.

$$\alpha = \alpha_c + \left(\frac{\alpha_v - \alpha_c}{\rho_o - \rho_c}\right)(\rho_s - \rho_c)\ ; \quad \beta = \beta_c + \left(\frac{\beta_v - \beta_c}{\rho_o - \rho_c}\right)(\rho_s - \rho_c) \tag{45}$$

where α_v and β_v are the coefficients for virgin state of the material while α_c and β_c are the coefficients for the charred state.

2.2.6 Secondary Materials

Energy transfer within the secondary materials (designated by the subscripts S1, S2, etc.) is assumed to be solely by conduction. It is further assumed that the thermal expansion coefficient of these materials is small, the governing equations including temperature dependent properties are of the form of equation (46) where the region of validity is

$$\ell_i < x < \ell_{i+1} \; ; \quad i = 1, 2 \ldots$$

$$(\rho c)_{si} \frac{\partial T}{\partial t} = \frac{\partial}{\partial x}\left(k_{si} \frac{\partial T}{\partial x}\right); \quad i = 1, 2 \ldots \tag{46}$$

2.2.7 Summary of Internal Equations

The complete set of differential and auxiliary equations governing energy and mass transfer within the composite heat shield of Figure 1 is then given by a combination of equations (6), (14), (22), (23), (32), (33), (36), and (37). The resulting set of equations are as follows:

$s < x < \ell_1$:

$$\rho_s C_{ps} \frac{\partial T}{\partial t} = \frac{\partial}{\partial x}\left(k_s \frac{\partial T}{\partial x}\right) + C_{pg} w \frac{\partial T}{\partial x} + \dot{\rho}_s \left(\Delta H_c + C_{pg} T - C_{pa} T\right)$$

$$- a F_o (1 - R_o)\left(\frac{\exp\left[-a(x-s)\right] + R_\ell \exp\left[-a(2\ell_1 - x - s)\right]}{1 - R_c R_\ell \exp\left[-2a(\ell_1 - s)\right]}\right) \tag{47}$$

$$C_{ps} = C_{pa}\left(\frac{\rho_s - \rho_c}{\rho_s}\right) + C_{pc}\left(\frac{\rho_c}{\rho_s}\right) \tag{48a}$$

$$k_s = k_o - \left(\frac{k_o - k_c}{\rho_o - \rho_c}\right)(\rho_o - \rho_s) \tag{48b}$$

$$\frac{\partial w}{\partial x} = \dot{\rho}_s \quad \text{or} \quad w = \int_x^\ell \dot{\rho}_s \, dx \tag{49}$$

$$\dot{\rho}_s = -\sum_{i=1}^{3} A_i \rho_{oi} \left(\frac{\rho_s - \rho_{o,i+1}}{\rho_{oi}} \right)^{n_i} \exp\left(-\frac{B_i}{T} \right) \tag{50}$$

$$P = \left\{ P_s^2 + 2R \int_s^x \alpha \mu T \omega \, dx + 2R \int_s^x \beta T \omega^2 \, dx \right. \tag{51}$$

$$\alpha = \alpha_c + \left(\frac{\alpha_v - \alpha_c}{\rho_o - \rho_c} \right)(\rho_s - \rho_c) \quad ; \quad \beta = \beta_c + \left(\frac{\beta_v - \beta_c}{\rho_o - \rho_c} \right)(\rho_s - \rho_c) \tag{52}$$

$\ell_1 < x < \ell_2$

$$(\rho c)_{s1} \frac{\partial T}{\partial t} = \frac{\partial}{\partial x} \left(k_{s1} \frac{\partial T}{\partial x} \right) \tag{53a}$$

$\ell_2 < x < L$

$$(\rho c)_{s2} \frac{\partial T}{\partial t} = \frac{\partial}{\partial x} \left(k_{s2} \frac{\partial T}{\partial x} \right) \tag{53b}$$

Equations (47) through (53) together with an appropriate set of initial and boundary conditions completely describe the system.

2.3 Initial Conditions

As initial conditions to the problem, both the temperature and density are specified throughout the primary material and the temperature is specified in the secondary materials. Any arbitrary distributions may be specified, i.e., the initial conditions may be in the form of equations (54).

$$T(x, 0) = T(x), \tag{54a}$$

$$\rho(x, 0) = \rho(x). \tag{54b}$$

2.4 Heat Transfer to a Highly Cooled Non-Ablating Surface

For the cases considered here the surface recedes in a continuous fashion. Discontinuous removal based on a thermal stress criterion can be easily introduced into the computational scheme for those materials which exhibit such phenomena. Based on a continuous material removal process, a heat balance at the receding surface can be written in the form of equation (55).

$$q = -k_s \frac{\partial T}{\partial x} + \dot{s}\left\{\rho_c H_v + (\rho_s - \rho_c)\Delta H_c\right\} - \epsilon\sigma T^4 \; ; \; \text{at } x = s \qquad (55)$$

where the left-hand side of the above equation, q, represents the convective heat transfer rate to a hot wall in the presence of mass transfer and chemical reactions. The terms on the right-hand side represent the rates of heat conduction into the solid surface, vaporization of the solid surface and radiation from the solid surface.

Some discussion is needed to explain the form and method of calculation of the heat transfer term, q. Since the heat transfer depends on the temperature (or enthalpy) and mass transfer at the solid surface as well as boundary layer flow parameters, it is apparent that a simultaneous solution of the variable property, chemically reacting boundary layer and the charring heat shield energy equations is necessary to determine heat transfer rates. Realizing that such a simulatneous solution is needed at many times during the re-entry it is believed that such a method is impractical for use as a design tool. In practice what is done is to perform analytical and experimental boundary layer studies and obtain solutions for a wide range of wall conditions. The solutions are then correlated to relate heated wall and boundary layer conditions.

The usual procedure is to define a "cold wall" heat transfer rate q_c as in equation (56).

$$q_c = \frac{q_o}{\left(\frac{H_r}{H_s} - \frac{H_w}{H_s}\right)} \qquad (56)$$

where q_o is the heat transfer to a "hot" non-ablating surface, H_r is the recovery enthalpy, H_s is the stagnation enthalpy and H_w is the enthalpy of the environmental fluid at the temperature of the heated surface. For most applications the "cold wall" heat flux (which is essentially a heat transfer coefficient) depends only slightly on the wall temperature and this variation could be ignored on the grounds that the correction is less than the uncertainty in the value of the heat transfer coefficient itself. In certain cases, however, the corrections become numerically, if not physically, significant and probably should be employed if for no other

reason than consistency. This is particularly true since the appropriate corrections are easily introduced into most numerical calculations.

2.4.1 Stagnation Point Heat Transfer

In the case of stagnation point flow the treatment of Fay and Riddell (Reference 4) shows the cold wall heat transfer rate depends on conditions at the wall in accordance with the following proportionality.

$$q_c \sim (\rho_w \mu_w)^{0.1} \tag{57}$$

In equation (57) ρ_w and μ_w are the density and viscosity at the wall temperature and pressure. It is desirable to obtain a correction term which gives q_c as a function of the wall temperature. Figure 3 is a graph of log ($\rho_w \mu_w$) as a function of log (H_w). The range of temperatures covered by this figure is from room temperature to 18000°R. The density and enthalpy are from Reference 5 and the viscosity from Reference 6. It can be seen that in the range of surface enthalpies of interest the product ($\rho_w \mu_w$) is nearly proportional to $(H_w)^{-0.037}$. The "cold wall" heat transfer rate evaluated for a wall at temperature T_w in terms of the value obtained for a wall at T_{wr} is then given by equation (58).

$$q_c = (q_c)_r \left(\frac{H_w}{H_{wr}}\right)^{-0.037} \tag{58}$$

The data in Figure (3) are for a pressure of 1, 10 and 100 atmospheres and demonstrates that the exponent in equation (58) is insensitive to pressure and, hence, equation (58) is recommended for use at least in the near atmospheric pressure range.

2.4.2 Turbulent Heat Transfer

In the case of turbulent boundary layers the method of Eckert (Reference 7) gives the "cold wall" heat flux as a function of the properties evaluated at a reference conditions.

$$q_c \sim (\rho^*)^{0.8} (\mu^*)^{0.2} \tag{59}$$

The properties in (59) are evaluated at a reference enthalpy H* which is defined by equation (60).

$$H^* = \frac{1}{2}(H_e + H_w) + 0.22 H_s \left(\frac{H_r}{H_s} - \frac{H_e}{H_s}\right) \tag{60}$$

FIGURE 3

STAGNATION POINT

HEAT TRANSFER PARAMETER VARIATION WITH ENTHALPY

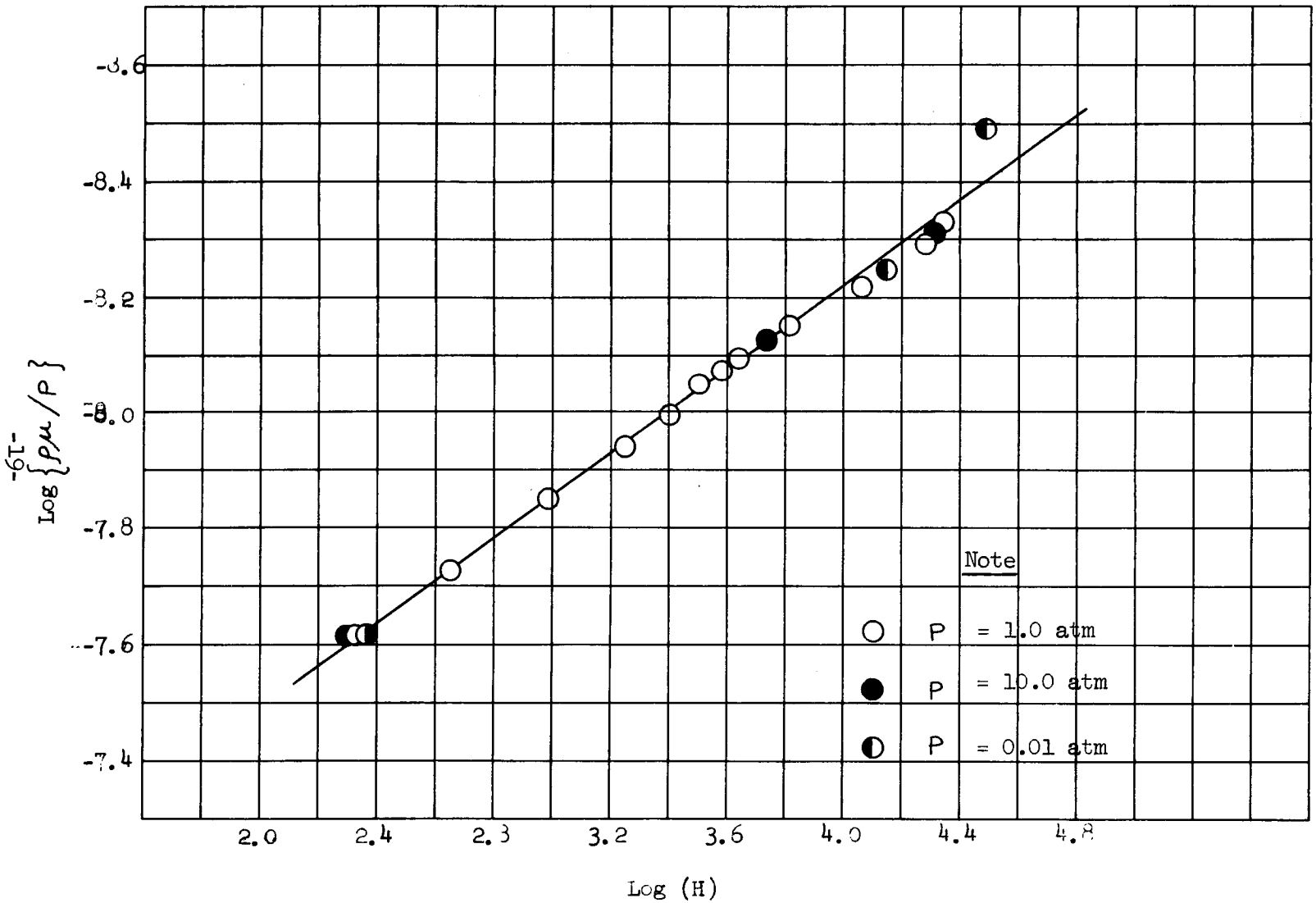

NOTE: USE TYPE B PENCIL FOR VUGRAPHS AND REPORT DATA.

where H_r and H_e are, respectively, the recovery and local free stream static enthalpy.

The ratio involving the local static enthalpy is a function of the recovery enthalpy through equation (61) where r is the recovery factor.

$$\frac{H_e}{H_s} = \frac{\frac{H_r}{H_s} - r}{1 - r} \tag{61}$$

Figure 4 is a plot of $(\rho^*)^{0.8}(\mu^*)^{0.2}$ as a function of enthalpy. Over the range of reference enthalpies of interest equation (62) is obtained as a correction for wall temperature effects on the "cold wall" heat transfer rate for the turbulent boundary layer.

$$q_c = (q_c)_R \left(\frac{H^*}{H^*_R}\right)^{-0.502} \tag{62}$$

2.4.3 Laminar Heat Transfer

A correlation similar to the above may be formulated for laminar boundary layer flow at locations away from the stagnation region. Again employing the method of Eckert results in the following expression for corrected "cold wall" heat transfer.

$$q_c = (q_c)_R \left(\frac{H^*}{H^*_R}\right)^{-0.185} \tag{63}$$

2.5 Heat Transfer with Air Injection

The injection of the ablated species into the boundary layer has a pronounced effect on the cold wall heat transfer coefficient. The injected species, with its normal velocity component, tends to decelerate the flow and decrease the skin friction while also acting as a distributed heat sink. The left-hand side of equation (55) may be written as follows:

$$q = q_o \left(\frac{q}{q_o}\right) = q_o \phi \tag{64}$$

where ϕ is the ratio of heat transfer to a "hot wall" with mass injection to heat transfer to a hot wall and no mass injection. The ratio ϕ depends on the vehicle geometry, type of boundary layer flow and properties of the injected species. By employing the results of analytical and experimental boundary layer studies, correlations may be developed for ϕ. Analytical studies for laminar flow of air to air injection for the stagnation region, cones and wedge shapes

FIGURE 4

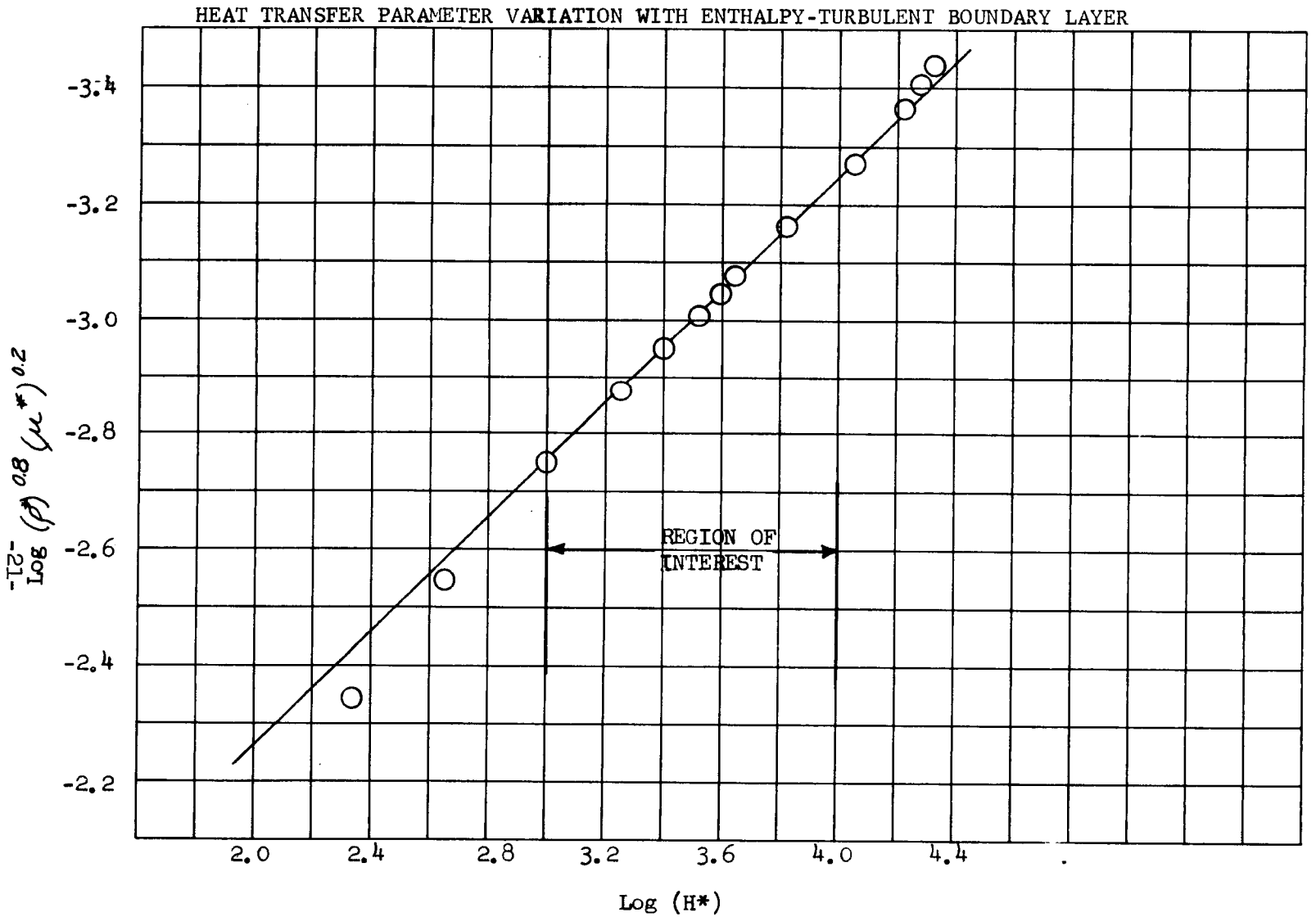

NOTE: USE TYPE B PENCIL FOR VUGRAPHS AND REPORT DATA.

have yielded solutions which are in good agreement with experimental data. For turbulent flow the evaluation of the heat transfer ratio, ϕ, depends primarily on experimental studies. The effects of foreign gas injection has also been studied and correlations have been proposed which permit rather simple expressions to describe the interaction of heat and mass transfer. Reference (8) gives a review of binary boundary layer characteristics based on both analytical and experimental studies. This same reference presents the exact solutions of air to air injection when the edge velocity varies as some power of the distance along the solid surface, i.e., $u_e \sim z^n$. These solutions are shown in Figure 5 and of particular interest are the special cases of the flat plate (n = 0) and the plane and axisymmetric stagnation regions (n = 1). The heat transfer ratio ϕ is plotted against a boundary layer mass transfer parameter, $\rho_w v_w / \rho_e u_e \sqrt{R_{ez}}$, where R_{ez} is the Reynolds number based on edge velocity and Z-distance along the surface. Since the heat transfer to a non-ablating wall depends on the local Reynolds number a more suitable form for the mass transfer parameter may be deduced which eliminates the Reynolds number. The result is a new parameter $\dot{m}_w h_r / q_c$ where the advantage is evident since both cold wall heat transfer, q_c and recovery enthalpy h_r are assumed to be known functions of time. The quantity $\dot{m}$ is the total mass transfer rate from the surface. In this way there is no need to add a new input, Reynolds number, to the input format of the computer program. Figure 6 shows the heat transfer ratio, ϕ, in terms of $\dot{m}_w h_r / q_c$. Also indicated is a curve fit of ϕ which agrees well with the exact solutions for the region of interest, i.e.,

$$\phi = \exp \left\{ - f \, (1 + 0.618 f) \right\} , \tag{65}$$

where $$f = \eta \, \frac{\dot{m}_w \, h_r}{q_c} ,$$

and η, the so called blowing coefficient or transpiration factor is

$$\eta = 0.603 \quad \text{for the stagnation region,}$$

$$\eta = 0.764 \quad \text{for the laminar flat plate.}$$

2.6 Heat Transfer with Foreign Gas Injection

For the injection of a gas other than air into an air boundary layer the analytical and experimental data for ϕ may be correlated by introducing a molecular weight ratio into the mass transfer parameter. The transpiration factors may now be generalized.

$$\eta = 0.603 \left(\frac{M_a}{M_i} \right)^{1/3} \quad \text{for the stagnation region,} \tag{66a}$$

$$\eta = 0.764 \left(\frac{M_a}{M_i} \right)^{1/3} \quad \text{for the laminar flat plate,} \tag{66b}$$

where: M_a is the molecular weight of air, M_i is the molecular weight of the

FIGURE 5

LAMINAR BOUNDARY LAYER HEAT TRANSFER
AIR TO AIR INJECTION

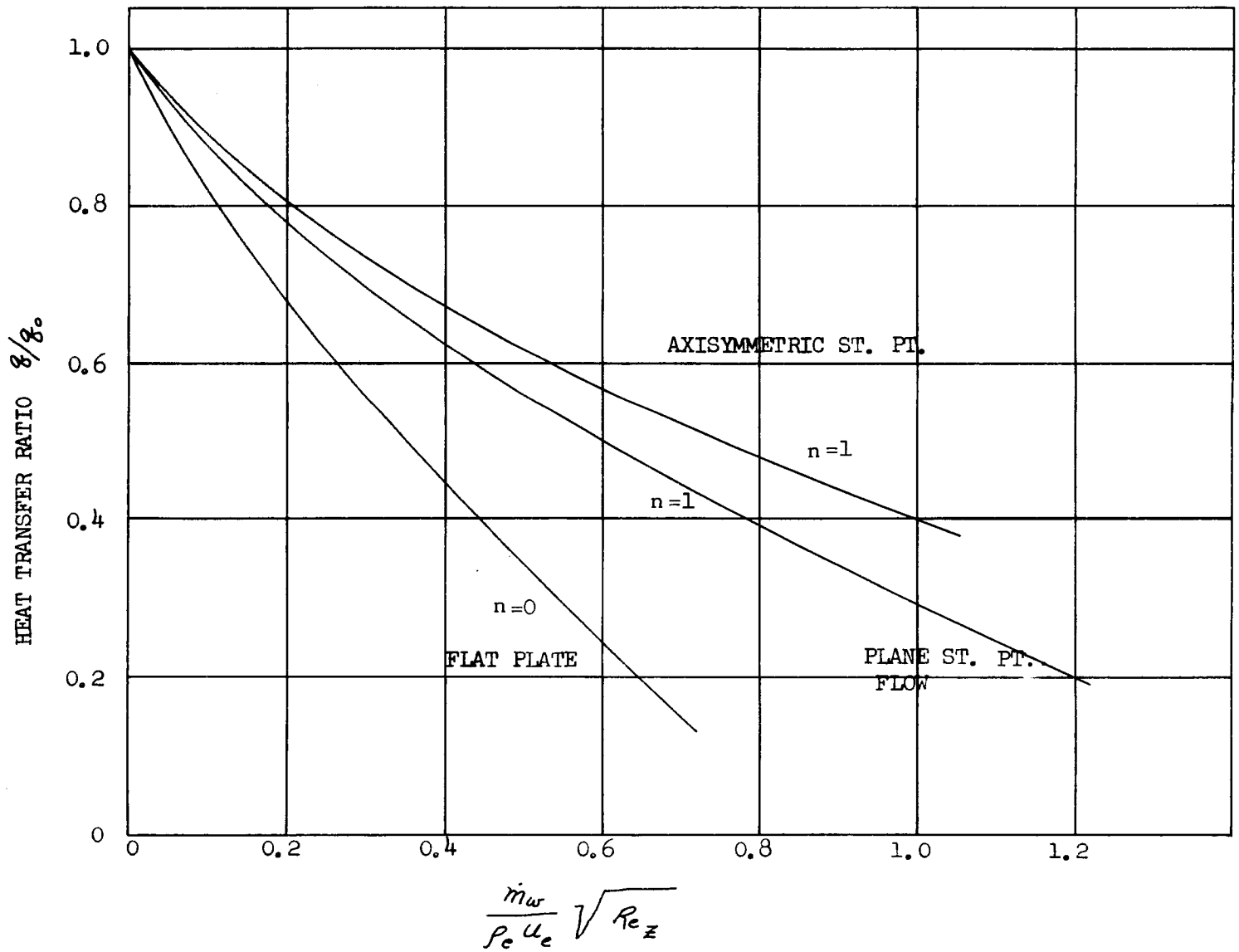

FIGURE 6

LAMINAR BOUNDARY LAYER HEAT TRANSFER
AIR TO AIR INJECTION

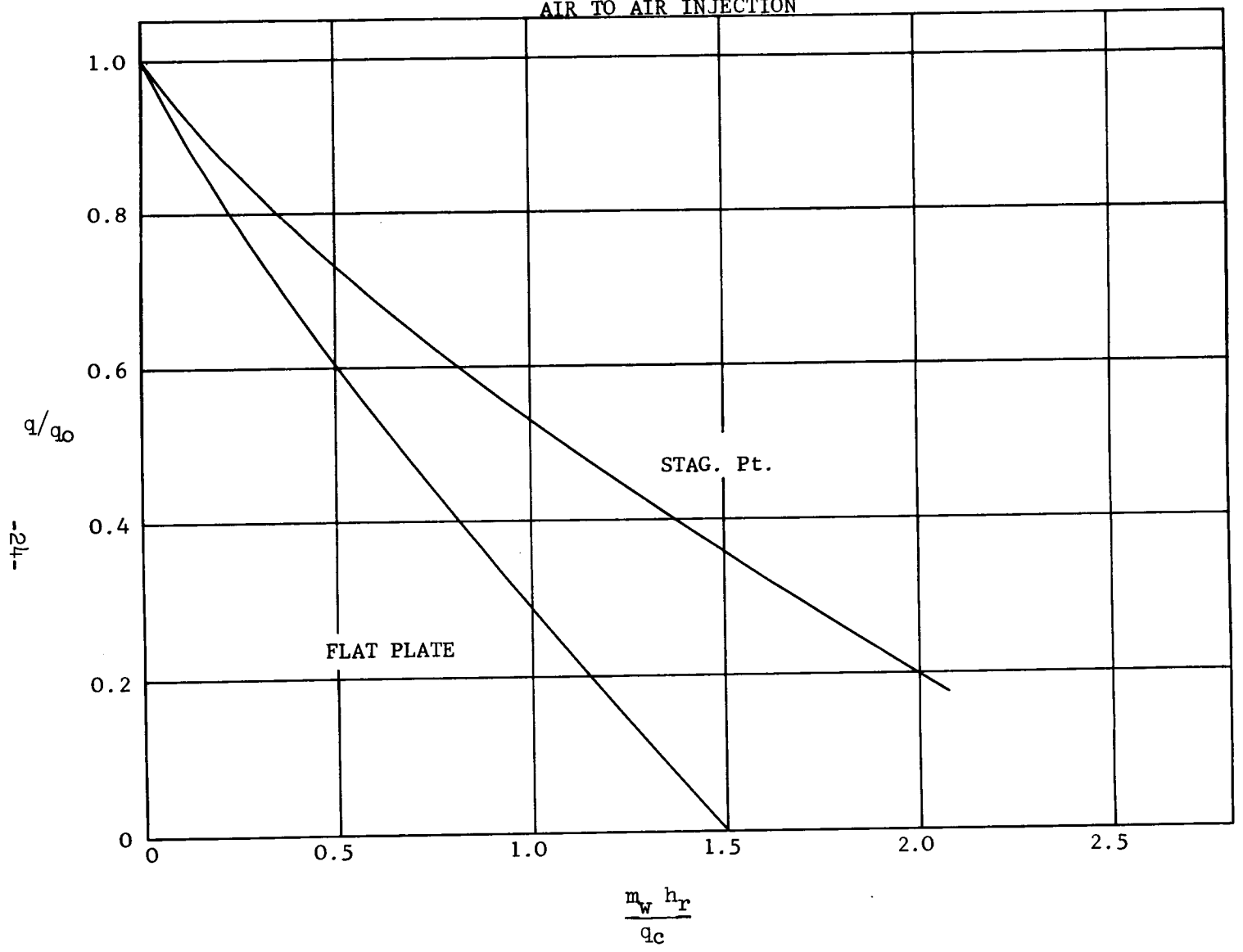

injected gas, and the value of the exponent is (1/3) justified on the bases of data reported in reference 8.

For turbulent flow much less analysis and experimental work have been done especially for foreign gas injection. Figure (7) shows the results of several analysis (Ref. 9, 10, 11) for air to air injection. The molecular weight ratio may again be employed and from the available data on foreign gas injection the transpiration factor becomes:

$$\eta = 0.347 \left(\frac{M_a}{M_i}\right)^{0.1} \quad \text{for turbulent flow.} \tag{67}$$

The above value of η for turbulent flow is found to be insensitive to pressure gradient along the body.

2.7 Heat Transfer with Multicomponent Gas Injection

To apply the analytical and experimental results of heat and mass transfer studies mentioned above to a charring heat shield is complicated by the fact that the ablated species have many components and the boundary layer is not a binary mixture. For charring materials, the procedure followed is to assume the mass transfer parameter for the composite injected mixture of surface material and subsurface gases is the sum of the individual mass transfer parameters, i.e.,

$$f = \frac{h_r}{q_c}\left\{\eta_s \rho_s \dot{S} + \eta_g w\right\} , \tag{68}$$

where:

$\dot{S}$ is the linear surface recession rate,

ρ_s is the density of the solid surface,

w is the mass flow role per unit area of subsurface rat decomposition gases,

η_s is the transpiration factor for the injection of the subliming surface,

η_g is the transpiration factor for the injection of decomposition gaseous products.

By combining (56), (58), (62), (63) and (64) the heat transfer to a "hot" ablating surface is

$$q = (q_c)_R \left\{1 - \frac{H_w}{H_s}\right\} \left\{\frac{H_w}{H_{wr}}\right\}^{-0.037} \exp\left\{- f\,(1 + 0.618f)\right\} \tag{69a}$$

FIGURE (7)

TURBULENT BOUNDARY LAYER HEAT TRANSFER WITH
MASS TRANSFER COOLING

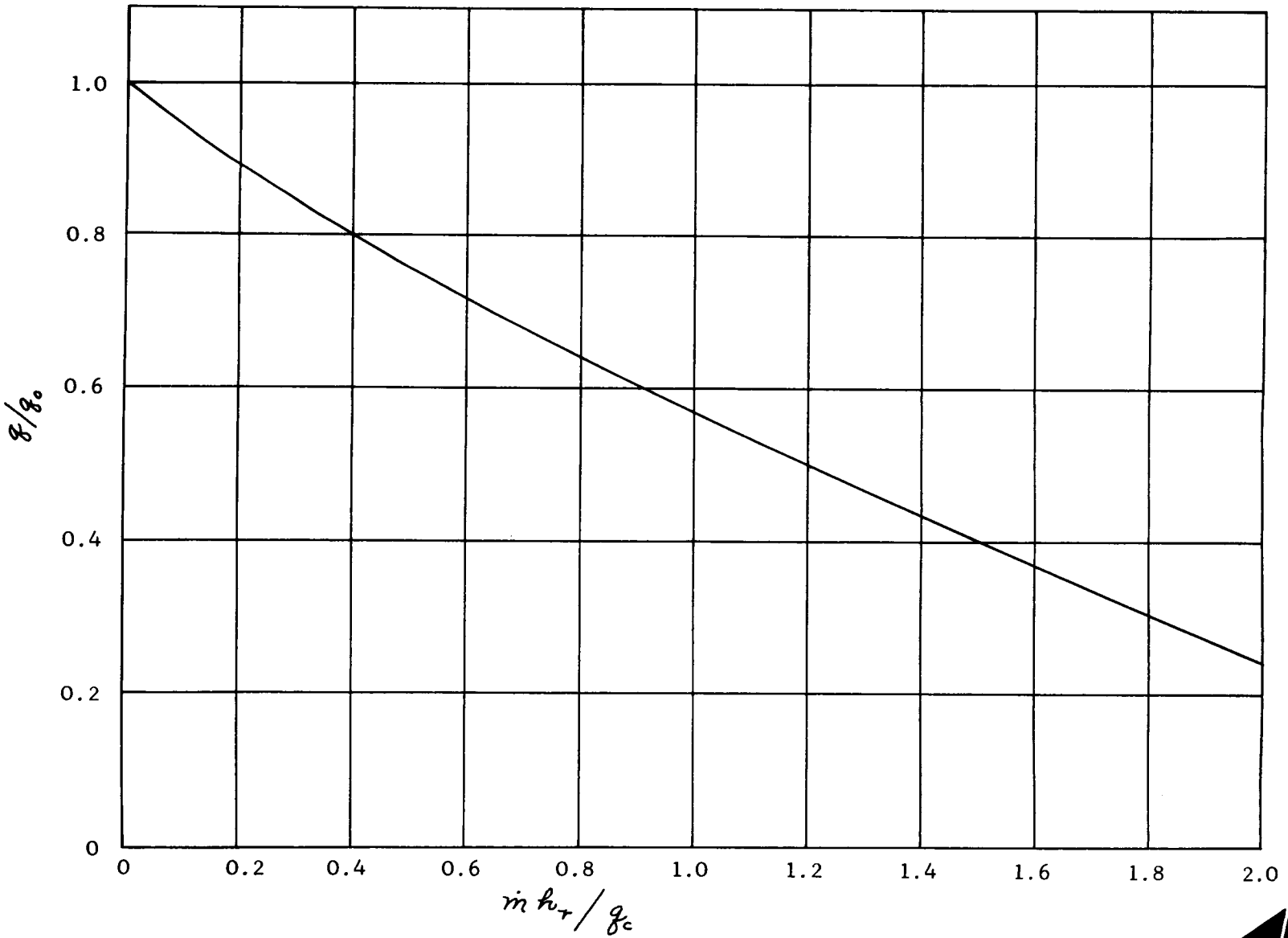

at the stagnation region, and

$$q = (q_c)_R \left\{ \frac{H_r}{H_s} - \frac{H_w}{H_s} \right\} \left\{ \frac{H_w^*}{H\bar{x}_{wr}} \right\}^{E2} \cdot \exp \left\{ - f (1 + 0.618f) \right\} \qquad (69b)$$

at body stations away from the stagnation point. In equation (69b) the value of the exponent E2 is dependent on whether the external flow is laminar or turbulent as the previous discussion indicates. In either case it is understood that the $(q_c)_R$ is cold wall heat transfer to a fixed set of wall conditions and is therefore explicitly only a function of time and body station.

2.8 Wall Enthalpy Relations

The enthalpy, H_w , of the environmental fluid at the temperature and pressure of the heated surface is computed under the assumption of an equilibrium mixture involving O_2, N_2 and O.

Consider an equilibrium mixture of molecular nitrogen, molecular oxygen and atomic oxygen. One unit of "cold" gas will be taken to contain δ_1, gram moles of molecular nitrogen and δ_2 gram moles of molecular oxygen. At any temperature, T, and total pressure, P, the amount of molecular oxygen present in the equilibrium mixture is (δ_2 - X) moles and the amount of atomic oxygen is (2X) moles. The thermodynamic equilibrium criterion for the mixture can then be written as Equation (70) where K is the equilibrium constant for oxygen dissociation.

$$K = \frac{4 X^2 P}{(\delta_1 + \delta_2 + X)(\delta_2 - X)} \qquad (70)$$

The physically real solution of Equation (70) is given by Equation (71).

$$X = \frac{\left[K^2 \delta_1^2 + 4K(K+4P)(\delta_1 + \delta_2 + \delta_2^2) \right]^{1/2} - K\delta_1}{2(K + 4P)} \qquad (71)$$

In general, the equilibrium constant K can be written to a high degree of approximation in the form of Equation (72).

$$K = A \exp \left\{ - B_{e/T} \right\} . \qquad (72)$$

Designating the enthalpy of the equilibrium mixture as H_w and the enthalpy of the species N_2, O_2 and O by the subscripts 1 through 3, respectively, we can write the enthalpy of the unit of gas in the following form.

$$H_w = \delta_1 H_1 + (\delta_2 - X) H_2 + 2X H_3 \quad . \tag{73}$$

Also to a high degree of approximation, it is possible to write the species enthalpies, H_i, as quadratic functions of temperature in the form of Equation (74) where the γ are empirical constants obtained by curve fitting.

$$H_i = \gamma_{i1} + \gamma_{i2} T + \gamma_{i3} T^2 \quad . \tag{74}$$

In terms of these coefficients, the enthalpy of the mixture can be written as equation (75).

$$H_w = (\delta_1 \gamma_{11} + \delta_2 \gamma_{21}) + (\delta_1 \gamma_{12} + \delta_2 \gamma_{22}) T + (\delta_1 \gamma_{13} + \delta_2 \gamma_{23}) T^2 + [(2\gamma_{31} - \gamma_{21}) + (2\gamma_{32} - \gamma_{22}) T + (2\gamma_{33} - \gamma_{23}) T^2] X . \tag{75}$$

Using the following definitions:

$$\left.\begin{aligned} \Gamma_1 &= (\delta_1 \gamma_{11} + \delta_2 \gamma_{21}) + (2\gamma_{31} - \gamma_{21}) X , \\ \Gamma_2 &= (\delta_1 \gamma_{12} + \delta_2 \gamma_{22}) + (2\gamma_{32} - \gamma_{22}) X , \\ \Gamma_3 &= (\delta_1 \gamma_{13} + \delta_3 \gamma_{23}) + (2\gamma_{33} - \gamma_{23}) X , \end{aligned}\right\} \tag{76}$$

Equation (75) then becomes:

$$H_w = \Gamma_1 + \Gamma_2 T + \Gamma_3 T^2 \quad . \tag{77}$$

Equations (71) and (72) together with either Equation (75) or the equivalent Equations (76) and (77) then serve to define the enthalpy of the equilibrium mixture for all areas of the temperature pressure field in which the dissociation of nitrogen is negligible.

Values of the various constants appearing in the preceding equations have been obtained by least squares techniques based on the data of Reference

(12). The composition of normal air has been taken from Reference (13). The resulting constants appropriate to normal air are given in Table (1) and are for use with pressure in atmospheres, temperature in degrees Rankine and yield the enthalpy in BTU/lb.

Figure (8) shows the error between the present method and "exact" calculations for air as a function of temperature for several values of total pressure. As can be seen from this figure, the agreement is excellent and is in fact within the uncertainties in the so-called "exact" calculations.

Figure (9) presents the enthalpy of air as a function of temperature for several values of pressure as computed using the present method together with the constants given in Table (1).

2.9 Surface Ablation Theory

The ablative performance of the materials considered may be regarded as falling into two regimes. In the first of these regimes a heterogeneous reaction takes place between a charred carbonaceous surface and the oxygen in the free stream fluid. This reaction is exothermic and the rate at which this reaction occurs is a function of the kinetics of the surface reaction and the rate at which oxygen can diffuse to the reacting surface. In the discussion which follows consideration is limited to pure carbon for illustrative purposes. An analogous analysis for char-forming materials adds nothing but more involved algebra to the system.

2.9.1 Rate Limited Surface Oxidation

It is assumed that the heterogeneous surface combustion of carbon is of arbitrary order, N, in the partial pressure of oxygen at the surface. Under this assumption, and writing the heterogeneous rate constant as an Arrhenius function of temperature, the rate of removal of carbon due to this oxidation reaction can be written in the form of Equation (78)

$$\dot{m}_r = A_r \left\{ \mu_1 W_s P_e \right\}^{N_r} \exp \left\{ - B_{r/T} \right\} . \tag{78}$$

In this equation the quantity P_e is the local static pressure, W_s in the weight fraction of oxygen at the reacting surface and μ_1 is a molecular weight ratio which converts W_s from a weight fraction to a mole fraction.

2.9.2 Diffusion Limited Surface Oxidation

A second relation involving W_s and $\dot{m}$ can be written in terms of the rate of diffusion of oxygen to the reacting surface. Since any reaction at the surface requires that oxygen migrate to the surface in order to

TABLE 1

VALUES OF CONSTANTS FOR NORMAL AIR

The following constants are those appropriate to normal air with T in ^{o}R and P in atmospheres. The resultant enthalpy is in BTU/lb.

δ_1	12.7657
δ_2	2.9984
A	1.1105×10^{7}
B	1.1112×10^{5}
γ_{11}	-0.858
γ_{12}	16.151×10^{-3}
γ_{13}	0.321×10^{-6}
γ_{21}	-0.903
γ_{22}	16.620×10^{-3}
γ_{23}	0.416×10^{-6}
γ_{31}	234.341
γ_{32}	11.089×10^{-3}
γ_{33}	-0.0054×10^{-6}
$(\delta_1\gamma_{11} + \delta_2\gamma_{21})$	-13.654
$(\delta_1\gamma_{12} + \delta_2\gamma_{22})$	256.012×10^{-3}
$(\delta_1\gamma_{13} + \delta_2\gamma_{23})$	5.345×10^{-6}
$(2\gamma_{31} - \gamma_{21})$	469.585
$(2\gamma_{32} - \gamma_{22})$	5.558×10^{-3}
$(2\gamma_{33} - \gamma_{23})$	-0.427×10^{-6}

FIGURE 8

ERRORS IN APPROXIMATE METHOD

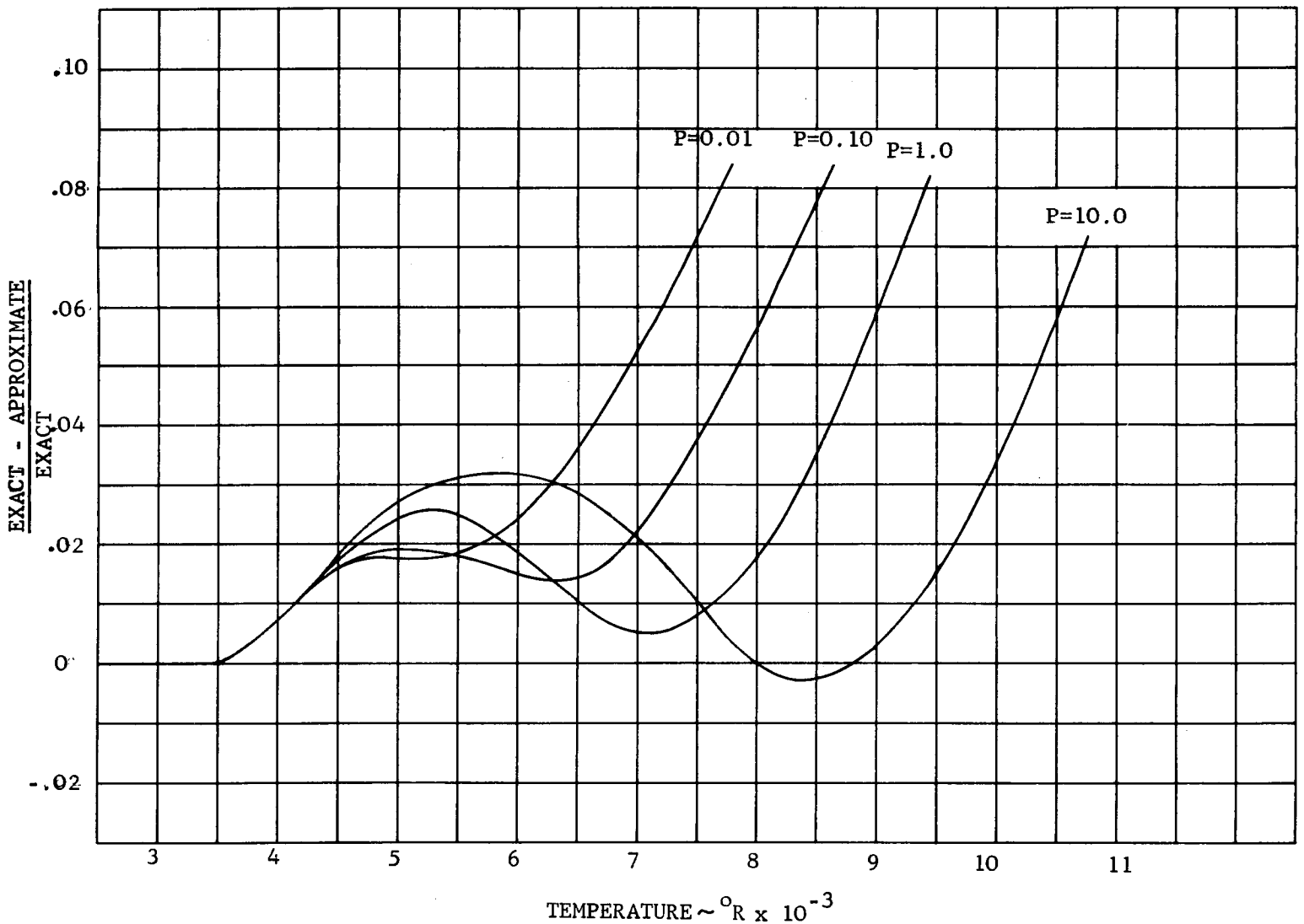

FIGURE 9

ENTHALPY Vs. TEMPERATURE FOR NORMAL AIR

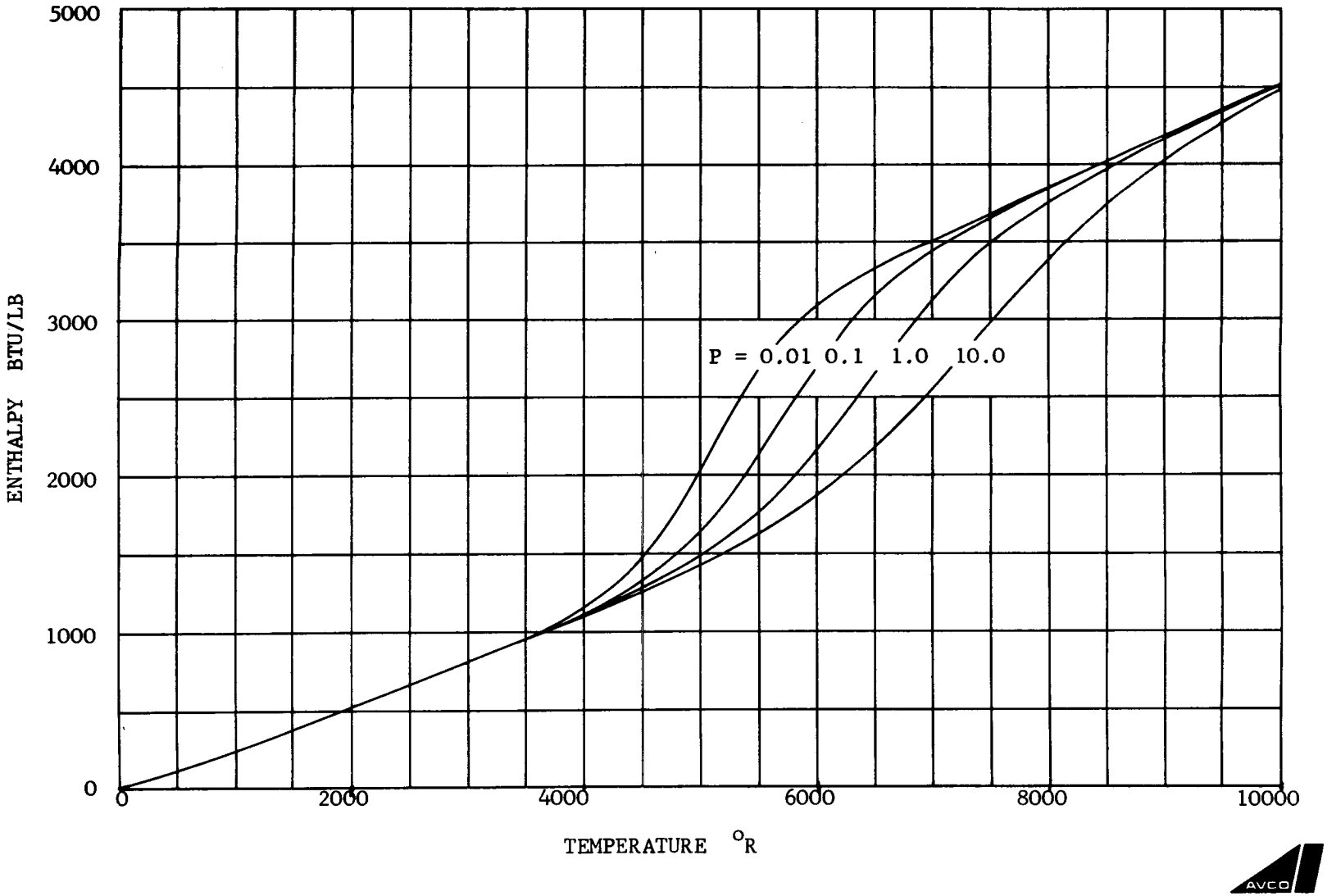

react, the mass removal rate of carbon is not only given by equation (78) but is limited by the rate at which oxygen diffusion can occur. The rate at which this diffusion process can take place leads to equation (79) for the mass removal rate of carbon from the surface for the case where the Lewis number is unity.

$$\dot{m}_{\ell} = \mu_2 (w_e - w_s) \bar{h} \quad . \tag{79}$$

In equation (79) W_e is the weight fraction of oxygen in the free stream, μ_2 is a molecular weight ratio which describes the ratio in which oxygen and carbon enter the surface reaction, and $\bar{h}$ is the heat transfer coefficient. Writing $\bar{h}$ in terms of the heat transfer coefficient without mass transfer and the reduction due to mass injection yields equation (80) for the mass removal rate of carbon at the surface.

$$\rho_s \dot{s} = \mu_2 (w_e - w_s) \left(\frac{q_c}{H_o}\right) \exp\left\{-f(1-\alpha f)\right\} \tag{80}$$

where:

$$f = \rho_s \dot{s} \eta_s \left(\frac{H_s}{q_c}\right)$$

2.9.3 Transition from Rate to Diffusion Limited Regimes

Since equations (78) and (80) must be simultaneously satisfied throughout the regime in which the controlling ablation process is the heterogeneous surface oxidation they may be combined to eliminate the quantity W_s and yield a single relationship for $\dot{m}$ which is valid over the entire regime. Equation (81) is easily found to be the result of eliminating W_s between (78) and (80).

$$\dot{m} = \dot{m}_D \left\{1 - \left(\frac{\dot{m}}{\dot{m}_r}\right)^{1/N_r}\right\} \tag{81}$$

where:

$$\dot{m}_D = \mu_2 w_e \left(\frac{q_c}{H_o}\right) \exp\left\{-f(1+\alpha f)\right\} \tag{82}$$

$$\dot{m}_R = A_r \left\{\mu_1 w_e \rho_e\right\}^{N_r} \exp\left\{-\frac{B_r}{T_s}\right\} \tag{83}$$

In the analysis of Scala (References 14, 15) the limiting forms corresponding to Equations (82) and (83) are employed and what is

referred to as the "concept of resistances in series" is invoked to yield a relationship for the "transition zone" between the two limiting cases. The present analysis requires no such treatment of the "transition zone" since the process is considered to be a continuous one over the entire region and, unlike the analysis of Scala, is not restricted to "half-order kinetics" but is equally valid for all values of the order N_r.

2.9.4 Sublimation Regime

In order to consider the full range of conditions under which carbon ablates it is necessary to examine the regime in which direct vaporization of the carbonaceous char takes place and any chemical interaction with the free stream gas takes place in a homogeneous fashion. In this homogeneous reaction regime the only effects of the chemical interactions between carbon vapor and oxygen are to modify the heat transfer to the surface. These effects will be discussed later and for the present it is sufficient to consider the vaporization process itself as if the gas near the surface were chemically inert. The net rate of vaporization is the difference between the rate of vaporization and the rate of condensation. If it is assumed that the maximum vaporization rate or "vaporization potential" is independent of the conditions on the gas side of the interface and depends only on conditions in the solid at the surface the maximum rate may be found from a combination of thermodynamic and kinetic theory considerations (See Reference 16). The resulting expression for this vaporization rate is Equation (84).

$$\dot{m}_v = \gamma \left\{ \frac{\mu_v}{2\pi R T_s} \right\}^{1/2} P_v \tag{84}$$

In Equation (84) μ_v is the molecular weight of the vaporizing species, P_v is its equilibrium vapor pressure, γ is an accomodation coefficient for condensation and R is the universal gas constant. Based on kinetic theory a similar expression for the condensation rate may be obtained.

$$\dot{m}_c = \gamma \left\{ \frac{\mu_v}{2\pi R T_g} \right\}^{1/2} P_a \tag{85}$$

In Equation (85) T_g is the temperature on the gas side of the vaporizing interface and P_a is the existing partial pressure associated with the condensing species. In principle equations (84) and (85) should be written as summations over the individual species which either vaporize or condense, however, in the present treatment we will consider a "mean molecule" for which these equations hold. Under the assumption that T_g can be approximated by T_s over a distance of a few mean free paths near the surface equation (86) then represents the net vaporization rate.

$$\dot{m}_s = \gamma \left\{ \frac{\bar{\mu}}{2\pi R T_s} \right\}^{1/2} P_v \left\{ 1 - \left(\frac{P_a}{P_v} \right) \right\} \tag{86}$$

It should be noted that the equilibrium vapor pressure, P_v, is a function of surface temperature only and that the only quantity in Equation (85) which depends on the environmental conditions is the partial pressure P_a. This partial pressure is related to the local static pressure, P_e, through a concentration function N_c which is the mole fraction of carbon vapor in the gas phase at the vaporizing surface. It can be shown that Equation (87) is a reasonable approximation to the weight fraction of injected gas at the wall.

$$W_{es} = 1 - \phi, \tag{87}$$

where:

$$\phi = \exp \left\{ - f (1 + \alpha f) \right\} .$$

For the conditions under which the vaporization analysis is to be applied, the gas at the wall may be considered to consist of carbon vapor of molecular weight $\bar{\mu}$ and molecular nitrogen and carbon monoxide of molecular weight μ_o. (If CN is a boundary layer constituent the molecular weight μ_o is still a good approximation since CN, CO and N_2 all have nearly the same molecular weights.) Using these molecular weights and Equation (87) for the weight fraction yields Equation (88) for the mole fraction of carbon at the surface.

$$N_c = \frac{1 - \phi}{1 + \left\{ \left(\frac{\bar{\mu}}{\mu_o} \right) - 1 \right\} \phi} \tag{88}$$

The partial pressure, P_a, for use in Equation (86) is then given by Equation (89).

$$P_a = \frac{(1 - \phi) P_e}{1 + \left\{ \left(\frac{\bar{\mu}}{\mu_o} \right) - 1 \right\} \phi} \tag{89}$$

Equations (86) and (89) form the basis for evaluating the surface mass transfer rate in the regime of homogeneous chemical interactions between the free stream gas and the ablating carbonaceous char.

2.9.5 Combustion Energy Effects

An expression of the energy balance at the surface is required in order to complete a description of the ablation process. This energy balance includes terms accounting for the basic aerodynamic heating, contributions due to any combustion processes which may occur, surface radiation losses, energy conducted into the material, and the energy required to remove the solid

material. The energy balance at the surface can then be written in the form of Equation (90).

$$\frac{\rho_c}{H_s}\left\{H_r - H_w\right\}\phi + Q_1 - \epsilon\sigma T_w^4 = -\left(k\frac{\partial T}{\partial x}\right)_{x=s} \tag{90}$$

In Equation (90) the first term is the aerodynamic heating corrected for wall enthalpy and mass transfer effects, Q_1 is the energy of mass removal (including combustion effects), the third term is the surface re-radiation and the right-hand side is the energy conducted into the solid material. Consider the quantity Q_1 which contains the terms associated with the surface ablation. In the regime of heterogeneous chemical reactions the overall energy associated with the ablation process is that associated with the surface reaction. In this regime the total energy involved could be given as a single term involving the product of the ablation rate, $\dot{m}$, and the heat of combustion per unit mass of solid carbon. For reasons which will become apparent in the subsequent discussion it is more convenient to separate this energy term into two parts whose sum is exactly equivalent to that stated above. For the purposes of evaluating Q_1 consider the energy to be separable into that required to vaporize the surface plus the energy associated with the carbon vapor - air reaction. This process is identical with that for the reaction of oxygen and solid carbon to produce gaseous products. As has been pointed out in the development of equation (81) the rate at which carbon can react at the surface is exactly equal to the rate at which oxygen can diffuse to the surface. This rate is given by Equation (91) which is identical to Equation (80) with the exception of the molecular weight ratio μ_2.

$$\dot{m}_o = (W_e - W_s)\left(\frac{\rho_c}{H_s}\right)\phi \tag{91}$$

The concentration potential in Equation (91) can be written in the same manner as was employed in developing Equation (81) which yields equation (92) for the rate at which oxygen reacts at the surface.

$$\dot{m}_o = W_e\left(\frac{\rho_c}{H_s}\right)\phi\left\{1 - \left(\frac{\dot{m}}{\dot{m}_R}\right)^{1/Nr}\right\} \tag{92}$$

Designating the heat of reaction of oxygen and gaseous carbon as H_c for unit mass of oxygen and the heat of vaporization per unit mass of carbon as H_v yields equation (93) as the appropriate expression for Q_1.

$$Q_1 = W_e H_c\left(\frac{\rho_c}{H_s}\right)\phi\left\{1 - \left(\frac{\dot{m}}{\dot{m}_R}\right)^{1/Nr}\right\} - \dot{m} H_v \tag{93}$$

The negative sign in equation (93) is dictated by the convention that the endothermic process of vaporization is assigned a positive energy, H_v. Thus, according to our convention H_v will always be a positive quantity. Equations (90) and (93) can then be combined to yield the energy balance appropriate to the heterogeneous reaction regime. The resulting expression is Equation (94).

$$\frac{q_c}{H_s}\left\{H_r + H' - H_w\right\}\phi - \epsilon\sigma T_w^4 = -\left(k\frac{\partial T}{\partial x}\right)_{x=s} + \dot{m}H_v \qquad (94)$$

where:

$$H' = W_e H_c\left\{1 - \left(\frac{\dot{m}}{\dot{m}_R}\right)^{1/N_r}\right\} \qquad (95)$$

Equations (81), (82), (83), (94) and (95) then represent a complete set of equations which may be applied as a boundary condition to the Fourier equation to describe the transient ablation of carbon throughout the heterogeneous reaction regime.

In the regime in which only homogeneous chemical interactions take place the energy quantity Q_1 in Equation (90) can no longer be considered as a single term representing the energy of reaction of gaseous oxygen with solid carbon since two distinct processes take place at different locations in the system. The first of these is the direct vaporization of the carbon surface followed by a diffusion of the carbon vapor out into the boundary layer where it interacts with the oxygen diffusing towards the surface. This chemical interaction occurs at some distance from the surface and has the effect of modifying the convective heat transfer to the surface. Lees (Reference 17) has shown that for Lewis numbers of unity the location of the zone of chemical interaction with respect to the surface is immaterial and that the effect on heat transfer is to increase the enthalpy potential by an amount equal to the enthalpy change for the chemical reaction. This enthalpy change per unit mass of free stream gas is simply the heat of reaction per unit mass of oxygen time the weight fraction of oxygen in the free stream. In this regime the energies associated with the ablation process can then be written in the form of Equation (96).

$$Q_1' = \frac{q_c}{H_s}\left\{W_e H_c\right\}\phi - \dot{m}H_v \qquad (96)$$

Consider the conditions under which direct vaporization takes place in a typical problem. It is easily seen that in the region associated with the homogeneous reaction process the ratio $(\dot{m}/\dot{m}_R) \ll 1$ and under these conditions Q_1 as defined by Equation (93) approaches Q_1' as defined by Equation (96). Equations (94) and (95) then represent the proper energy balance at the surface over the full range of conditions under which carbon ablation occurs.

2.10 Interface Boundary Conditions

Boundary at X = ℓ_1

The first condition is a statement of the energy balance at the interface. Since the secondary materials are assumed to transport energy by conduction only, all energy entering the boundary leaves as a conduction flux.

at x = ℓ_1:

$$k_{s1} \frac{\partial T_{s1}}{\partial x} = k_s \frac{\partial T}{\partial x} - (1-R_0) F_0 \left\{ \frac{(1-R_\ell) \exp\left[-a(\ell_1 - s)\right]}{1 - R_0 R_\ell \exp\left[-2a(\ell_1 - s)\right]} \right\} \quad (97)$$

The second boundary condition at X = ℓ_1, is required by the continuity equation (49). The assumption of nonporous secondary materials then requires that Equation (98) be satisfied.

$$w(\ell_1) = 0 \quad (98)$$

Boundary at X = ℓ_2:

The boundary condition at the X = ℓ_2 interface is obtained simply by equating the conduction flux entering to that leaving the boundary.

$$\left(k_{s1} \frac{\partial T_{s1}}{\partial x}\right)_{x=\ell_2} = \left(k_{s2} \frac{\partial T_{s2}}{\partial x}\right)_{x=\ell_2} \quad (99)$$

Boundary at X = L:

A number of boundary conditions may be written at this rear face. These include a constant temperature, radiative cooling, convective cooling, or a condition of insulation. For the present purposes the surface is assumed to be insulated and the applicable condition is given by Equation (100).

$$\left(k_{s2} \frac{\partial T_{s2}}{\partial x}\right)_{x=L} = 0 \quad (100)$$

2.11 Coordinate Transformation

Since the heated surface generally recedes in a fixed coordinate system, the numerical solution of equations (47) to (52) are conceptually complicated by the displacement of the surface through temperature and density nodes in the fixed x coordinate system. This means that the space subdivisions near

the surface undergo rapid changes in size as the ablation front approaches and furthermore that once the front goes by the nodes must be discarded from the calculation. These large changes in space increments produce large change in the coefficients of the finite difference equations, making accurate solutions more difficult to obtain. To minimize these rapid changes and to efficiently utilize the number of nodes present transformation from a fixed, x, to a moving, y, coordinate system is introduced for the region $S \leq x \leq \ell_1$. Defining

$$y = \frac{x - s}{\ell_1 - s}$$

then:

$$\left(\frac{\partial T}{\partial t}\right)_x = \left(\frac{\partial T}{\partial t}\right)_y + \left(\frac{\partial T}{\partial y}\right)_t \left(\frac{\partial y}{\partial s}\right)_x \left(\frac{\partial s}{\partial t}\right)_x$$

$$= \frac{\partial T}{\partial t} + \frac{\partial T}{\partial y}\left(\frac{y-1}{\ell_1 - s}\right)\dot{s}$$

$$\left(\frac{\partial T}{\partial x}\right)_t = \left(\frac{\partial T}{\partial y}\right)_t \left(\frac{\partial y}{\partial x}\right)_t = \left(\frac{1}{\ell_1 - s}\right)\frac{\partial T}{\partial y}$$

$$\left(\frac{\partial \omega}{\partial x}\right)_t = \left(\frac{\partial \omega}{\partial y}\right)_t \left(\frac{\partial y}{\partial x}\right)_t = \left(\frac{1}{\ell_1 - s}\right)\frac{\partial T}{\partial y} \qquad \text{(100a)}$$

It is readily seen that an additional term will enter the energy equation through the operator

$$\left(\frac{\partial}{\partial t}\right)_x = \left(\frac{\partial}{\partial t}\right)_y + \dot{s}\left(\frac{y-1}{\ell_1 - s}\right)\left(\frac{\partial}{\partial y}\right)_t$$

This new term accounts for the convection of energy due to the motion of the medium toward the fixed boundary. Applying the above operations to the region $S \leq x \leq \ell_1$ gives the following new form to equations (47) to (52):

$$\rho_s C_{p_s}\frac{\partial T}{\partial t} + \rho_s C_{p_s}\left(\frac{y-1}{\ell_1 - s}\right)\frac{\partial T}{\partial y} = \left(\frac{1}{\ell_1 - s}\right)\frac{\partial}{\partial y}\left(\frac{k}{\ell_1 - s}\frac{\partial T}{\partial y}\right) \qquad \text{(100b)}$$

$$+\left(\frac{C_{p_g}\omega}{\ell_1 - s}\right)\frac{\partial T}{\partial y} + \dot{\rho}_s\left(\Delta H_c + C_{p_g}T - C_{p_a}T\right)$$

$$- a_o F_o (1 - R_o)\left\{\frac{\exp[-a y(\ell_1 - s)] + R_\ell \exp[-a(2\ell_1 - y(\ell_1 - s))]}{1 - R_o R_\ell \exp[-2a(\ell_1 - s)]}\right\}$$

$$C_{p_s} = C_{p_a}\left(\frac{\rho_s - \rho_c}{\rho_s}\right) + C_{p_c}\left(\frac{\rho_c}{\rho_s}\right) \qquad \text{(100c)}$$

$$k_s = k_o - \left(\frac{k_o - k_c}{\rho_o - \rho_c}\right)(\rho_o - \rho_s) \tag{100d}$$

$$\left(\frac{1}{l_1 - s}\right)\frac{\partial \omega}{\partial y} = \dot{\rho}_s \quad \text{or:} \quad \omega = (l_1 - s)\int_y^1 \dot{\rho}_s \, dy \tag{100e}$$

$$\dot{\rho}_s = -\sum_{i=1}^{3} A_i \rho_{oi} \left(\frac{\rho_s - \rho_{o,i+1}}{\rho_{oi}}\right)^{n_i} \exp\left\{-\frac{B_i}{T}\right\} \tag{100f}$$

$$P = \left\{\rho_s^2 + 2R(l_1 - s)\int_0^y \alpha \mu T w \, dy + 2R(l_1 - s)\int_0^y \beta T w^2 \, dy\right\}^{1/2} \tag{100g}$$

$$\alpha = \alpha_c + \left(\frac{\alpha_v - \alpha_c}{\rho_o - \rho_c}\right)(\rho_s - \rho_c) \tag{100h}$$

$$\beta = \beta_c + \left(\frac{\beta_v - \beta_c}{\rho_o - \rho_c}\right)(\rho_s - \rho_c) \tag{100i}$$

In the above equations it is understood that:

$$T = T(y,t)$$

$$\rho = \rho(y,t)$$

$$w = w(y,t)$$

The boundary conditions (55) and (95) are also transformed to the following:

at y = 0

$$q = -\left(\frac{k_{s1}}{\ell_1 - s}\right)\frac{\partial T}{\partial y} + \dot{s}\left\{\rho_c H_v + (\rho_s - \rho_c)\Delta H_c\right\} - \epsilon\sigma T^4 \qquad (100j)$$

at y = 1

$$\left(\frac{k_{s1}}{\ell_1 - s}\right)\left(\frac{\partial T_{s1}}{\partial y}\right)_{y=1} = \left(k_{s2}\,\frac{\partial T_{s2}}{\partial x}\right)_{x=\ell_1} - (1-\rho_c)\,F_0\left\{\frac{(1-R_\ell)\exp\left[-a(\ell_1 - s)\right]}{1 - R_0 R_\ell \exp\left[-2a(\ell_1 - s)\right]}\right\} \qquad (100k)$$

The preceding equations together with the initial and boundary conditions represented by equations (54) through (100) constitute the mathematical model employed for the transient behavior of charring ablators. The digital computer program described in Volume II is based on this analysis and solves the problem presented in this analysis.

3.0 Interpretation of Test Data

The successful design of an ablative thermal protection system requires first that the system provide adequate protection for the mission payload and second that this be accomplished by means of a system of minimum weight consistant with the reliability requirements and with good design practice. The problem of the choice of appropriate design safety factors is more philosophical than technical and will not be considered here. On the other hand it is usually critical that the heat shield designer be quite aware of the degree of controlled conservatism that is being introduced into the design of the system. If he is not in control of this conservatism the designer is open to deserved criticism either upon failure of the payload to survive or for having penalized the overall system through overdesign of the heat shield. Generally speaking flight test programs provide little useful information to the designer since, barring initial flight test disaster, the information is received too late to influence anything other than the design of subsequent systems which may employ the same material.

The preceding considerations lead directly to the requirement for a physically valid analytical model together with a characterization of the basic ablative material within the framework of the model. By characterization is meant the process by which values are established for the material dependent parameters which appear in the model. The general lack of usable flight test information requires that this characterization process be accomplished by means of test data obtained in laboratory facilities under conditions which are far removed from the flight environment. The analytical model thus in a very real sense represents the scaling law which must be employed to predict the flight performance of a system in terms of the performance of the system in ground test facilities.

In practice a number of types of experimental data must be examined in the process of compiling an appropriate set of material dependent characteristics for use in any given analytical model of the ablation and heat transfer processes. The data which have been examined in the case of the Apollo material are discussed in some detail in the following sections.

3.1 Ablation Test Data

3.1.1 General Considerations

Ablation data are obtained from experiments in which both energy and mass transfer effects play a significant role. These tests are run in facilities where the ablation process is induced by means of a controlled energy source and in which the several material performance parameters can be carefully measured. In order that these data be useful for the purpose of obtaining quantitative information for use in the mathematical model it is required that the experiments be run in such a way that near steady state ablation is achieved over a significant portion of the total test time. Unless the time variable can be removed from the data analysis process it becomes impractical

if not impossible to interpret a series of tests in a way which yields quantitative values for the several material dependent parameters which appear in any realistic model of the ablation process. In the case of test data obtained in experiments where such quantities as surface recession rate are deduced on the basis of pre-test and post-test dimensions together with the total test time the condition that steady state be achieved over a significant portion of the test time is of particular importance. Generally the question of whether this condition has been met by a given set of test data cannot be completely answered on the basis of the test data alone. Generally speaking tests run at less severe conditions require longer running times to satisfy this requirement than do those which have been run under more severe environmental conditions. This implies that there is some lower limit on the total surface recession during a test below which the data become meaningless for the purpose of quantitative interpretation. This, however, is only a portion of the story. In order for an experiment to be interpreted as a steady state experiment in the case of a charring ablator the post-test char thickness must be small compared to the sum of the post-test char thickness and the total surface recession. This condition arises as a result of the fact that tests are initiated on samples of the virgin material in which no charring has taken place and one of the conditions for steady state ablation requires that the rate of char propagation into the virgin material be identical with the surface recession rate.

A quantitative statement of the condition stated above is given by equation (101).

$$(\Delta S/\Delta t) = \Delta(S + \delta_c)/\Delta t \tag{101}$$

In equation (101) S is the coordinate of the surface, t is the time, δ_c is the char depth measured from the heated surface and the operation indicated by Δ is the usual one of differences between initial and final states. It is clear from equation (101) that in tests which are initiated on virgin material samples this condition can never be rigorously satisfied.

Steady state is defined as a process in which the energy and mass transfer processes which take place remain invariant in a coordinate system fixed on the heated surface. This requires that the rate of surface motion is constant in a laboratory coordinate system. It also requires that the char thickness remain constant and that the temperature distribution remain fixed with respect to the moving boundary. A consequence of these requirements is that the location of any isotherm must be a linear function of time in a laboratory coordinate system. A further consequence of the definition of the steady state is that the weight loss experienced by a sample as a result of a steady state ablation experiment is given exactly by the product of the virgin material density, the sample cross sectional area and the sample length loss. This may be expressed as the following:

$$\Delta W = \rho_o A \Delta L \tag{102}$$

The initial sample weight, W_1, can be expressed in terms of the initial length, L_1, by means of a simple relationship.

$$W_1 = \rho_o A L_1 \tag{103}$$

Combining these equations results in a relationship between the length loss, the weight loss, the initial weight and the initial length which must hold for any experiment carried out under steady state conditions.

$$L_1 \Delta W = W_1 \Delta L \tag{104}$$

This relationship can be used as the basis of a test to be applied to ablation test data as a criterion of steady state ablative performance. The measure which is adopted is the ratio of the fractional weight loss to the fractional length loss. For experiments in which both weight loss and length loss are directly measured quantities this parameter, F, is simply defined by equation (105).

$$F = \frac{L_1 \Delta W}{W_1 \Delta L} \tag{105}$$

In equation (105) L is the sample length, W is the sample weight, the subscript 1 refers to the pre-test values and Δ is the same operation indicated in connection with equation (101).

In application to experimental data the quantity F as defined by equation (105) is the ratio of the experimental weight loss to the weight loss which would have been experienced by a sample in a steady state experiment where the length loss was ΔL. In those experiments in which the post test char thickness, δ_c, is measured an alternate definition of F can be formulated. The calculated experimental weight loss based on the length loss and char thickness is given by equation (106).

$$\Delta W_m = \rho_o A \Delta L + (\rho_o - \rho_c) A \delta_c \tag{106}$$

The calculated weight loss based on ΔL for a steady state experiment is given by equation (102). The ratio of these two weight losses leads directly to the alternate definition of F given by equation (107).

$$F = \frac{\Delta L + (1 - \rho_c/\rho_o)\delta_c}{\Delta L} \tag{107}$$

Although the quantity F as defined by equation (105) is in principle the same as that defined by equation (107) the two definitions are effected quite differently by experimental errors. In the case where the weight loss is directly measured the errors in length and weight measurement allow F to scatter to values less than unity depending on the accuracy and consistency of the measurements. Such items as non-uniform recession of the heated surface also can contribute to a large scatter in this case. On the other hand in those cases where the weight loss is deduced on the basis of the length loss and the post-test char thickness values of F less than unity are clearly impossible since δ_c is a finite, positive quantity. The general trends in the test data would be expected to be similar however, even though the experimental scatter will have a different appearance for the two definitions of F.

It is of interest to exhibit the parameter F as a function of some other test parameter which might be expected to indicate an approach to steady state ablation. As stated earlier it is expected that tests run under more severe environments will more nearly approach the required steady state condition. Generally speaking there is no single experimental environmental parameter which is an adequate measure of its severity. A material response parameter is available, however, in the average surface recession rate, ($\Delta L/\Delta t$). The larger values of this rate are expected to be associated with the more nearly steady state experiments.

Figure (10) shows values of the parameter F plotted as a function of the average surface recession rate for a large number of experiments in which the only available data are pre-test and post-test sample measurements. The data are those obtained by NASA/MSC in the Plasmadyne facility, the NASA/MSC data from the radiative test facility at Southwest Research Institute and a sampling of data points from the AVCO/OVERS test facility. As is evident from the figure the data from all of these facilities departs significantly from the requirement that F be very close to unity in order for the data to be quantitatively useful. The trend expected with increasing average recession rate is clearly evident in the test data and no clear cut differences between radiative and convective tests are evident.

Figure (11) is an expanded view of the radiative data from the Southwest Research Institute in which the nature of the environmental gas present in the chamber during the test is indicated. Again no significant differences are apparent in the behavior of the parameter F.

The AVCO/Model 500 test data are free from several of the problems associated with the data shown in Figures (10) and (11). In general the average surface recession rate is in the range of 2×10^{-2} to 10×10^{-2} inches per second which places the data far to the right of the data shown in Figures (10) and (11). More importantly, however, is the fact that surface recession rates are obtained from high speed silhouette movies taken during the test. The rate is then obtained during the latter part of the run when the initial transients have dissipated and the surface position is a linear function of time.

FIGURE 10

TRANSIENT BEHAVIOR IN TEST DATA

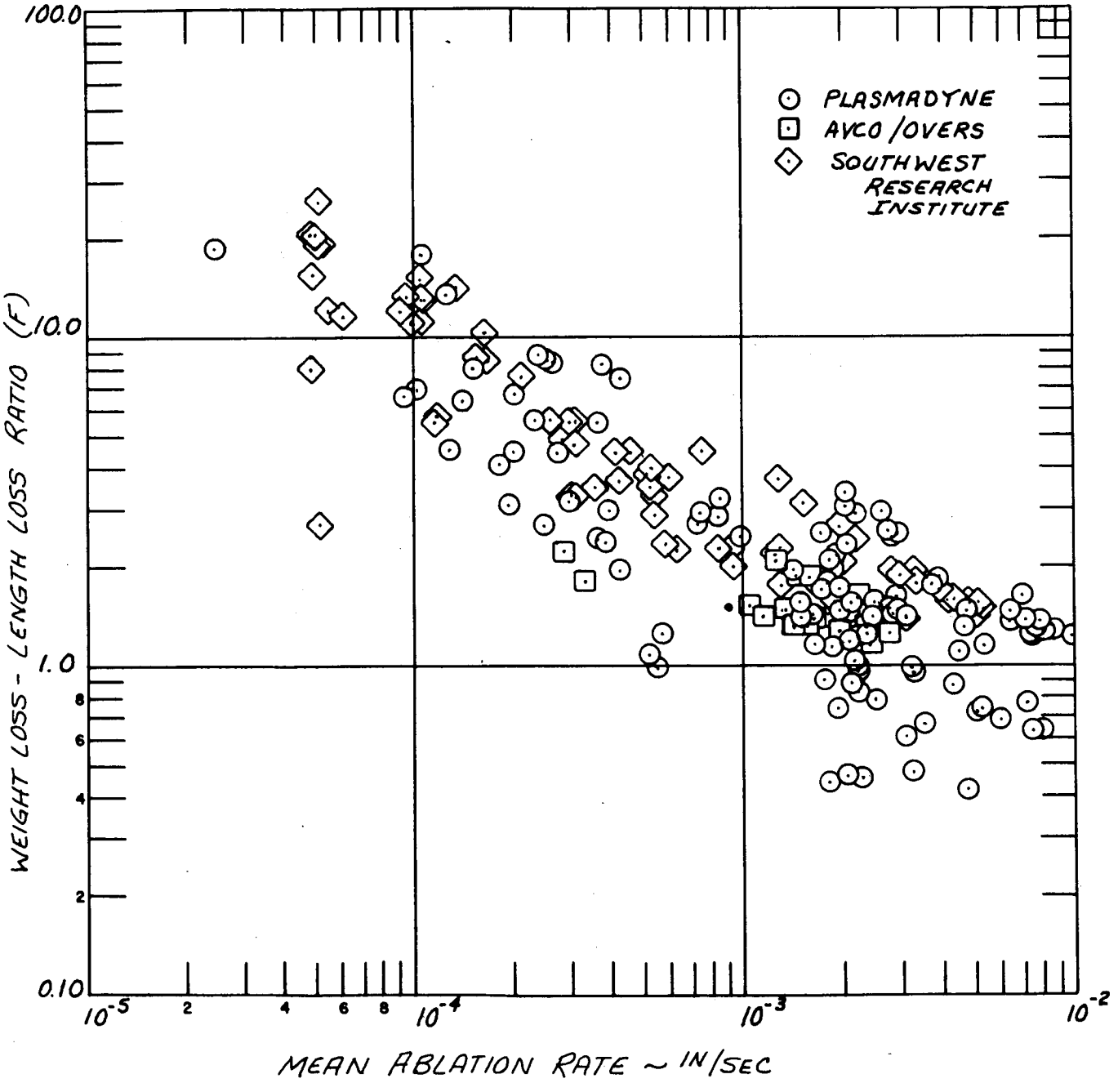

NOTE: USE TYPE B PENCIL FOR VUGRAPHS AND REPORT DATA.

FIGURE 11
RADIATIVE TEST DATA (SWRI)

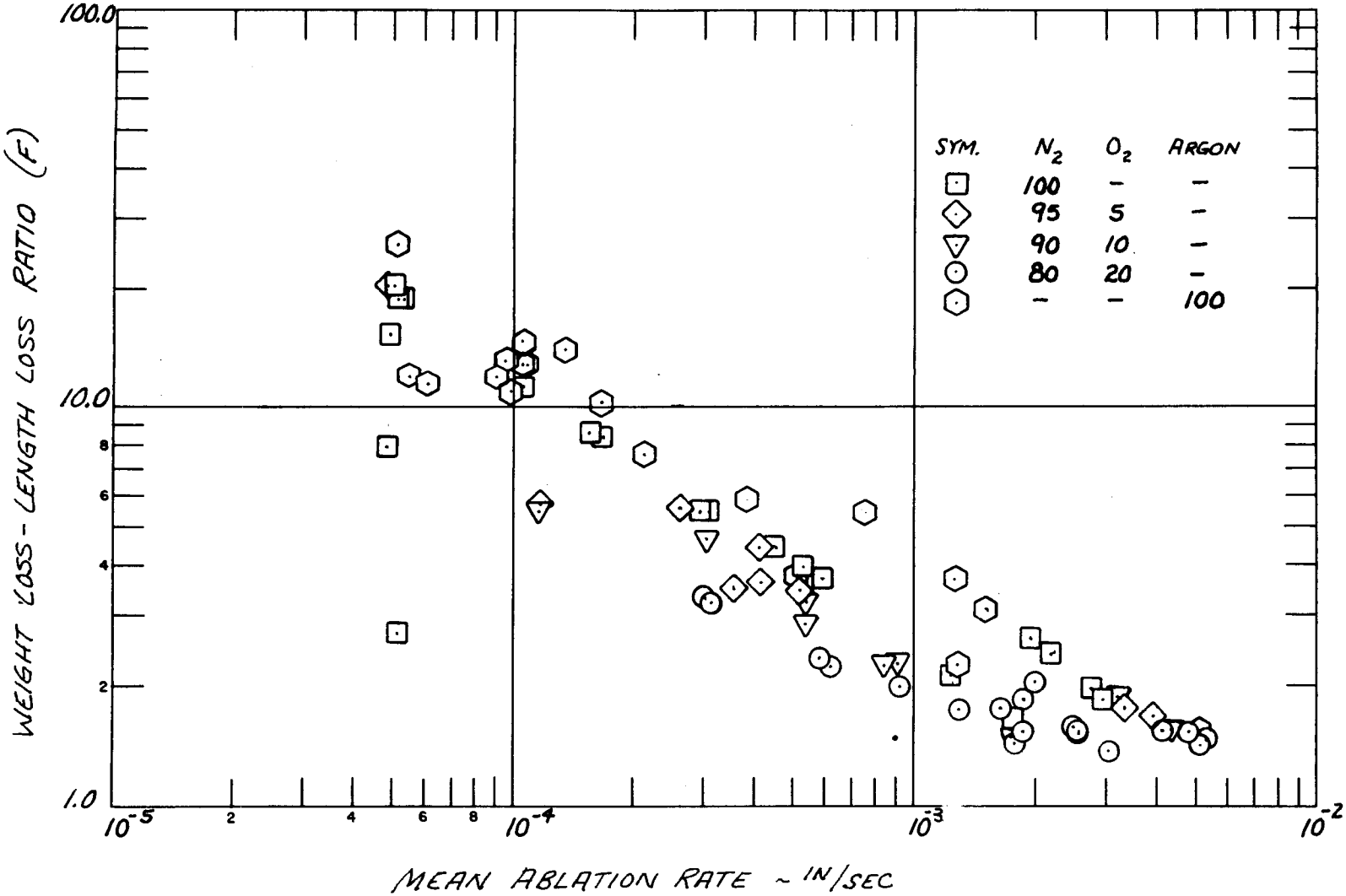

NOTE: USE TYPE B PENCIL FOR VUGRAPHS AND REPORT DATA.

In employing the parameter F as defined by equations (105) or (107) it is useful to make an estimate of the maximum value of F which will allow a usable interpretation of the data within the framework of a steady state analysis. Although such an estimate is of necessity subjective it is believed that for the material under consideration here the maximum value of F should not exceed 1.2 for useful quantitative data interpretation.

3.1.2 Stagnation Point Ablation Data

The technique for examining steady state ablation test data is quite general and applies to any data that satisfies the requirement that the data be reducible within the framework of a steady state analysis. The analysis is then applied to the Avco/Model 500 data as being the only available data which satisfy the data reduction requirement. In the bulk of stagnation point ablation tests the observational quantities which are reported are a calorimetrically determined heat flux, q_{cal}, a stagnation pressure, P, and a stagnation enthalpy, H_s, describing the environmental conditions of the test. The material related quantities which are normally reported are a surface recession rate, $\dot{S}$, and either a surface temperature or the total surface radiation loss, q_r. In some cases total length loss and test duration are reported in place of surface recession rate and in some cases an external radiant energy flux, F_s, is imposed. Although the environmental parameters of heat flux, enthalpy and pressure are not strictly independent they will be treated as such in the present analysis since they are, generally speaking, determined independently.

The steady state ablative behavior of a char forming material can be described by an energy balance in the form of equation (108).

$$\frac{q_c}{H_s}\ (H_s + W_e Q_2 - H_w)\ \phi + (1 - R_o)\ F_s - q_r - \dot{m}\ \bar{C}_p\ (T_s - T_{ref}) = \dot{m}\ Q_1 \qquad (108)$$

In equation (108) q_c is a "cold wall" heat flux, ϕ is the ratio of heat transfer with mass addition to that without, $\bar{C}_p$ is an average specific heat of the char and gaseous products at the surface temperature T_s, and T_{ref} is a reference surface temperature or "standard ablation temperature" to which the energy terms Q_1 and Q_2 are being corrected. In particular, since no material ablates at a fixed temperature, the term in C_p removes this variation from Q_1 thus making Q_1 a "true constant". The quantity Q_1 contains the latent heats of charring and vaporization of the material together with the sensible or $C_p\ \Delta\ T$ heats for the system. Q_1 will be a constant if the heat of vaporization is independent of temperature over the range of surface temperatures in the test series and if the "reaction zone" temperature for the char forming reaction is nearly constant in the series. Equation (108) can be re-written in the form of equation (109) which is a linear form suitable for statistical treatment.

$$Y = Q_1 - Q_2\ X \qquad (109)$$

where:

$$Y = \frac{q_c}{\dot{m} H_s} (H_s - H_w) \phi + \frac{(1 - R_o) F_s - q_r}{\dot{m}} - \bar{C}_p (T_s - T_{ref})$$

$$X = \frac{W_e q_c}{\dot{m} H_s} \phi$$

The quantity ϕ , which is the effect of mass addition on heat transfer, has been written in numerous ways in the literature. The form most frequently employed at Avco is given by equation (110) and is a result of a survey of existing analytical and experimental work on this subject.

$$\phi = \text{EXP} \left\{ - f (1 + \alpha f) \right\} \tag{110}$$

where:

$$f = \frac{\eta \dot{m} H_s}{q_c}$$

The parameter η is to be determined from the test data and depends on the material, on the free stream gas and on the flow conditions, i.e., axisymmetric stagnation point, laminar flat plate, etc. The quantity α in equation (110) has been found to be independent of flow conditions and material and to have a "best value" near 0.618. (See Sections 2.5 and 2.6).

To be precise, the combination ($\eta \dot{m}$) appearing in the definition of f should be separated into a portion due to the surface removal and a portion due to the gaseous products of the charring reaction. It is impossible, however, to separate these two components on the basis of steady state ablation experiments hence the use of a lumped term with the necessary separation to be accomplished by other means.

For each experimental point, values are obtained for the quantities Y and X as defined by equations (109) and (110). The procedure for finding best values of Q_1, Q_2 and η is based on finding least squares values of Q_1 and Q_2 for a sequence of values of η then finding the best values of the three constants such that equation (111) is satisfied.

$$\frac{\partial}{\partial \eta} \sum_{i=1}^{N} (Y_i - \bar{Y}_i)^2 = 0 \tag{111}$$

In equation (111) the summation is over all experimental points, X_i is the "observed" value of Y_i and $\bar{Y}_i$ is the value computed on the basis of the least squares values of Q_1 and Q_2. This procedure will be discussed in more

detail in a later section.

Since not all of the quantities appearing in equation (108) are directly observed in the experiments their values must be obtained in terms of the observed quantities. Some of the quantities require a knowledge of other derived quantities for their evaluation and thus require a series of successive approximations involving the entire set. A description of the iterative technique employed will be given in a later section.

A. Surface Temperature, T_s

The surface temperature plays an important role in the data reduction being required for several terms in the calculation including the wall enthalpy, H_w, and the radiative flux, q_r, in some cases. Several optional situations arise when dealing with this quantity and they are discussed separately. The choice of which technique is employed depends upon what type of data are available and prior knowledge regarding the ablation system being considered.

1. In some few cases the surface temperature is either known or is measured and hence poses no problem since it then becomes an input to the calculation.

2. In many cases the observational quantity is the net radiative loss from the ablating surface. In those cases where a surface emissivity, ϵ, is also known the surface temperature is obtained from equation (112) where σ_B is the Stephen-Boltzmann constant.

$$T_s = \left\{ \frac{q_r}{\epsilon \sigma_B} \right\}^{\frac{1}{4}} \tag{112}$$

3. In some cases where q_r is a measured quantity the surface recession rate, $\dot{s}$, and the surface temperature bear a known relationship to each other either on the basis of theoretical or empirical considerations. In such cases the surface temperature is obtained by solution of equation (113) for T_s and combining this temperature with q_r to obtain a value for the emissivity.

$$\dot{S} = \beta_1 + \beta_2 T_s^{\beta_3} \text{ EXP} \left\{ - \beta_4 / T_s \right\} \tag{113}$$

$$\epsilon = q_r / \sigma_B T_s^4 \tag{114}$$

B. Wall Enthalpy, H_w

A solution for the wall enthalpy H_w is entirely straightforward once the surface temperature and stagnation pressure are known. Current practice at Avco considers an equilibrium mixture of nitrogen molecules, oxygen molecules and oxygen atoms. (See Section 2.8).

C. "Cold Wall" Heat Flux, q_c

The cold wall heat flux, q_c, is defined as the heat flux to a non-ablating wall at which the enthalpy of the free stream fluid is zero. When divided by the local static enthalpy this quantity then becomes the heat transfer coefficient in terms of the enthalpy as a driving potential. The cold wall flux as defined in this manner is not independent of the wall temperature as might be expected since the "average" values of the properties of the gas which determine the heat transfer coefficient depend to some extent on the temperature associated with the gas at the gas-wall interface.

The cold wall flux associated with the calorimeter measurement, q_c', is obtained in terms of the calorimeter flux, q_{cal}, the stagnation enthalpy, H_s, and the wall enthalpy associated with the calorimeter measurement, H_{wr}.

$$q_c' = q_{cal} \; H_s/(H_s - H_{wr}) \tag{115}$$

In order to estimate the wall enthalpy associated with the calorimeter measurement it is necessary to obtain a value for the calorimeter wall temperature T_{sr}. In many cases the calorimeters employed are of the water cooled steady state type. For these cases the value of T_{sr} can be obtained from equation (116) where ℓ is the calorimeter wall thickness, k is its thermal conductivity and T_w is the mean temperature of the cooling water.

$$T_{sr} = \left(\frac{\ell}{k}\right) q_{cal} + T_w \tag{116}$$

In the case of transient calorimeters T_{sr} must be estimated as the average surface temperature during the calorimeter run.

Having obtained T_{sr} the calorimeter wall enthalpy is obtained by the same process used to obtain H_w in the preceding section only using T_{sr} and P as the primary quantities.

In order to obtain the cold wall flux associated with the ablation experiment it is necessary to account for the effects of wall temperature on the heat transfer coefficient. This process has been discussed in another section of this report where it is shown that these effects can be correlated in terms of the wall enthalpy and recovery factor. For an axisymmetric stagnation point it is shown that this effect can be accounted for by means of equation (117).

$$q_c = q_c' \left(\frac{H_w}{H_{wr}}\right)^{-0.037} \tag{117}$$

The final combined expression for q_c in terms of the observed quantities together with H_{wr} and H_s is then equation (118).

$$q_c = q_{cal} \left(\frac{H_s}{H_s - H_{wr}} \right) \left(\frac{H_w}{H_{wr}} \right)^{-0.037} \tag{118}$$

D. Radiative Loss, q_r

1. In most cases q_r is given as an experimentally observed quantity and hence is used as an input to the data reduction process.

2. In some cases, of which certain low temperature ablators are examples, measured values of q_r are not available and this quantity must be obtained from other input information. These correspond to those in which the surface temperature is obtained by methods A.1 or A.3 above. Having obtained the surface temperature by either of these two methods this temperature is combined with a known emissivity to obtain q_r by means of equation (119).

$$q_r = \epsilon \sigma_B T_s^4 \tag{119}$$

In some cases where q_r is not measured the emissivity should in reality be written as a function of the ablation rate as a result of internal self glowing of certain materials. These cases are not considered here, however, since their frequency is small.

Having obtained all of the quantities required to evaluate Y and X in equation (109) the problem becomes one of obtaining "best values" of the parameters Q_1, Q_2 and η based on a set of experimental data. The procedure currently in use considers a best fit subject to Y errors only. A value of η is selected and values of Y_i and X_i are obtained for each of the N experimental points and values of $Q_1(\eta)$ and $Q_2(\eta)$ are obtained by least squares using equations (120) and (121).

$$Q_1(\eta) = \frac{S_1 \cdot S_4 - S_2 \cdot S_5}{S_1 \cdot S_3 - S_2^2} \tag{120}$$

$$Q_2(\eta) = \frac{S_2 \cdot S_4 - S_3 \cdot S_5}{S_1 \cdot S_3 - S_2^2} \tag{121}$$

where:

$$S_1 = \sum_i W_i \cdot X_i^2$$

$$S_2 = \sum W_i \cdot X_i$$

$$S_3 = \sum W_i$$

$$S_4 = \sum W_i \cdot X_i$$

$$S_5 = \sum W_i \cdot X_i \cdot Y_i$$

The quantities W_i are the weights assigned to each point and their evaluation will be discussed in a later section. A measure of the "goodness" of the fit is obtained by evaluating $\sigma^2(\eta)$ which has been defined as in equation (122).

$$\sigma^2(\eta) = \sum_i W_i \left\{ Y_i - Q_1(\eta) + Q_2(\eta) X_i \right\}^2 \Big/ \sum_i W_i \qquad (122)$$

Values of $\sigma^2(\eta)$ are computed for a sequence of values of η. Successive values of η are selected such that a minimum in $\sigma^2(\eta)$ is found. Five values of $\sigma^2(\eta)$ are selected such that at least two values lie on either side of the minimum as determined numerically. These five values are then fit by least squares to a cubic equation in η and the best value of η found as the solution of the quadratic obtained by setting the first derivative of this equation equal to zero. Finally, "best" values of Q_1 and Q_2 are obtained for this value of η as explained previously.

The weights associated with the experimental points are obtained on the basis of the degree to which the individual data points agrees with the least squares fit of equation (108) on the entire set. If enough information were available regarding the probable errors in each of the experimentally determined quantities a more rigorous weighting process could be used but this is not practical at the present time since in general this information is lacking. For the present analysis the weights are taken as proportional to the probability that an observed value of Y will deviate from the least squares adjusted "best" value by as much as the observed deviation. The weights employed are then given by equation (123).

$$W_i = \frac{K}{\sqrt{2\pi}} \int_{t_i}^{\infty} e^{-\frac{t^2}{2}} dt \qquad (123)$$

where:

$$t_i = (N-1) \left\{ Y_i - \bar{Y}_i \right\} \Big/ \sum_i \left\{ Y_i - \bar{Y}_i \right\} \qquad (124)$$

$$K = N / \sum_i W_i \tag{125}$$

A rational expression for the integral appearing in equation (123) is available resulting in equation (126) as the final expression for the weights.

$$W_i = K \left\{ E_1 U_i + E_2 U_i^2 + E_3 U_i^3 \right\} e^{-t_i^2/2} \tag{126}$$

where:

$$U_i = 1/(1 + E_4 t_i)$$

$$E_1 = 0.17401$$

$$E_2 = -0.047944$$

$$E_3 = 0.37393$$

$$E_4 = 0.33267$$

3.1.3 Turbulent Pipe Data Analysis

The interpretation of the data obtained from the AVCO "turbulent pipe" ablation test facility is subject to a number of uncertainties. Several of these uncertainties arise from the variation in pipe diameter during a test and from the necessity for deducing the behavior on the basis of measurements made before and after the test rather than from direct observation during the test itself.

The present analysis is based primarily on the assumption that the "hot wall" convective heat flux to the walls of the pipe varies during a test in accordance with Equation (127).

$$q_o = q_{oo} (D_o/D)^{\alpha} \tag{127}$$

where:

q_o = "hot wall" flux

q_{oo} = "hot wall" flux for diameter D_o

D = instantaneous pipe diameter

D_o = initial pipe diameter

Under the assumption that the heat of ablation, H_a, and the radiation loss, q_r, are constant the assumption that the ablation process can be represented by a series of instantaneous steady states yields Equation (128) as the differential equation governing the time variation of pipe diameter.

$$\dot{D} = B_1 \cdot D^{-\alpha} - B_2 \tag{128}$$

$$B_1 = \frac{2\, q_{oo}\, D_o^{\alpha}}{\rho\, H_a} \tag{128a}$$

$$B_2 = \frac{2\, q_r}{\rho\, H_a} \tag{128b}$$

In equation (128) ρ is the sample density. We now introduce the time, τ, as measured from the beginning of the steady state ablation process. Equation (128) can then be formally integrated to yield Equation (129) where λ has been introduced as a variable of integration.

$$D(\tau) = D_o - B_2 \tau + B_1 \int_{\lambda=0}^{\tau} \left\{ D(\lambda) \right\}^{\alpha} d\lambda \tag{129}$$

Successive approximations to the function $D(\tau)$ can be obtained using Equation (129) and the method of Picard which requires a first approximation to the function. In order to obtain this first approximation consider Equation (128). It is assumed that the radiative loss from the pipe is small compared to the convective heat transfer rate. The first approximation, $D_1(\tau)$, is then obtained by integrating Equation (128) with $B_2 = 0$. The resulting relation for D_1 is that given by Equation (130).

$$D_1(\tau) = \left[(1+\alpha)\, B_1\, \tau + D_o^{1+\alpha} \right]^{\frac{1}{1+\alpha}} \tag{130}$$

Making the appropriate substitution, the second approximation $D_2(\tau)$ is obtained by combining Equations (129) and (130).

$$D_2(\tau) = D_o - B_2(\tau) + B_1 \int_{\lambda=0}^{\tau} \left\{ (1+\alpha)\, B_1 \lambda + D_o^{1+\alpha} \right\}^{-\frac{\alpha}{1+\alpha}} d\lambda \tag{131}$$

Equation (131) can be easily integrated to yield the function $D_2(\tau)$.

$$D_2(\tau) = \left\{ (1+\alpha)\, B_1\, \tau + D_o^{1+\alpha} \right\}^{\frac{1}{1+\alpha}} - B_2\, \tau \tag{132}$$

It should be noted that Equation (132) can also be written:

$$D_2(\tau) = D_1(\tau) - B_2 \cdot \tau \tag{133}$$

It can be shown that for this situation, where D is a single valued function of τ, this method converges on the true function, $D(\tau)$, in an alternating fashion and hence the maximum error in a given approximation is less than one half the difference between successive approximations. Thus, in the present case, the maximum error in $D_2(\tau)$ is less than $(\frac{1}{2} B_2 \tau)$. As a result of these considerations, the variation of pipe diameter with time is then taken as Equation (134) where the quantity R is a factor whose value lies between 0.5 and 1.0 and whose "best" value can be found by numerical integration of Equation (128) for several typical cases.

$$D(\tau) = \left\{(1+\alpha)\, B_1 \tau + D_o^{1+\alpha}\right\}^{\frac{1}{1+\alpha}} - R\, B_2 \tau \tag{134}$$

If τ is the time interval during which the pipe changes diameter and ΔW is the total loss in weight of a pipe of length L the foregoing assumptions lead to a second expression for $D(\tau)$.

$$D(\tau) = \left\{\frac{4\,\Delta W}{\pi \rho L} + D_o^2\right\}^{1/2} \tag{135}$$

Equations (134) and (135) can then be employed to eliminate the diameter D and to obtain an expression for B_1.

$$B_1 = \frac{1}{(1+\alpha)\tau}\left\{\left(\frac{4\,\Delta W}{\pi \rho L} + D_o^2\right)^{1/2} + R B_2 \tau\right\}^{1+\alpha} - \frac{D_o}{(1+\alpha)\tau} \tag{136}$$

Equations (136) and (128) can then be employed to yield an expression for the "initial" mass transfer rate, $\dot{m}_o$.

$$2\dot{m}_o = \rho\, \dot{D}(o) = \rho B_1 D_o^{-\alpha} - B_2 \rho \tag{137}$$

or:

$$2\dot{m}_o = \frac{\rho D_o^{-\alpha}}{(1+\alpha)\tau}\left\{\left(\frac{4\,\Delta W}{\pi \rho L} + D_o^2\right)^{1/2} + R B_2 \tau\right\}^{1+\alpha} - \frac{\rho D_o^{1+\alpha}}{(1+\alpha)\tau} - \rho B_2 \tag{138}$$

Equation (138) contains the quantities τ and H_a (in B_2) which are not a part of the experimental data and as a result these quantities must be estimated by other means. The time, τ, must be distinguished from the total test time t since it is assumed that some period of time is required before ablation begins. This time is known as an "induction time" and can be

estimated by means of the following considerations.

For the present purposes, assume that the temperature distribution at the "initial time", t_o, is given by the usual steady state approximation.

$$(T - T_o) = (T_s - T_o) \exp\left\{ \frac{C_p \dot{m}_o y}{K} \right\} \tag{139}$$

In equation (139) C_p is the specific heat, K is the thermal conductivity, T_s is the surface temperature, T_o is the initial temperature and y is the coordinate measured from the surface. The amount of thermal energy stored in the material is then given by Equation (140).

$$Q_s = \rho C_p \int_{y=o}^{\infty} (T - T_o)\, dy = \frac{\rho K (T_s - T_o)}{\dot{m}_o} \tag{140}$$

It is further assumed that the average convective flux during the "induction" period is q_{oo}. This assumption somewhat overestimates the induction time but is consistent with there being internal decomposition processes which make Equation (140) a low estimate of the stored energy. The resulting expression for the time in terms of the induction time, t_o, and the total test time, t is given by Equation (141).

$$\tau = t - t_o = t - \frac{\rho K (T_s - T_o)}{q_{oo}\ \dot{m}_o} \tag{141}$$

In the tests as currently run, the heat flux to a calorimeter is measured in a pipe having the initial diameter D_o. The "hot wall" heat flux q_o in terms of this calorimeter heat flux can be shown to be given by Equation (142) where q_{cal} is the calorimeter flux, H_w is the enthalpy at the ablating wall, H_s is the stagnation enthalpy of the flow and H_{cal} is the wall enthalpy associated with the calorimeter.

$$q_{oo} = q_{cal} \left\{ \frac{H_s - H_w}{H_s - H_{cal}} \right\} \left\{ \frac{H_s + H_w}{H_s + H_{cal}} \right\}^{-0.508} \tag{142}$$

The surface temperature associated with the ablation process is needed in order to obtain H_w and q_r, the radiation loss. The resulting values obtained for the heat of ablation are not overly sensitive to this surface temperature, and it is, therefore, assumed to be constant during the course of a test. The value of the surface temperature is obtained from the model 500 test data.

The equation employed for the heat of ablation is Equation (143).

$$H_a = \frac{1}{\dot{m}_o} \left\{ q_{oo} - q_r \right\} \tag{143}$$

where:

$$q_r = \epsilon_{eff} \sigma T_s^4 \tag{144}$$

In equation (144) the quantity ϵ_{eff} is an effective emissivity which accounts for both the natural emissivity of the material and the geometric factors peculiar to the pipe test.

In summary, the preceding discussion yields a set of equations which can be solved simultaneously by numerical methods to yield the initial mass transfer rate, the heat of ablation, the induction time, the surface temperature and the corrected hot wall convective heat transfer rate in terms of the material properties and the test data. For convenience, this set of equations is repeated below:

$$H_a = \frac{1}{\dot{m}_o} \left\{ q_{oo} - q_r \right\} \tag{145a}$$

$$q_{oo} = q_{CAL} \left\{ \frac{H_s - H_w}{H_s - H_{CAL}} \right\} \left\{ \frac{H_s + H_w}{H_s + H_{CAL}} \right\}^{-0.508} \tag{145b}$$

$$H_w = H_w (T_s, P) \tag{145c}$$

$$q_r = \epsilon_{eff} \sigma T_s^4 \tag{145d}$$

$$\dot{m}_o = \frac{\rho}{2(1+\alpha)\tau} \left[D_o^{-\alpha} \left\{ \left(\frac{4 \Delta W}{\pi \rho L} + D_o^2 \right)^{1/2} + R B_2 \tau \right\}^{1+\alpha} - D_o - (1+\alpha) B_2 \tau \right] \tag{145e}$$

$$B_2 = \frac{2 q_r}{\rho H_a} \tag{145f}$$

$$\tau = t - \frac{\rho K (T_s - T_o)}{q_{oo} \cdot \dot{m}_o} \tag{145g}$$

It should be emphasized that the above analysis assumes that the test is of sufficient duration that the steady state assumptions apply. If, on the other hand, the test does not approach steady state, then any interpretation in terms of a meaningful "heat of ablation" is impossible since the entire "H_a" concept is one of steady state and has no meaning in terms of a transient problem. This situation may well pose serious problems in the interpretation of test data for materials having high values of H_a, k and T_s. This is at least qualitatively evident from an examination of the expression for the "induction time" which can be written in the form of Equation (146).

$$t_o = \frac{\rho k (T_s - T_o) H_a}{(q_w)^2} \tag{146}$$

Equation (146) indicates that high values of k, T_s and H_a all tend to increase the "induction time" and hence for a fixed test time to decrease the value of $\hat{z}$ and thus increase the uncertainties in the analysis. It should also be noted that the effect of going to small heat flux levels is profound in terms of the induction time t_o.

3.1.4 Numerical Analysis of the Test Data

The data employed for an interpretation of the Apollo material ablative performance are those resulting from tests in the Avco Model 500 test facility. The reasons for rejecting data from other sources have been detailed earlier in this section. The data available from the Model 500 facility consist of some 91 test points covering the range of stagnation enthalpies from 1000 to 10000 BTU/lb. The reduction of the raw test data follows the procedure given in the preceding paragraphs. Figure (12) shows the data plotted in the form of a heat of ablation as a function of stagnation enthalpy. The heat of ablation as plotted is defined as the net heat flux to the sample (apart from combustion effects) divided by the steady state mass transfer rate.

$$H_a = \frac{q_c}{\dot{m} H_s} \left\{ H_s - H_w \right\} - \frac{\epsilon \sigma T_s^4}{\dot{m}} \tag{147}$$

Also appearing in Figure (12) are a group of seven test points obtained in the Avco 10 Megawatt turbulent subsonic pipe test facility. These data have been reduced in the manner previously described with the quantity H_a being defined by equation (143). These data will be discussed in a later paragraph.

As can be seen from the figure the Model 500 data are reasonably consistent although the scatter in the points is about $\pm$ 35% in the heat of ablation at stagnation enthalpies near 6000 BTU/lb.

It is generally considered that the interaction between the charred surface of the Apollo material and the environment presented by flight through the earths atmosphere is controlled by a chemical interaction on

FIGURE 12
HEAT OF ABLATION AS A FUNCTION
OF STAGNATION ENTHALPY

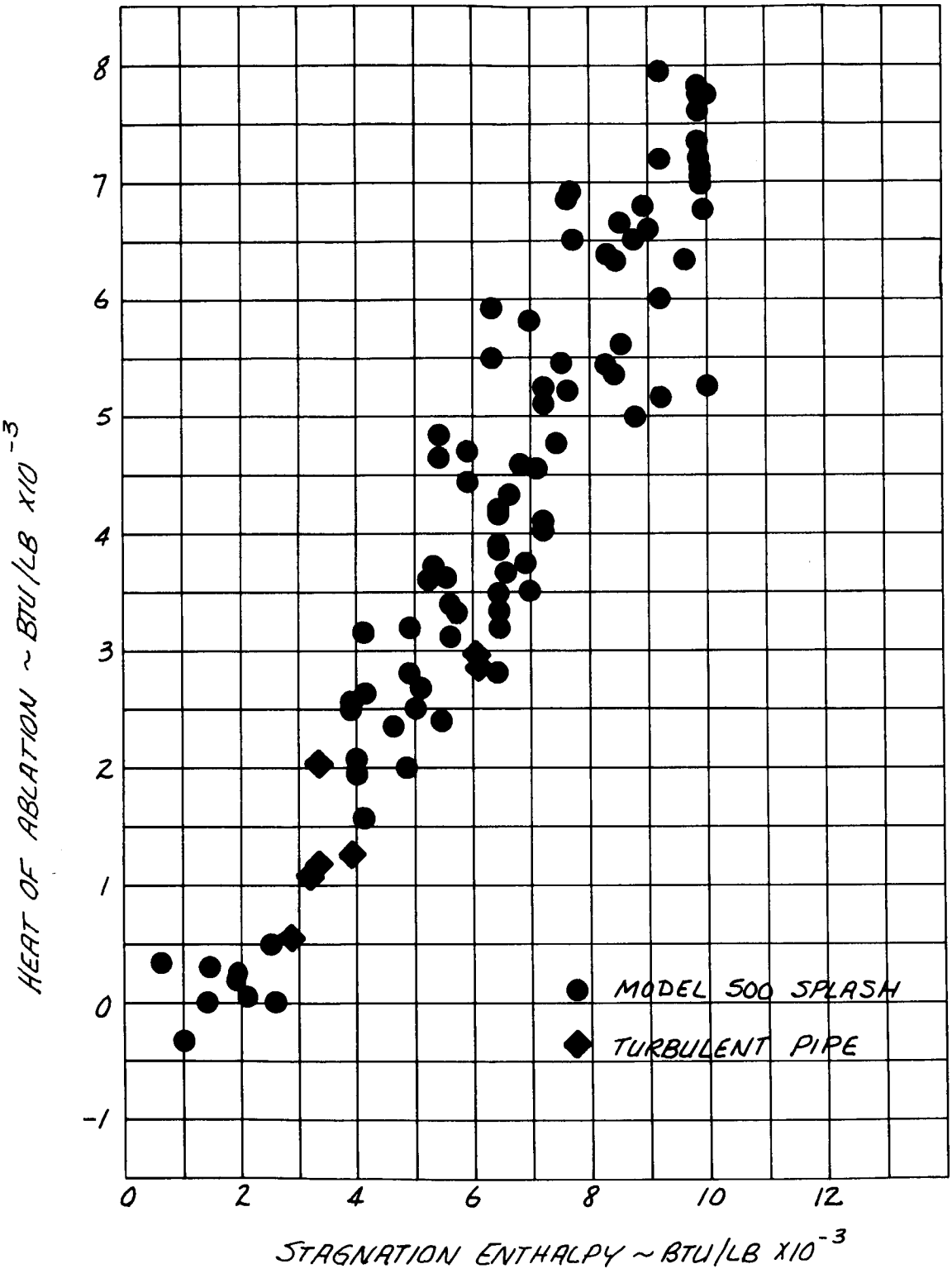

the condensed surface. If this is the case and the reaction is controlled by the diffusion of either reactants or products across the boundary layer then to a good approximation the ablation rate should be proportional to the product of the heat transfer coefficient and the concentration potential associated with the rate limiting species. Figure (13) shows the ratio of mass transfer rate to the heat transfer coefficient as a function of surface temperature as obtained from the Model 500 test data plotted as a function of surface temperature. As can be seen from the figure there is no apparent trend in the diffusion parameter with surface temperature and the scatter in the data is similar to that found in the heat of ablation-stagnation enthalpy plot of Figure (12). Conclusions to be drawn from Figure (13) are that the diffusion controlled mechanism is indeed entirely consistent with the experimental data and further that the concentration potential associated with this diffusion process is not a sensitive function of surface temperature over the range indicated in the figure.

The conclusion that the concentration potential associated with the rate controlling diffusion process is insensitive to the surface temperature is an important one. If the diffusion process which limits the ablation rate involves the movement of reaction products away from the heated surface toward the edge of the boundary layer the validity of this conclusion requires that the concentration of this species at the wall be independent of temperature over the range represented by the experimental data. If the rate limiting process involves the diffusion of a component of the environmental gas toward the surface, then the heterogeneous reaction rate between this component and the solid surface must be sufficiently large to reduce the concentration of the diffusing component to near zero at the surface. In addition the product of this heterogeneous reaction must be quite stable relative to the reactants such that the equilibrium at the surface conditions greatly favors the products over the reactants. With these considerations in mind one can then proceed to examine in some detail the situation involving the Apollo material exposed to an air environment. Such an examination can be aided by a consideration of the thermodynamic equilibrium between air and the Apollo material over the range of temperatures, pressures and air concentrations associated with the experimental data.

Such calculations have been performed using data from the JANAF Thermochemical Tables and employing a total of 38 gaseous species. The gaseous species considered were: C, CH, HCN, HCNO, HCO, CH_2, CH_2O, CH_3, CH_4, CN, CO, CO_2, C_2, C_2N_2, C_3O_2, H, NH, OH, SiH, H_2, NH_2, H_2O, NH_3, N_2H_4, SiH_4, N, NO, NO_2, SiN, N_2, N_2O, O, SiO, O_2, SiO_2, Si, Si_2, Si_3. The charred surface in equilibrium with this mixture was assumed to consist of carbon and SiO_2. Calculations were performed over a wide range of temperatures (1800-5500°R), pressures (0.01-10.0 atm) and weight fractions of air (0.0 - 0.7). The only species which satisfy the condition of yielding a near constant concentration potential were oxygen and carbon monoxide. All other species either showed concentration variations of several orders of magnitude over the range of the experiments or were found to be present in such small amounts as to preclude being responsible for the ablation process. The question of whether the diffusion of oxygen or the diffusion of carbon monoxide is the rate limiting step in the present case is also

FIGURE 13-
DIFFUSION PARAMETER
MODEL 500 TEST DATA

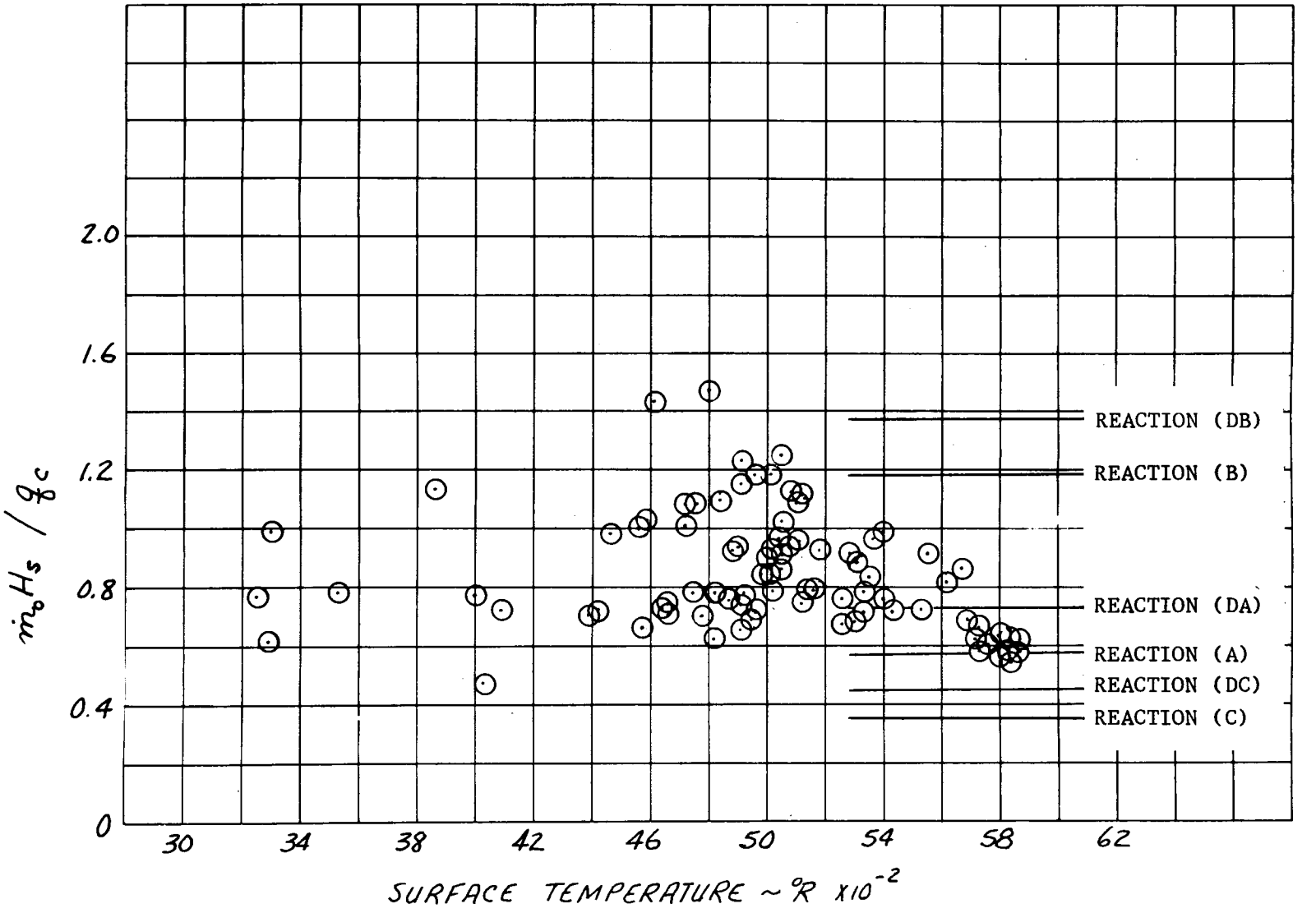

answerable on the basis of the equilibrium calculations referred to above. If the process were due to the diffusion of carbon monoxide then there would be appreciable amounts of uncombined oxygen in equilibrium at the surface. Such is indeed not the case and the calculations indicate that the concentration of free oxygen at the ablating wall is negligible over the range considered. The ablation controlling process is thus taken to be the diffusion of oxygen to the surface from the outer edge of the boundary layer over the entire range of the experimental data indicated in Figures (12) and (13).

Although it appears clear that the only diffusion process which satisfies the requirements associated with the test data is that involving oxygen moving toward the heated surface, it is of some interest to examine the possible range of ablation performance associated with other diffusion processes. For example, consider the process in which nitrogen is the reactant at the wall to yield CN as a primary gaseous product. Although this reaction undoubtedly contributes to the overall ablation process, as do a number of other chemical reactions at the surface, the nitrogen diffusion process cannot be the limiting one since nitrogen is very stable with respect to the possible products of its reaction with the charred surface. If this were not the case, however, and one postulates surface reaction to be carbon and nitrogen to yield CN, it then is possible to evaluate the theoretical value of the diffusion parameter plotted in Figure 13. Assuming the charred surface to be 40% carbon and a ratio of virgin to char density of 2.0 the analysis as presented in Section 2.9.2 can be used to evaluate a "theoretical" value for the diffusion parameter for several possible reactions.

Equation (80) of Section 2.9.2 represents the diffusion limited mass ablation rate for a surface which is a pure reactant. Application of the analysis in that section to a material whose surface is not pure carbon but rather which has a weight fraction W_c of available carbon and $(1 - W_c)$ of an inert component yields equation (148).

$$\dot{m}_o = \rho_o \dot{s} = \mu_2 \left(\frac{\rho_o W_e}{\rho_c W_c}\right)\left(\frac{q_c}{H_s}\right) \exp\left\{-f\left(1 + 0.618\, f\right)\right\} \tag{148}$$

where:

$$f = \frac{\dot{m}_o \eta H_s}{q_c}$$

Equation (148) can be readily solved for the diffusion parameter, $(\dot{m}_o H_s/q_c)$, based on a postulated chemical interaction at the ablating surface. Consider for example the reaction of carbon and oxygen to yield carbon monoxide as represented by reaction (A)

$$C_{(s)} + 1/2\ O_{2(g)} \longrightarrow CO_{(g)} \tag{A}$$

Application of equation (148) to this reaction yields the following results.

$$W_e = 0.2314$$

$$W_c = 0.4$$

$$\mu_2 = (12/16)$$

$$\eta = 0.6$$

$$\left(\frac{\dot{m}_o H_s}{q_c} \right)_A = 0.571 \tag{149}$$

Equation (149) can be re-written in terms of the surface recession rate, $\dot{S}$. This rate is given by equation (149a).

$$\dot{S}_A \text{(in/sec)} = 0.208 \left(\frac{q_c}{H_s} \right) \tag{149a}$$

$q_c \sim$ BTU/ft^2-sec

$H_s \sim$ BTU/lb

In the case of a postulated reaction between carbon and nitrogen the appropriate chemical reaction is (B).

$$C_{(s)} + 1/2\ N_{2(g)} \rightarrow CN_{(g)} \tag{B}$$

Application of equation (148) to this chemical system yields the following results.

$$W_e = 0.7686$$

$$W_c = 0.4$$

$$\mu_2 = (12/14)$$

$$\eta = 0.6$$

$$\left(\frac{\dot{m}_o H_s}{q_c} \right)_B = 1.182 \tag{150}$$

$$\dot{S}_B \text{(in/sec)} = 0.430 \left(\frac{q_c}{H_s} \right) \tag{150a}$$

A third reaction which can be postulated is the reaction carbon and oxygen to yield carbon dioxide.

$$C_{(s)} + O_{2(g)} \rightarrow CO_{2(g)} \qquad (C)$$

In the case of this reaction the use of the diffusion approximation leads to the following results.

$$W_e = 0.2314$$

$$W_c = 0.4$$

$$\mu_2 = (12/32)$$

$$\eta = 0.6$$

$$\left(\frac{\dot{m}_o H_s}{q_c} \right)_C = 0.345 \qquad (151)$$

$$\dot{s}_c \text{ (in/sec)} = 0.125 \left(\frac{q_c}{H_s} \right) \qquad (151a)$$

The values for the diffusion parameter for these postulated surface reactions are indicated in Figure 13 for comparison with the test data.

It is also possible that a reaction between the silica and carbon in the charred material can take place which would have an effect on the values obtained for the several reactions. One such reaction which has been postulated involves the reaction of SiO_2 and carbon to yield CO and SiO. Assuming the weight fraction of carbon which is left by the pyrolysis reaction is W_c', this reaction can be written as (D).

$$\left(\frac{1 - W_c'}{60} \right) Si O_{2(s)} + \left(\frac{W_c'}{12} \right) C_{(s)} \rightarrow \left(\frac{1 - W_c'}{60} \right) Si O_{(g)} + \left(\frac{6 W_c' - 1}{60} \right) C_{(s)} \qquad (D)$$

The excess free carbon is represented by the last term on the right hand side of reaction (D). The weight fraction of the char which is excess carbon and available to react with the free stream gas is then given in terms of W_c' by equation (152).

$$W_c = 12 \left(\frac{12 W_c' - 2}{120} \right) = \left(\frac{6 W_c' - 1}{5} \right) \qquad (152)$$

Under the conditions previously assumed, namely that the pyrolysis reaction produces a material with a weight fraction of carbon equal to 0.4, equation (152) yields an effective value of the carbon weight fraction equal to 0.28. Use of this value of W_c for the reactions considered previously yields a new set of chemical reactions and diffusion parameters.

$$\left(\frac{1-W_c'}{60}\right) Si O_{2(s)} + \left(\frac{W_c'}{12}\right) C_{(s)} + \left(\frac{6W_c'-1}{120}\right) O_{2(g)} \rightarrow \left(\frac{1-W_c'}{60}\right) Si O_{(g)} + \left(\frac{6W_c'-1}{60}\right) CO_{(g)} \quad (DA)$$

$$\left(\frac{\dot{m}_o H_s}{q_c}\right)_{DA} = 0.716 \quad (153)$$

$$\dot{S}_{DA}(in/sec) = 0.260 \left(\frac{q_c}{H_s}\right) \quad (153a)$$

$$\left(\frac{1-W_c'}{60}\right) Si O_{2(s)} + \left(\frac{W_c'}{12}\right) C_{(s)} + \left(\frac{6W_c'-1}{120}\right) N_{2(g)} \rightarrow \left(\frac{1-W_c'}{60}\right) Si O_{(g)} + \left(\frac{6W_c'-1}{60}\right) CN_{(g)} \quad (DB)$$

$$\left(\frac{\dot{m}_o H_s}{q_c}\right)_{DB} = 1.366 \quad (154)$$

$$\dot{S}_{DB}(in/sec) = 0.498 \left(\frac{q_c}{H_s}\right) \quad (154a)$$

$$\left(\frac{1-W_c'}{60}\right) Si O_{2(s)} + \left(\frac{W_c}{12}\right) C_{(s)} + \left(\frac{6W_c'-1}{60}\right) O_{2(g)} \rightarrow \left(\frac{1-W_c'}{60}\right) Si O_{(g)} + \left(\frac{6W_c-1}{60}\right) CO_{2(g)} \quad (DC)$$

$$\left(\frac{\dot{m}_o H_s}{q_c}\right)_{DC} = 0.451 \quad (155)$$

$$\dot{S}_{DC}(in/sec) = 0.164 \left(\frac{q_c}{H_s}\right) \quad (155a)$$

The values obtained for the diffusion parameters for reactions (DA), (DB) and (DC) are also compared with the test data in Figure 13.

As can be seen from the figure the Avco Model 500 are entirely consistent with a diffusion reaction involving the production of carbon monoxide. On the surface the most consistent explanation of the data appears to be reaction (DA) although the choice between (A) and (DA) is not clear cut when it is considered that the ablation indicated by reaction (A) is without doubt augmented by other processes such as (B) and (C) as well as a number of other minor reactions which have not been considered in detail. The question of the chemical details of the ablation process must be answered on the basis of a detailed multicomponent boundary layer analysis in which the ablating surface is coupled into the problem. In the absence of such an analysis, it is assumed, as stated earlier, that the ablation mechanism in the diffusion controlled regime can be adequately accounted for in terms of an "effective" reaction resulting from the diffusion of oxygen to the heated surface. As indicated in Figure 13, this "effective" reaction probably involves more than the simple reaction of carbon and oxygen to yield carbon monoxide. Using this reaction as the major factor and providing the form of the equations to be employed, the effective weight fraction of carbon at the surface and the ablation energies are then deduced from the experimental data.

The Model 500 data have been reduced employing the weight fraction of oxygen in normal air (0.23) for the quantity W_e appearing in equation (108). It should be noted that no set of convective experiments in a gas of fixed composition (all experimental data falling in the diffusion ablation regime) will serve to separate the quantities Q_1 and Q_2 of equation (109). The reason for this is obvious. The quantity defined by equation (156) is constant for a diffusion controlled process.

$$f' = \dot{m}_o H_s / q_c \tag{156}$$

This being the case and since the quantity η is a constant the ratio of heat transfer coefficient with mass transfer to the heat transfer without mass transfer is constant.

$$\phi = EXP\left\{-\eta f'(1+\alpha \eta f')\right\} \tag{157}$$

It is easily seen that with f' and ϕ constant as well as W_e that X is also a constant.

$$X = \frac{W_e q_c}{\dot{m} H_s}\phi = \frac{W_e}{f'}\phi \tag{158}$$

Thus only the combination $(Q_1 + Q_2 X)$ can be determined from the present test data. A unique separation of Q_1 and Q_2 must await adequate steady state

ablation data over a range of compositions for the environmental gas. For the present purposes the value of Q_2 has been selected to be consistent with the formation of carbon monoxide.

Section 2.9.5 develops in detail the arguements associated with assigning the energy quantity corresponding to the combustion energy H_c; this is the same parameter as the Q_2 of equation (109). In the present situation this energy is that associated with the homogeneous reaction involving equilibrium carbon vapor and oxygen to yield carbon monoxide. The boundary condition in which this quantity appears can be written as equation (159) which is the same as equation (108)

$$\frac{q_c}{H_s}\left(H_s + W_e Q_2 - H_w\right)\phi + (1-R_o)F_s - \epsilon\sigma T_s^4 = \rho_c \dot{s} H_v - k_c\left(\frac{\partial T}{\partial y}\right)_s \qquad (159)$$

Based on the data in the JANAF tables of thermodynamic properties the energy associated with the reaction of equilibrium carbon vapor with oxygen to yield carbon monoxide is approximately 10000 BTU/lb oxygen and this value has been chosen for Q_2 (the H_c of Section 2.9.5). On this basis and using the values of the virgin and char densities discussed in a later section together with 500 BTU/lb for the heat of pyrolysis per pound of gas produced best values of the several parameters associated with the ablation process are as follows.

$$\eta = 0.6 \qquad (160)$$

$$H_v = 580 \text{ BTU/lb} \qquad (161)$$

$$X = \frac{W_e q_c \phi}{\dot{m}_o H_s} = 0.2220 \qquad (162)$$

The mean value of X as given in (162) has been obtained by giving more weight to the larger values of X_i as being more probable in the light of the possible experimental errors involved in the test data.

Equation (162) can be written in the form employed in equations (150) and (150a)

$$\left(\frac{\dot{m}_o H_s}{q_c}\right)_{\text{expt.}} = 0.650 \qquad (162a)$$

$$\dot{s}_{(\text{in/sec})} = 0.236 \left(q_c/H_s\right) \qquad (162b)$$

The analysis of the test data also provide a value of the emissivity, ϵ ,

based on the measured brightness temperature and the measured radiative loss as described in Section 3.1.2. The emissivity obtained is given by equation (163).

$$\epsilon = \frac{1}{\sigma N} \sum_{i=1}^{N} \left(\frac{q_{r_i}}{T_{s_i}^4} \right) = 0.667 \tag{163}$$

It is also impossible in the present set of data to separate the blowing parameter associated with the pyrolysis products from that associated with the surface mass transfer. In principle, this can be accomplished by means of steady state ablation experiments on fully charred samples. A by-product of the equilibrium calculations described earlier allows such a separation to be made however. The calculations done for the case with no air present yield an estimate of the molecular weight of the pyrolysis products which, when combined with the correlation for the effects of mass injection on heat transfer described in another section of this report, yield a value of 0.8 for the blowing parameter, η_g, associated with these gases. This value allows the separation to be accomplished according to equation (164).

$$\rho_o \eta = \rho_c \eta_s + (\rho_o - \rho_c) \eta_g \tag{164}$$

$$\eta = 0.6$$

$$\eta_g = 0.8$$

$$\eta_s = 0.4$$

It should be noted at this point that an apparent pressure dependence of the ablation process can be falsely inferred from the transient data obtained in the facilities other than the Model 500 arc. When the data from the MSC Plasmadyne series or from the Avco/OVERS facility are incorrectly interpreted as being steady state experiments an apparent pressure dependence appears in the "diffusion parameter" as defined by equation (165).

$$\text{Apparent Diffusion Parameter} = \left\{ \frac{W_e \Delta t \, q_c \phi'}{\rho_o A \Delta L H_s} \right\} \tag{165}$$

$$\phi' = EXP \left\{ -f'(1 + \alpha f'') \right\}$$

$$f'' = \frac{\rho_o A \Delta L H_s \eta}{q_c}$$

This apparent pressure dependence is a direct result of interpreting the test data as being steady state. The apparent pressure dependence is such that it would appear that the product of the diffusion parameter and the cube root of the pressure is a constant. The interaction between the pressure and the measure of transient behavior, F, defined by equation (105) or (107) is quite apparent. Tests run at low pressures correspond to low heating rates, low values of the mean ablation rate and consequently to high values of the parameter F. There is a strong correlation between the pressure at which a test was run and the measure of transient behavior. This is to be expected because of the fact that heat flux and pressure cannot be varied independently over wide ranges. The apparent pressure dependence of the ablation behavior is thus a property of the operating map of the particular facility rather than of the ablative material as such.

The turbulent pipe data shown in Figure (13) are of interest since they appear to be the only reasonably reliable data on the material at elevated pressure and shear levels. The data are tabulated in Table (2). As can be seen from the Figure there is no evidence that the performance of the material is adversely affected by pressure and shear levels up to those listed in Table (2).

3.1.5 Alternate Presentation of Test Data

It is of some interest to display the Model 500 ablation data in several forms in addition to those thus far employed in this report. Figure 14 shows the surface recession rate as a function of the heat transfer coefficient. This figure is similar to Figure 13 with the additional indication of the range of heat transfer coefficients over which data have been obtained. Also indicated on Figure 14 are the theoretical functions for several of the chemical reactions discussed in the preceeding section.

One of the common attempts at ablation data correlation involves the use of a unique relationship between surface recession rate and surface temperature. Such a relationship exists only for materials where the controlling ablation mechanism is a vaporization process. Figure 15 shows the surface recession rate as a function of surface temperature for the Model 500 ablation data. As can be seen from the figure no unique relationship is apparent in the test data.

Figures (16), (17) and (18) present the data in the form of the surface recession rate as a function of the "cold wall" heat flux. Again it is not expected that any unique relationship between these parameters should exist for the body of data taken as a whole. It is desirable, however, to indicate some comparison between the test data and some theoretical model. The theoretical relationships for the several chemical reactions considered in the preceeding section can be written in the form of equation (166) where the quantity C is a constant which depends on the chemical reaction being considered.

$$\dot{s} = C\left(\frac{q_c}{H_s}\right) \qquad (166)$$

TABLE 2

Avco Pipe Test Data

Apollo Heat Shield Material

Initial Diameter 1.25 in., Length 5.0 Inches

Sample	q_{cal} Btu/ft^2-sec	ρ_o lb/ft^3	H_o Btu/lb	Δ D inches	Δ W lb	P_o atm	Δ t sec	Shear lb/ft^2	H_a Btu/lb
AP1382-1	450.	29.97	3352.	0.818	0.2092	4.8	13.81	4.65	1156
-2	440.	29.97	3217.	0.803	0.2041	4.8	13.63	4.64	1081
AP1483-1	310.	28.22	3318.	0.358	0.09215	13.2	12.60	0.76	2023
-2	500.	28.34	3894.	1.314	0.3018	5.1	19.17	4.81	1249
-3	505.	27.91	2844.	1.355	0.3047	12.1	19.15	3.01	645
AP1553-1	660.	29.65	6129.	0.587	0.1598	2.2	9.63	12.9	2865
-2	650.	29.59	6027.	0.669	0.1468	2.2	9.20	12.8	2959

FIGURE 14

MODEL 500 ABLATION DATA

ABLATION VELOCITY AS A FUNCTION OF HEAT TRANSFER COEFFICIENT

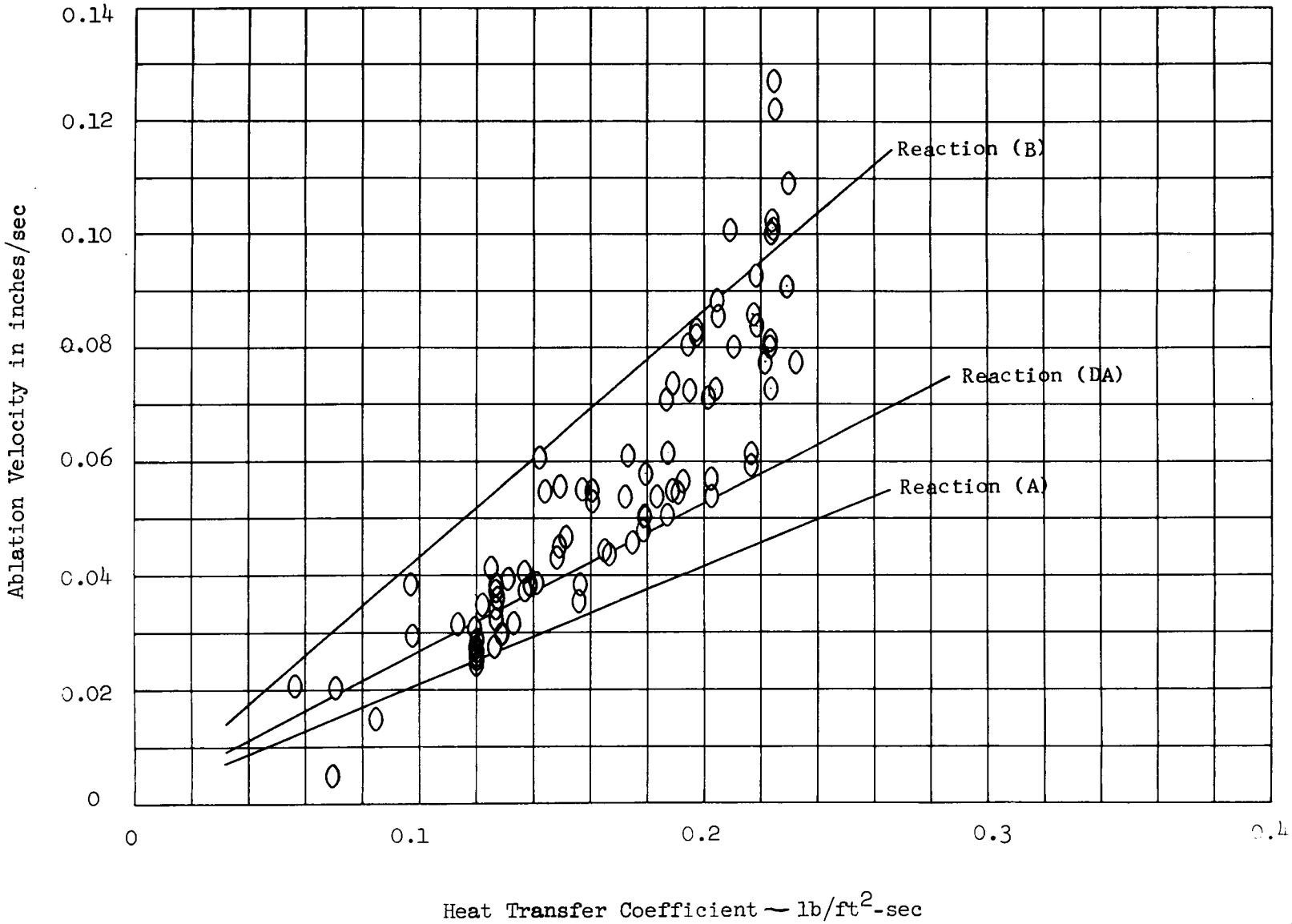

FIGURE 15

MODEL 500 ABLATION DATA

ABLATION VELOCITY AS A FUNCTION OF SURFACE TEMPERATURE

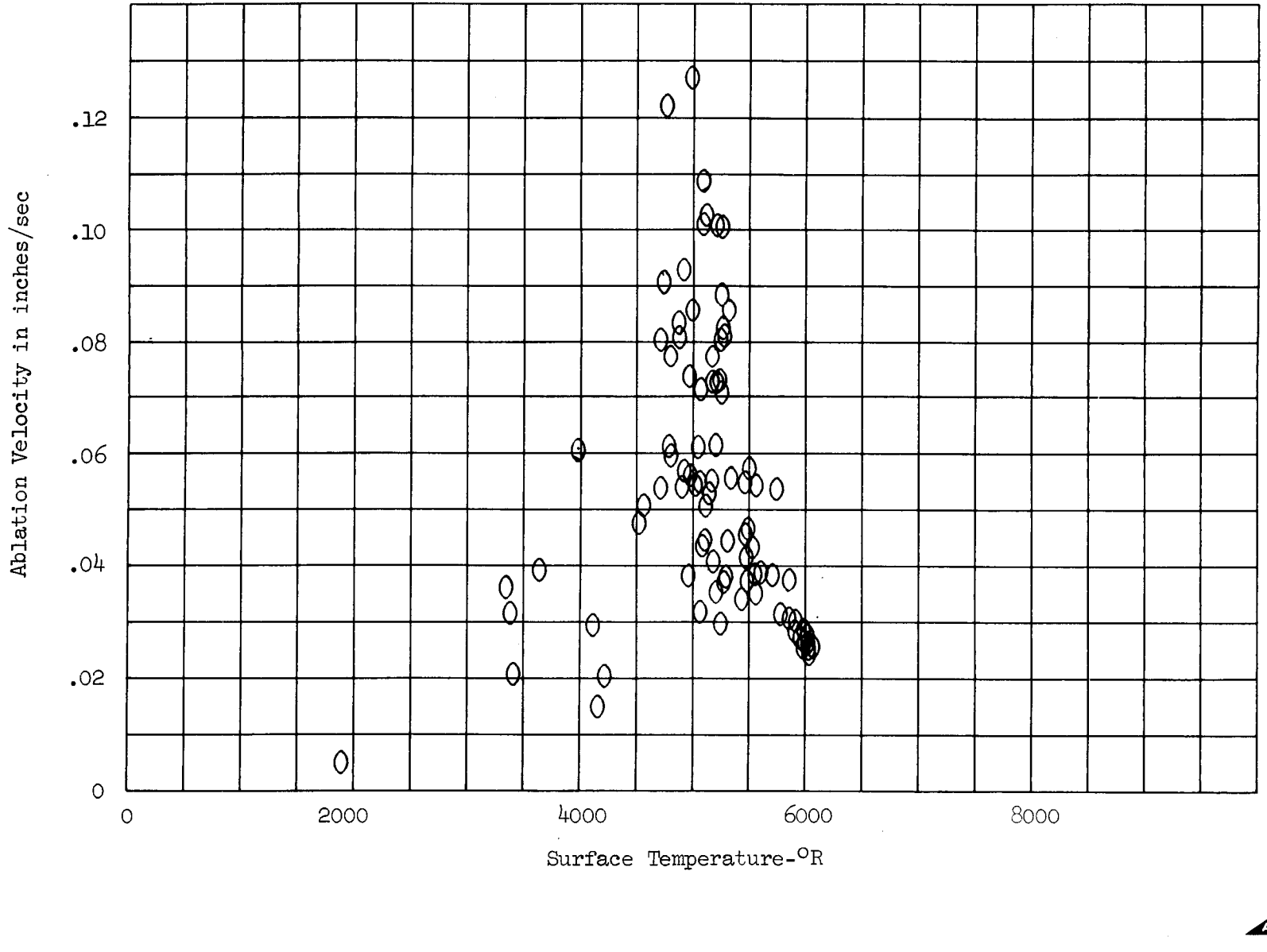

NOTE: USE TYPE B PENCIL FOR VUGRAPHS AND REPORT DATA.

FIGURE 16

MODEL 500 ABLATION DATA

ABLATION VELOCITY AS A FUNCTION OF HEAT FLUX ENTHALPY (I.G.1000-5000) BTU/lb

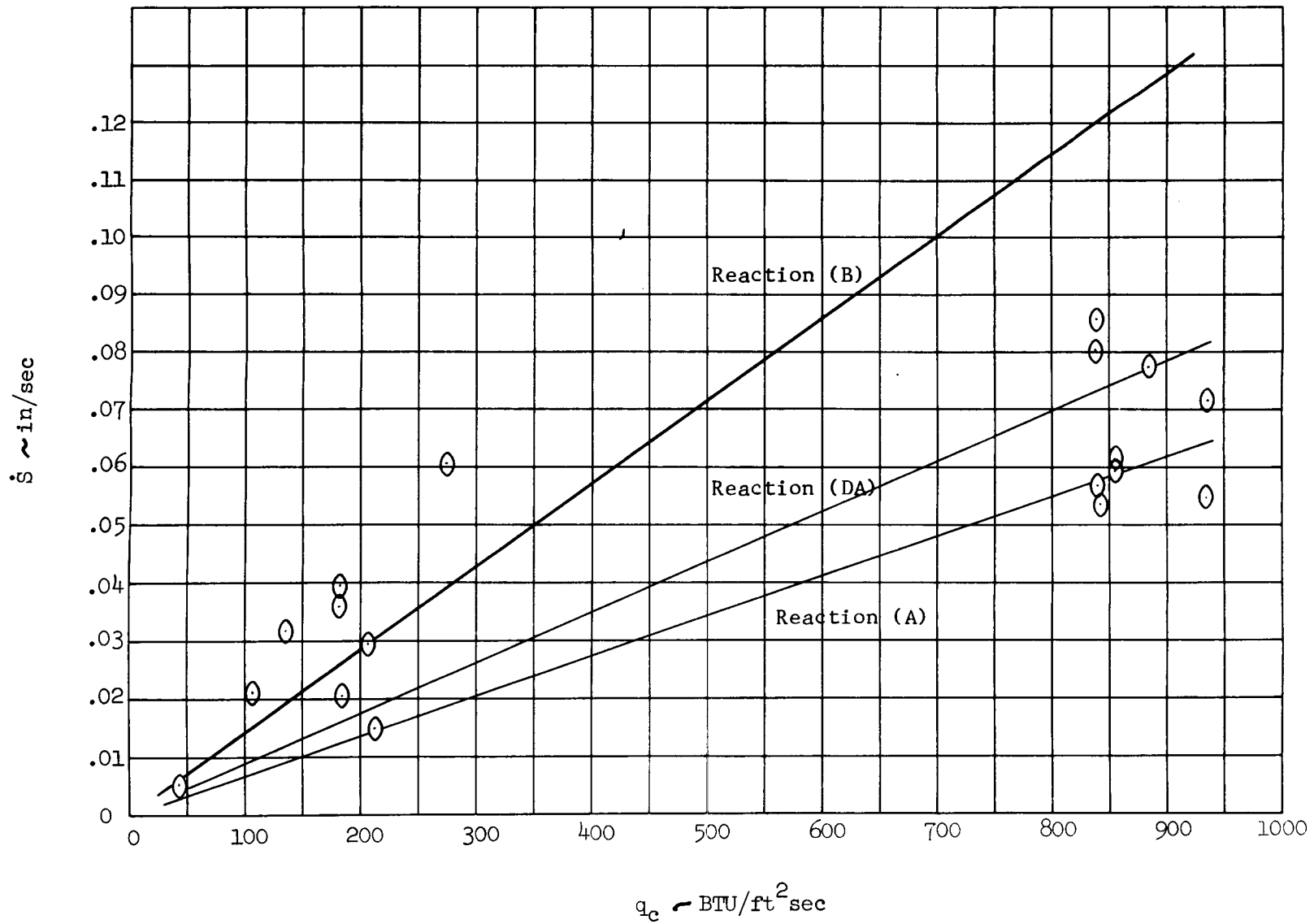

NOTE: USE TYPE B PENCIL FOR VUGRAPHS AND REPORT DATA.

FIGURE 17

MODEL 500 ABLATION DATA

ABLATION VELOCITY AS A FUNCTION OF HEAT FLUX ENTHALPY (I.G. 5000-7000) BTU/lb

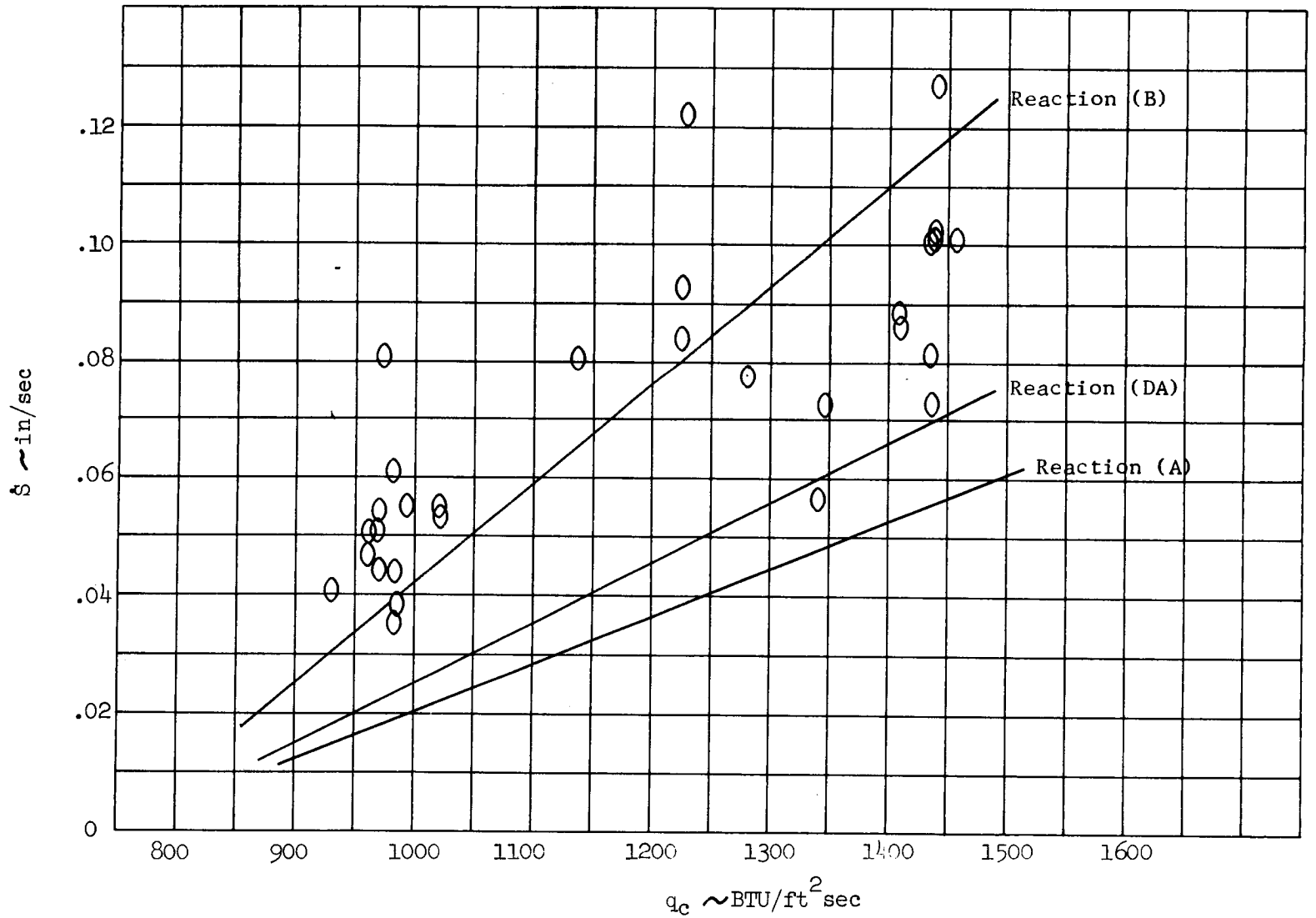

FIGURE 18

MODEL 500 ABLATION DATA

ABLATION VELOCITY AS A FUNCTION OF HEAT FLUX ENTHALPY (I.G.7000-10000)BTU/lb

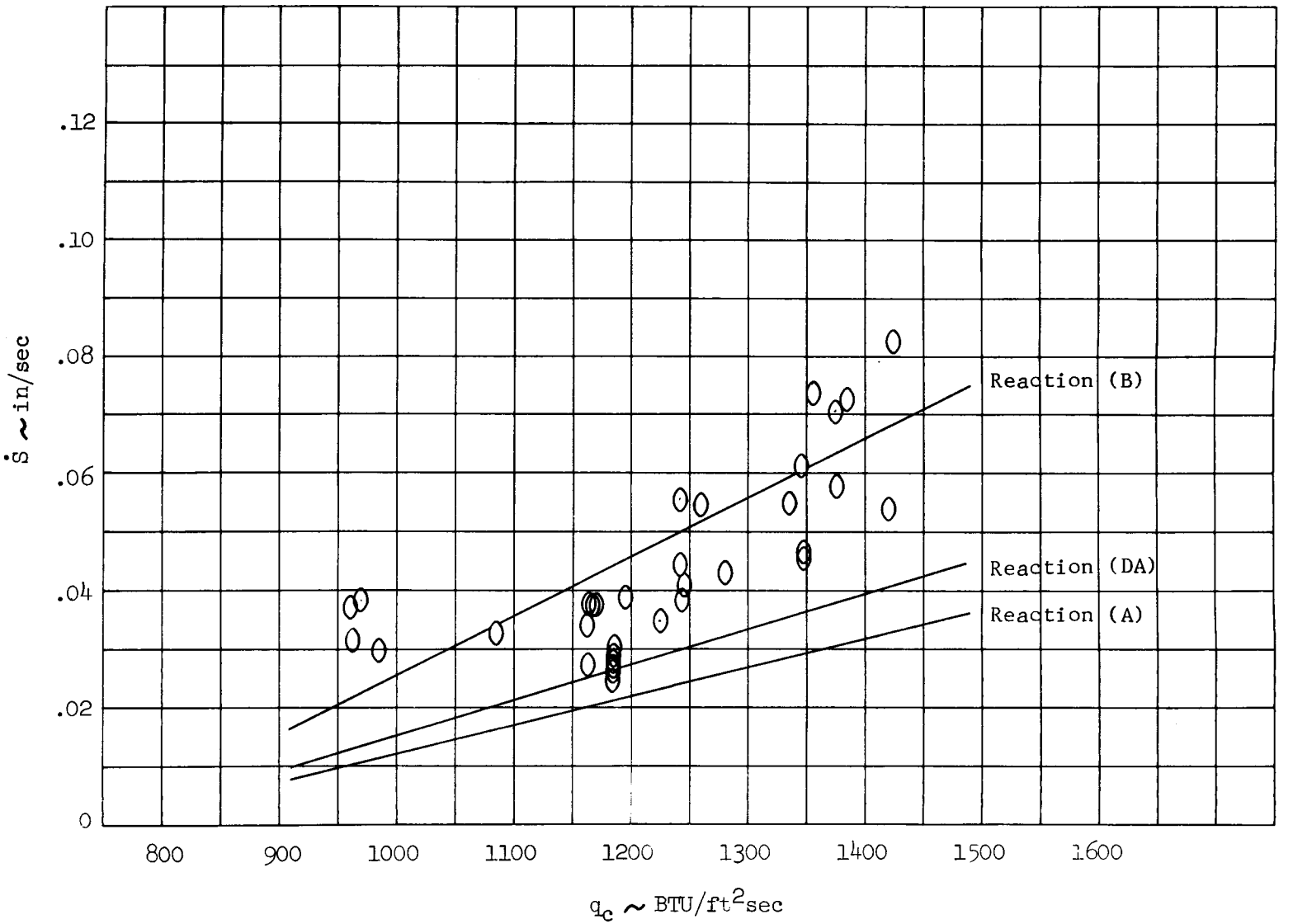

Over a limited range of stagnation enthalpies equation (166) can be written in an approximate fashion as equation (167) where the quantity $\bar{H}_s$ is the mean enthalpy in the range of data selected.

$$\dot{s} \approx \left(\frac{C}{\bar{H}_s}\right) q_c \qquad (167)$$

The Model 500 data have been divided into three groups as indicated on the figures and the theoretical lines for reactions (A), (B) and (DA) obtained from equation (167) by means of equations (149a), (150a) and (153a).

3.2 Pressure and Mass Flow Data

3.2.1 Analysis Method

The porous nature of ablative materials, particularly in the charred state, together with the internal production of gaseous pyrolysis products leads to a non-uniform pressure distribution through the material. The equation chosen for describing this process in the design computer program can be written in the form of equation (168).

$$\left(\frac{1}{RT}\right)\frac{d(P)^2}{dy} = 2\mu\alpha\dot{m}_g + 2\beta\dot{m}_g^2 \tag{168}$$

where:

P	pressure
$\dot{m}_g$	gas flow rate per unit area
μ	gas viscosity
R	specific gas constant
α	viscous resistance coefficient
β	inertial resistance coefficient

Values of the resistance coefficients, α and β, are obtained by measuring w, the mass flow of gas per unit area per unit time; P_u, the pressure immediately upstream of the sample; and P_d, the pressure downstream of the sample. If the sample thickness L, is small enough such that the mass flow rate and temperature are essentially constant across the sample, then equation (168) may be integrated to yield the following expression.

$$\frac{P_u^2 - P_d^2}{RTL\,\omega^2} = 2\alpha\left(\frac{\mu}{\omega}\right) + 2\beta \tag{169}$$

Equation (169) suggests that for a series of experiments varying the gas, sample thickness, temperature, and pressure level, all the data for a specific porous medium could be correlated in terms of a friction factor per unit length, C, and a Reynolds number per unit length, R_e, where

$$C = \frac{P_u^2 - P_d^2}{RTL\omega^2}$$

and

$$R_e = \frac{\omega}{\mu}$$

Equation (169) may be re-written as

$$C = 2\alpha\left(\frac{1}{R_e}\right) + 2\beta \tag{170}$$

Equation (170) is linear in the reciprocal Reynolds number per unit length so that the resistance coefficients may be easily obtained by a least square analysis of the experimental data. Letting the subscript i denote the value of any quantity corresponding to the i^{th} datum point and N be the total number of experiments considered, then α and β are given by equations (171) and (172).

$$\alpha = \frac{N\sum_{i=1}^{N}\frac{C_i}{(R_e)_i} - \left(\sum_{i=1}^{N} C_i\right)\left(\sum_{i=1}^{N}\frac{1}{(R_e)_i}\right)}{2\left\{N\sum_{i=1}^{N}\frac{1}{(R_e)_i^2} - \left(\sum_{i=1}^{N}\frac{1}{(R_e)_i}\right)^2\right\}} \tag{171}$$

$$\beta = \frac{\left(\sum_{i=1}^{N} C_i\right)\left(\sum_{i=1}^{N}\frac{1}{(R_e)_i^2}\right) - \left(\sum_{i=1}^{N}\frac{1}{(R_e)_i}\right)\left(\sum_{i=1}^{N}\frac{C_i}{(R_e)_i}\right)}{2\left\{N\sum_{i=1}^{N}\frac{1}{(R_e)_i^2} - \left(\sum_{i=1}^{N}\frac{1}{(R_e)_i}\right)^2\right\}} \tag{172}$$

where

$$C_i = \frac{(P_u)_i^2 - (P_d)_i^2}{R_i T_i L_i \omega_i^2} \quad ; \quad i = 1, 2, \ldots N$$

$$(R_e)_i = \frac{\omega_i}{\nu_i} \quad ; \quad i = 1, 2, \ldots N$$

Equations (171) and (172) are readily obtained by applying the method of least squares to equation (170). (Reference 14). However, if the data are primarily in the viscous range, then a small amount of scatter may force a negative value of the inertial coefficient, β. In such a case it is assumed that the inertial effects are actually small and that $\beta = 0$. The best straight line through the data in the viscous region is then given by

$$\alpha = \frac{1}{N}\sum_{i=1}^{N}\alpha_i = \frac{1}{N}\sum_{i=1}^{N} C_i (R_e)_i \tag{173}$$

3.2.2 Apollo Material Data

Experiments measuring mass flow of gas and pressure have been performed at Avco for the virgin and charred states of the Apollo heat shield material. Tests were run for flow parallel and perpendicular to the honeycomb cell walls, using air as the gas. Gas flow perpendicular to the cell walls was reported to be much less than parallel flow, however, no interpretation of these experiments is offered here. The following discussion then concerns only parallel flow.

Tests were performed on 0.50 inch thick samples, the virgin sample having a 2.0 inch diameter and charred sample having 1.78 inch diameter. The charred sample was prepared from material pre-charred at 1840°R and is assumed to be fully decomposed. The measured flow rate, upstream pressure, downstream pressure, temperature, sample thickness, and computed value of friction factor per foot, C, and Reynolds number per foot, R_e, are given in Table (3) for the virgin material and Table (4) for the charred material. The data reported in Tables (3) and (4) range in mass flow from .0012 lb_m/ft^2-sec to 0.80 lb_m/ft^2-sec and pressure drops across the sample from 0.02 lb_f/in^2 to about 15.0 lb_f/in^2 with the downstream pressure varying only slightly from one atmosphere. Some tests were performed outside this range, both higher and lower mass flows, but these test results are not included here because of the large scatter in the data at the low end and evidence of mechanical sample failure at the higher mass flows.

Figure (19) is a plot of the data given in Table (3) and Table (4) in the form of w vs. $P_u^2 - P_d^2$. Also indicated in Figure (19) is the curve generated using equation (169) and values of α and β derived from equations (171), (172), and (173). For the fully charred Apollo material, the resistance coefficients derived from equations (171) and (172) are:

$$\alpha_c = 5.781 \times 10^9 \text{ ft}^{-2} \qquad (174a)$$

$$\beta_c = 1.924 \times 10^5 \text{ ft}^{-1} \qquad (174b)$$

For the virgin Apollo material, equations (171) and (172) give a negative value of the inertial coefficient, i.e.

$$\alpha_v = 6.626 \times 10^{10} \text{ ft}^{-2}$$

$$\beta_v = -7.473 \times 10^3 \text{ ft}^{-1}$$

A measure of the importance of the inertial effects may be obtained by rewriting equation (170) as

$$C = \frac{2\alpha}{R_e}\left(1 + \frac{\beta}{\alpha} R_e\right) \qquad (175)$$

TABLE 3 AIR MASS FLOW-PRESSURE DROP DATA FOR CHARRED AVCOAT 5026-39-HCG

$w \sim lb_m/ft^2\text{-sec}$	$P_u \sim lb/ft^2$	$P_d \sim lb/ft^2$	$T \sim {}^oR$	$L \sim ft$	$C \sim ft^{-1}$	$R_e \sim ft^{-1}$
2.1800E-03	1.5020E+01	1.5000E+01	5.3500E+02	4.1567E-02	7.0437E+07	1.6769E+02
5.8000E-03	1.5050E+01	1.5000E+01	5.3500E+02	4.1567E-02	2.4902E+07	4.4615E+02
7.5600E-03	1.5060E+01	1.5000E+01	5.3500E+02	4.1567E-02	1.7594E+07	5.8154E+02
8.6200E-03	1.5080E+01	1.5000E+01	5.3600E+02	4.1567E-02	1.4856E+07	6.6308E+02
9.8200E-03	1.5090E+01	1.5000E+01	5.3600E+02	4.1567E-02	1.5557E+07	7.5538E+02
1.0960E-02	1.5100E+01	1.5000E+01	5.3600E+02	4.1567E-02	1.3971E+07	8.4308E+02
1.3300E-02	1.5120E+01	1.5000E+01	5.3600E+02	4.1667E-02	1.1392E+07	1.0231E+03
1.3560E-02	1.5130E+01	1.5000E+01	5.3600E+02	4.1567E-02	1.1877E+07	1.0431E+03
1.6880E-02	1.5160E+01	1.5000E+01	5.3600E+02	4.1567E-02	9.4424E+06	1.2985E+03
1.9100E-02	1.5180E+01	1.5000E+01	5.3600E+02	4.1567E-02	8.3023E+06	1.4692E+03
2.0700E-02	1.5200E+01	1.5000E+01	5.3600E+02	4.1567E-02	7.8591E+06	1.5923E+03
2.0700E-02	1.5200E+01	1.5000E+01	5.3600E+02	4.1567E-02	7.8591E+06	1.5923E+03
2.2900E-02	1.5220E+01	1.5000E+01	5.3600E+02	4.1567E-02	7.0684E+06	1.7615E+03
3.3300E-02	1.5410E+01	1.5090E+01	5.3600E+02	4.1567E-02	4.9072E+06	2.5615E+03
4.2800E-02	1.5520E+01	1.5090E+01	5.3600E+02	4.1567E-02	4.0061E+06	3.2923E+03
5.3200E-02	1.5650E+01	1.5090E+01	5.3600E+02	4.1567E-02	3.3911E+06	4.0923E+03
6.1700E-02	1.5760E+01	1.5090E+01	5.3600E+02	4.1567E-02	3.0272E+06	4.7462E+03
7.0600E-02	1.5880E+01	1.5100E+01	5.3600E+02	4.1567E-02	2.7030E+06	5.4308E+03
7.9100E-02	1.5980E+01	1.5110E+01	5.3600E+02	4.1567E-02	2.4102E+06	6.0846E+03
8.8500E-02	1.6130E+01	1.5120E+01	5.3600E+02	4.1567E-02	2.2468E+06	6.8077E+03
9.7000E-02	1.6260E+01	1.5130E+01	5.3600E+02	4.1567E-02	2.1018E+06	7.4615E+03
1.0600E-01	1.6390E+01	1.5140E+01	5.3700E+02	4.1567E-02	1.9520E+06	8.1538E+03
1.1400E-01	1.6520E+01	1.5150E+01	5.3700E+02	4.1567E-02	1.8579E+06	8.7692E+03
1.2300E-01	1.6670E+01	1.5160E+01	5.3700E+02	4.1567E-02	1.7679E+06	9.4615E+03
1.2300E-01	1.6680E+01	1.5160E+01	5.3740E+02	4.1567E-02	1.7789E+06	9.4615E+03
1.3200E-01	1.6820E+01	1.5180E+01	5.3740E+02	4.1567E-02	1.6749E+06	1.0154E+04
1.4100E-01	1.6960E+01	1.5190E+01	5.3740E+02	4.1567E-02	1.6017E+06	1.0846E+04
1.5000E-01	1.7120E+01	1.5210E+01	5.3820E+02	4.1567E-02	1.5239E+06	1.1538E+04
1.6800E-01	1.7380E+01	1.5230E+01	5.3860E+02	4.1567E-02	1.3783E+06	1.2923E+04
1.7600E-01	1.7540E+01	1.5250E+01	5.3860E+02	4.1567E-02	1.3150E+06	1.3538E+04
2.0000E-01	1.7750E+01	1.5210E+01	5.3700E+02	4.1567E-02	1.1547E+06	1.5385E+04
2.9300E-01	1.9310E+01	1.5260E+01	5.3700E+02	4.1567E-02	9.0758E+05	2.2538E+04
3.3500E-01	2.0090E+01	1.5290E+01	5.3700E+02	4.1567E-02	8.4212E+05	2.5769E+04
3.7500E-01	2.0790E+01	1.5320E+01	5.3700E+02	4.1567E-02	7.8166E+05	2.8846E+04
3.9600E-01	2.1080E+01	1.5330E+01	5.3700E+02	4.1567E-02	7.4296E+05	3.0462E+04
4.3200E-01	2.1770E+01	1.5360E+01	5.4000E+02	4.1567E-02	7.0577E+05	3.3231E+04
4.7100E-01	2.2490E+01	1.5400E+01	5.4000E+02	4.1567E-02	6.7015E+05	3.6231E+04
4.9200E-01	2.2880E+01	1.5420E+01	5.4000E+02	4.1567E-02	6.5321E+05	3.7846E+04
5.1000E-01	2.3180E+01	1.5440E+01	5.4000E+02	4.1567E-02	6.3609E+05	3.9231E+04
5.5000E-01	2.3980E+01	1.5480E+01	5.4000E+02	4.1567E-02	6.1362E+05	4.2308E+04
5.9200E-01	2.4690E+01	1.5520E+01	5.4000E+02	4.1567E-02	5.9274E+05	4.5538E+04
6.2300E-01	2.5550E+01	1.5570E+01	5.4000E+02	4.1567E-02	5.8613E+05	4.7923E+04
6.6700E-01	2.6340E+01	1.5630E+01	5.4000E+02	4.1567E-02	5.5914E+05	5.1308E+04
7.1000E-01	2.7170E+01	1.5680E+01	5.4000E+02	4.1567E-02	5.4251E+05	5.4615E+04
7.4600E-01	2.8050E+01	1.5740E+01	5.4000E+02	4.1567E-02	5.3604E+05	5.7385E+04
7.8500E-01	2.8700E+01	1.5790E+01	5.4000E+02	4.1567E-02	5.1582E+05	6.0385E+04

TABLE 4 AIR MASS FLOW-PRESSURE DROP DATA FOR VIRGIN AVCOAT 5026-39-HCG

$w \sim lb_m/ft^2\text{-sec}$	$P_u \sim lb/ft^2$	$P_d \sim lb/ft^2$	$T \sim {}^oR$	$L \sim ft.$	$C \sim ft^{-1}$	$R_e \sim ft^{-1}$
4.8000E-03	1.5395E+01	1.4951E+01	5.3600E+02	4.1567E-02	3.2504E+08	3.6923E+02
5.7000E-03	1.5493E+01	1.4953E+01	5.3600E+02	4.1567E-02	2.8213E+08	4.3846E+02
6.7000E-03	1.5612E+01	1.4956E+01	5.3600E+02	4.1667E-02	2.4906E+08	5.1538E+02
7.7000E-03	1.5691E+01	1.4958E+01	5.3600E+02	4.1567E-02	2.1126E+08	5.9231E+02
8.7000E-03	1.5812E+01	1.4963E+01	5.3600E+02	4.1567E-02	1.9246E+08	6.6923E+02
9.7000E-03	1.5931E+01	1.4966E+01	5.3600E+02	4.1567E-02	1.7667E+08	7.4615E+02
1.0800E-02	1.6052E+01	1.4971E+01	5.3600E+02	4.1567E-02	1.6039E+08	8.3077E+02
1.1800E-02	1.6156E+01	1.4976E+01	5.3600E+02	4.1567E-02	1.4710E+08	9.0769E+02
1.2800E-02	1.6270E+01	1.4980E+01	5.3600E+02	4.1567E-02	1.3718E+08	9.8462E+02
1.4000E-02	1.6375E+01	1.4985E+01	5.3600E+02	4.1567E-02	1.2400E+08	1.0769E+03
1.5000E-02	1.6500E+01	1.4990E+01	5.3600E+02	4.1567E-02	1.1783E+08	1.1538E+03
1.6200E-02	1.6616E+01	1.4996E+01	5.3600E+02	4.1567E-02	1.0380E+08	1.2462E+03
1.7200E-02	1.6744E+01	1.5004E+01	5.3600E+02	4.1567E-02	1.0411E+08	1.3231E+03
1.8200E-02	1.6860E+01	1.5010E+01	5.3600E+02	4.1567E-02	9.9240E+07	1.4000E+03
1.2900E-02	1.6270E+01	1.4980E+01	5.3600E+02	4.1567E-02	1.3506E+08	9.9231E+02
7.7000E-03	1.5691E+01	1.4958E+01	5.3600E+02	4.1567E-02	2.1126E+08	5.9231E+02
2.8300E-02	1.7697E+01	1.5017E+01	5.3600E+02	4.1567E-02	5.1034E+07	2.1769E+03
3.5200E-02	1.8380E+01	1.5020E+01	5.3600E+02	4.1567E-02	5.0498E+07	2.7077E+03
4.2000E-02	1.9060E+01	1.5025E+01	5.3600E+02	4.1567E-02	4.3469E+07	3.2308E+03
4.9200E-02	1.9800E+01	1.5030E+01	5.3600E+02	4.1567E-02	3.8256E+07	3.7846E+03
5.6000E-02	2.0505E+01	1.5035E+01	5.3600E+02	4.1567E-02	3.4562E+07	4.3077E+03
6.2800E-02	2.1200E+01	1.5043E+01	5.3600E+02	4.1567E-02	3.1546E+07	4.8308E+03
7.0200E-02	2.1870E+01	1.5050E+01	5.3600E+02	4.1567E-02	2.8487E+07	5.4000E+03
7.7000E-02	2.2580E+01	1.5060E+01	5.3600E+02	4.1567E-02	2.5617E+07	5.9231E+03
8.3800E-02	2.3320E+01	1.5070E+01	5.3600E+02	4.1567E-02	2.5145E+07	6.4462E+03
9.1200E-02	2.3950E+01	1.5080E+01	5.3600E+02	4.1567E-02	2.3206E+07	7.0154E+03
9.8000E-02	2.4640E+01	1.5093E+01	5.3600E+02	4.1567E-02	2.2071E+07	7.5385E+03
1.0400E-01	2.5270E+01	1.5104E+01	5.3600E+02	4.1567E-02	2.1157E+07	8.0000E+03
1.1220E-01	2.5910E+01	1.5104E+01	5.3600E+02	4.1567E-02	1.9529E+07	8.6308E+03
1.1900E-01	2.6623E+01	1.5133E+01	5.3600E+02	4.1567E-02	1.8889E+07	9.1538E+03
1.1900E-01	2.6690E+01	1.5133E+01	5.3600E+02	4.1567E-02	1.9030E+07	9.1538E+03
1.2580E-01	2.7256E+01	1.5136E+01	5.3600E+02	4.1567E-02	1.8101E+07	9.6769E+03
1.3320E-01	2.7900E+01	1.5166E+01	5.3600E+02	4.1567E-02	1.7233E+07	1.0246E+04
1.0480E-01	2.5120E+01	1.4930E+01	5.3600E+02	4.1567E-02	2.0717E+07	8.0615E+03
7.7000E-02	2.2490E+01	1.4930E+01	5.3600E+02	4.1567E-02	2.6602E+07	5.9231E+03
3.5200E-02	1.8540E+01	1.4930E+01	5.3600E+02	4.1567E-02	5.4369E+07	2.7077E+03
1.2000E-03	1.5054E+01	1.4930E+01	5.3600E+02	4.1667E-02	1.4395E+09	9.2308E+01
1.4600E-03	1.5081E+01	1.4930E+01	5.3600E+02	4.1567E-02	1.1853E+09	1.1231E+02
1.7400E-03	1.5113E+01	1.4930E+01	5.3600E+02	4.1567E-02	1.0124E+09	1.3385E+02
1.8300E-03	1.5118E+01	1.4930E+01	5.3600E+02	4.1567E-02	9.4547E+08	1.4077E+02
4.2000E-03	1.5353E+01	1.4930E+01	5.3600E+02	4.1567E-02	4.0487E+08	3.2308E+02
6.5000E-03	1.5504E+01	1.4930E+01	5.3600E+02	4.1567E-02	2.6053E+08	5.0000E+02
7.7000E-03	1.5704E+01	1.4930E+01	5.3600E+02	4.1567E-02	2.2297E+08	5.9231E+02
9.7200E-03	1.5920E+01	1.4930E+01	5.3600E+02	4.1567E-02	1.8023E+08	7.4769E+02
1.1800E-02	1.6117E+01	1.4930E+01	5.3600E+02	4.1567E-02	1.4756E+08	9.0769E+02
1.3900E-02	1.6290E+01	1.4930E+01	5.3600E+02	4.1567E-02	1.2252E+08	1.0692E+03

FIGURE 19

PRESSURE DROP - MASS FLOW DATA FOR
AIR FLOW THROUGH THE APOLLO HEAT SHIELD MATERIAL

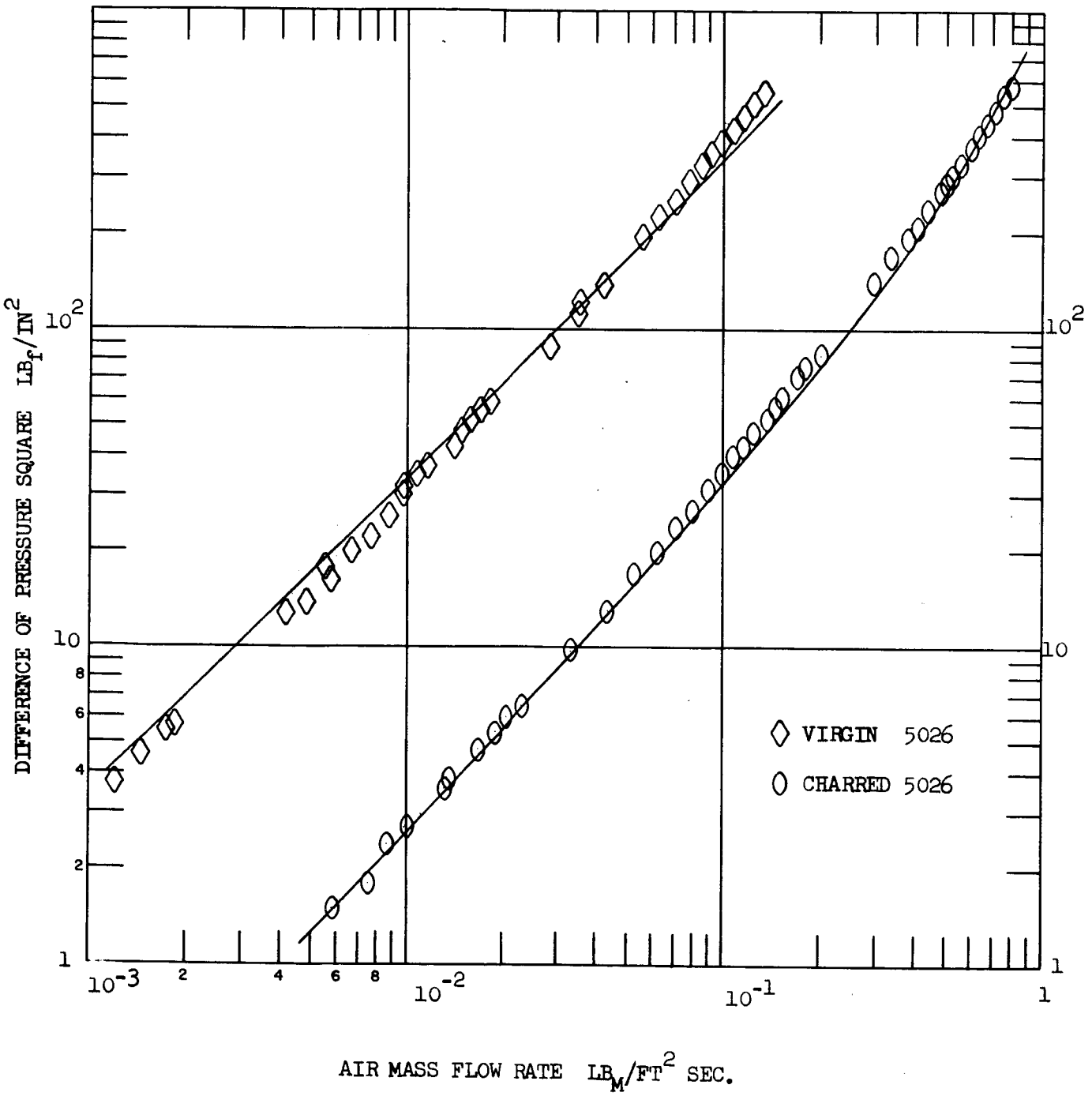

NOTE: USE TYPE B PENCIL FOR VUGRAPHS AND REPORT DATA.

The second term in the brackets of equation (175) is the ratio of the viscous force to inertial force. If the data of Tables (3) and (4) are applied to equation (175) the following inferences may be drawn. For the charred state of the material the test data extend into the region where the inertial effect is of the same order of importance as the viscous forces, i.e.

$$\left(\frac{\beta_c}{\alpha_c} R_e\right) \approx 2.0$$

However, the test data for the virgin state of the material is entirely in the viscous region, i.e.

$$\left(\left|\frac{\beta_v}{\alpha_v} R_e\right|\right)_{MAXIMUM} \approx 1.0 \times 10^{-3}$$

It appears that the negative value of the inertial coefficient, β_v is the result of trying to fit a parabola to data which will only justify a straight line. The small amount of scatter in the data which is all in the viscous region is sufficient to produce the physically meaningless negative β_v, at least when considered within the context of the assumed model given by equation (168). The least square straight line through the data for the virgin state results from making $\beta_v = 0$ and calculating α_v from equation (173). This calculation gives;

$$\alpha_v = 7.153 \times 10^{10} \text{ ft}^{-2} \tag{176a}$$

$$\beta_v = 0.0 \tag{176b}$$

Since no measurements have been made for intermediate states of the Apollo material, the assumption is made that the inertial and viscous resistance coefficients are linear functions of the density of the material, i.e.

$$\alpha = \alpha_v - \left(\frac{\alpha_v - \alpha_c}{\rho_o - \rho_c}\right)(\rho_o - \rho) \tag{177a}$$

$$\beta = \beta_c \left(\frac{\rho_o - \rho}{\rho_o - \rho_c}\right) \tag{177b}$$

Some further comments are necessary concerning the derivation of resistance coefficients from test data on mass flow through the Apollo material. In order to show conclusively that the coefficients α and β appearing in equation (169) are material characteristics and are independent of the flowing gas it would be necessary to include in the test program a series of experiments with gases having significantly different molecular weights, e.g. helium and nitrogen. Equation (169) also dictates that both

pressure level and not merely pressure drop must be varied to demonstrate the validity of the model. Since the test data for the Apollo material were obtained by using one gas, air, and varying only the pressure drop, the application to another gas and other pressures is at present an extrapolation of the data.

3.2.3 Verification of The Model

There is some support given to equation (169) from other test data obtained at Avco for charred RAD-60 PMTS (a silica phenolic heat shield material) using nitrogen and helium as gases. These data were also taken for various sample thicknesses which is theoretically equivalent to changing pressure levels since either parameter varies the gradient of pressure squared appearing in equation (168). The data from these experiments are shown in Figures (20) and (21) plotted as pressure drop variation with mass flow for a constant thickness. Figure (20) shows the nitrogen results and Figure (21) those for helium.

By applying a least square analysis to these data for charred RAD-60 PMTS all of the test points are made to fall near one curve representing equation (169) as demonstrated in Figure (22).

Additional support for the proposed correlation may be found in the literature. Green and Duwez, Reference (15), applied equation (171) to gas flow through porous metal with excellent correlation. Green, Reference (16) reports good agreement of equation (169) for flow through packed beds of sphere and wire screen matrices. Finally, Muskat, Reference (17) discusses various models and presents data for the flow of water through shot of uniform size and air flow through packed glass beads. In both cases Muskat employs a simple quadratic equation in mass flow to correlate the differential of squares of pressure.

Pressure distribution for Apollo application are calculated using equation (168) and the values of the resistance coefficients given by equation (174), (176), and (177).

3.3 Radiative Test Data

Many situations of interest in thermal protection system design involve significant radiative heating. One of the more important properties of the material in such circumstances is the absorptivity. Among the unfortunate facts of life for the analyst, there does not appear to be any currently available method for the direct measurement of this quantity under the conditions appropriate to the problem. Reflectivity measurements made at room temperature on surfaces previously exposed to a high temperature environment are at best of questionable value since the temperatures of interest may be higher by several thousand degrees and a different physical state may actually be involved for the surface material. As a result of this state of affairs, it is necessary to examine possible indirect techniques for deducing a value for the absorptivity. One such technique based on data obtained in experiments involving pure radiative transfer is described in the following paragraphs.

Consider an experiment in which a sample of material is exposed to a radiative energy source in a gaseous environment which plays no role in the ablation process. In the case where the experimental conditions approach steady state an energy balance on

FIGURE 20

MASS FLOW RATE OF HELIUM RESULTING FROM A PRESSURE DROP ACROSS CHARRED RAD 60 PMTS SAMPLES

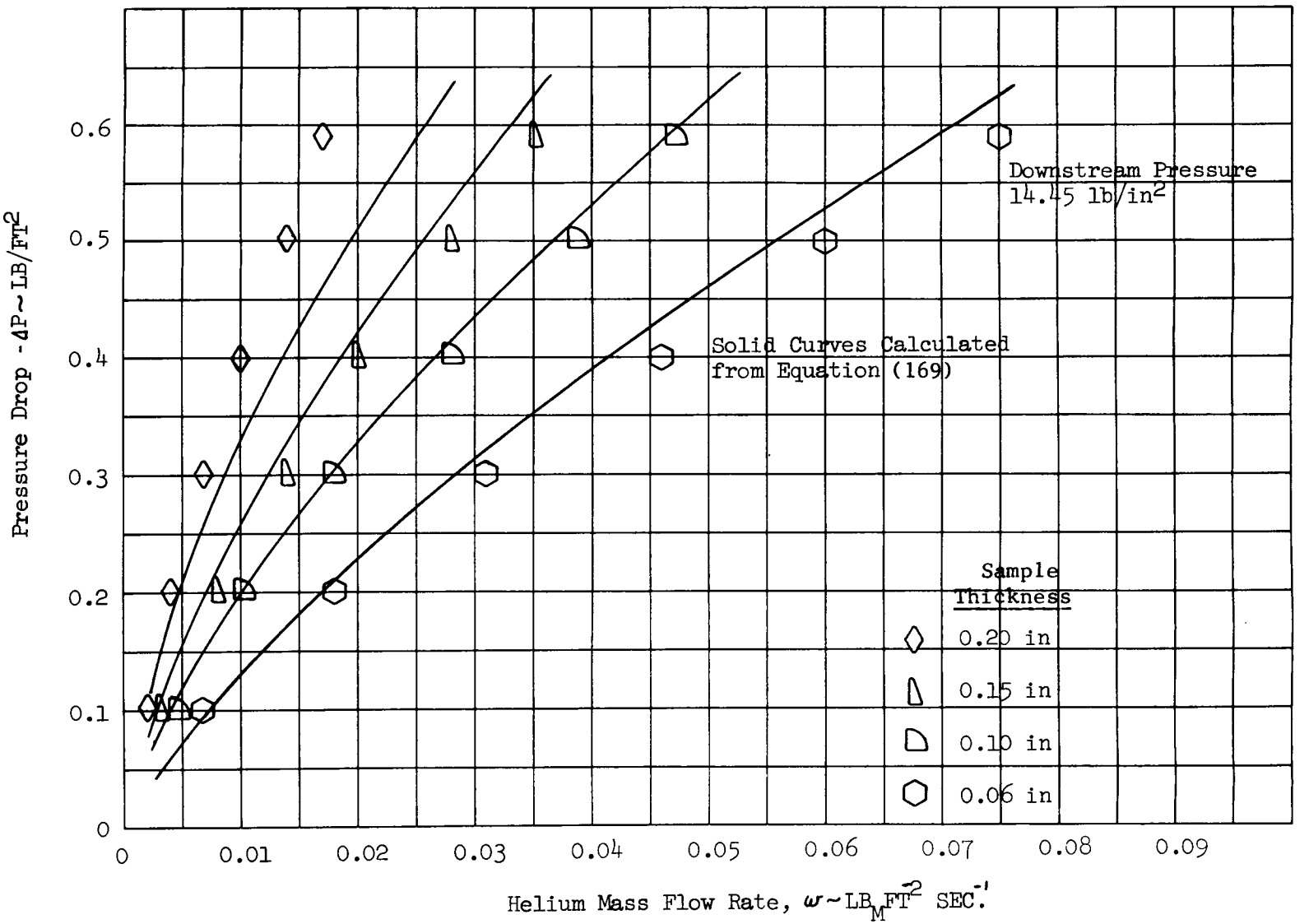

FIGURE 21

MASS FLOW RATE OF NITROGEN RESULTING FROM A
PRESSURE DROP ACROSS CHARRED RAD 60 PMTS SAMPLES

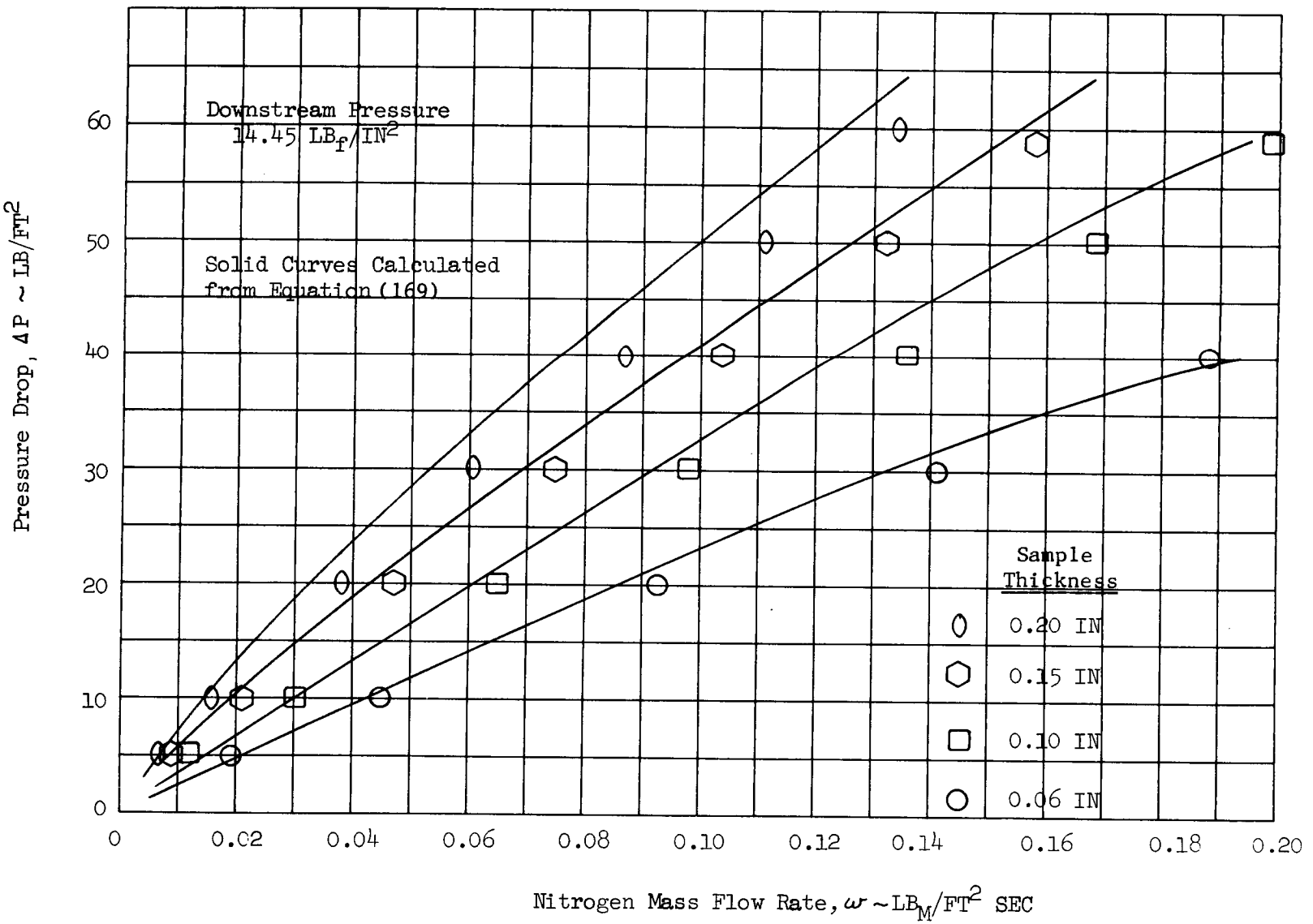

FIGURE 22

CORRELATION OF NITROGEN AND HELIUM MASS FLOW DATA WITH PRESSURE FOR VARIOUS THICKNESSES OF CHARRED RAD 60 PMTS

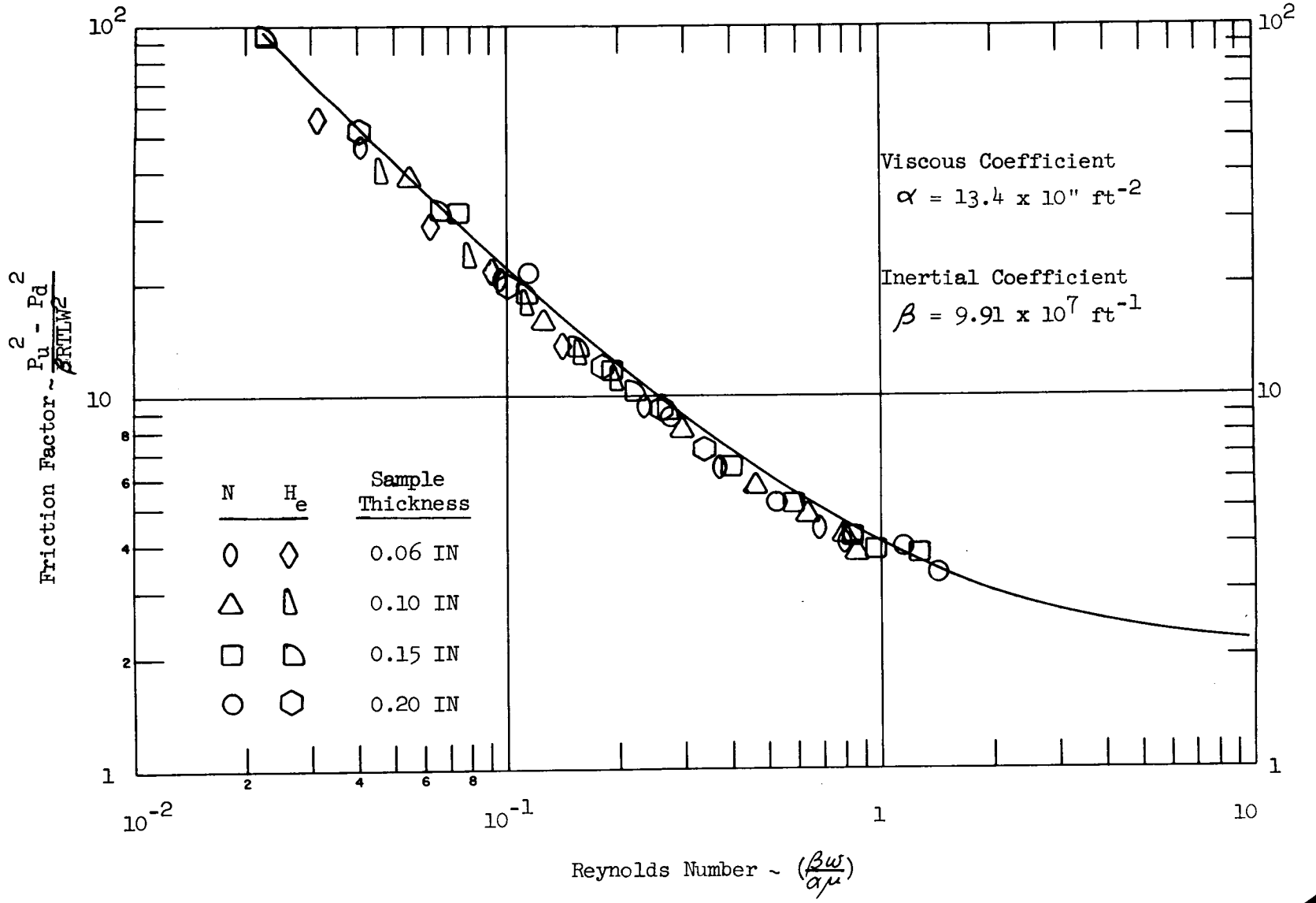

NOTE: USE TYPE B PENCIL FOR VUGRAPHS AND REPORT DATA.

the system can be written in the form of equation (178).

$$\alpha F_s - \epsilon \sigma T_s^4 = \dot{m} H_a \tag{178}$$

In equation (178) α is the absorptivity, F_s is the incident radiant flux, ϵ is the surface emissivity, T_s is the surface temperature, $\dot{m}$ is the steady state mass transfer rate, and H_a is a heat of ablation. Equation (178) can be re-arranged to yield equation (179).

$$\epsilon Y = - H_a + \alpha X \tag{179}$$

where: $Y = T_s^4/\dot{m}$

$X = F_s/\dot{m}$

Given a set of experiments in which F_s, T_s and $\dot{m}$ are measured, equation (179) provides the basis for a relationship between the absorptivity, α, and the emissivity, ϵ. In principle equation (179) also offers the possibility of obtaining the heat of ablation H_a from the same set of test data. In practice this is impractical due to the large differences in the magnitudes of H_a and the quantities X and Y. This will be apparent by an examination of a set of test data.

Figure (23) shows a set of test results obtained by the Southwest Research Institute on Avcoat 5026-39 using an arc imaging furnace in an argon atmosphere. The data are plotted in the form of Y as a function of X as defined in equation (179). As can be seen from the figure, an apparently linear relationship exists as indicated by equation (179). Also apparent are the difficulties inherent in an attempt to obtain the intercept with any accuracy. Since the apparent intercept is near zero and the data analysis can be simplified if it is assumed to be zero this assumption is made in the present case.

The non-steady effects discussed in Section 3.1.1 have an effect on the interpretation of the data in the present case since equation (178) is strictly valid only for a steady state experiment. In the present case, however, this effect is smaller than in the interpretation in terms of ablative performance. This is due to the fact that H_a is small compared to the X and Y of equation (179) and since the non-steady effects appear primarily in $\dot{m}$, both X and Y are affected in the same fashion. Unlike the usual treatment of linear relationships where one or the other variable is assumed to be free from error the present technique assumes equal probable errors in both Y and X. Under this assumption the application of the principle of least squares leads to equation (180) as the appropriate relationship between α and ϵ.

$$\alpha^2 + \left\{ \frac{\sum x_i^2 - \epsilon^2 \sum y_i^2}{\epsilon \sum x_i y_i} \right\} \alpha - 1 = 0 \tag{180}$$

FIGURE 23 SWRI RADIATIVE TEST DATA

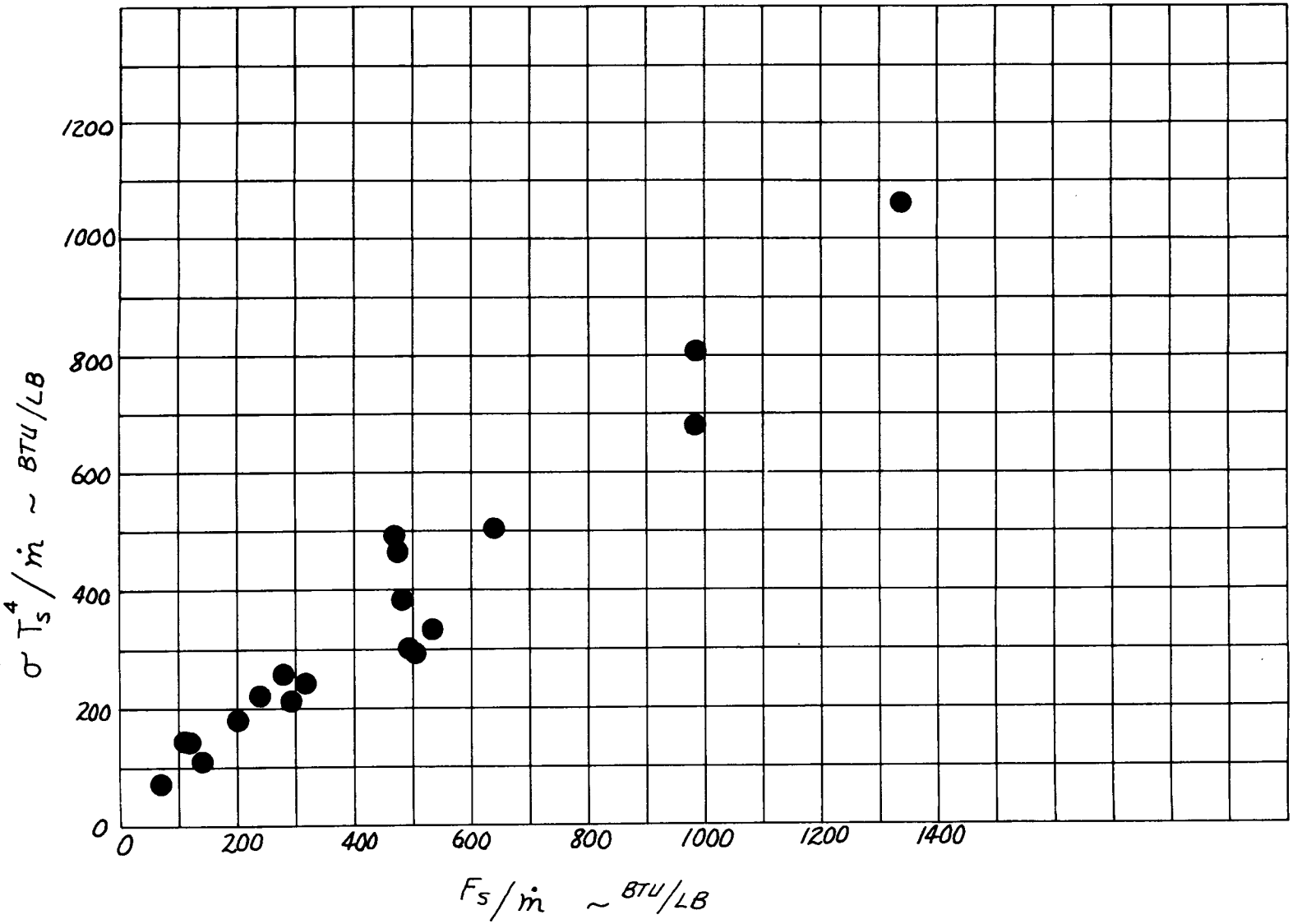

Application of equation (180) to the SWRI test data yields the relation between α and ϵ plotted in Figure (24). Also indicated on Figure (24) is the relation frequently employed for opaque materials, namely, that the absorptivity equals the emissivity.

Use of the value 0.667 obtained for the emissivity during the analysis of the ablation data in Section 3.1.4 yields a value of 0.5 for the absorptivity.

3.4 Treatment of Pyrolysis Kinetics Data

One of the problems associated with a proper analysis of the performance of char forming materials for thermal protection systems is that of obtaining an accurate mathematical description of the kinetics of the char forming pyrolysis reaction. The treatment of this reaction as a part of the overall analysis of charring ablator performance is limited by the techniques available for experimentally determining the proper kinetics of these reactions. Even within the framework of currently available tecnniques for experimental measurement very limited attention has been given to the problem of obtaining realistic kinetic parameters from the experimental data. In general the groups which carry out the experimental investigations either attempt on interpretation of their data or when such an interpretation is made it is entirely inadequate for the purposes of the engineer who must utilize the information in the design of thermal protection systems.

The most common type of experiment employed for the purpose of defining the pyrolysis kinetics of charring ablators is the linear thermogravimetric analysis (LTG) experiment in which simultaneous measurements are obtained for sample weight and temperature under conditions such that the sample temperature is a linear function of time. The analysis usually employed is limited to those materials in which the limiting fully charred sample weight is independent of temperature or to situations in which the application of the material to a vehicle allows this assumption to be made without significant error. This latter class of applications includes most ballistic missile systems which are quite insensitive to the details of the pyrolysis kinetics. The assumption of a temperature independent limiting sample weight is totally inadequate for the analysis of manned reentry vehicle thermal protection systems. The sensitivity of these latter systems to the pyrolysis kinetics is a result of the relatively mild environmental conditions and ling soak times associated with this type of entry.

3.4.1 Analysis Method

The analysis of Section 2.0 and the computer program described in Volume II employs equation (181) as the differential equation describing the pyrolysis kinetics.

$$\frac{\partial \xi}{\partial t} = -\sum_{i=1}^{3} A_i \left\{ \xi - \xi_{c_i} \right\}^{N_i} \exp\left\{ -\frac{B_i}{T} \right\} \tag{181}$$

In equation (181) the quantity ξ is the instantaneous weight of material in the control volume and ξ_c is the limiting weight associated with the i'th reaction step. The program allows all quantities A, N, ξ_c and B to be arbitrary functions of temperature, time, space, etc. Equation (181) thus provides the basis for a very versatile description

FIGURE 24

ABSORBTIVITY BASED ON SWRI ABLATION DATA

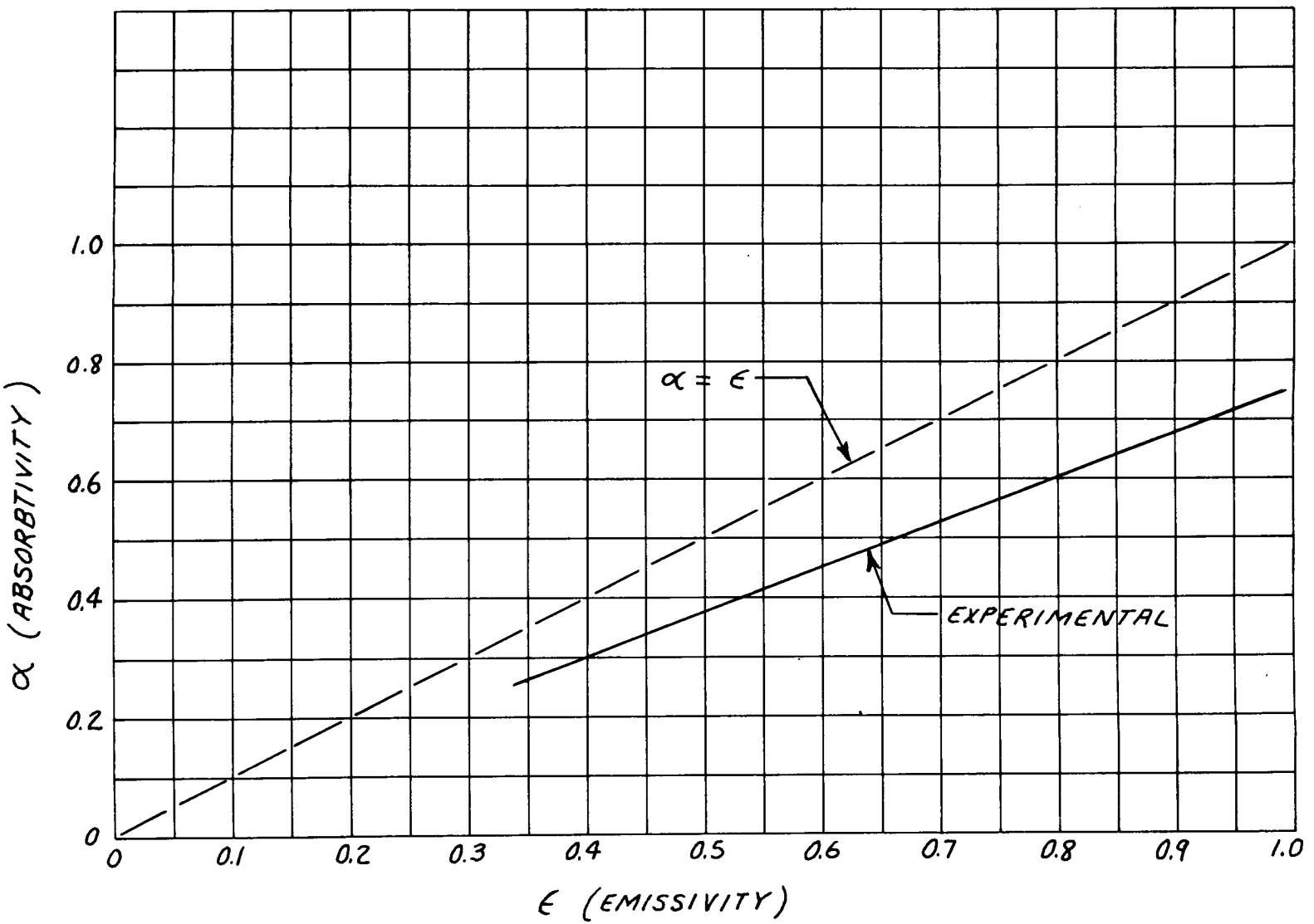

of the pyrolysis kinetics. On the basis of the observed LTG curves for materials of interest it would appear to be of dubious value to attempt a data analysis which employs more than one term in equation (181). The sole exception to this is that group of materials which appears to undergo an initial dehydration or curing process at temperatures somewhat below those required for the primary pyrolysis. Application of a single term of equation (181) to the experimental situation presented by the LTG tests yields equation (182) where the quantity is the instantaneous fractional sample weight and (T) is its limiting value which is considered an arbitrary function of temperature. The quantity β is the reciprocal of the time rate of change of temperature. Although in an LTG experiment β is a constant the present data analysis does not require this restriction and it will therefore not be imposed and β will be taken as an arbitrary function of temperature.

$$\frac{d\omega}{dT} = A\beta(T)\left\{\omega - \bar{\omega}(T)\right\}^{N} \exp\left\{-\frac{B}{T}\right\} \tag{182}$$

Equation (182) may be integrated to yield an expression for a calculated fractional weight at the i'th experimental point in terms of the experimental LTG and limiting weight curves together with the constants A, N and B. Designating this calculated weight fraction as $\hat{\omega}$ (i) we obtain equation (183) where η has been introduced as a variable of integration.

$$\hat{\omega}(i) = 1 - A\int_{\eta=T_0}^{T_i} \beta(\eta)\left\{\omega(\eta) - \bar{\omega}(\eta)\right\}^{N} \exp\left\{-\frac{B}{\eta}\right\} d\eta \tag{183}$$

It should be noted that the function $\bar{\omega}(\eta)$ is a limiting case of $\omega(\eta)$ as given by equation (184).

$$\bar{\omega}(\eta) = \lim_{\beta \to \infty} \omega(\eta) \tag{184}$$

An expression for the deviation between measured and computed values of ω can be obtained from equation (183).

$$\delta(i) = \omega(i) - \hat{\omega}(i) = \omega(i) - 1 + A H_1(i) \tag{185}$$

where:

$$H_1(i) = \int_{\eta=T_0}^{T_i} \beta(\eta)\left\{\Delta(\eta)\right\}^{N} \exp\left\{-\frac{B}{\eta}\right\} d\eta \tag{186}$$

$$\Delta(\eta) = \omega(\eta) - \bar{\omega}(\eta) \tag{187}$$

We now define the quantity F by equation (188) where a weighting function u(i) has been introduced.

$$F = \sum_i u(i) \left\{ \delta(i) \right\}^2 \tag{188}$$

The condition for a "best" fit to the experimental data is then taken as that given by equation (189).

$$\frac{\partial F}{\partial A} = \frac{\partial F}{\partial N} = \frac{\partial F}{\partial B} = 0 \tag{189}$$

The pyrolysis reaction which takes place in the material has been examined using the data which appear in the data library together with the analysis just described. Figure (25) is typical of the data obtained from the linear thermogravimetric experiments in an inert atmosphere. As can be seen from the figure, there is typically about a 5% loss in weight of the sample at low temperatures due to removal of water from the system. In the overall ablation problem this effect is not large but should be accounted for. Inclusion of this effect leads to a two term rate expression to describe the overall kinetics of the combined water loss and pyrolysis kinetics. The equation obtained for this system is thus given by equation (190).

$$\frac{d}{dt}\left(\frac{\rho}{\rho_0}\right) = A_1 \left\{ \left(\frac{\rho}{\rho_0}\right) - \left(\frac{\rho_{c1}}{\rho_0}\right) \right\}^{N_1} EXP\left\{ - \frac{B_1}{T} \right\} + A_2 \left\{ \left(\frac{\rho}{\rho_0}\right) - \left(\frac{\rho_{c2}}{\rho_0}\right) \right\}^{N_2} EXP\left\{ - \frac{B_2}{T} \right\} \tag{190}$$

The constants in the first term representing the water loss are estimated and those for the pyrolysis reaction obtained from the LTG data taken in an inert atmosphere. The values obtained by this process are shown in Table (5).

FIGURE 25
LTG DATA ON AVCOAT 5026-39
HELIUM ATMOSPHERE

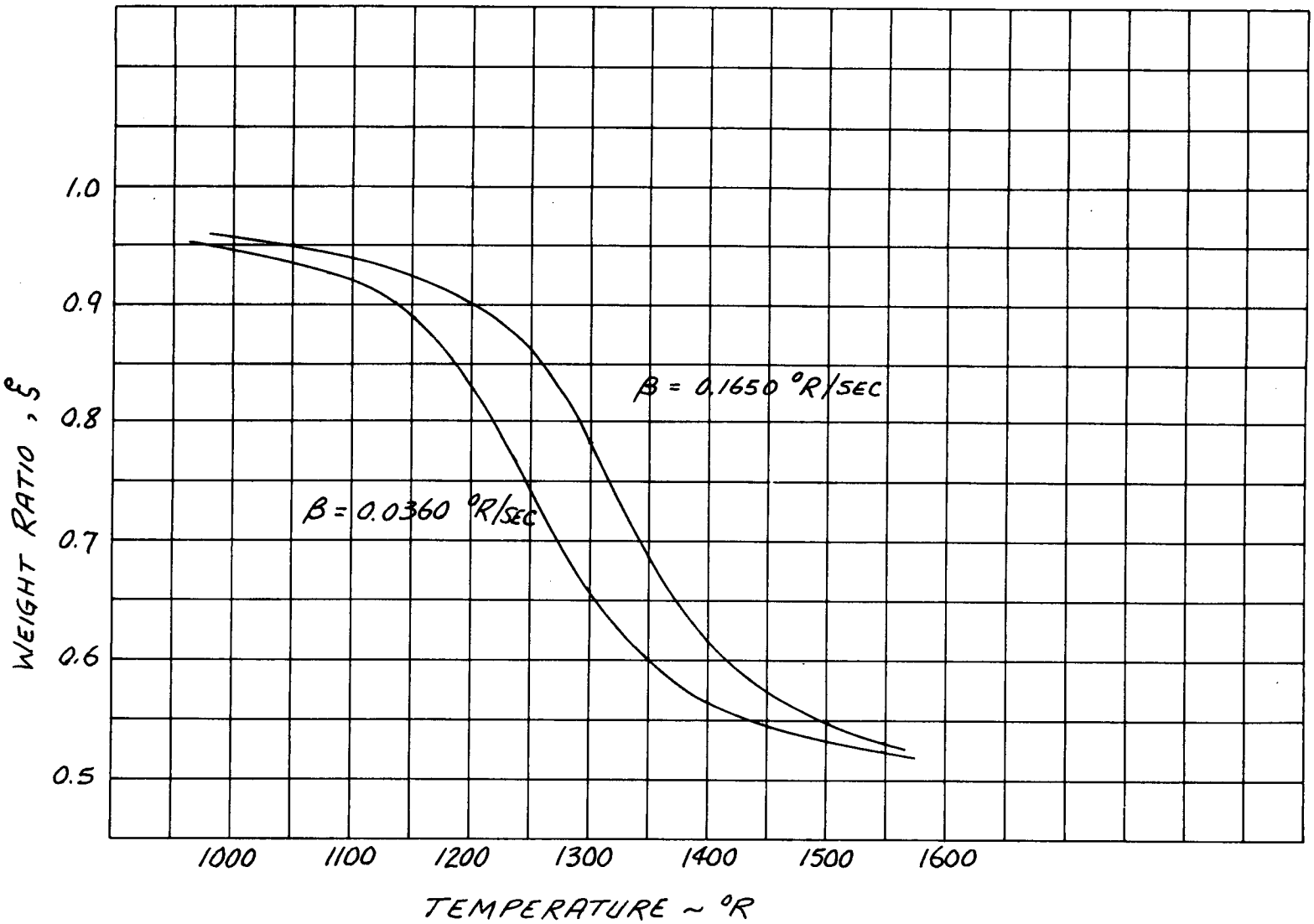

Table (5)

Water Loss and Pyrolysis Rate Constants

Equation (190)

	Detailed Analysis	Approximate Analysis
A_1	10^7 sec^{-1}	
N_1	1.0	
B_1	12000°R	
(ρ_{c1}/ρ_o)	0.95	
A_2	3.26×10^5 sec^{-1}	9.83×10^5 sec^{-1}
N_2	2.0	2.1
B_2	21480°R	22660°R

T °R	(ρ_{c2}/ρ_o)
0	0.95
1000	0.95
1100	0.945
1150	0.890
1200	0.860
1250	0.740
1300	0.655
1350	0.600
1400	0.565
1450	0.545
1500	0.525
1600	0.50
∞	0.50

3.4.2 Approximate Method

The values listed as approximate in Table 5 have been obtained by the following technique. An approximate method for obtaining pyrolysis rate constants from the thermogravimetric data without resort to a computer can be obtained on the basis of equation (182). Equation (182) can be written as equation (191)

$$\frac{(dw/dt)}{\beta(w-\bar{w})} = -A\left\{w-\bar{w}\right\}^{(N-1)} EXP\left\{-\frac{B}{T}\right\} \qquad (191)$$

The derivative appearing on the left hand side of (191) is then evaluated either numerically or graphically from the LTG data. Using these numerically obtained derivatives the quantities A, N and B can be obtained in a straight-forward manner by the method of least squares applied to equation (191) in the form of equation (192)

$$ln\left\{\frac{-(dw/dt)}{\beta(w-\bar{w})}\right\} = ln\,A + (N-1)\,ln\,(w-\bar{w}) - \frac{B}{T} \qquad (192)$$

The LTG data in Figure 25 have been employed to obtain graphically the derivatives (dw/dt). The limiting densities of Table 5 are also employed. Equation (192) can be written in a linear form by means of the following transformation.

$$Y_i = ln\left\{\frac{-(dw/dt)_i}{\beta(w_i-\bar{w}_i)}\right\} \qquad (193a)$$

$$X_i = ln\,(w_i - \bar{w}_i) \qquad (193b)$$

$$Z_i = -\left(\frac{1}{T_i}\right) \qquad (193c)$$

$$K_1 = ln\,A \qquad (193d)$$

$$K_2 = (N-1) \qquad (193e)$$

$$Y_i = K_1 + K_2 X_i + B Z_i \qquad (194)$$

The normal equations corresponding to this system are (195) through (197) where the summations extend over the number of points taken from the LTG curve, M.

$$\sum_i Y_i = K_1 M + K_2 \sum_i X_i + B \sum_i Z_i \qquad (195)$$

$$\sum_i X_i Y_i = K_1 \sum_i X_i + K_2 \sum_i X_i^2 + B \sum_i Z_i X_i \qquad (196)$$

$$\sum_i Z_i Y_i = K_1 \sum_i Z_i + K_2 \sum_i X_i Z_i + B \sum_i Z_i^2 \qquad (197)$$

Equations (195) through (197) are then easily solved for K_1, K_2, and B with A and N then obtained from (193d) and (193e).

Application of this technique to the LTG data on the Apollo material yields the rate constants appearing in Table (5). The temperature dependance of the limiting char density is taken to be the same as that indicated in Table (5). As can be seen by a comparison of the values in the two tables there is little difference between the two techniques for this case.

Figure 26 shows a comparison between the observed and calculated values of fractional weight loss for several points on the LTG curve.

3.5 Density, Thermal Conductivity and Specific Heat Data

The direct measurements of thermal conductivity and specific heats have been employed to obtain values for these quantities where possible. All of the available data have been reported in the data library. An examination of the data on the thermal conductivity of the virgin material indicates that this quantity is a function of both the individual sample density and the temperature. Equation (198) has been obtained from the data as a reasonable representation of this functional relationship with ρ_o being the virgin material density in lb/ft^3 and T being the temperature in degrees Rankine.

$$k_o \text{ (Btu/ft-hr-}^\circ\text{R)} = -0.0187 \quad 0.0020\rho_o + 0.217 \times 10^{-4}T \qquad (198)$$

Also based on the data in the library a value of 33.0 lb/ft^3 has been selected as a standard density for the virgin material. This selection together with equation (198) yields equation (199) for the nominal thermal conductivity of the virgin material.

$$k_o \text{ (Btu/ft-hr-}^\circ\text{R)} = 0.0473 + 0.217 \times 10^{-4}T \qquad (199)$$

The thermal conductivity of the charred material is somewhat more questionable than that of the virgin material. This is particularly true in the temperature region of primary interest for this quantity (1000 $\rightarrow$ 5000°R). Not enough data are available to justify the use of a temperature dependent thermal conductivity in the high temperature region, therefore the use of a constant value is indicated for design purposes. Based on the limited data available in the library and to some extent on a comparison of measured and predicted temperatures for instrumented ground test ablation experiments, a value of 0.19 Btu/ft-hr-°R has been selected as nominal. Further work with the instrumented ground tests and to some extent data from well instrumented flight tests may be able to improve this choice somewhat.

FIGURE 26

COMPARISON OF MEASURED AND PREDICTED LTG CURVE

β = 0.1650 °R/Sec.

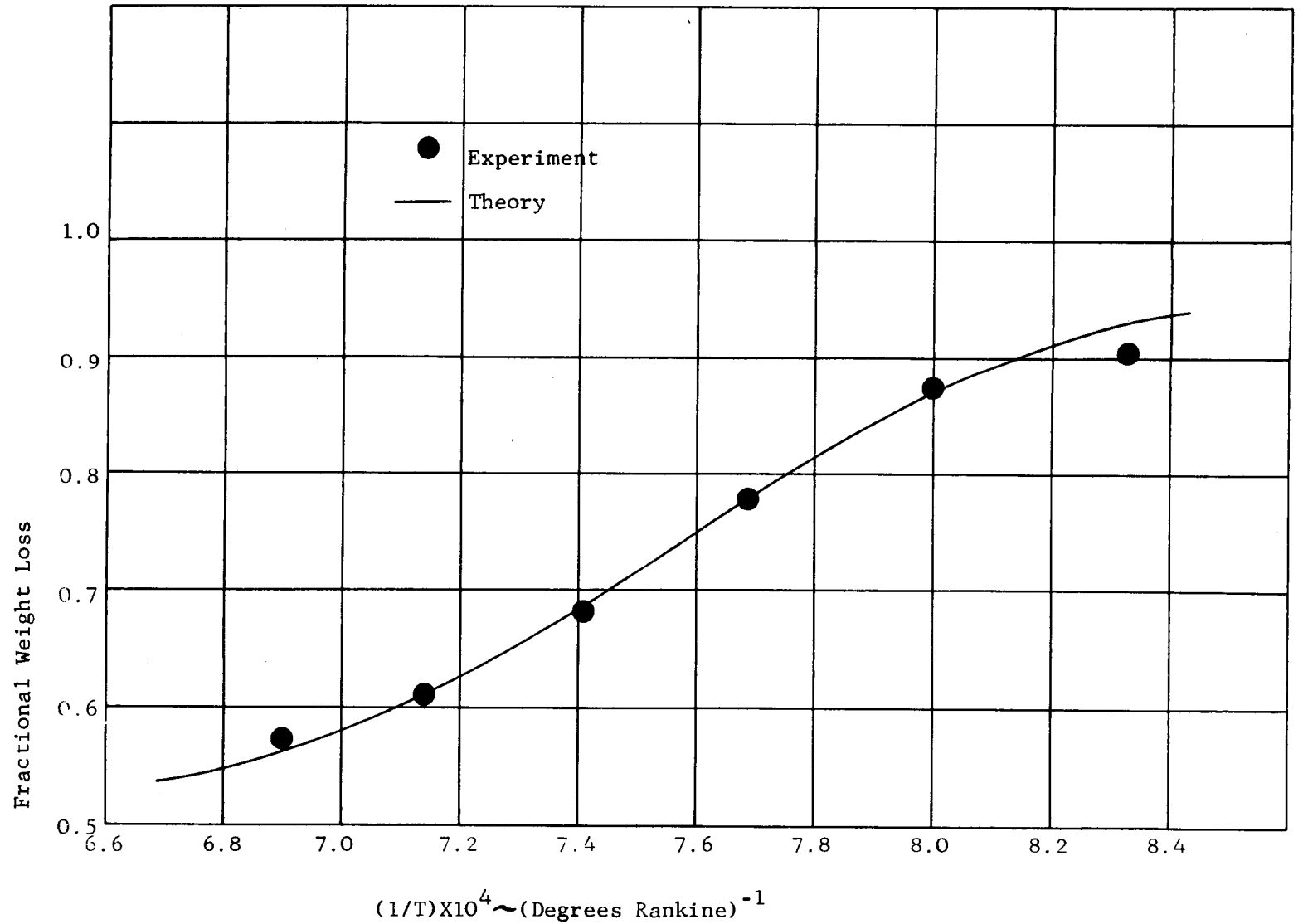

The specific heat of the virgin material is obtained from an examination of the direct measurements reported in the data library. Although some anomalies appear in the data, they appear to be due to the influence of the pyrolysis reaction which is considered separately. Equation (200) has been selected as representative of the virgin material specific heat.

$$C_{p_o}\ (\text{Btu/lb-}^{\circ}\text{R}) = 0.20 + 0.22 \times 10^{-3} T \qquad (200)$$

An assessment of the high temperature specific heats of the gaseous pyrolysis products and of the charred material is aided by a thermochemical equilibrium analysis of the non-silica components of the material. A product of the calculations described in Section 3.2 is an estimate of the high temperature specific heats of both the gaseous pyrolysis products and of the char residue. These results are shown in Figure (27). Also shown on this figure are several measurements of char specific heat as reported in the data library. As can be seen from the figure, excellent agreement is obtained between experiment and theory for this particular quantity. The theoretical values indicated in Figure (27) are taken as the nominal values for these two specific heats.

3.6 Estimated Properties

In order to completely describe the performance of the Apollo material using the formulation of Section 2.0, it is necessary to assign values to several quantities which are not uniquely determined by the existing experimental data.

At low values of surface temperature the heterogeneous reaction between the surface material and the environmental fluid will take place at a rate which is too small to allow a diffusion limited process to take place. This is the rate controlled ablation regime discussed in Section 2.9.1. In order to account for this fact and in order to provide a smooth transition into the diffusion controlled process it is necessary to provide estimates of the rate constants associated with this regime. Since it is unlikely that such a reaction takes place between the virgin material and the environmental fluid the reaction rate is assumed to be a function of both the surface temperature and the extent of the pyrolysis reaction at the heated surface. The form assumed for the reaction rate is given by equation (201) which is an extension of equation (78) of section 2.9.1.

$$\dot{S}_R = \left(\frac{W_c A_r}{\rho_s}\right)\left\{\frac{\rho_o - \rho_s}{\rho_o - \rho_c}\right\}\left\{\mu_e W_s P_e\right\}^{N_r} EXP\left\{-\frac{B_r}{T_s}\right\} \qquad (201)$$

Equation (201) differs from equation (78) by the factor $W_c(\rho_o - \rho_s)/(\rho_o - \rho_c)$ which is simply the available free carbon at the surface.

FIGURE 27
EQUILIBRIUM PREDICTIONS AVCOAT 5026-39
P = 1.0 ATM.

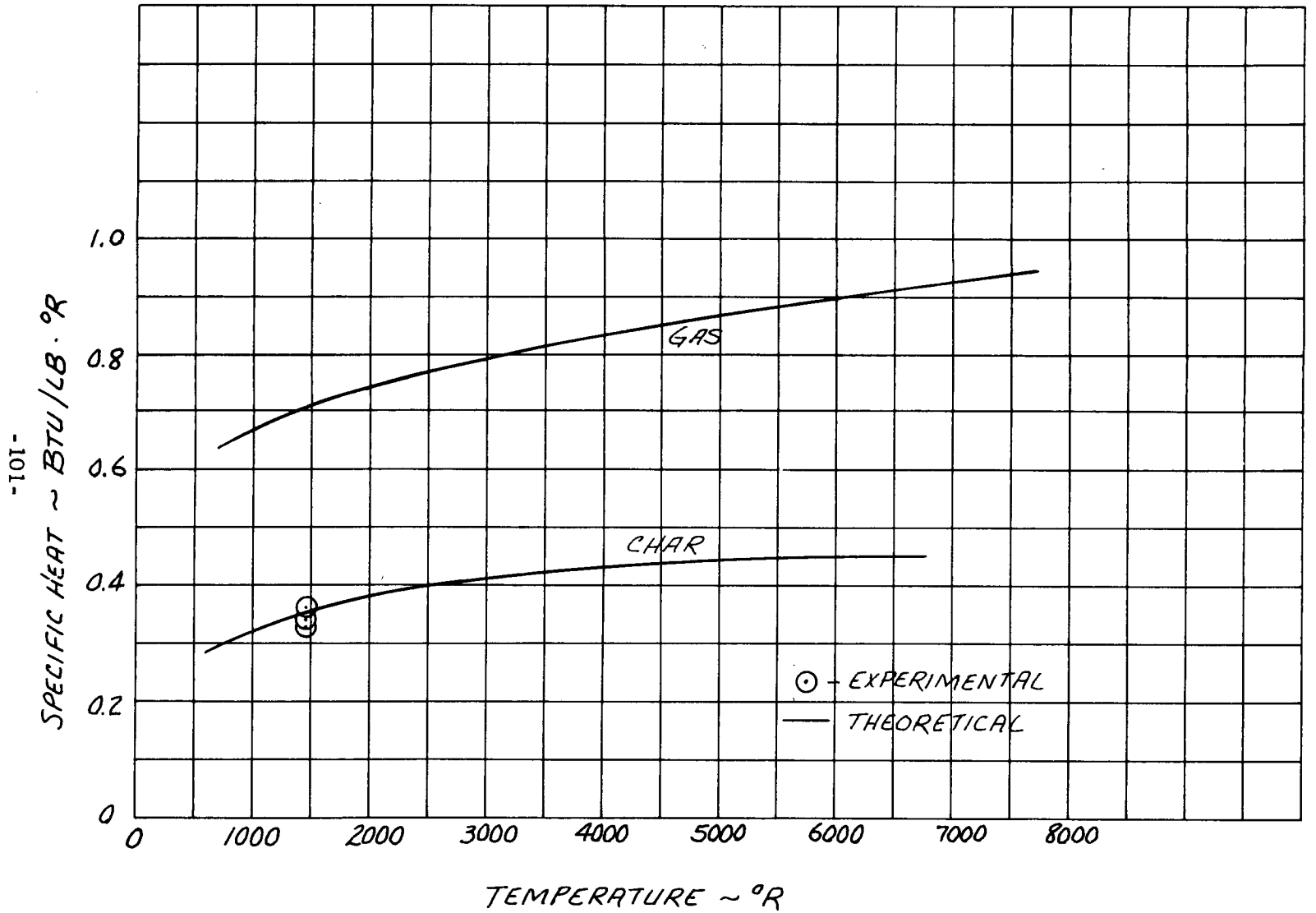

where:

A_r = 54.0 lb/ft^2-sec

N_r = 0.5

B_r = 17000°R

W_c = 0.329

μ_1 = 28.96/32.0

ρ_o = 33.0 lb/ft^3

ρ_c = 16.5 lb/ft^3

The numerical values of A_r, N_r and B_r have been assigned on the basis of data obtained on the porous carbon char surface of a carbon fiber reinforced phenolic material known as Avco REST 6300 HP. The use of these values in the case of the present material is highly suspect and is necessitated by the absence of appropriate test data on the Apollo material. Rather large changes in these constants have only minor effects on most design calculations and this fact allows their use with some confidence in the end product of a vehicle design which is, after all, the goal of any such model.

At the other extreme of the surface temperature range it is necessary to provide for a transition to some type of vaporization controlled mechanism as discussed in Section 2.9.4. In the case of the Apollo material it is assumed that at sufficiently high surface temperatures the surface recession process is controlled by the vaporization rate of carbon. Equations (86) and (89) of Section 2.9.4 can be written as equations (202) and (203).

$$\dot{S}_s = \left(\frac{1}{\rho'}\right)\left\{\frac{\bar{\mu}}{2\pi R T_s}\right\}^{1/2} P_v \left\{1 - \frac{P_a}{P_v}\right\} \qquad (202)$$

$$P_a = \frac{(1-\phi)\, P_e}{1 + \left\{\left(\bar{\mu}/\mu_o\right) - 1\right\}\phi} \qquad (203)$$

In these equations $\bar{\mu}$ is the mean molecular weight of the vaporizing gas, ρ' is the density of pure carbon, R is the universal gas constant, P_v is the equilibrium vapor pressure of the vaporizing species, μ_o is the mean boundary layer molecular weight, P_e is the local static pressure and ϕ is the usual blowing effect on heat transfer coefficient.

Using the data on carbon vapor from the JANAF tables (Reference 12) for the thermodynamic quantities appearing in these two equations leads to the following relations for the ablation rate in the sublimation regime.

$$\dot{S}_s\,(ft/sec) = \left[9.1 \times 10^{8}\; T_s^{0.28}\; EXP\left\{-\frac{161000}{T_s}\right\}\right]\bar{B} \qquad (204)$$

$$\bar{B} = 1 - \frac{(1-\phi)\, P_e}{0.174 \times 10^{12}\, \mathrm{EXP}\left\{-\frac{163200}{T_s}\right\}} \qquad (205)$$

It is of interest to examine the overall relationships between ablation rate and surface temperature throughout the temperature regime from very low to very high. In order to accomplish this an expression for the diffusion limited ablation rate is required. This is obtained from the experimental data in Section 3.1.4. Equation (162) can be written as equation (206).

$$\dot{S}_D \text{ (ft/sec)} = 0.03136 \left(\rho_c / H_s\right)\phi \qquad (206)$$

Equations (201) and (202) then combine to yield the ablation velocity in the heterogeneous reaction regime in accordance with the analysis of Section 2.9.3.

$$\dot{S}_H = \dot{S}_D \left\{1 - \left(\frac{\dot{S}_H}{\dot{S}_R}\right)^2\right\} \qquad (207)$$

At a given surface temperature the applicable ablation rate is the larger of the two given by equation (202) and (207). A complete description of the surface behavior requires an energy balance as given by equations (94) and (95). Equations (94) and (95) as applied to a steady state process yield equation (208)

$$\left(\frac{\rho_c}{H_s}\right)\left\{H_s - H_w + H'\right\}\phi - \epsilon\sigma T_s^4 = \rho_c \dot{s} H_v + (\rho_o - \rho_c)\dot{s} C_q (T_s - T_r)$$

$$+ (\rho_o - \rho_c)\dot{s}\,\Delta H_c + \rho_c \dot{s} C_{p_c}(T_s - T_r) + \rho_o \dot{s} C_{p_o}(T_r - T_o) \qquad (208)$$

where:

$$H' = W_e H_c \left\{1 - \left(\frac{\dot{s}}{\dot{s}_R}\right)^2\right\}$$

Using 1500° R as an average reaction zone temperature, T_m and the values previously selected for the quantities appearing in equation (208), equations (201), (202), (203), (204), (205) and (208) have been solved simultaneously for a number of conditions.

Figure 28 shows the ratio of the ablation velocity to the diffusion limited ablation velocity, $(\dot{S}/\dot{S}_D)$ as a function of surface temperature for several values of the total pressure. The values in Figure 28 are for stagnation point ablation and assume a fixed value for the stagnation point heat transfer parameter given by equation (209).

$$\frac{q_c}{H_s \sqrt{P}} = 0.10 \ \text{Lb/FT}^2 \cdot \text{sec} \cdot \text{atm}^{1/2} \qquad (209)$$

The value chosen for this parameter is typical of ground test facilities. It is noted that the curves for all pressures coincide in the regime of heterogeneous chemical ablation. The reason for this is easily seen when it is noted that at a given temperature $\dot{S}_R$ is proportional to the square root of pressure as shown in equation (201) and that $\dot{S}_D$ is also proportional to the square root of pressure through the heat transfer coefficient according to the ground rule of Figure 28 and expressed by equation (209). Since the curve in Figure 28 is governed by the ratio $(\dot{S}_R/\dot{S}_D)$ the pressure effect disappears in this regime where the surface chemistry is controlling. A different choice of surface reaction kinetics or a different assumption regarding the stagnation point heat transfer parameter would separate the curves.

In order to illustrate this effect Figure 29 shows the ablation velocity as a function of surface temperature for a fixed value of heat transfer coefficient, (q_c/H_s) with pressure as a parameter. It should be noted that this is generally speaking not a physically real situation since q_c, H_s and P are not independent physical quantities.

Figure 28

Predicted Ablation Rate - Surface Temperature Relationship
$(q_c/H_s P^{\frac{1}{2}}) = 0.1$ lb/ft^2-sec-atm$^{\frac{1}{2}}$

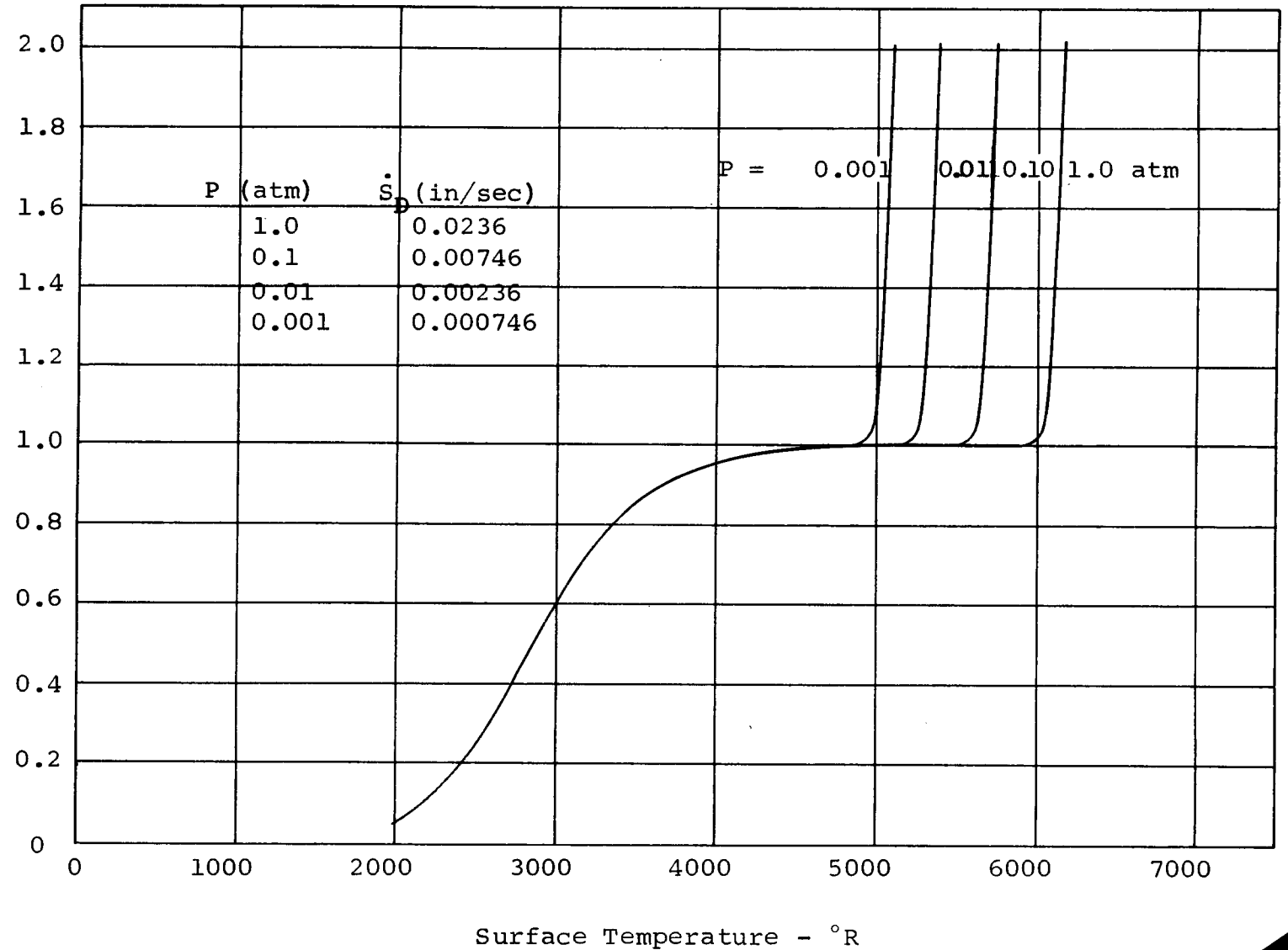

Figure 29

Predicted Ablation Rate-Surface Temperature Relationship for Fixed Heat Transfer Coefficient

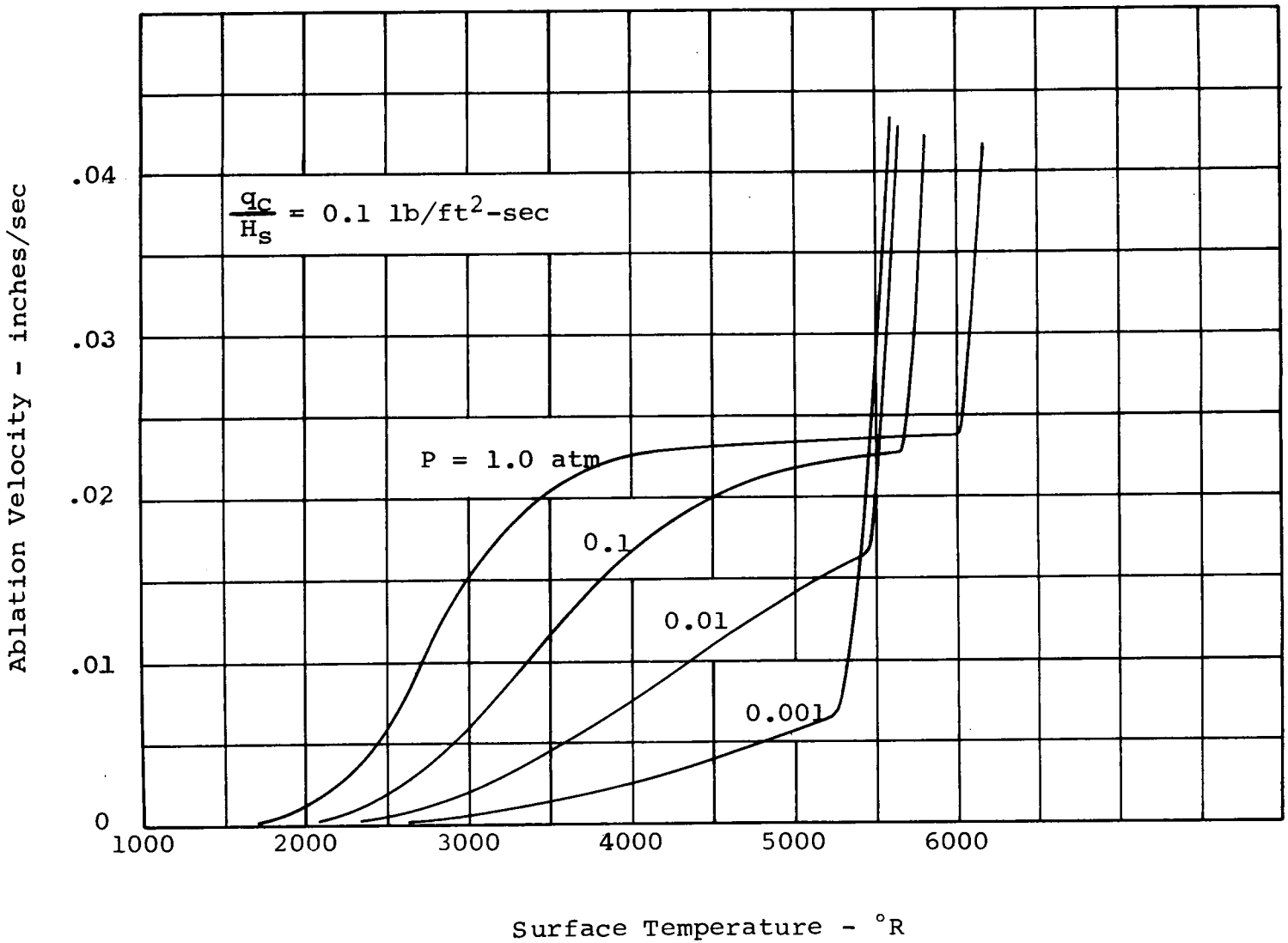

4.0 Apollo Material Physicomathematical Model

The model which has been selected to describe the coupled energy and mass transfer processes in the Apollo ablative thermal protection system is summarized in this section which combines the analytical discussion of Section 2.0 and the test data considerations of Section 3.0. The use of this model by means of the computer program described in Volume II of this report represents the present best estimate of the performance of this material in the Apollo application.

4.1 Energy Equation

$$\rho C_p \left(\frac{\partial T}{\partial t}\right) = \frac{\partial}{\partial x}\left(k \frac{\partial T}{\partial x}\right) + C_g(T)\,\omega \frac{\partial T}{\partial x} + \dot{\rho}\,\Delta H_c \tag{210}$$

$$\rho(x,t) = \rho(x,0) + \int_0^t \dot{\rho}(x,t')\,dt' \tag{211}$$

$$C_p(x,t) = C_{p_0}(T) - \left\{\frac{C_{p_0}(T) - C_{p_c}(T)}{\rho_0 - \rho_c}\right\}\left[\rho_0 - \rho(x,t)\right] \tag{212}$$

$$k(x,t) = k_0(T) - \left\{\frac{k_0(T) - k_c}{\rho_0 - \rho_c}\right\}\left\{\rho_0 - \rho(x,t)\right\} \tag{213}$$

$$\omega(x,t) = \int_x^{\ell_1} \dot{\rho}(x',t)\,dx' \tag{214}$$

$$\dot{\rho}(x,t) = -A_1 \rho_0 \left\{\frac{\rho(x,t) - \rho_{c1}(T)}{\rho_0}\right\}^{N_1} \exp\left\{-\frac{B_1}{T(x,t)}\right\} - A_2 \rho_0 \left\{\frac{\rho(x,t) - \rho_{c2}(T)}{\rho_0}\right\}^{N_2} \exp\left\{-\frac{B_2}{T(x,t)}\right\} \tag{215}$$

4.2 Gas Pressure Distribution

$$P(x,t) = \left\{ Z_1 P_e^2(t) - Z_2 \int_S^x \alpha(x',t)\,\mu(x',t)\,w(x',t)\,dx' - Z_2 \int_S^x \beta(x',t)\,w^2(x't)\,dx' \right\} \tag{216}$$

$$\mu(x,t) = (1.7765 \times 10^{-6}) \frac{\{T(x,t)\}^{3/2}}{T(x,t)+198.} \tag{217}$$

$$Z_1 = 4.478 \times 10^6 \tag{218}$$

$$Z_2 = 3.1489 \tag{219}$$

$$\alpha(x,t) = \alpha_v - \left(\frac{\alpha_v - \alpha_c}{\rho_o - \rho_c}\right)\{\rho_o - \rho(x,t)\} \tag{220}$$

$$\beta(x,t) = \beta_c \left\{ \frac{\rho_o - \rho(x,t)}{\rho_o - \rho_c} \right\} \tag{221}$$

The numerical constants in equations (217), (218) and (219) have been evaluated on the assumption that (1) the local static pressure, P_e, is given in atmospheres and (2) that the pyrolysis products have properties similar to normal air. The units of the output pressure, P, given by equation (216) are then lb/ft^2.

4.3 Boundary Conditions at $x = 5$

$$\bar{q}_c(t)\left[\frac{H_r}{H_s}(t) - \frac{\{H_w(t) - H'(t)\}}{H_s(t)}\right] + (1-R_o)F_s \tag{222}$$

$$-\epsilon\sigma T^4(s,t) = \left(k\frac{\partial T}{\partial x}\right)_{x=s} + \rho(s,t)\,\dot{s}\,H_v$$

$$\bar{q}_c = q_c \left(\frac{H_w}{H_{wR}}\right)^{E_1} \left(\frac{H^* + \frac{1}{2} H_w}{H^* + \frac{1}{2} H_{wR}}\right)^{E_2} \exp\left[-f(1 + 0.618 f)\right] \quad (223)$$

$$H^* = \left[(\tfrac{1}{2} - 0.22r)\, H_s \left\{\frac{\left(\frac{H_r}{H_s}\right) - r}{1 - r}\right\} + 0.22\, r\, H_s\right] \quad (224)$$

$$f = \left\{\rho(s,t)\, \dot{s}\, \eta_s - \omega(s,t)\, \eta_y\right\} \left(\frac{H_s}{\bar{q}_c}\right) \quad (225)$$

The quantities E_1 and E_2 in equation (223) are flow dependent as discussed in Sections 2.4.1, 2.4.2, and 2.4.3.

Stagnation Point Flow: $E_1 = -0.037$, $E_2 = 0.0$ (226a)

Laminar Boundary Layer: $E_1 = 0.0$, $E_2 = -0.185$ (226b)

Turbulent Boundary Layer: $E_1 = 0.0$, $E_2 = -0.502$ (226c)

$$H' = W_e\, H_c \left\{1 - \left(\frac{\dot{S}_T}{\dot{S}_R}\right)^{1/N_r}\right\} \quad (227)$$

$$\dot{S}_T = \dot{S}_D \left\{1 - \left(\frac{\dot{S}_T}{\dot{S}_R}\right)^{1/N_r}\right\} \quad (228)$$

$$\dot{S}_D = \frac{W_e\, \bar{q}_c}{W_c\, H_s\, \rho(s,t)} \left(\frac{u_3}{u_2}\right) \exp\left\{-f(1 + 0.618 f)\right\} \quad (229)$$

$$\dot{S}_R = \frac{W_e\, A_r}{\rho(s,t)} \left\{\frac{\rho_o - \rho(s,t)}{\rho_o - \rho_c}\right\} \left\{\left(\frac{u_o}{u_1}\right) \omega_e\, P_e\right\}^{N_r} \exp\left\{-\frac{B_r}{T(s,t)}\right\} \quad (230)$$

$$\dot{S} = \dot{S}_T + \left\{ \dot{S}_s - \dot{S}_T \right\} \quad \text{SUCH THAT} \quad \left\{ \dot{S}_s - \dot{S}_T \right\} \geq 0 \tag{231}$$

$$\dot{S}_s = \bar{B}\, \beta_5 \left\{ T(s,t) \right\}^{\beta_6} \exp\left\{ - \frac{\beta_7}{T(s,t)} \right\} \tag{232}$$

$$\bar{B} = 1 - \left[\frac{(1-\phi)\, P_e}{M_A} \exp\left\{ \frac{M_B}{T(s,t)} \right] \right. \tag{233}$$

$$\phi = \exp\left\{ - f\,(1 + 0.618\, f) \right\} \tag{234}$$

4.4 Boundary Condition at $x = \ell_1$

The boundary condition at the rear face of the ablative layer will normally be a statement of the equality of the conduction flux across the interface. Any appropriate boundary condition can be applied (See Volume II, Section 6.6).

4.5 Initial Conditions

The initial conditions consist of a specification of the temperature and density distributions at time zero.

$$\rho(x, 0) = f_1(x) \tag{235}$$

$$T(x, 0) = f_2(x) \tag{236}$$

4.6 Property Values

The various material dependent parameters appearing in equations (210) through (236) have been assigned values on the basis of the considerations in Section 3.0. The values assigned to the temperature independent quantities are collected in Table 6. Also indicated in Table 6 are the first equation in which the quantity appears and the computer program input symbol whenever this is appropriate. The temperature dependent properties are collected in Table 7. Linear interpolation is to be employed between entries in Table 7.

4.7 Environment Dependent Parameters

In addition to the material dependent characteristics listed in Tables 6 and 7 the physicomathematical model of this section requires certain characteristics of the flight environment to be given as functions of time. These are the cold wall flux, q_c, the stagnation enthalpy, H_s, the local static pressure, P_e, the ratio of recovery to stagnation enthalpy, (H_r/H_s), the recovery factor, r, and the radiant energy flux incident on the surface. Velocity may be specified instead of H_s.

Additional quantities which are generally constant for flight in the earths atmosphere are the weight fraction of oxygen in the free stream, W_e, the free stream molecular weight U_o and the molecular weight of oxygen. In the present model these quantities are taken to have the values 0.2314, 28.96 and 32.0 respectively.

TABLE 6

TEMPERATURE INDEPENDENT MATERIAL CHARACTERISTICS

Quantity	Program Symbol	Value	Description
ΔH_c	DELH	500. BTU/lb	Heat of pyrolysis (210)
ρ_o	—*	33.0 lb/ft^3	Virgin material density (212)
ρ_c	RHC	16.5 lb/ft^3	Fully charred density (212)
k_c	—*	0.19 BTU/ft-hr-$^\circ$F	Char conductivity (213)
A_1	GCBA1	1.0×10^7 sec^{-1}	Pyrolysis rate constants (215)
A_2	GCBA2	3.26×10^5 sec^{-1}	"
N_1	GCBN1	1.0	"
N_2	GCBN2	2.0	"
B_1	GCBB1	12000°R	"
B_2	GCBB2	21480°R	"
α_v	—*	7.153×10^{10} ft^{-2}	Viscous coefficient of virgin material (220)
α_c	—*	5.781×10^9 ft^{-2}	Viscous coefficient of charred material (220)
β_c	—*	1.924×10^5 ft^{-1}	Inertial coefficient of charred material (221)
ϵ	EFRØNT	0.667	Coefficient of emission (222)
R_o	—*	0.5	Surface reflectivity (222)
H_c	HC	10000. BTU/lb	Combustion energy (227)

*Not used directly in the computer program. See Table 13.

TABLE 6 (Con't)

A_r	—	54.0 lb/ft^2-sec	Heterogeneous rate constants (230)
N_r	E7	0.5	"
B_r	B3	17000.$^\circ$R	"
U_3	U3	12.0	Atomis weight of carbon (229)
U_2	U2	16.0	Atomic weight of oxygen (229)
W_c	$\left(\frac{1}{TW}\right)$	0.329	Weight fraction of surface carbon (230)
M_A	TRMA	0.174×10^{12} atm	Back pressure coefficient (233)
M_B	TRMB	163200.$^\circ$R	" (233)
β_5	BETA5	9.1×10^8 ft/sec-($^\circ$R)$^{0.28}$	Sublimation rate coefficients (234)
β_6	BETA6	0.28	"
β_7	BETA7	161000.$^\circ$R	"

In addition to the above there are two parameters which depend on the external flow conditions. These are the surface material blowing coefficient, η_s, and the pyrolysis products blowing coefficient, η_g.

Type of Flow	η_s	η_g
Stagnation point	0.400	0.800
Laminar boundary layer	0.507	1.014
Turbulent boundary layer	0.307	0.378

TABLE 7

TEMPERATURE DEPENDENT MATERIAL CHARACTERISTICS

T (^{o}R)	ρ_{c1} (lb/ft^3)	ρ_{c2} (lb/ft^3)	C_g (BTU/lb^{o}R)	C_{p_o} (BTU/lb^{o}R)	C_{p_g} (BTU/lb^{o}R)	k_o (BTU/ft-hr^{o}R)
0	33.0	31.35	0.55	0.25	0.20	0.0473
650	33.0	↓	—	—	—	—
700	31.35		—	—	—	—
1000	↓	31.35	0.66	0.32	—	—
1100		31.19	—	—	—	—
1150		29.37	—	—	—	—
1200		28.38	—	—	—	—
1250		24.42	—	—	—	—
1300		21.62	—	—	—	—
1350		19.80	—	—	—	—
1400		18.65	—	—	—	—
1450		17.98	—	—	—	—
1500		17.32	—	—	—	—
1600		16.50	—	—	—	—
2000		↓	0.74	0.38	—	—
3000			0.79	0.41	—	—
4000			0.83	0.43	—	—
6000				0.45	—	—
8000	↓	↓	0.96	↓	—	—
10000	31.35	16.50	0.96	0.45	2.40	0.2643

5.0 Comparison with Ground Test Data

The model described in the preceding section has been employed in a numerical simulation of several tests run on the Apollo material in the Plasmadyne and Southwest Research Institute facilities. This type of simulation serves to illustrate the adequacies or inadequacies of the model and to highlight several features of this type of test. The test points chosen for examination are shown in Table 8. The data obtained in the tests consist primarily of thermocouple histories, surface temperatures and total length loss. The detailed data are a part of the library described in Volume III of this report. The physicomathematical model of the preceding section together with the computer program described in Volume II of this report have been employed to make detailed predictions for the environmental conditions listed in Table 8.

The total output of the numerical calculations represents an extremely detailed picture of each of the tests and only selected results can be presented. One of the outputs is a prediction of the location of the 600°F and 1000°F isotherms as functions of time. These positions are also obtainable from the test data thermocouple histories. Figures 30 through 55 show the results obtained from the theoretical predictions compared with the experimental data reported by the Plasmadyne Facility. As is usual in comparisons of this type the agreement between theory and predictions is in some cases less than is desirable. On the other hand considering the scatter in the experimental data as indicated in Figures 10 and 12, it is not expected that a comparison which combines the scatter associated with the surface recession together with the internal heat transfer should yield strong agreement between selected experimental and theoretical results. Figures 56 through 62 present similar information in a different form by comparing measured and predicted thermocouple histories for selected models.

The results of the total length loss predictions for this sequence of test results are presented in Table 9. Again the comparison between predicted and measured total length loss is only fair. One feature of the material behavior which is not accounted for in the predictions and which may account for some of the discrepancies is the swelling and shrinking which occurs in the tests and introduces an unknown quantity into the measurements. Another problem is the exact way in which the posttest total length is measured. In most cases the post test profile is not uniform and the average length loss over the entire heated surface is difficult to define. This can introduce significant errors particularly in the cases where small values of length loss are observed. Table 9 also contains the predicted and "observed" surface temperatures. As can be seen from the data in the table the "observed" temperatures are consistently higher than the predicted values. No reasonable physical explanation has been found for this discrepancy. It can be noted, however, that the observed temperatures for test points 2 and 8 are very nearly the same even though the heat flux differs by a factor of two.

In the tests run in "inert" atmospheres of argon and nitrogen (test points 2A, 16A, 5N and 20N) it should be noted that the only mechanism allowed for surface recession is the vaporization mechanism described in Section 3.5. While this is probably very nearly correct for the case of the argon environment it is less valid for the case of the nitrogen tests as has been discussed in Section 3.1.

Table 8

TEST CONDITIONS

Test Point	Atmosphere	q_C(BTU/ft^2-sec)	H_S(BTU/lb)	$P_{(atm)}$	F_S(BTU/ft^2-sec)
1	air	26.7	3490	0.0082	-
2	air	113.0	10016	0.0120	-
3	air	223.3	17020	0.0180	-
4	air	55.6	3496	0.0333	-
5	air	56.0	10026	0.00335	-
7	air	116.0	17015	0.0041	-
8	air	224.2	10013	0.0440	-
2A	argon	85.3	8200	0.008	-
16A	argon	137.3	3320	0.099	-
5N	nitrogen	88.2	11050	0.008	-
20N	nitrogen	331.8	9100	0.097	-
SWRI 55	air	-	-	0.5	78.0
SWRI 120	air	-	-	3.0	507.0

Table 9

COMPARISON OF PREDICTED AND MEASURED TOTAL ABLATION AND SURFACE TEMPERATURE

Model	ΔS(obs)	ΔS(calc)	T(obs)	T(calc)
	(inches)	(inches)	(°R)	(°R)
PD120	0.040	0.011	2920	2425
PD121	0.070	0.064	2960	2586
PD122	0.050	0.132	2960	2631
PD157	0.160	0.526	2910	2709
PD140	0.170	0.075	—	3567
PD141	0.300	0.174	4360	3414
PD142	0.480	0.279	4410	3508
PD158	0.240	0.110	4760	4288
PD159	0.700	0.381	4830	4324
PD125	0.120	0.103	3635	3002
PD126	0.410	0.378	3600	3063
PD127	0.580	0.661	3610	3220
PD130	0.040	0.015	3110	2794
PD132	0.100	0.085	3180	3040
PD131	0.150	0.167	3200	3123
PD136	0.160	0.638	3760	3265
PD147	0.120	0.030	4010	3411
PD146	0.260	0.080	4010	3456
PD145	0.670	0.314	4100	3800
PD151	0.240	0.196	4440	4200
PD152	0.600	0.414	4390	4200
PD153	0.780	0.634	4410	4260
PD277	0.072	0.0005	4110	2966
PD251	0.055	0.007	3430	3387
PD267	0.247	0.0004	3885	3125
PD234	0.305	0.550	4760	4350
SWRI55	0.120	0.100	3360	3300
SWRI120	0.330	0.275	5390	5210

Figure 30

Comparison of Observed and Predicted Isotherm Progressions

TEST POINT 1

600°F

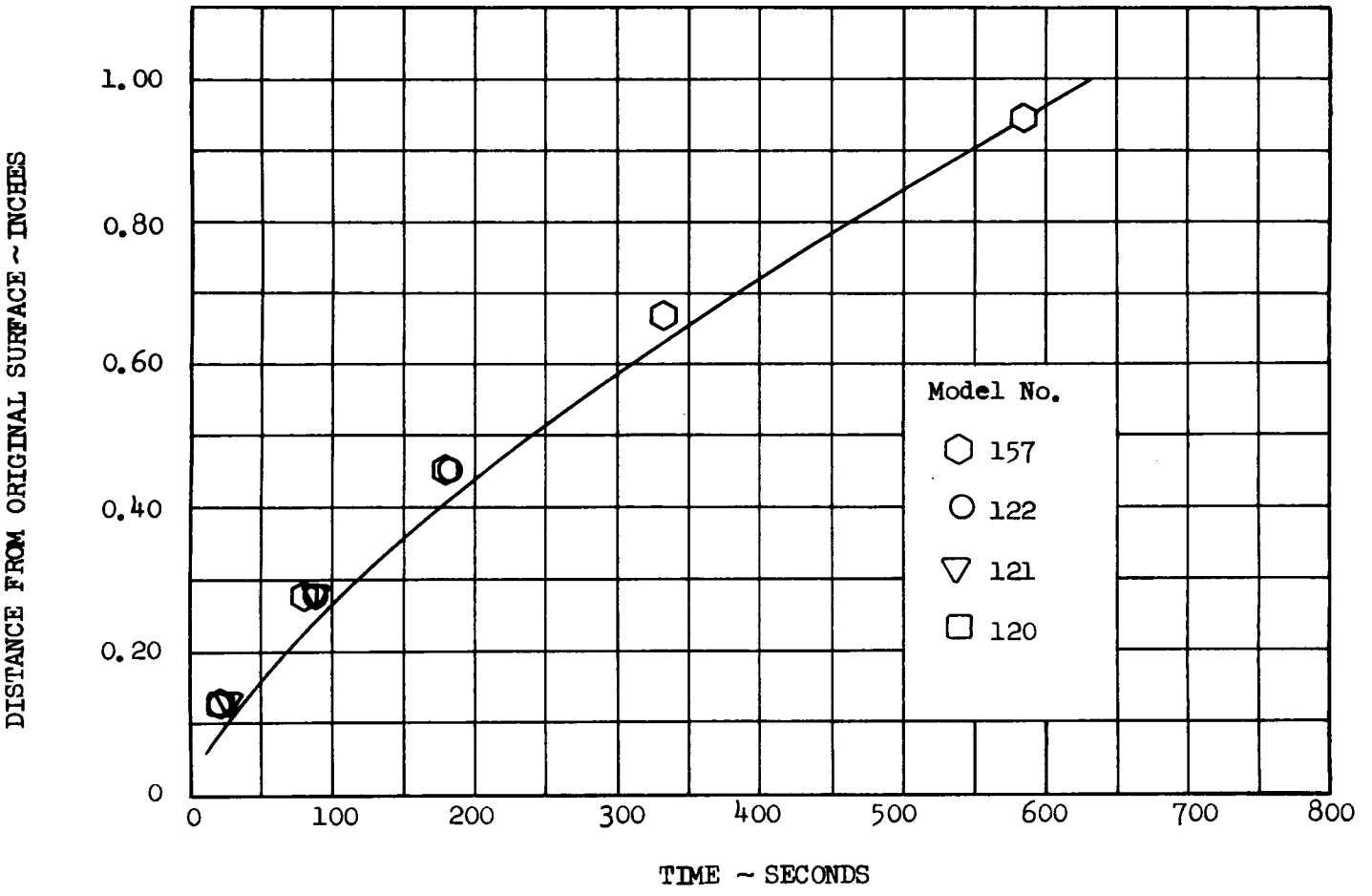

Figure 31

Comparison of Observed and Predicted Isotherm Progressions

TEST POINT 1

1000° F

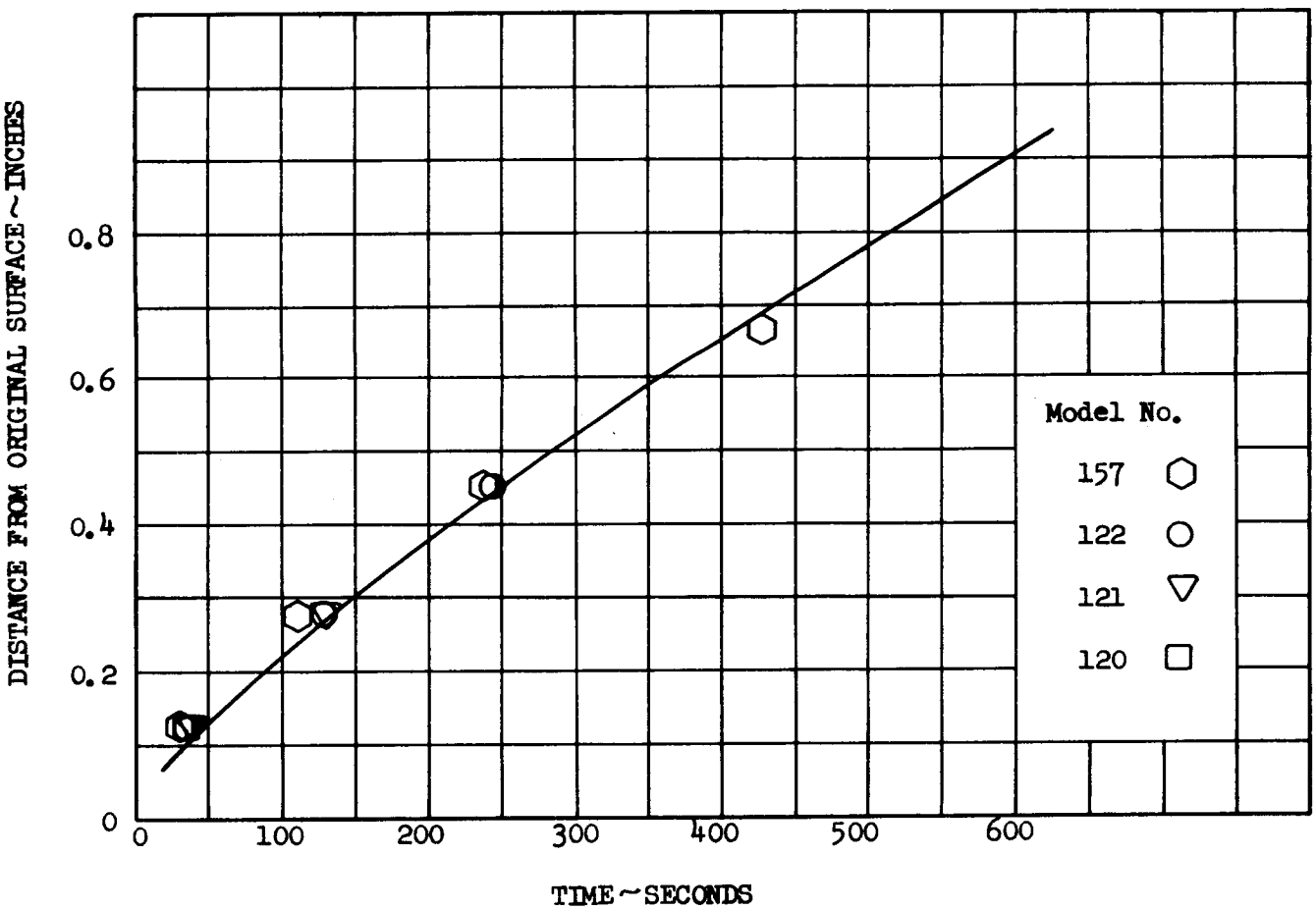

Figure 32

COMPARISON OF OBSERVED AND PREDICTED ISOTHERM PROGRESSIONS

TEST POINT 2

600°F

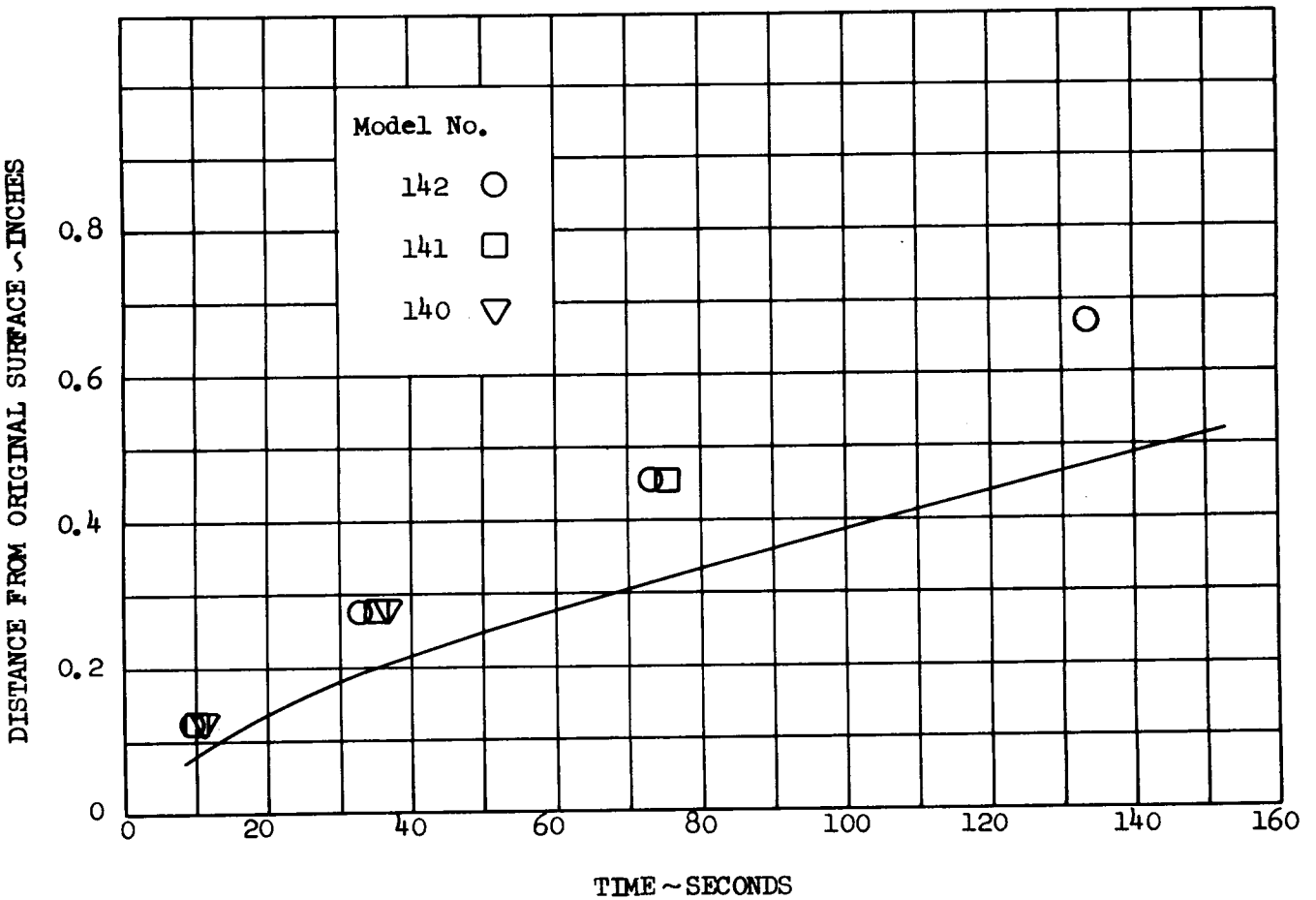

FIGURE 33

COMPARISON OF OBSERVED AND PREDICTED ISOTHERM PROGRESSIONS

TEST POINT 2

1000°F

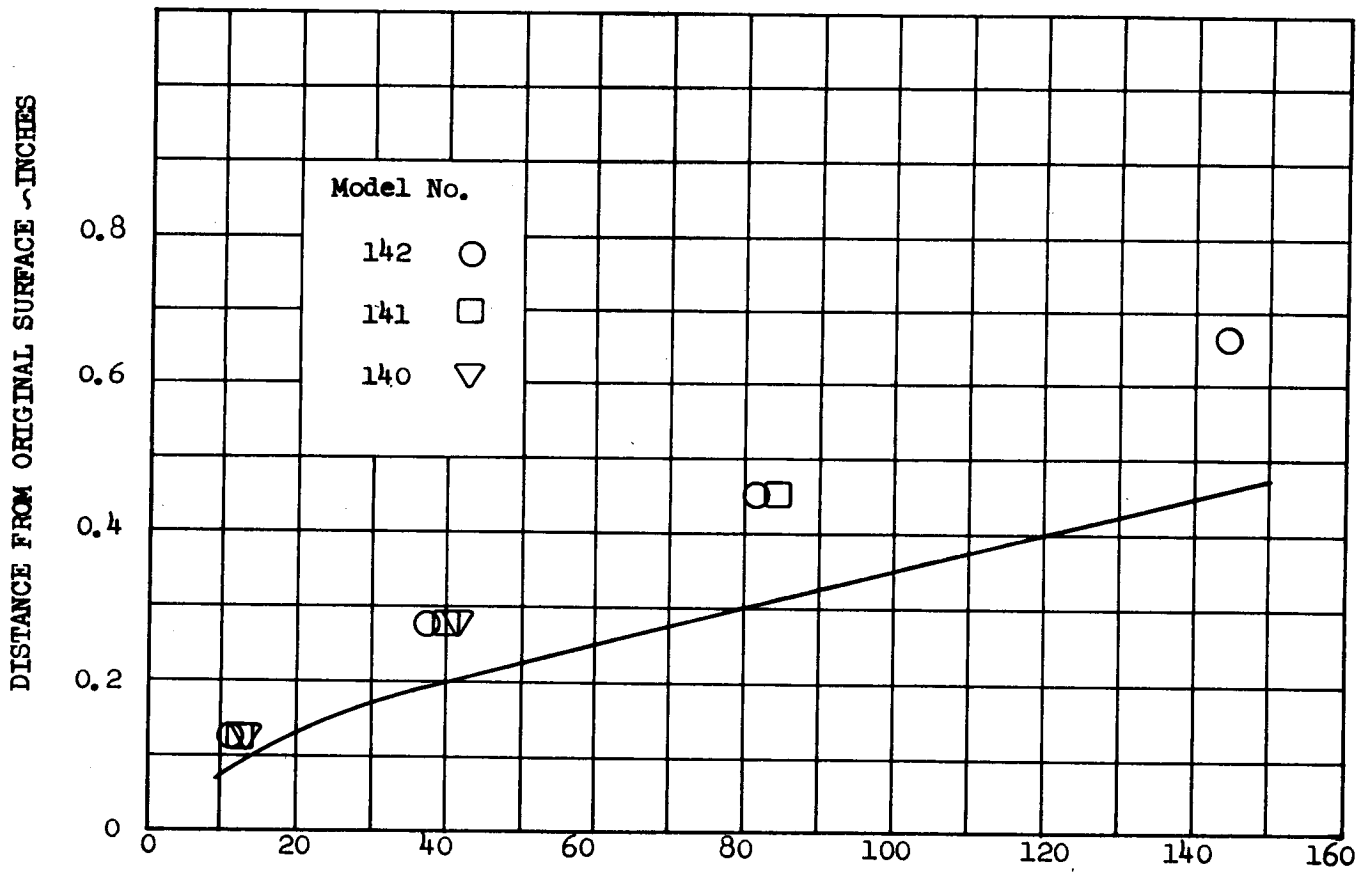

FIGURE 34

COMPARISON OF OBSERVED AND PREDICTED ISOTHERM PROGRESSIONS

TEST POINT 3

600°F

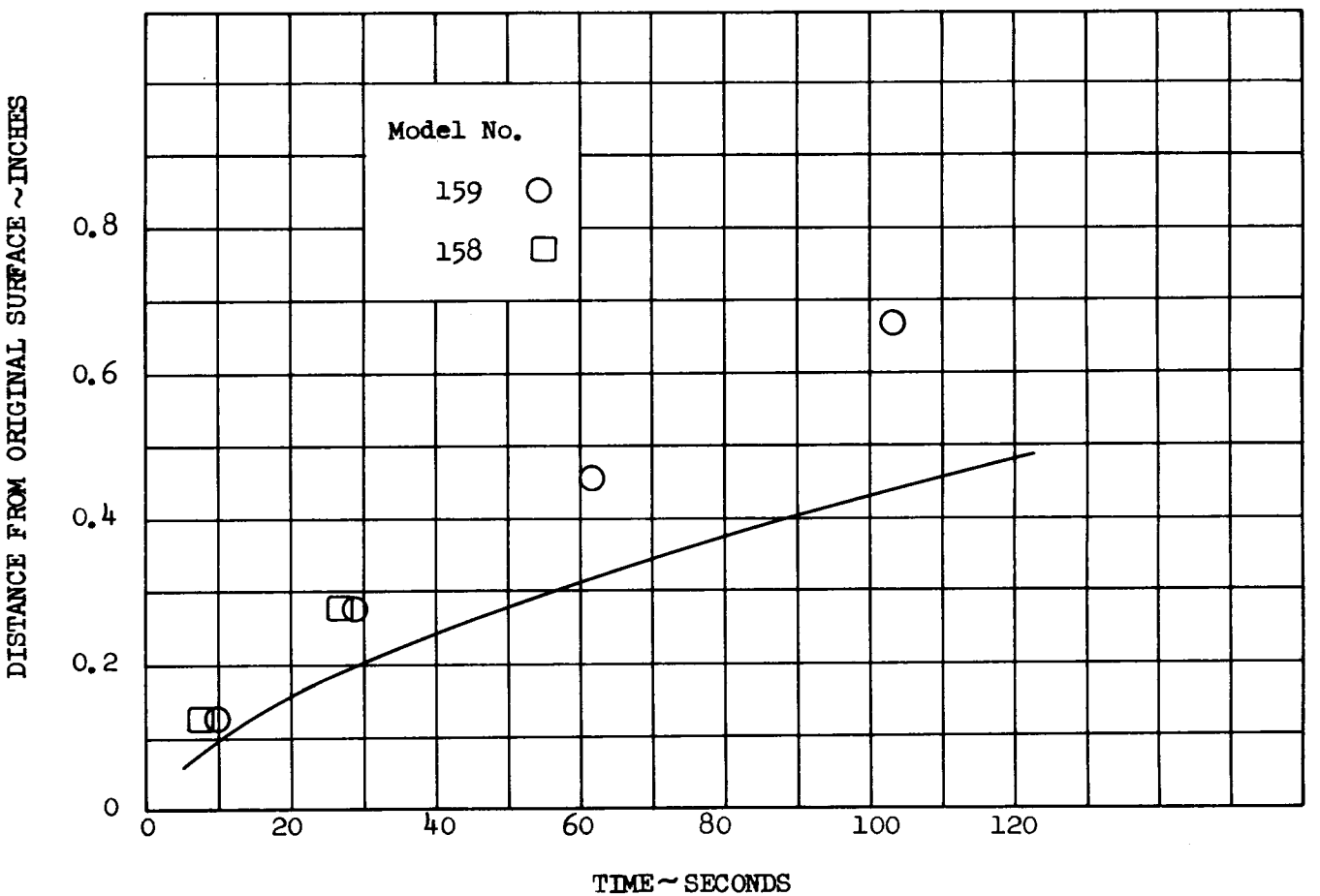

FIGURE 35

COMPARISON OF OBSERVED AND PREDICTED ISOTHERM PROGRESSIONS

TEST POINT 3

1000°F

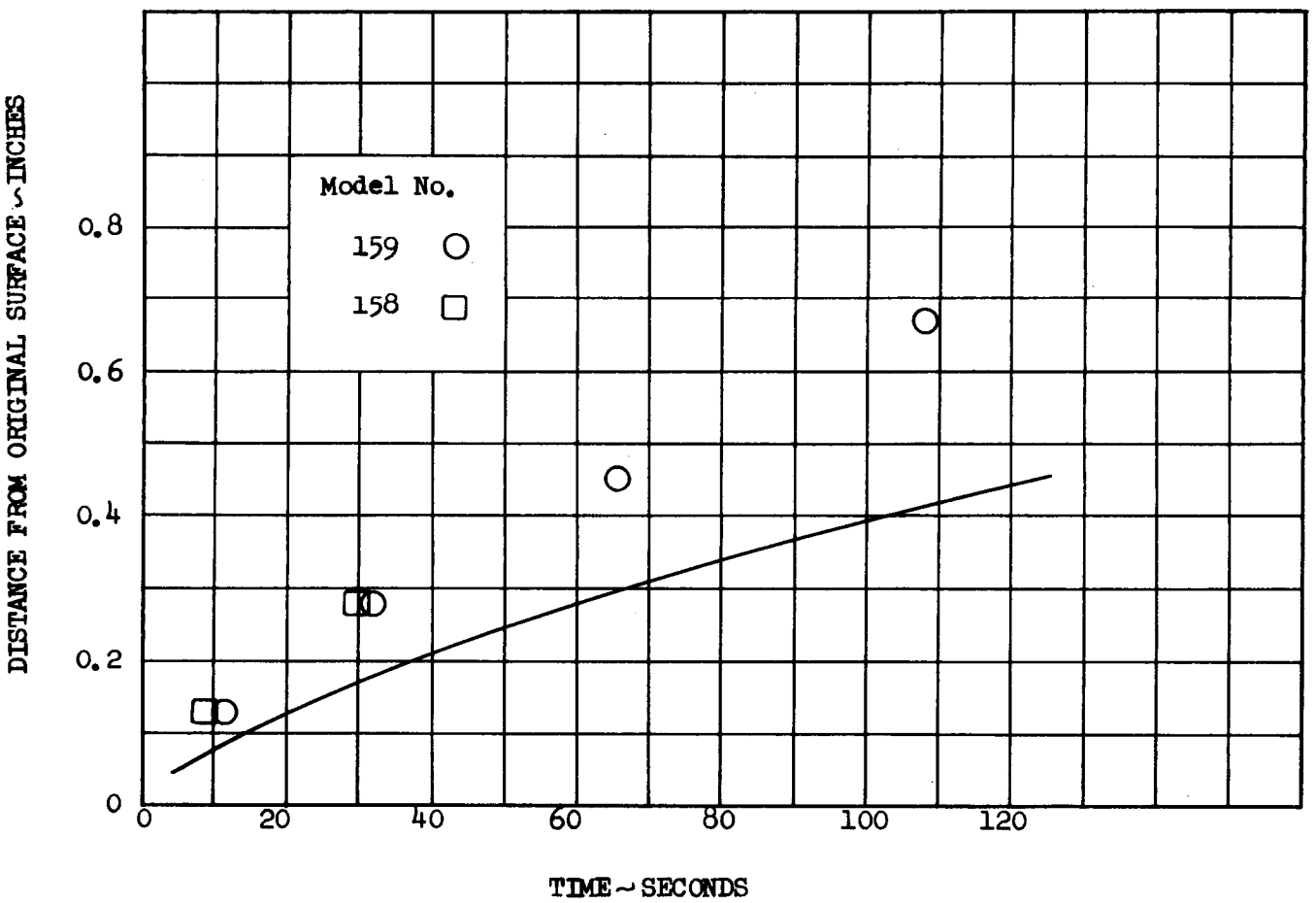

FIGURE 36

COMPARISON OF OBSERVED AND PREDICTED ISOTHERM PROGRESSIONS

TEST POINT 4

600°F

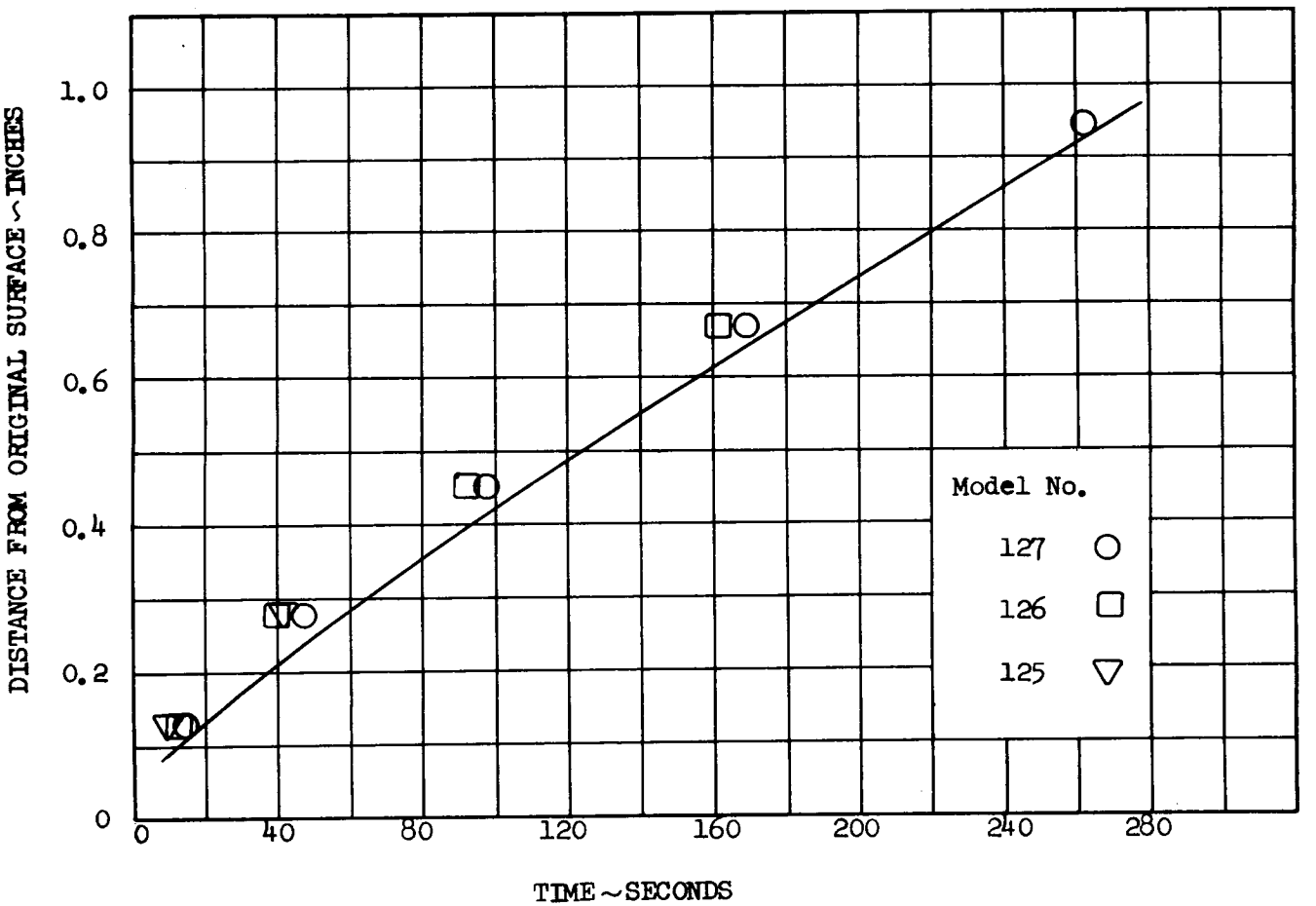

FIGURE 37

COMPARISON OF OBSERVED AND PREDICTED ISOTHERM PROGRESSIONS

TEST POINT 4

1000°F

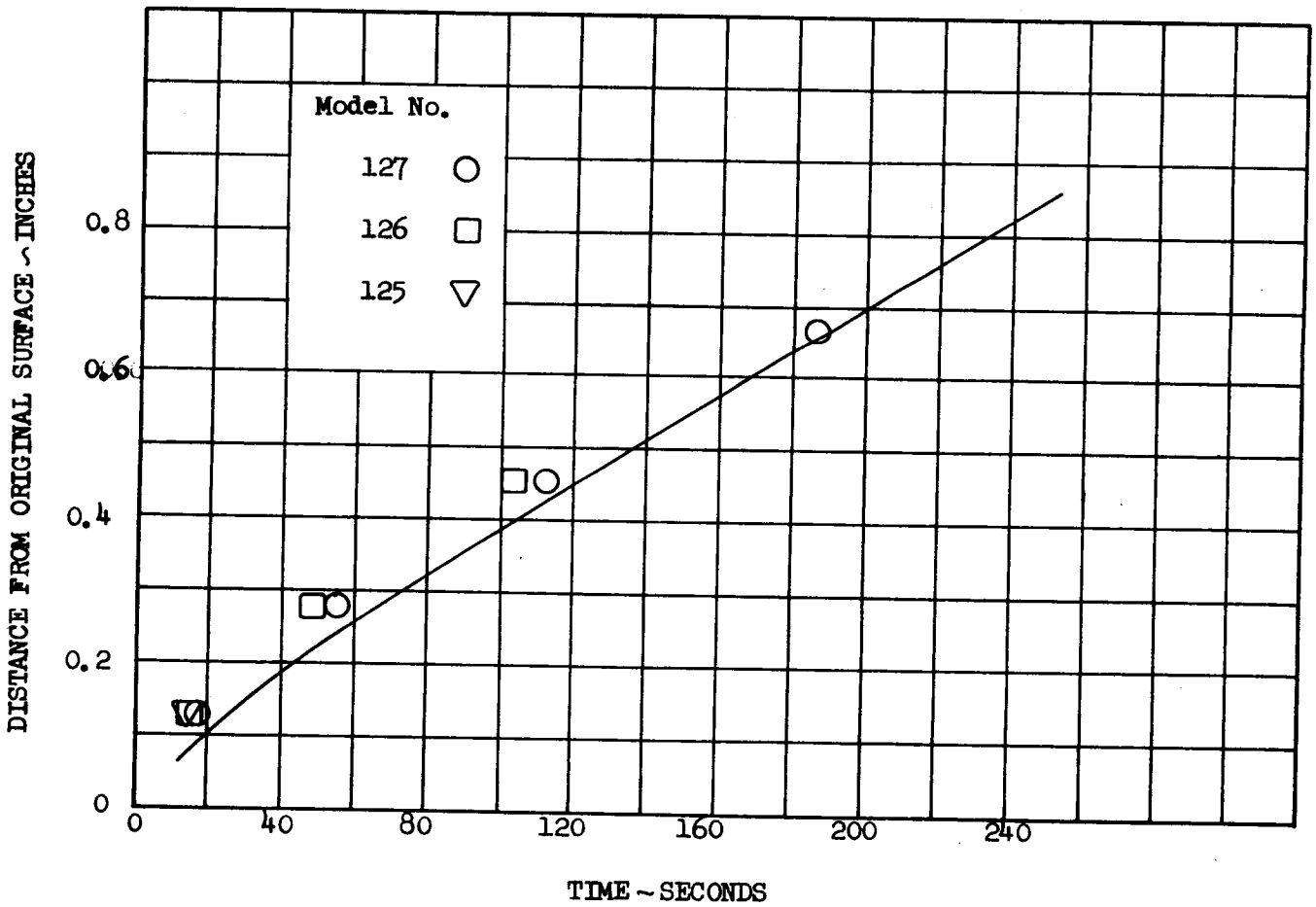

FIGURE 38

COMPARISON OF OBSERVED AND PREDICTED ISOTHERM PROGRESSIONS

TEST POINT 5

600°F

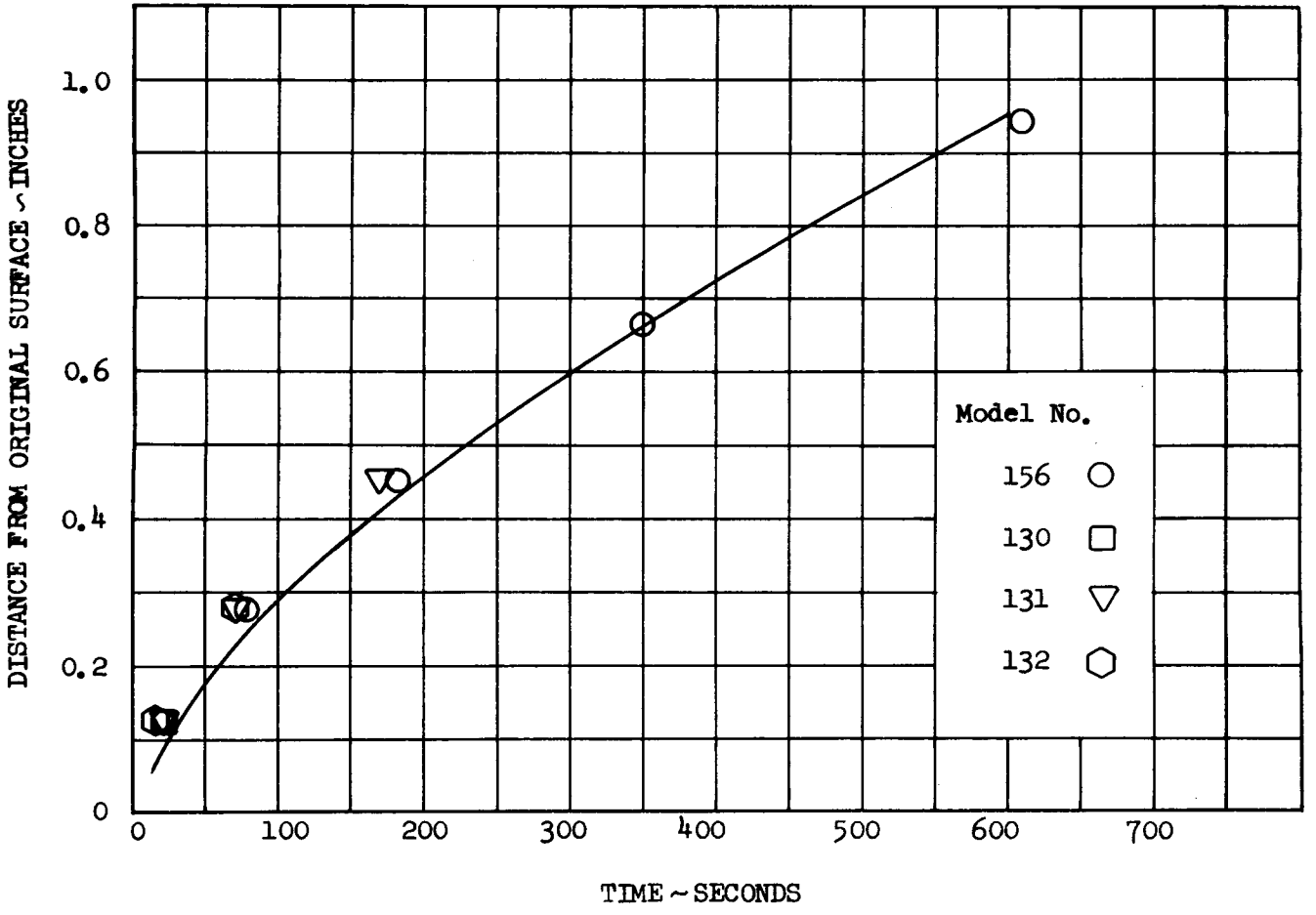

FIGURE 39

COMPARISON OF OBSERVED AND PREDICTED ISOTHERM PROGRESSIONS

TEST POINT 5

1000°F

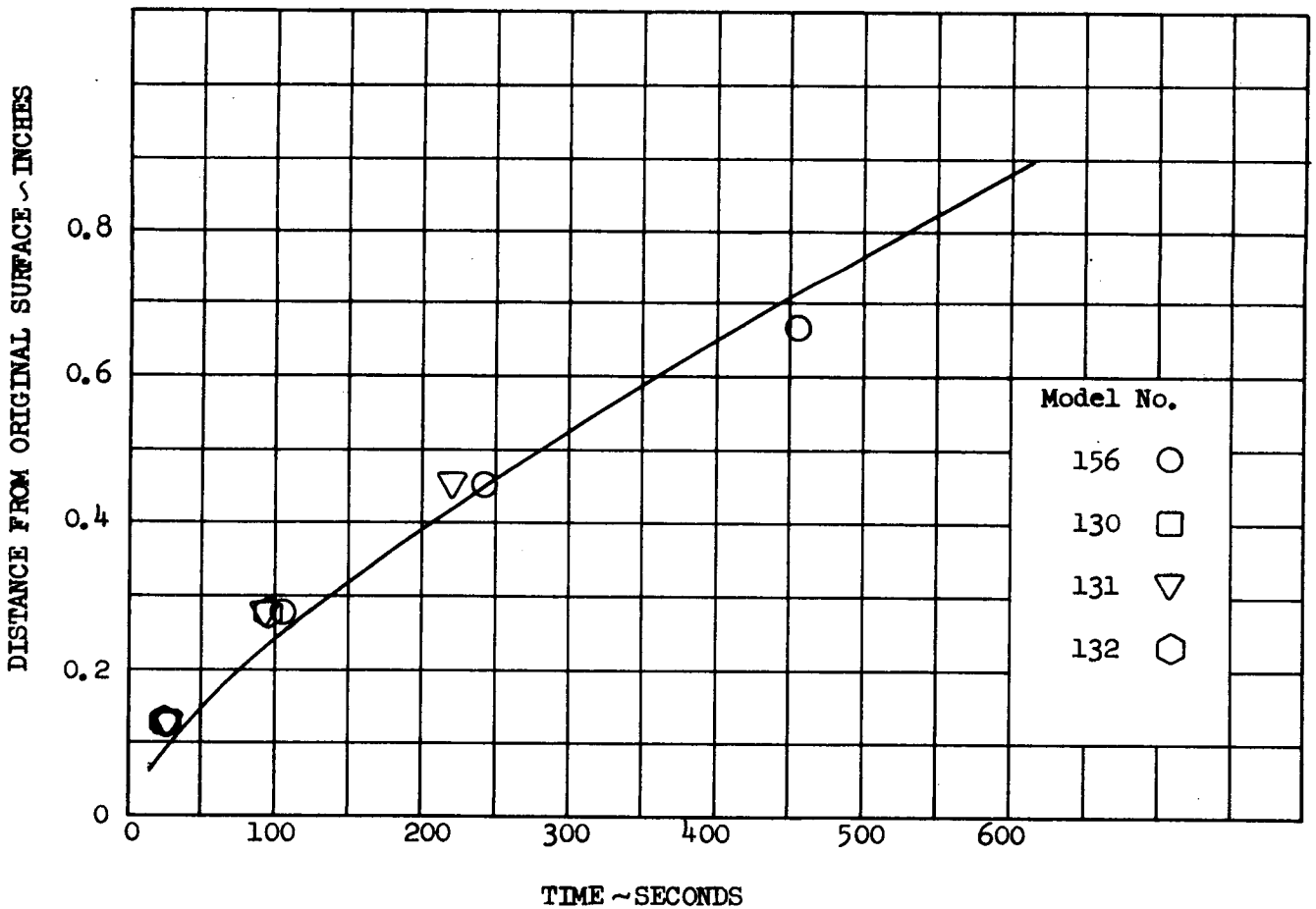

FIGURE 40

COMPARISON OF OBSERVED AND PREDICTED ISOTHERM PROGRESSIONS

TEST POINT 7

600°F

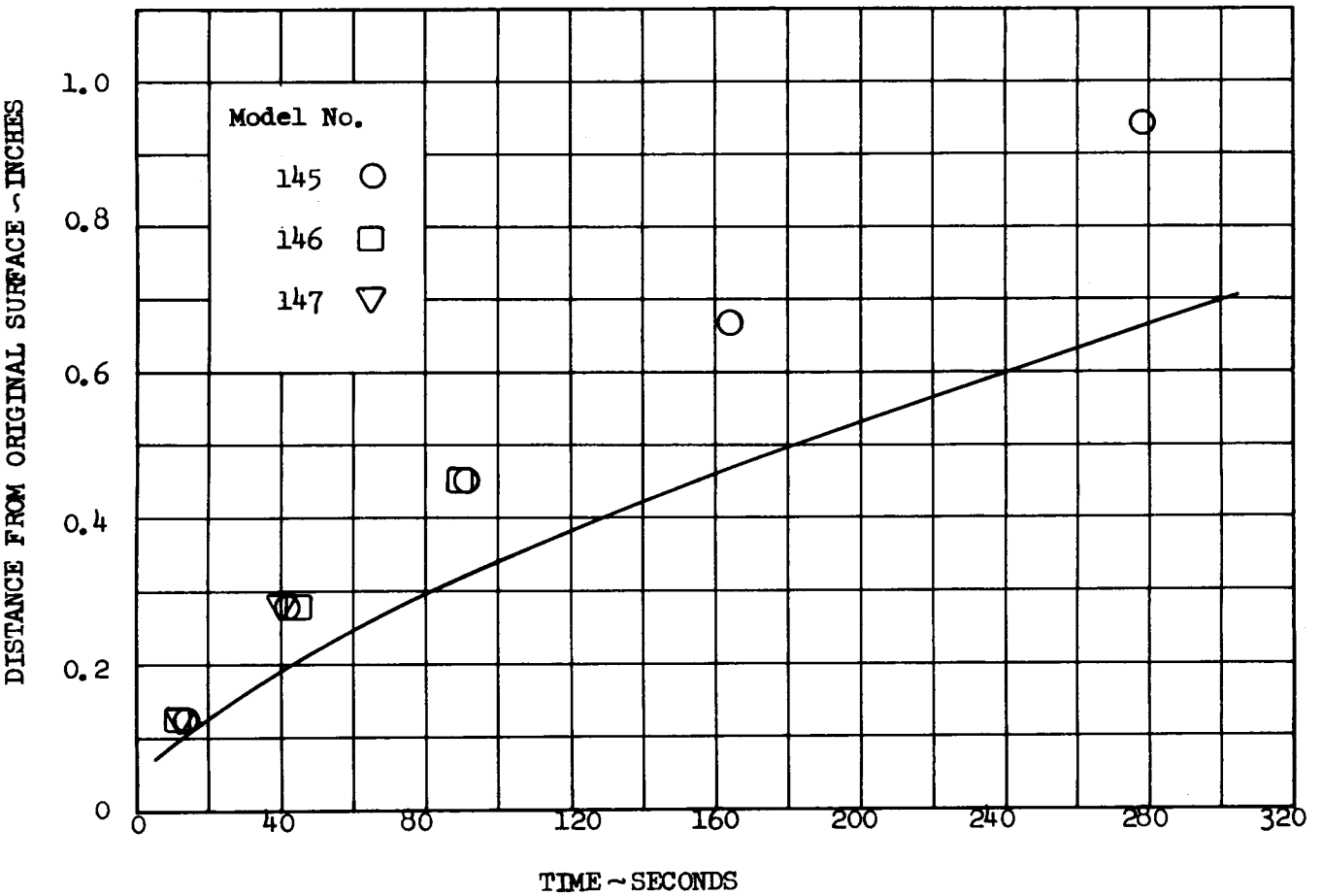

FIGURE 41

COMPARISON OF OBSERVED AND PREDICTED ISOTHERM PROGRESSIONS

TEST POINT 7

1000° F

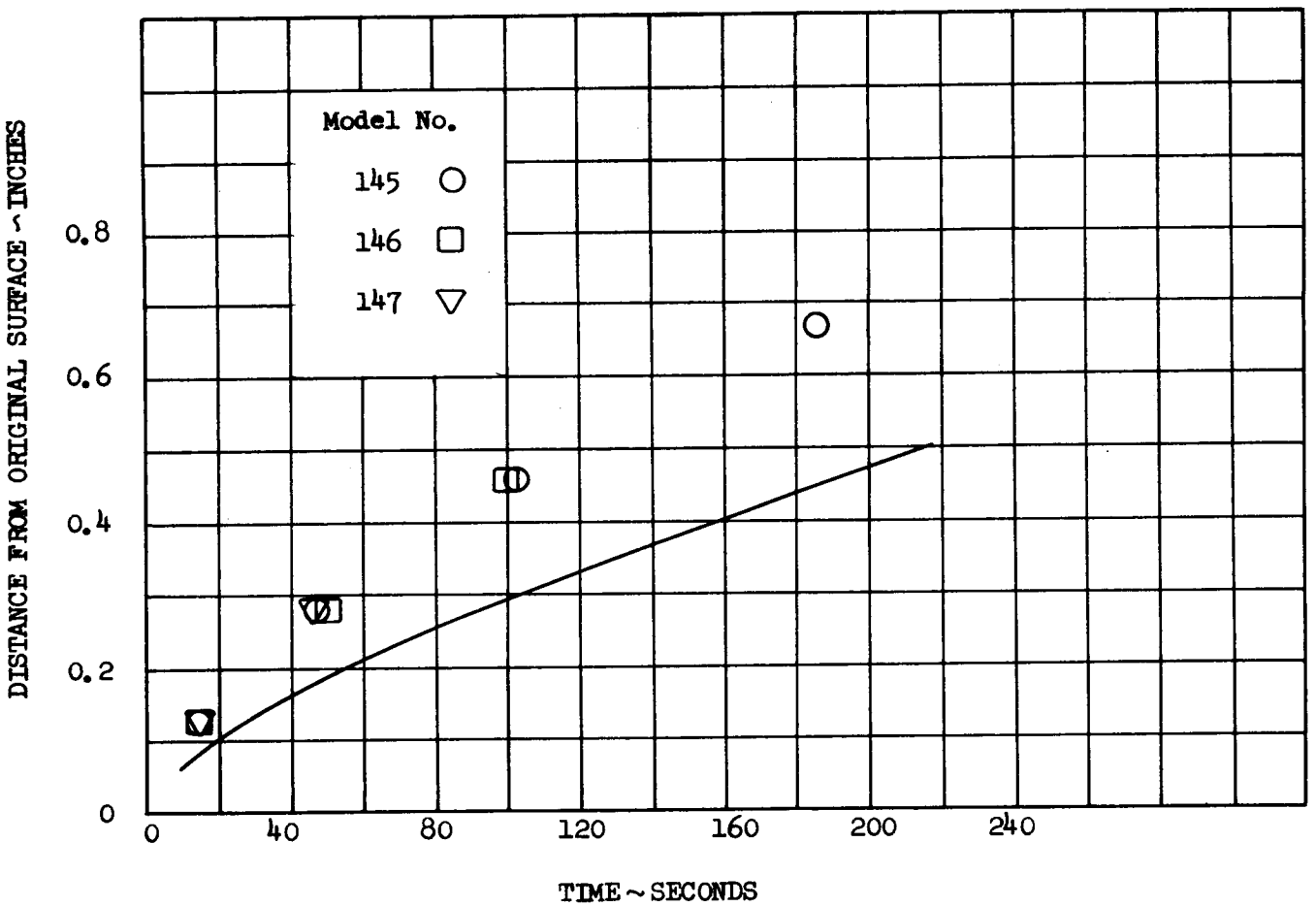

FIGURE 42

COMPARISON OF OBSERVED AND PREDICTED ISOTHERM PROGRESSIONS

TEST POINT 8

600°F

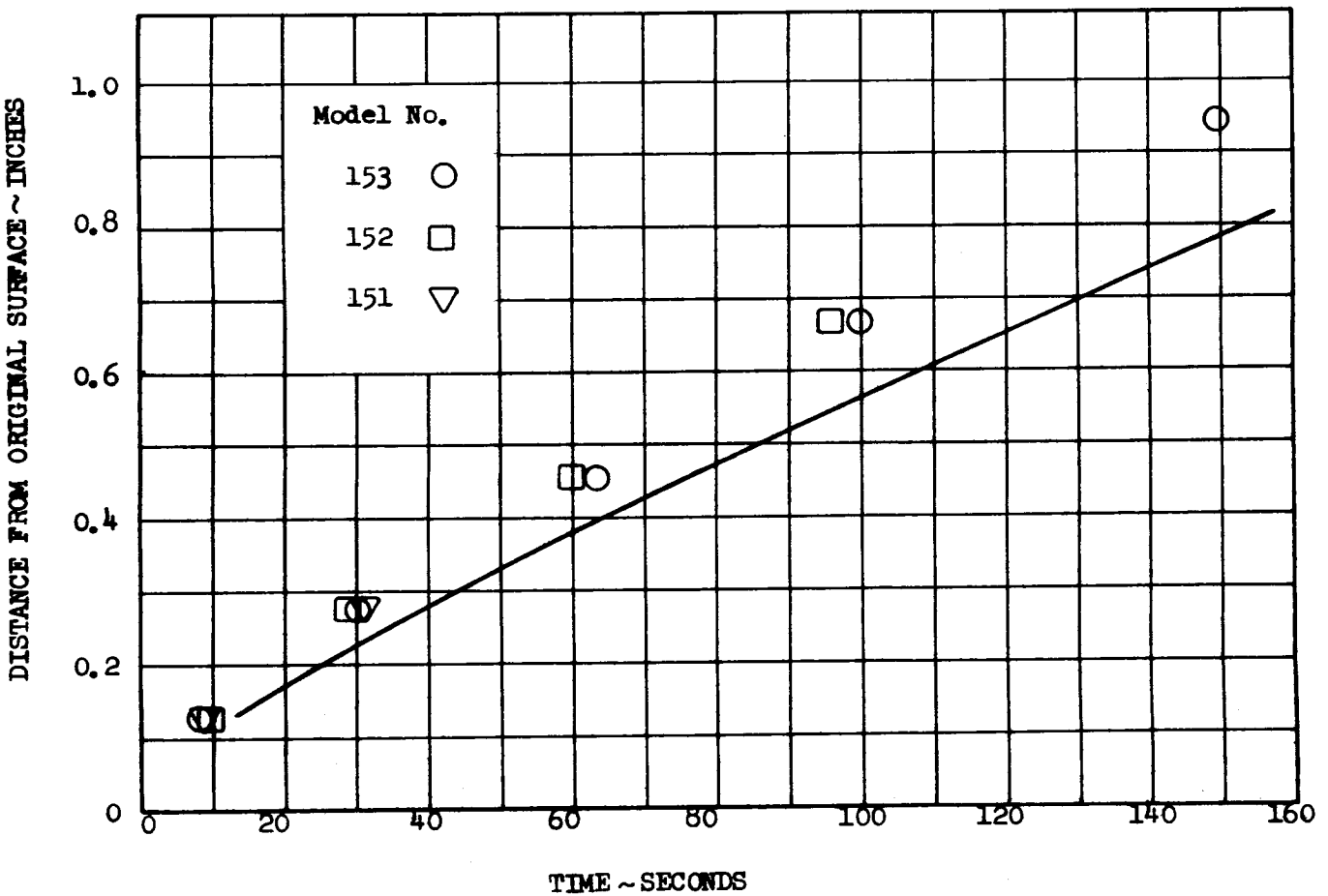

FIGURE 43

COMPARISON OF OBSERVED AND PREDICTED ISOTHERM PROGRESSIONS

TEST POINT 8

1000°F

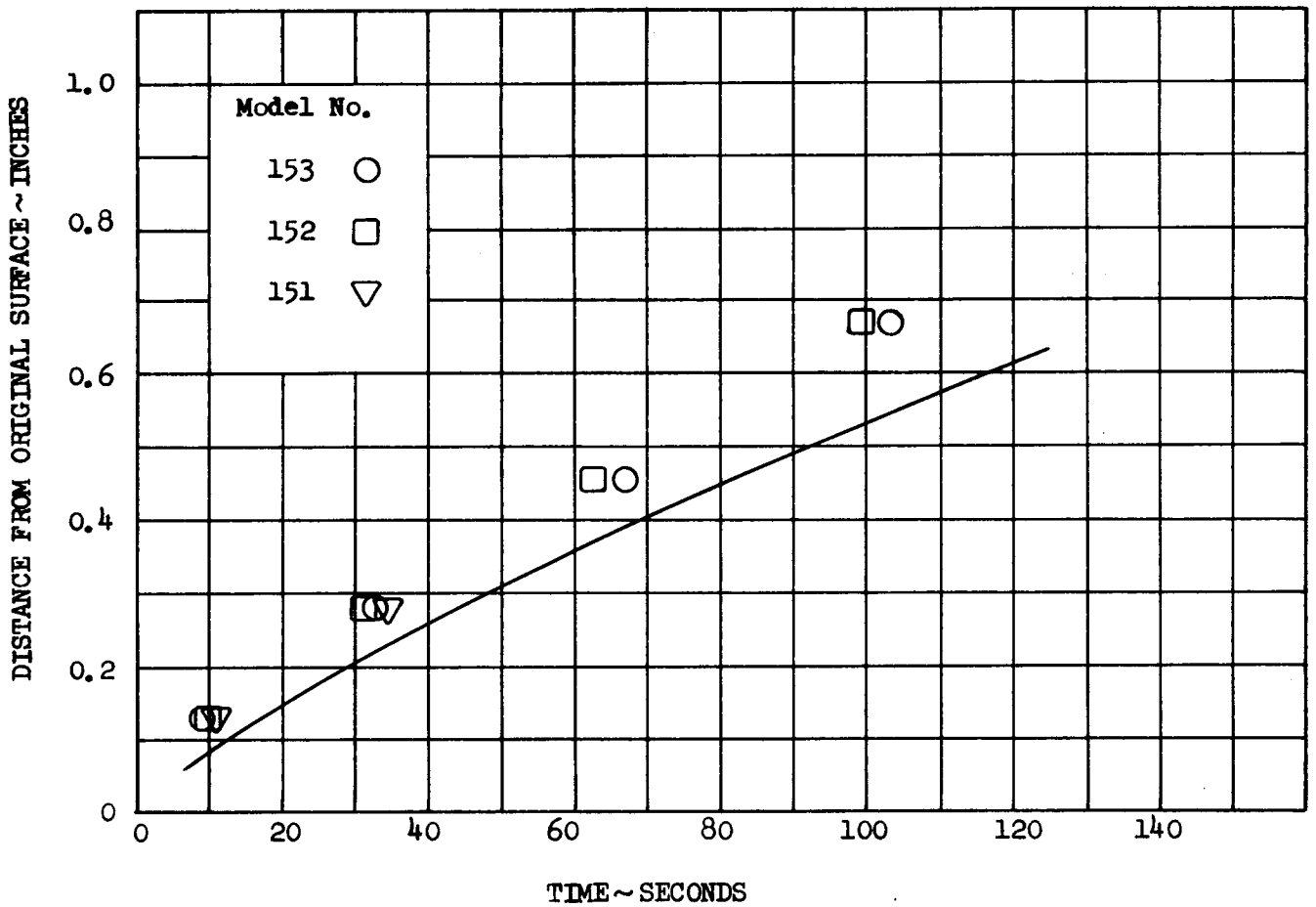

FIGURE 44

COMPARISON OF OBSERVED AND PREDICTED ISOTHERM PROGRESSIONS

TEST POINT 2A - MODEL 277
600°F

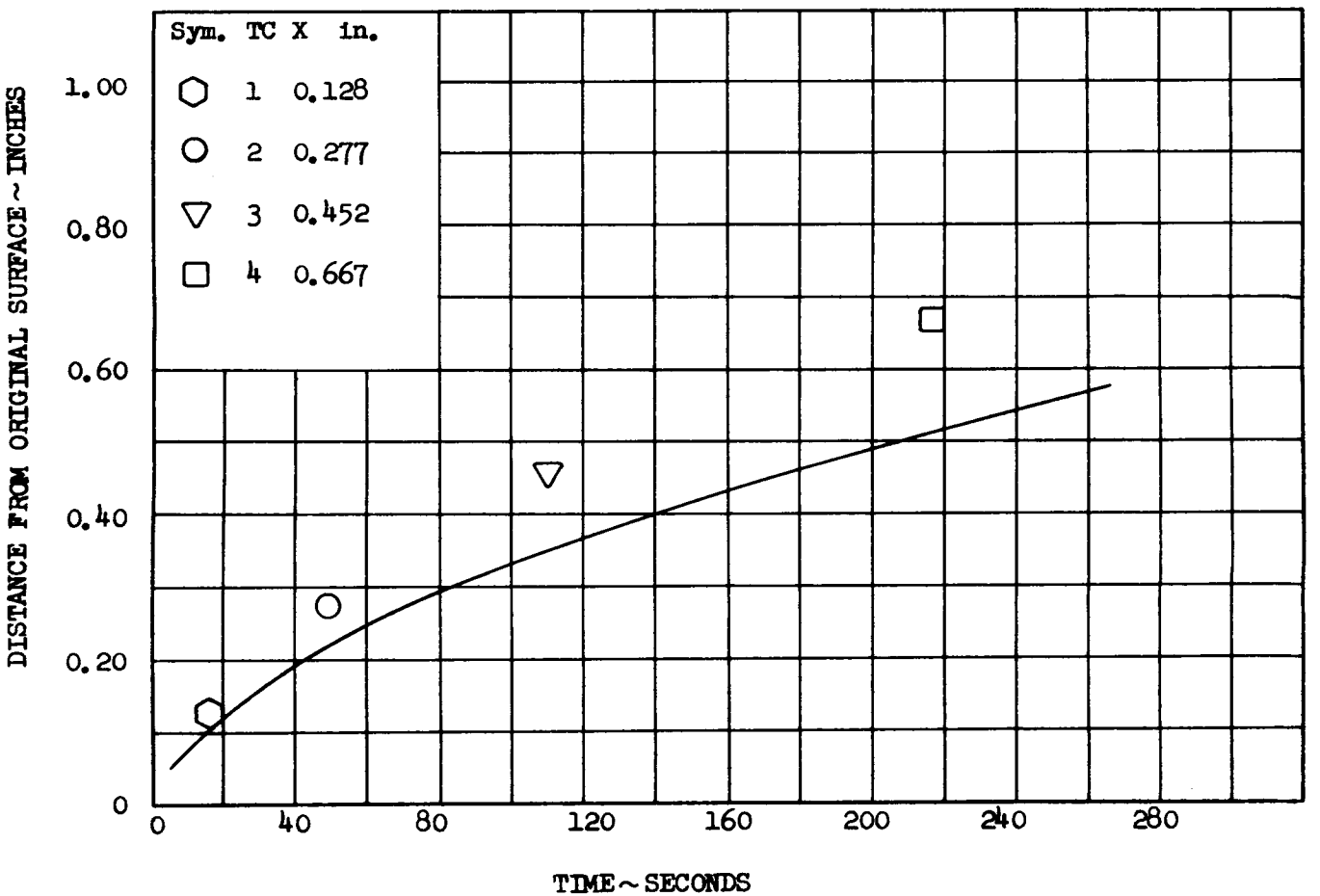

FIGURE 45

COMPARISON OF OBSERVED AND PREDICTED ISOTHERM PROGRESSIONS

TEST POINT 2A - MODEL 277
1000°F

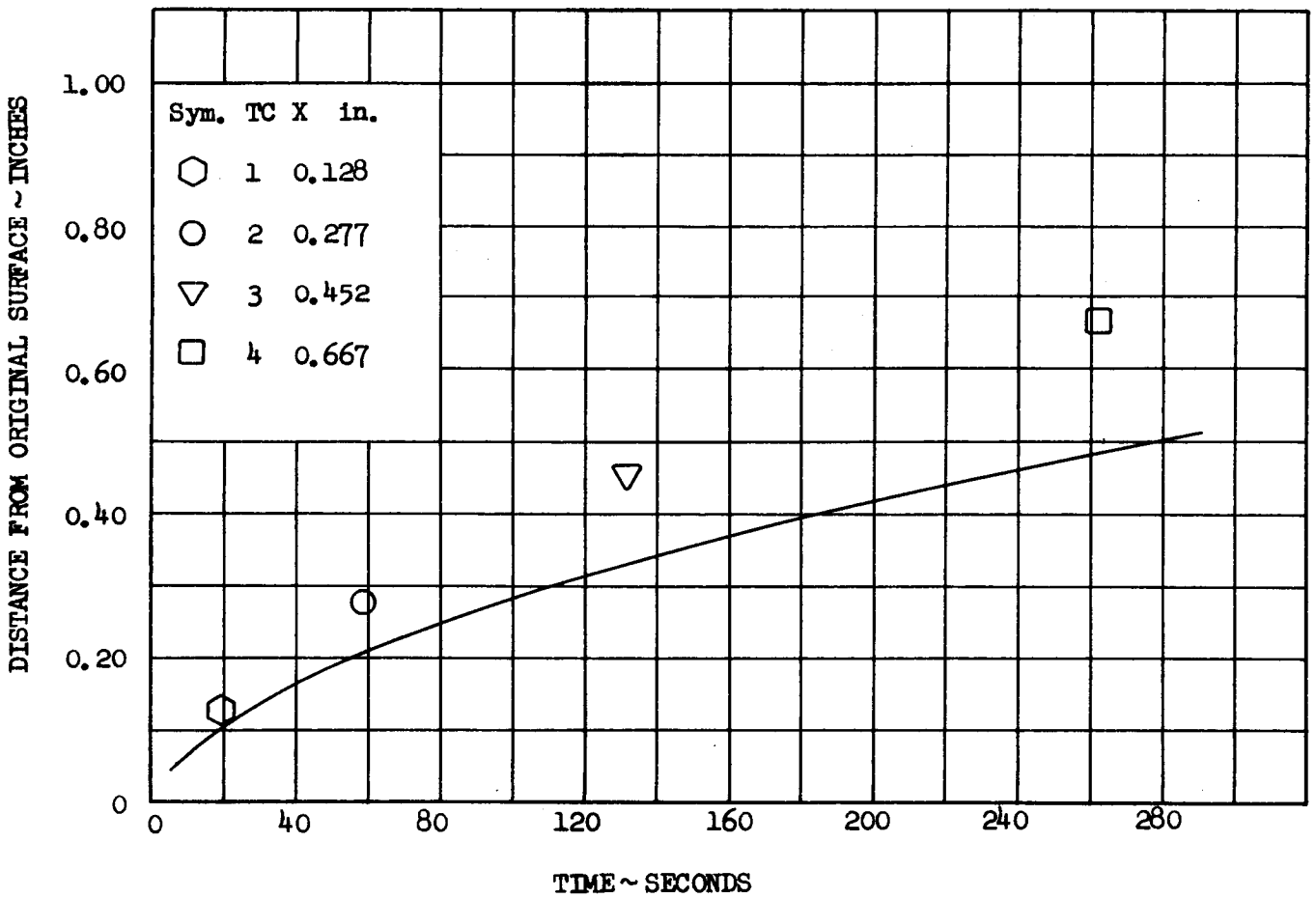

FIGURE 46

COMPARISON OF OBSERVED AND PREDICTED ISOTHERM PROGRESSIONS

TEST POINT 16A - MODEL 251
600°F

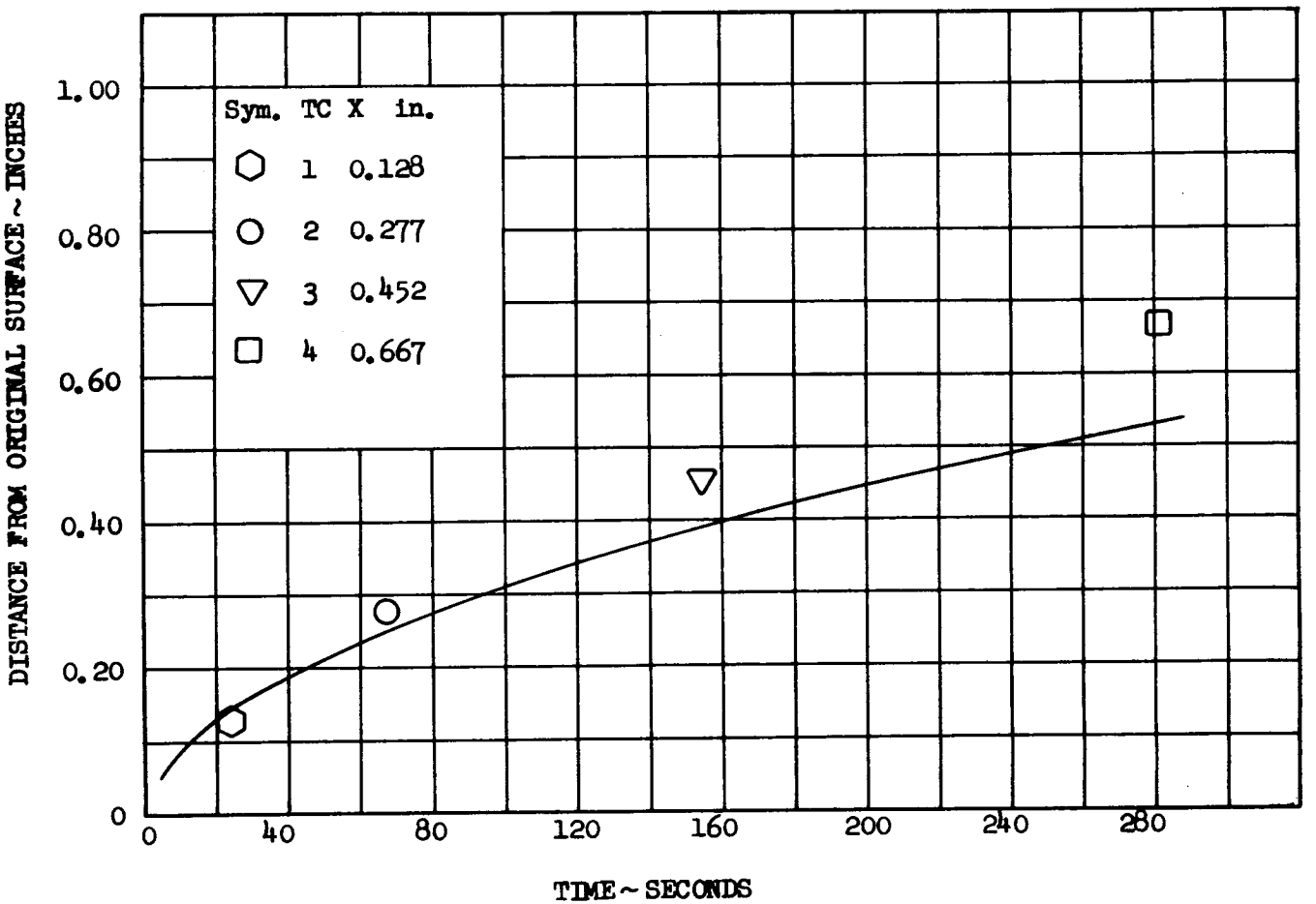

FIGURE 47

COMPARISON OF OBSERVED AND PREDICTED ISOTHERM PROGRESSIONS

TEST POINT 16A - MODEL 251
1000°F

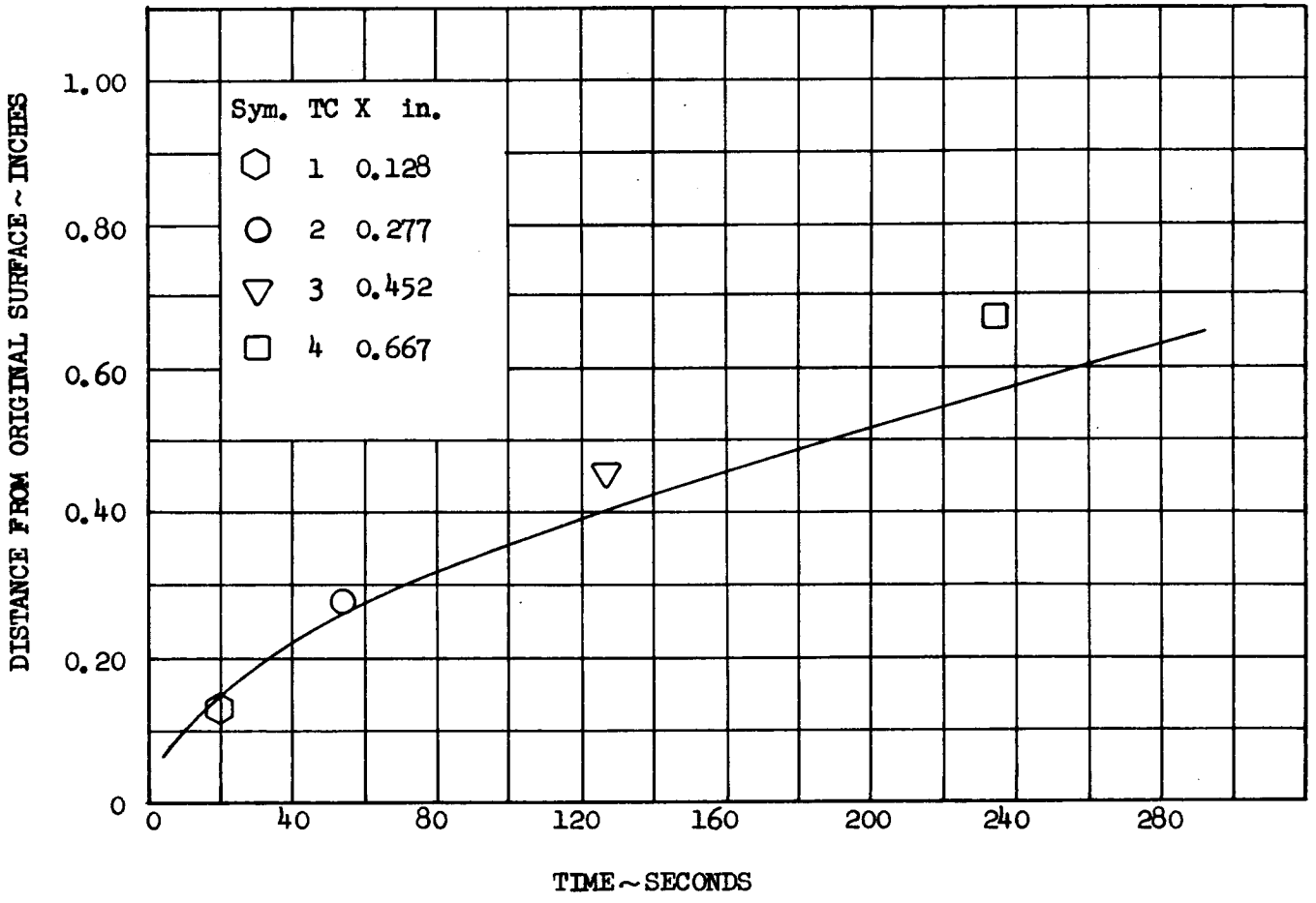

FIGURE 48

COMPARISON OF OBSERVED AND PREDICTED ISOTHERM PROGRESSIONS

TEST POINT 5N - MODEL 267
600°F

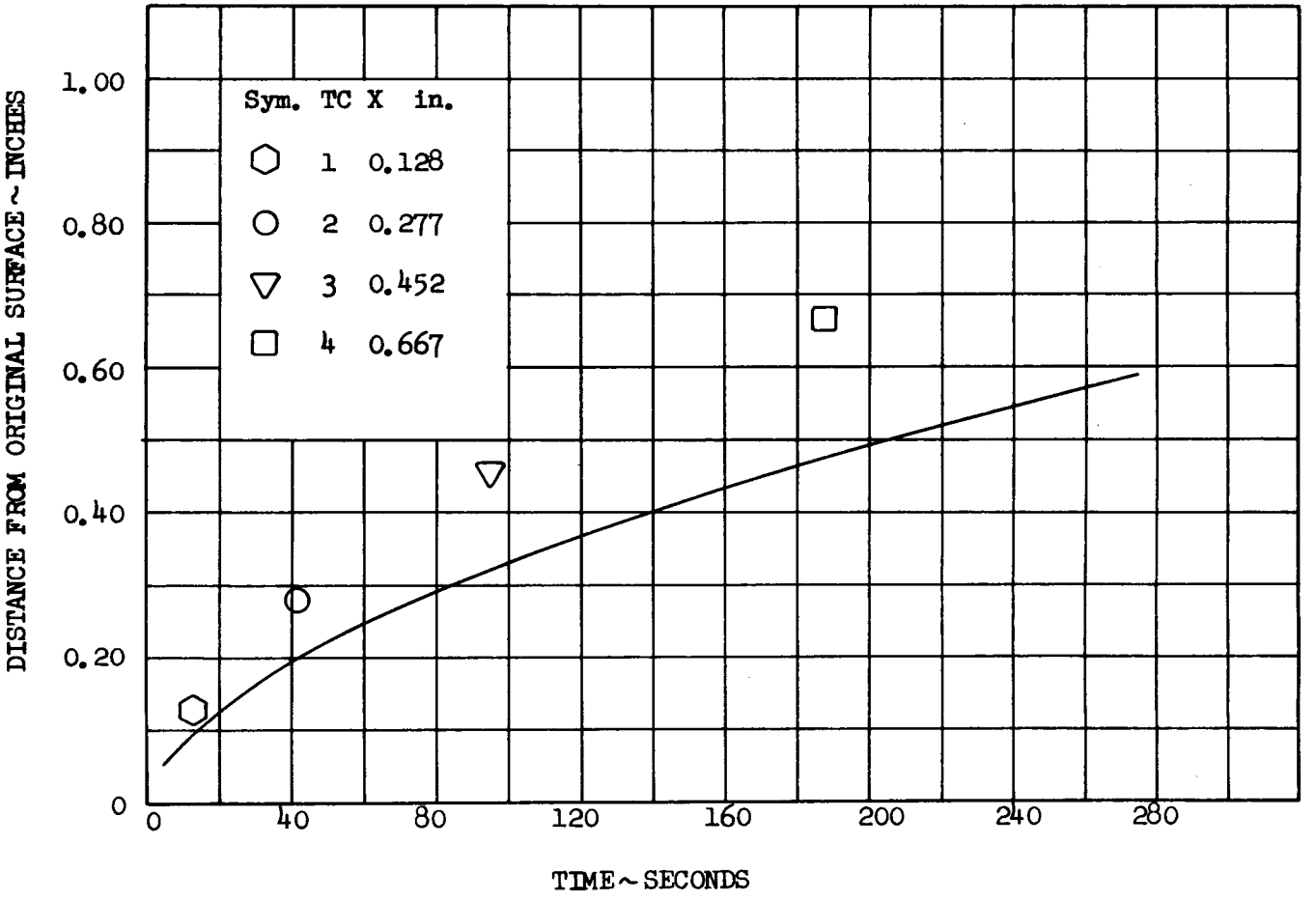

FIGURE 49

COMPARISON OF OBSERVED AND PREDICTED ISOTHERM PROGRESSIONS

TEST POINT 5N - MODEL 267
1000°F

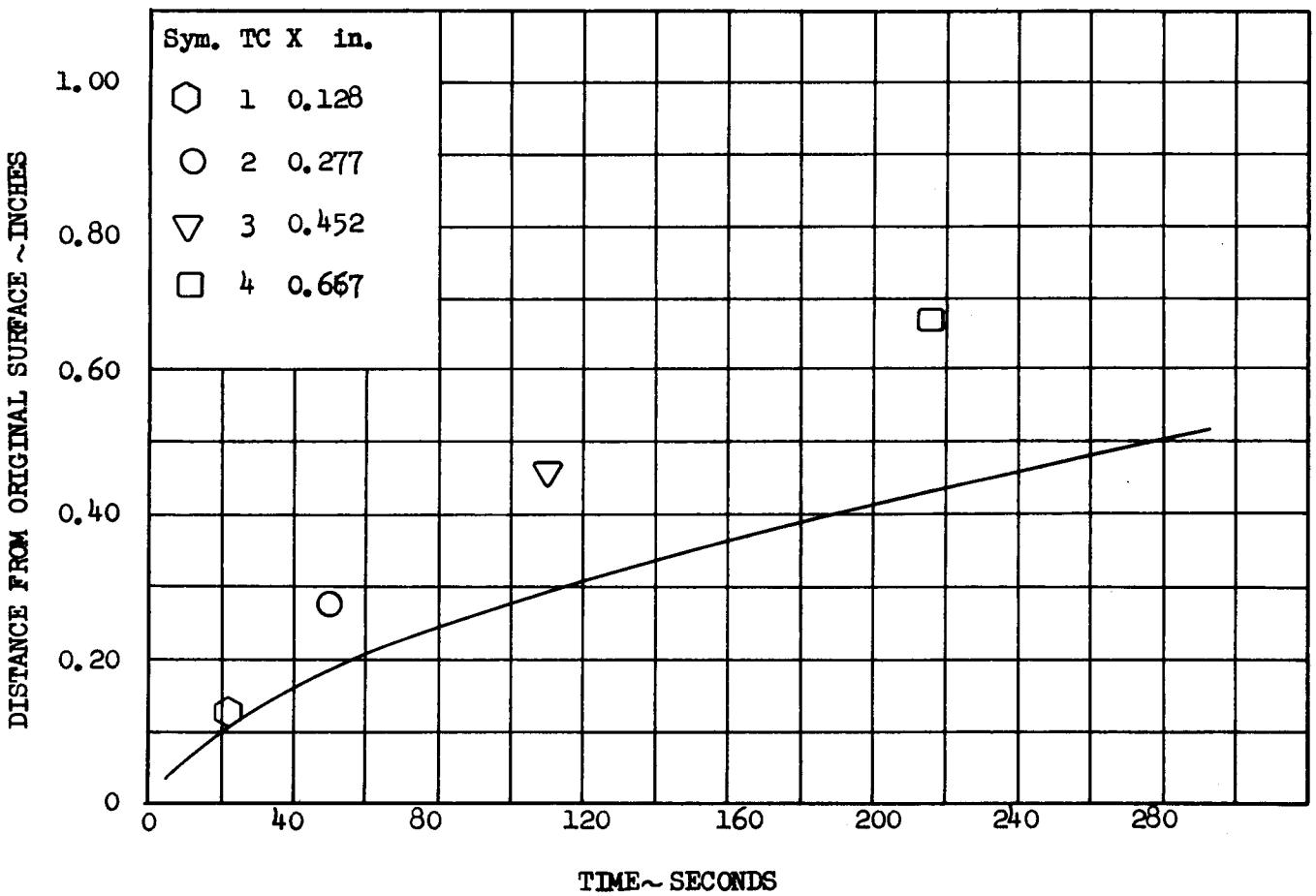

FIGURE 50

COMPARISON OF OBSERVED AND PREDICTED ISOTHERM PROGRESSIONS

TEST POINT 20N - MODEL 234
600°F

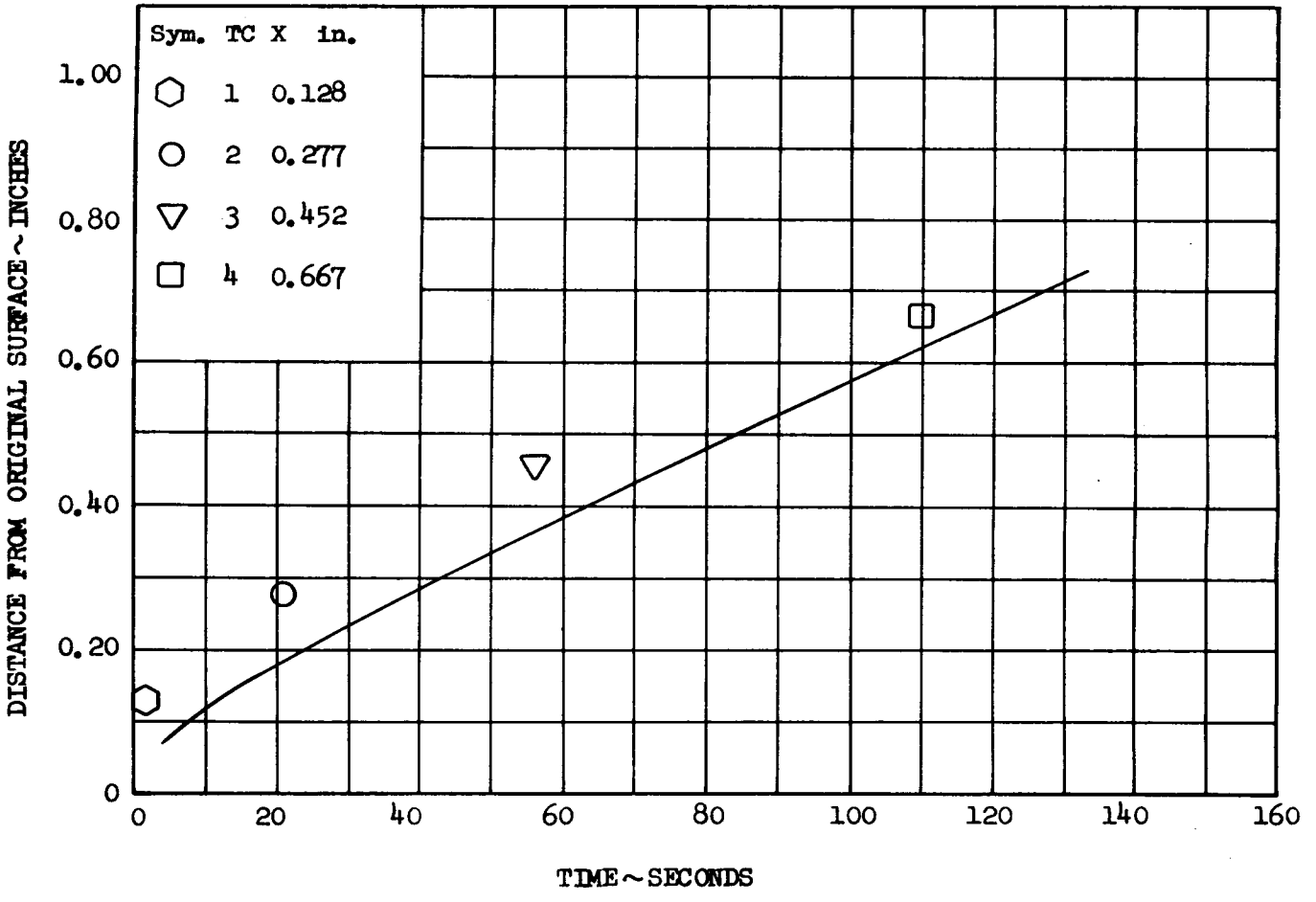

FIGURE 51

COMPARISON OF OBSERVED AND PREDICTED ISOTHERM PROGRESSIONS

TEST POINT 20N - MODEL 234
1000°F

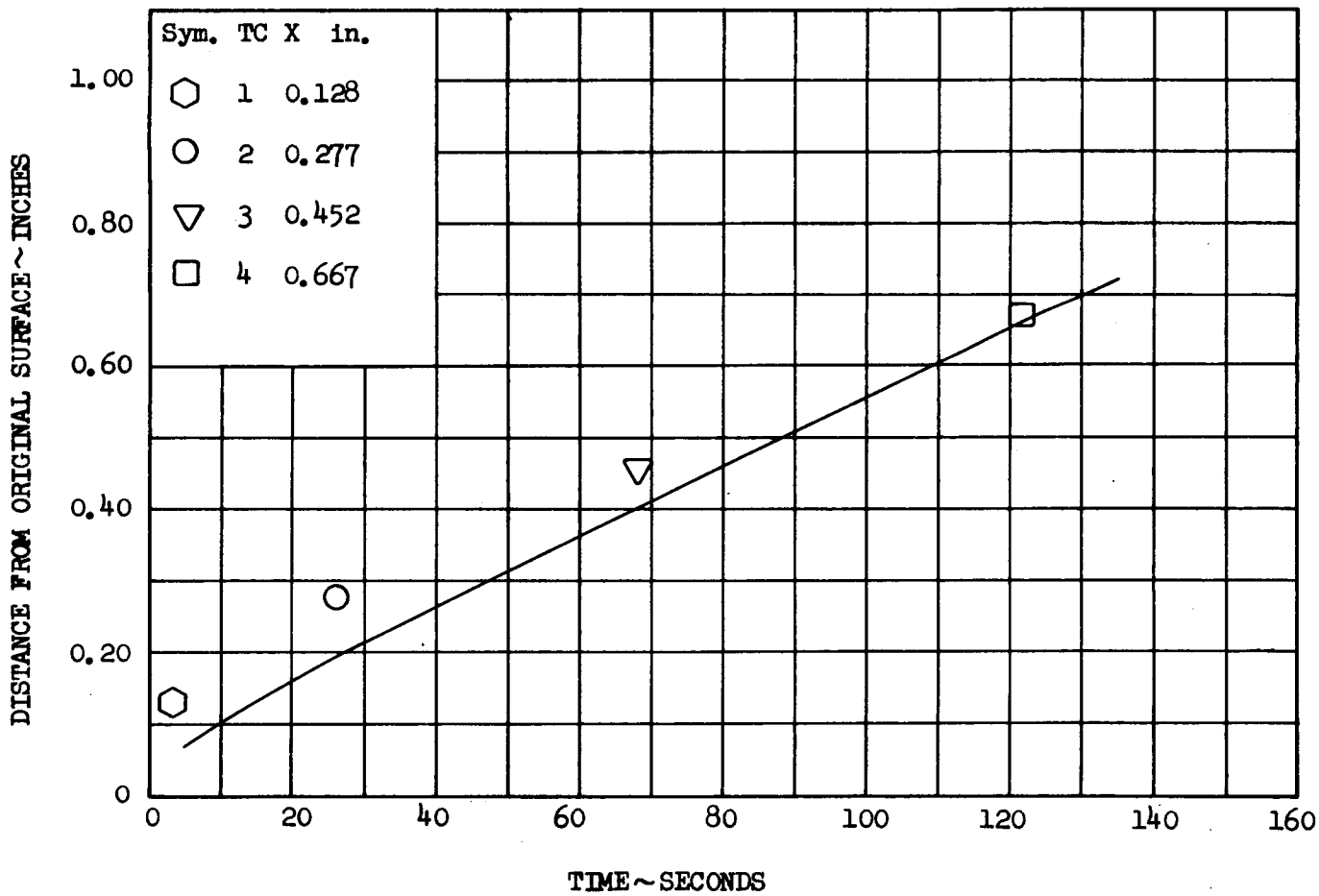

FIGURE 52
SWRI 55 600°F
COMPARISON OF OBSERVED AND PREDICTED ISOTHERM PROGRESSIONS

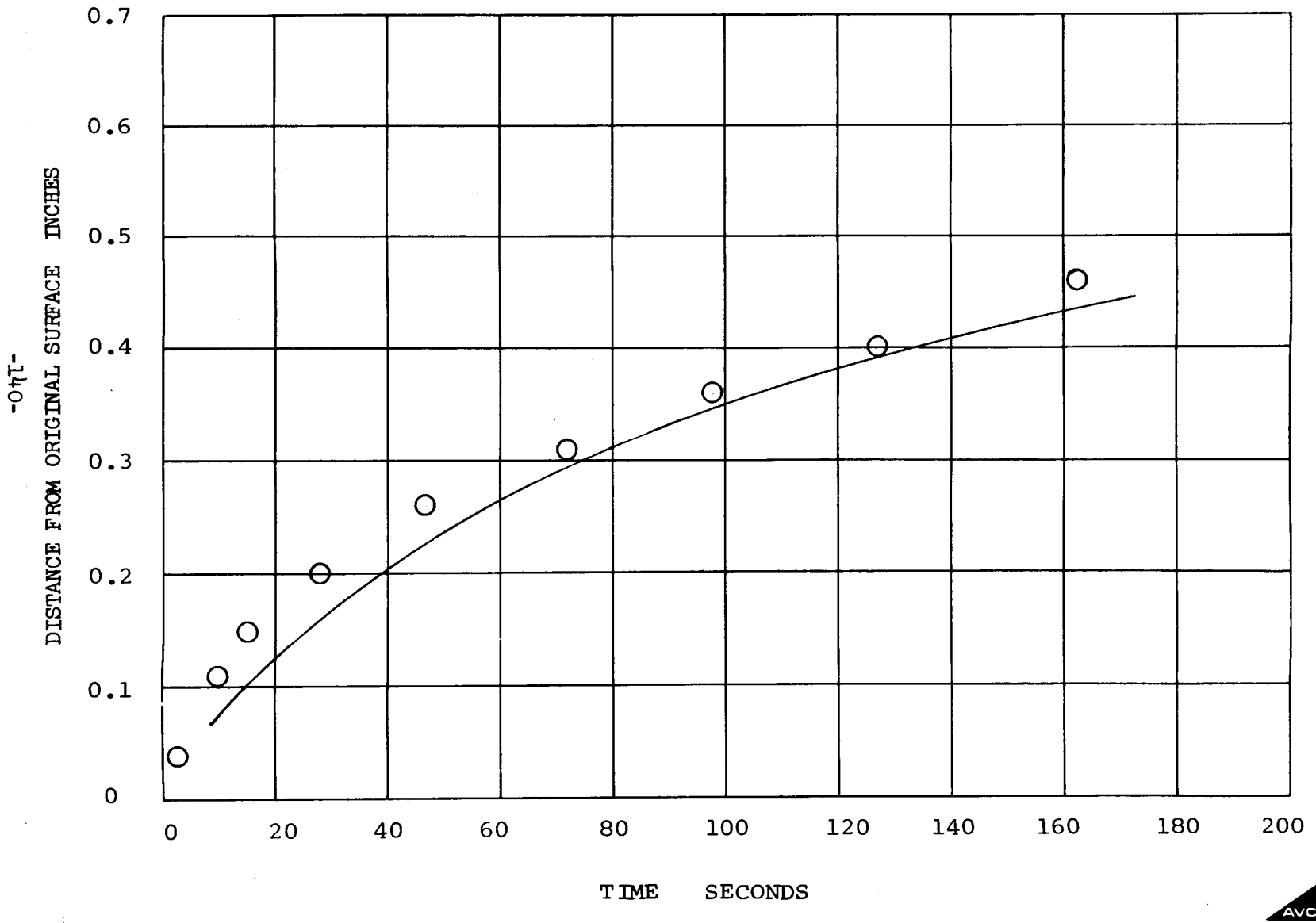

FIGURE 53
SWRI 55 1000°F
COMPARISON OF OBSERVED AND PREDICTED ISOTHERM PROGRESSIONS

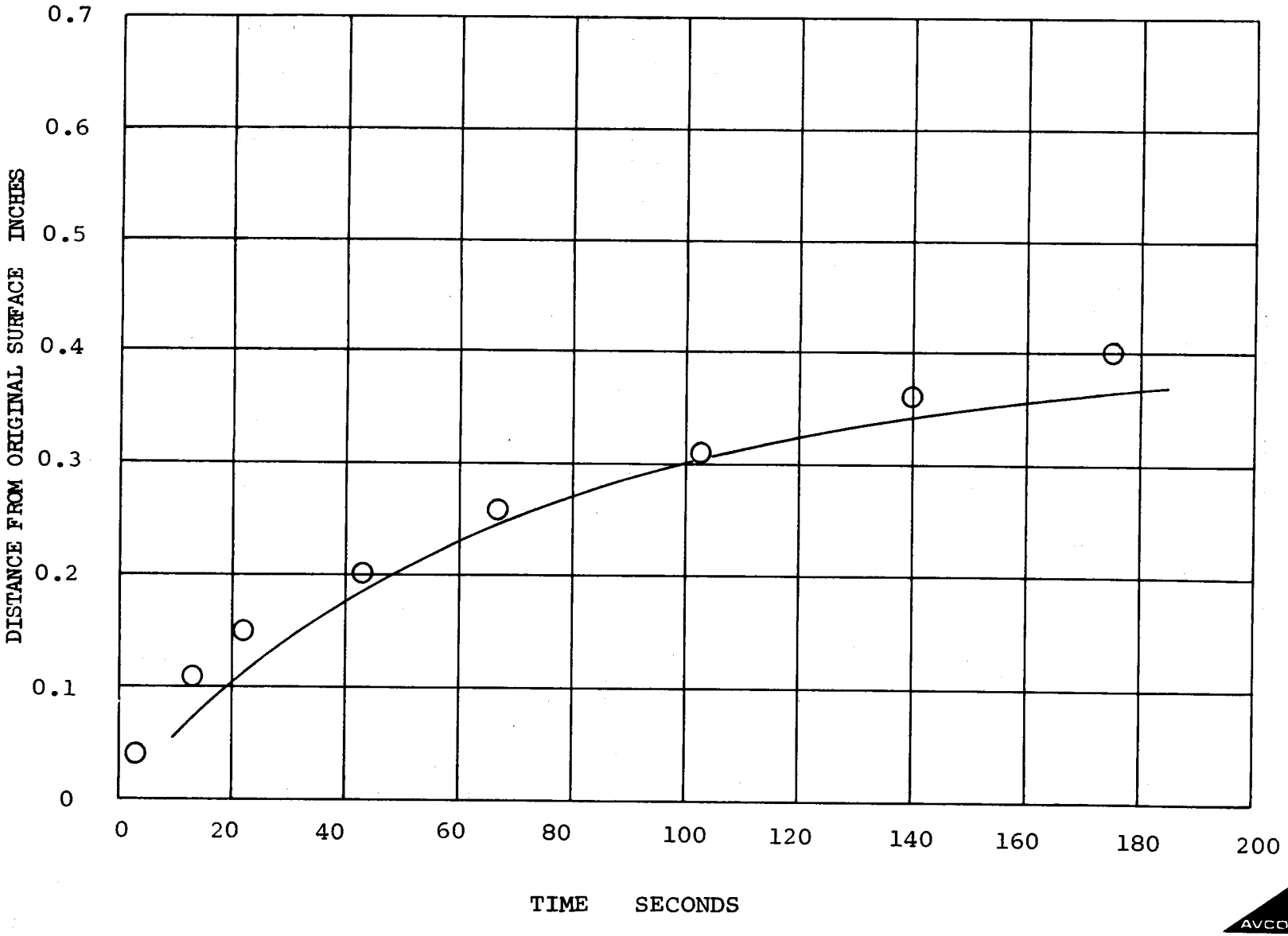

FIGURE 54
SWRI 120 600°F
COMPARISON OF OBSERVED AND PREDICTED ISOTHERM PROGRESSIONS

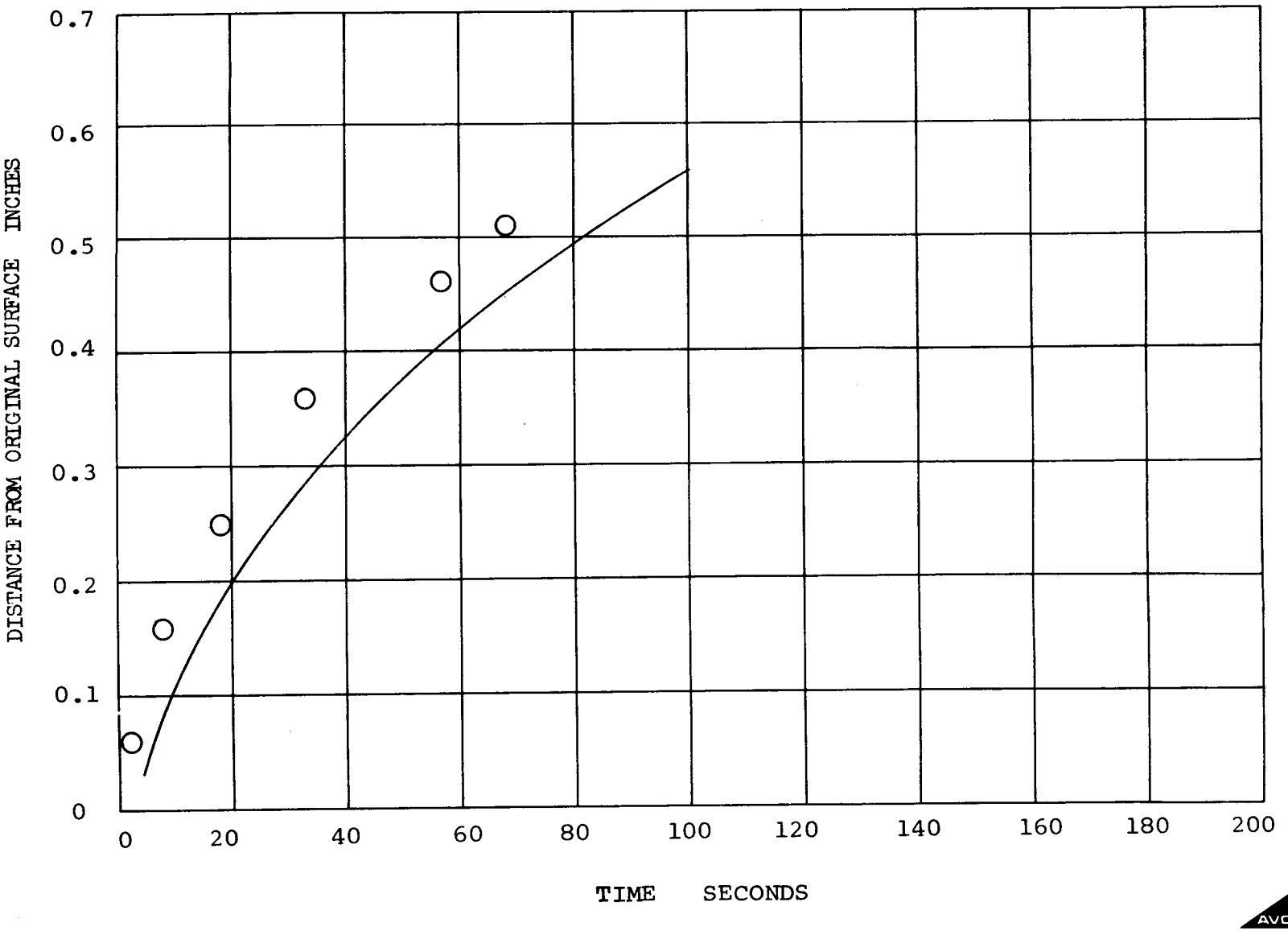

FIGURE 55
SWRI 120 1000°F

COMPARISON OF OBSERVED AND PREDICTED ISOTHERM PROGRESSIONS

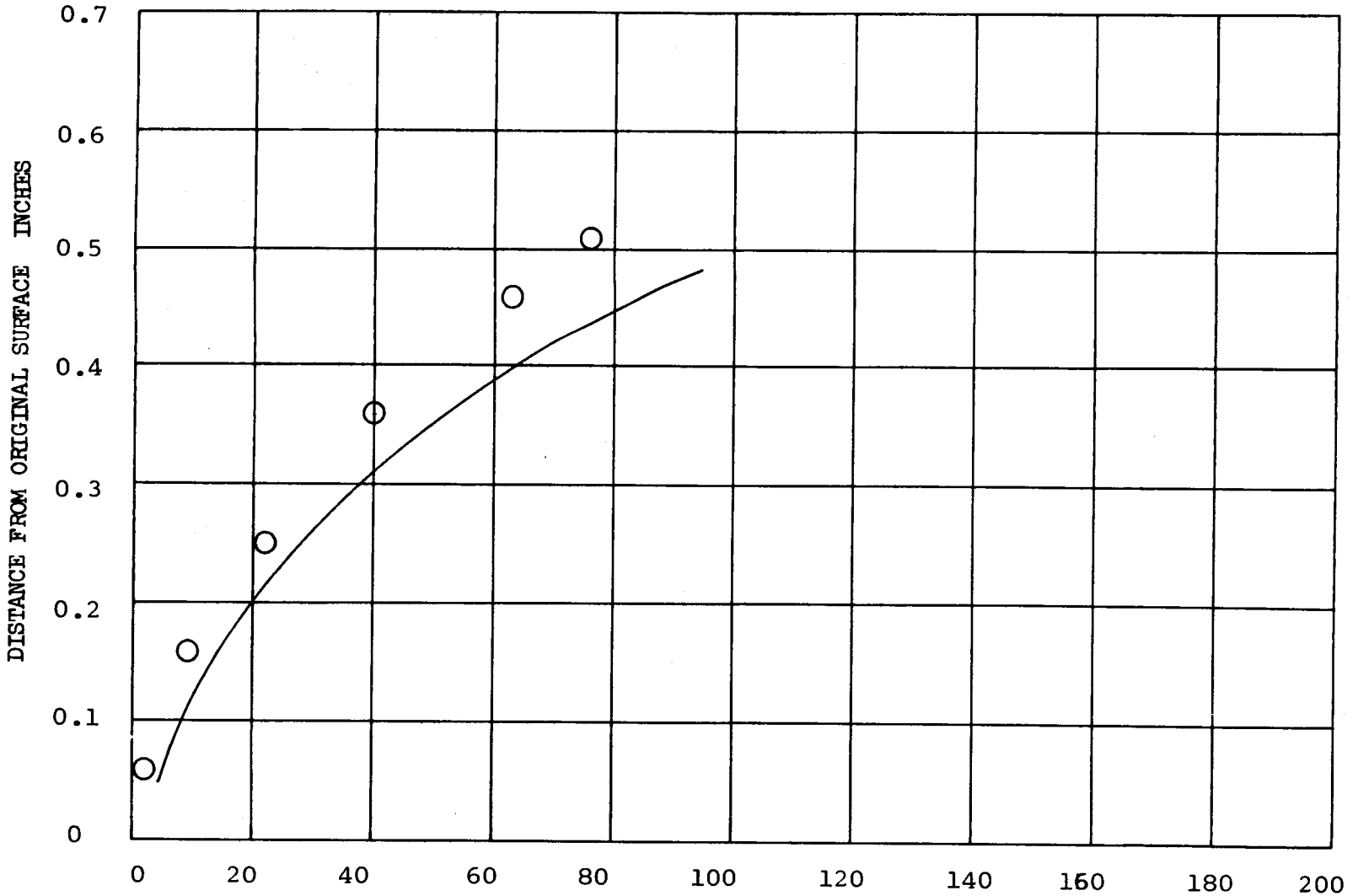

FIGURE 56

COMPARISON OF MEASURED AND PREDICTED THERMOCOUPLE HISTORIES
MODEL 157

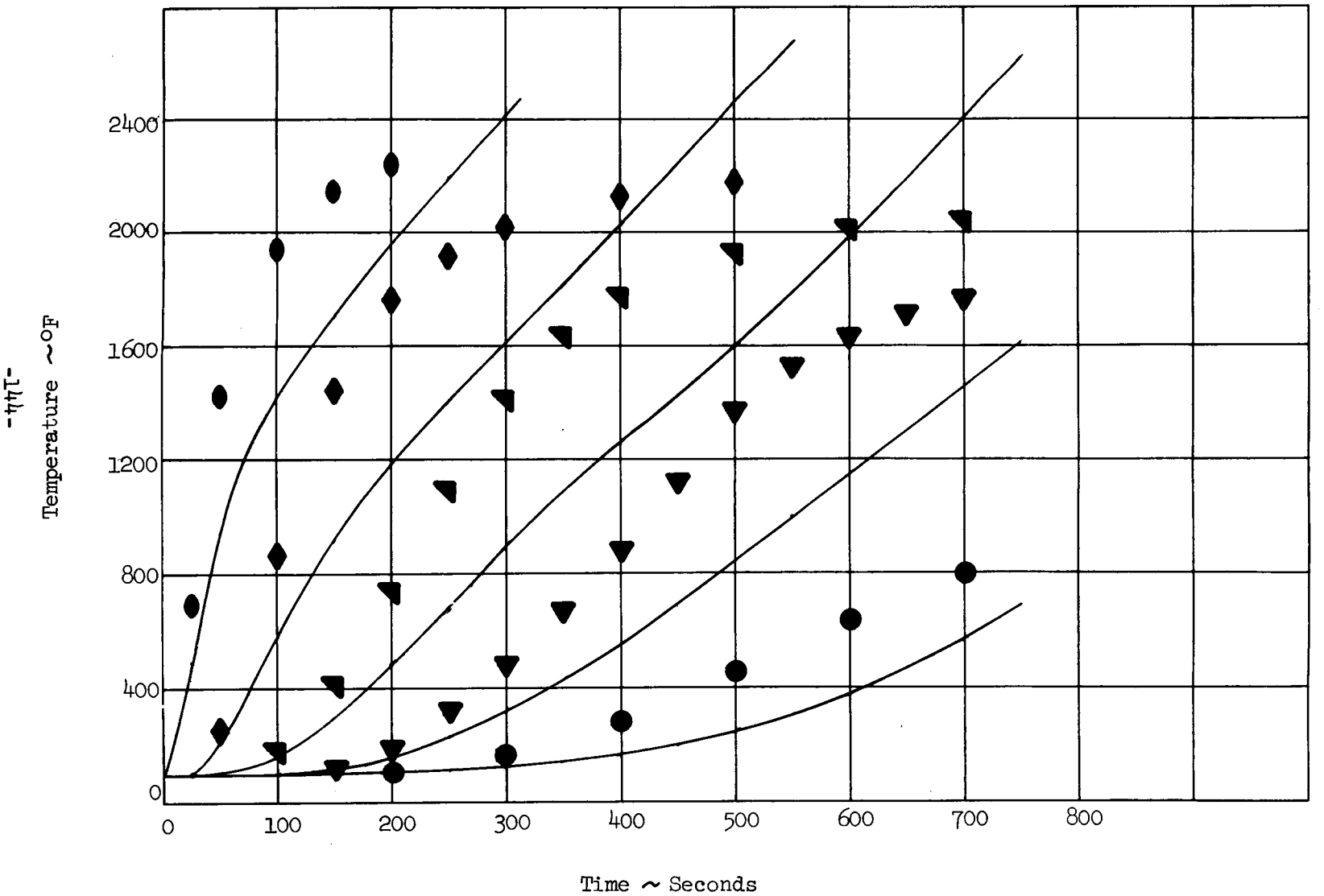

FIGURE 57

COMPARISON OF MEASURED AND PREDICTED THERMOCOUPLE HISTORIES
MODEL 142

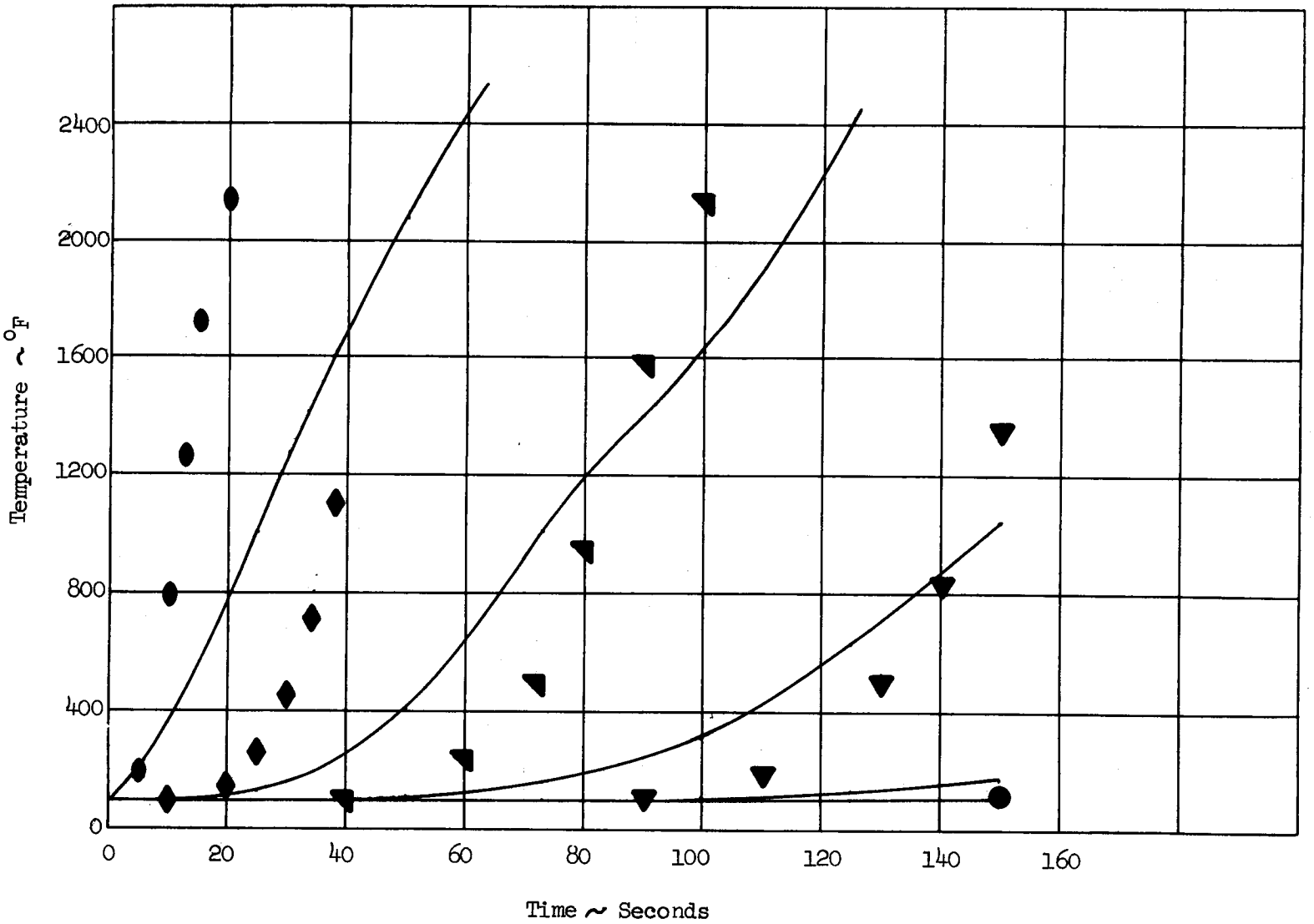

FIGURE 58

COMPARISON OF MEASURED AND PREDICTED THERMOCOUPLE HISTORIES
MODEL 159

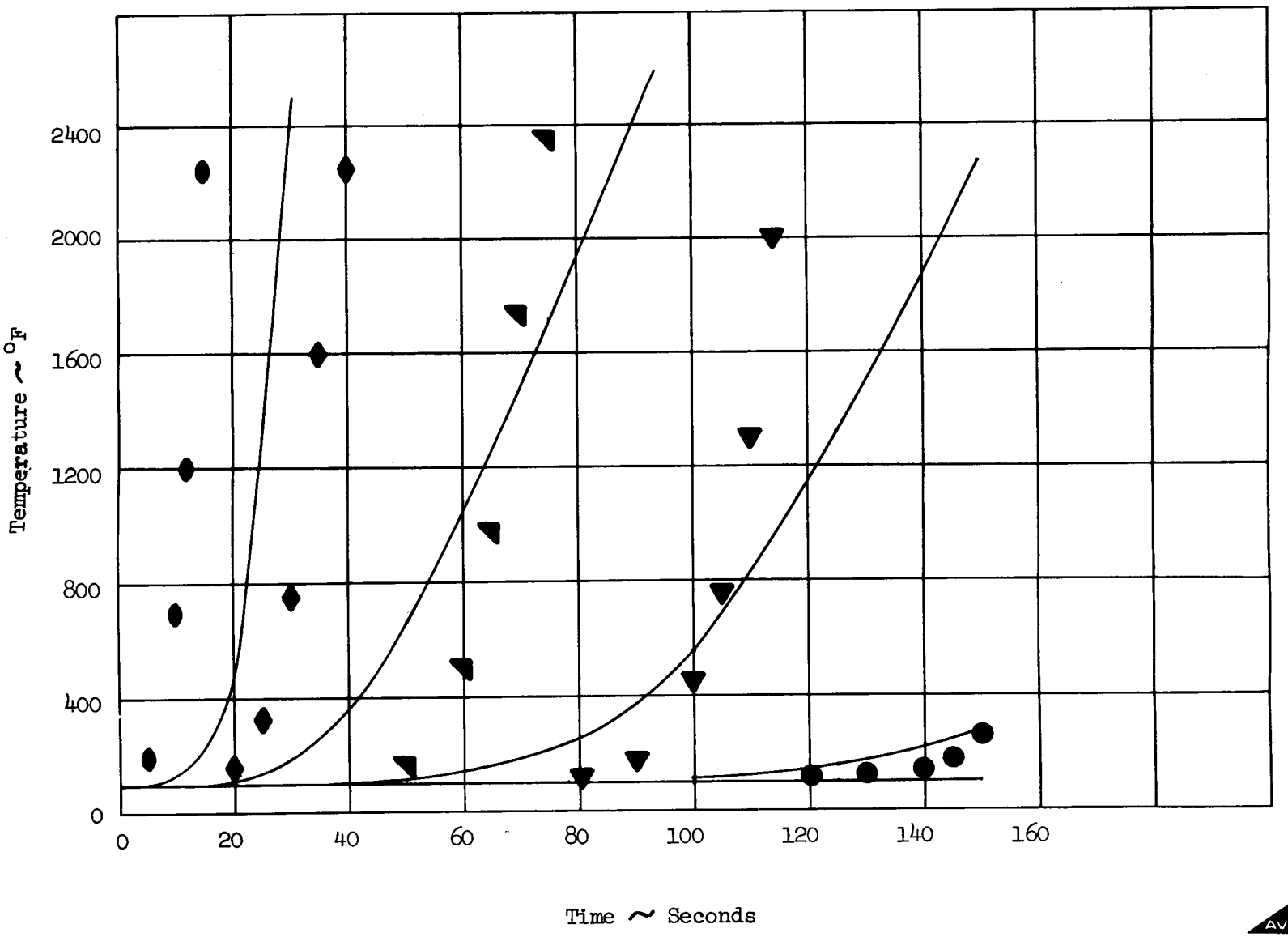

FIGURE 59

COMPARISON OF MEASURED AND PREDICTED THERMOCOUPLE HISTORIES
MODEL 127

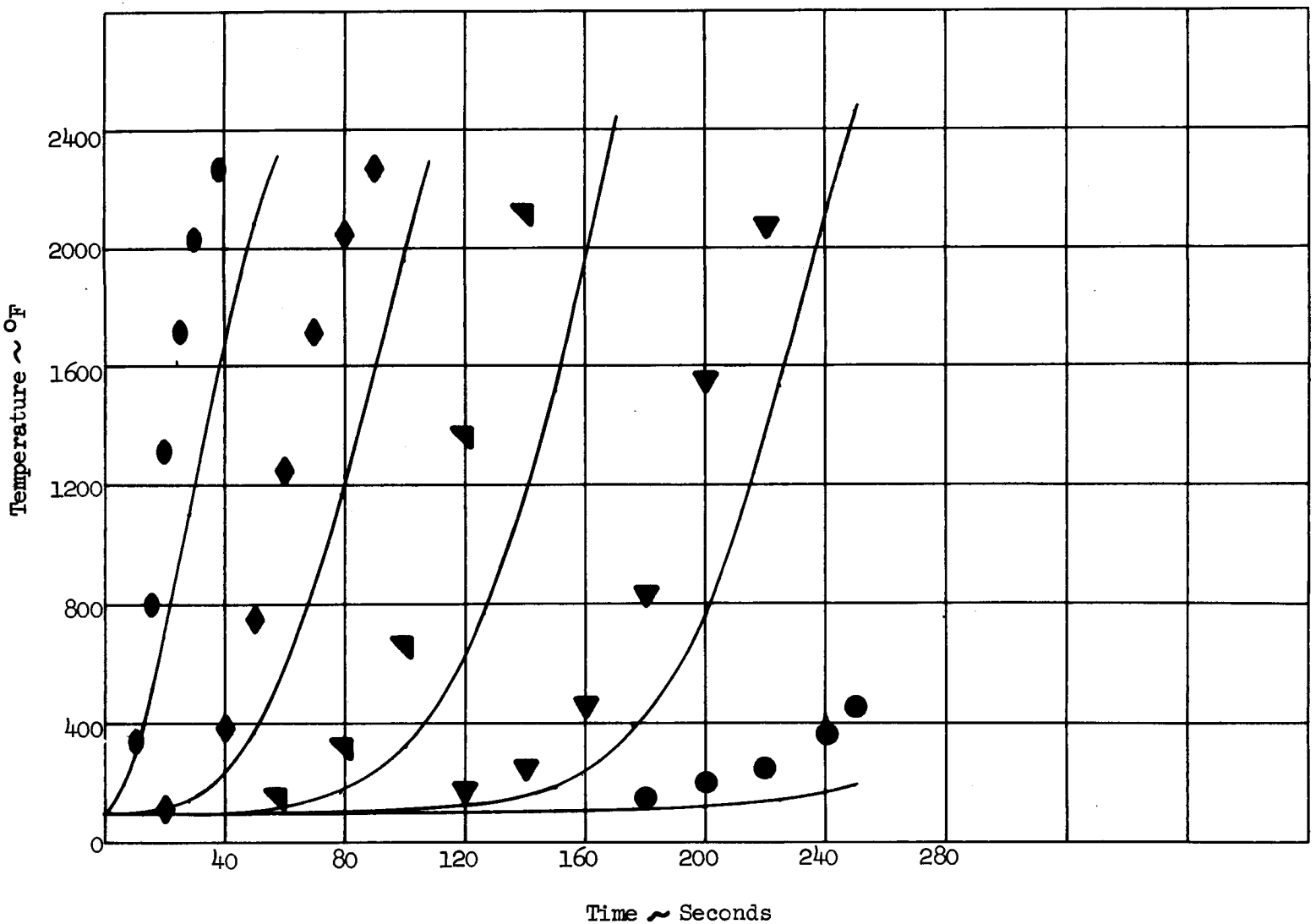

FIGURE 60

COMPARISON OF MEASURED AND PREDICTED THERMOCOUPLE HISTORIES
MODEL 131

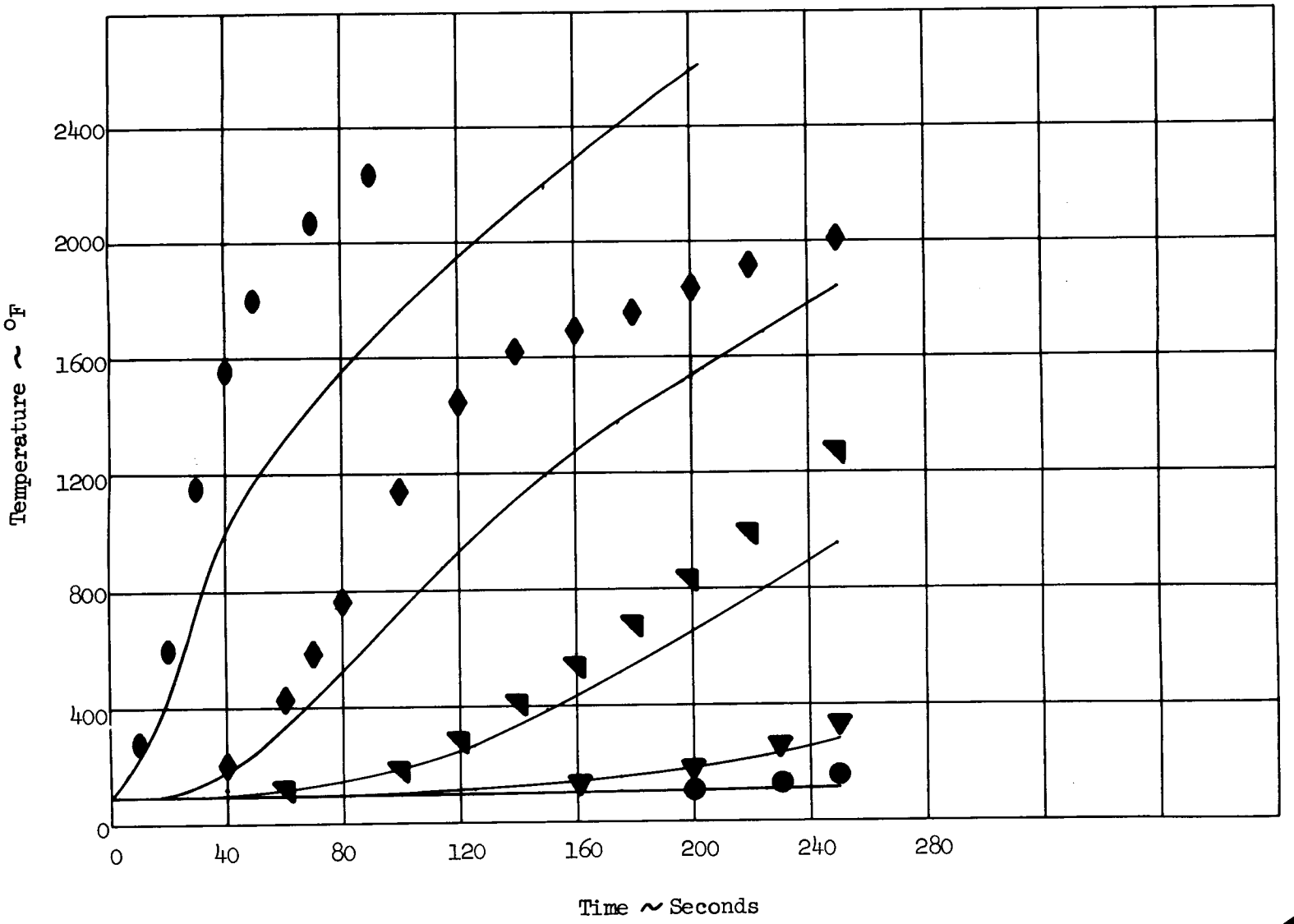

FIGURE 61

COMPARISON OF MEASURED AND PREDICTED THERMOCOUPLE HISTORIES
MODEL 145

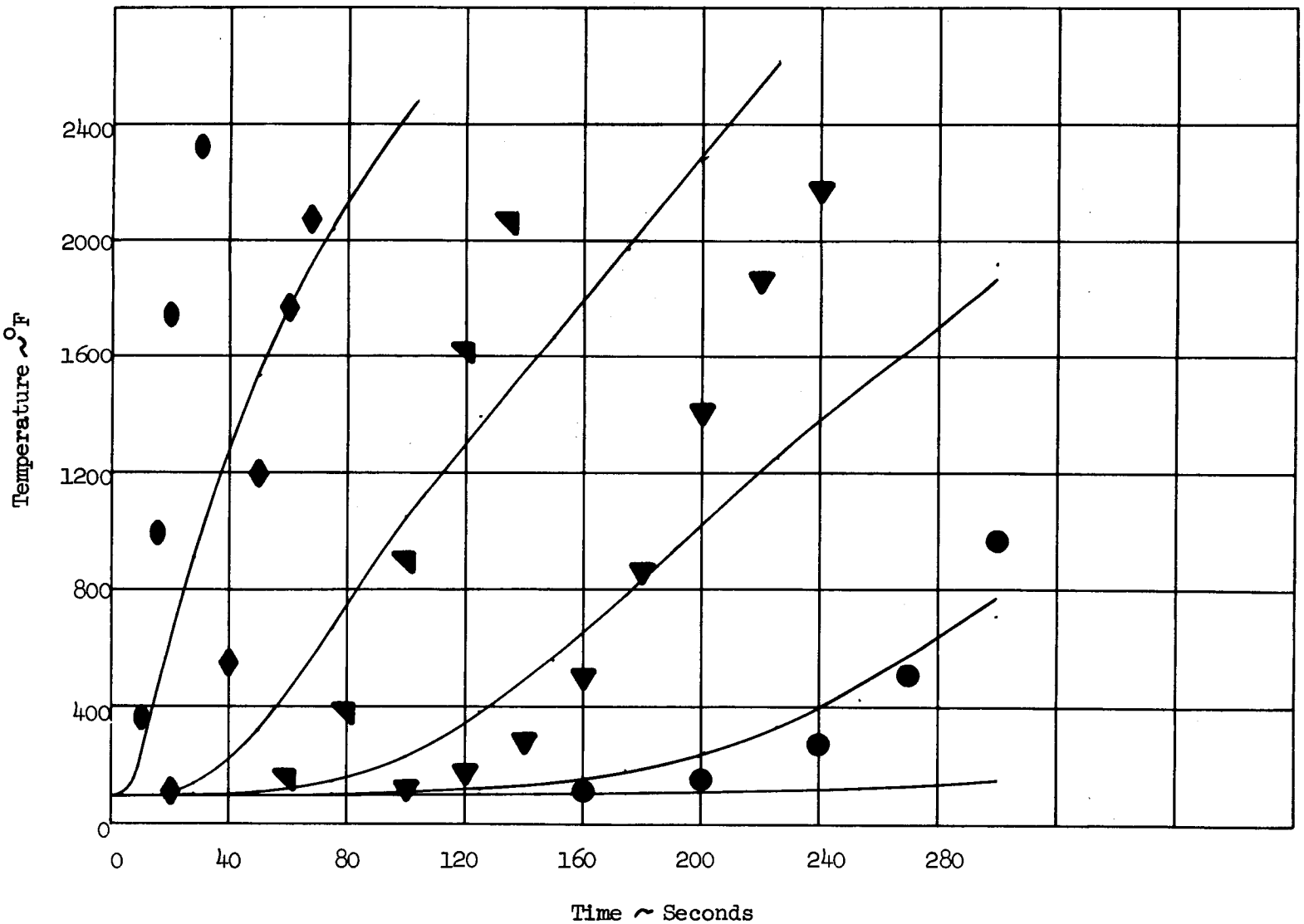

FIGURE 62

COMPARISON OF MEASURED AND PREDICTED THERMOCOUPLE HISTORIES
MODEL 153

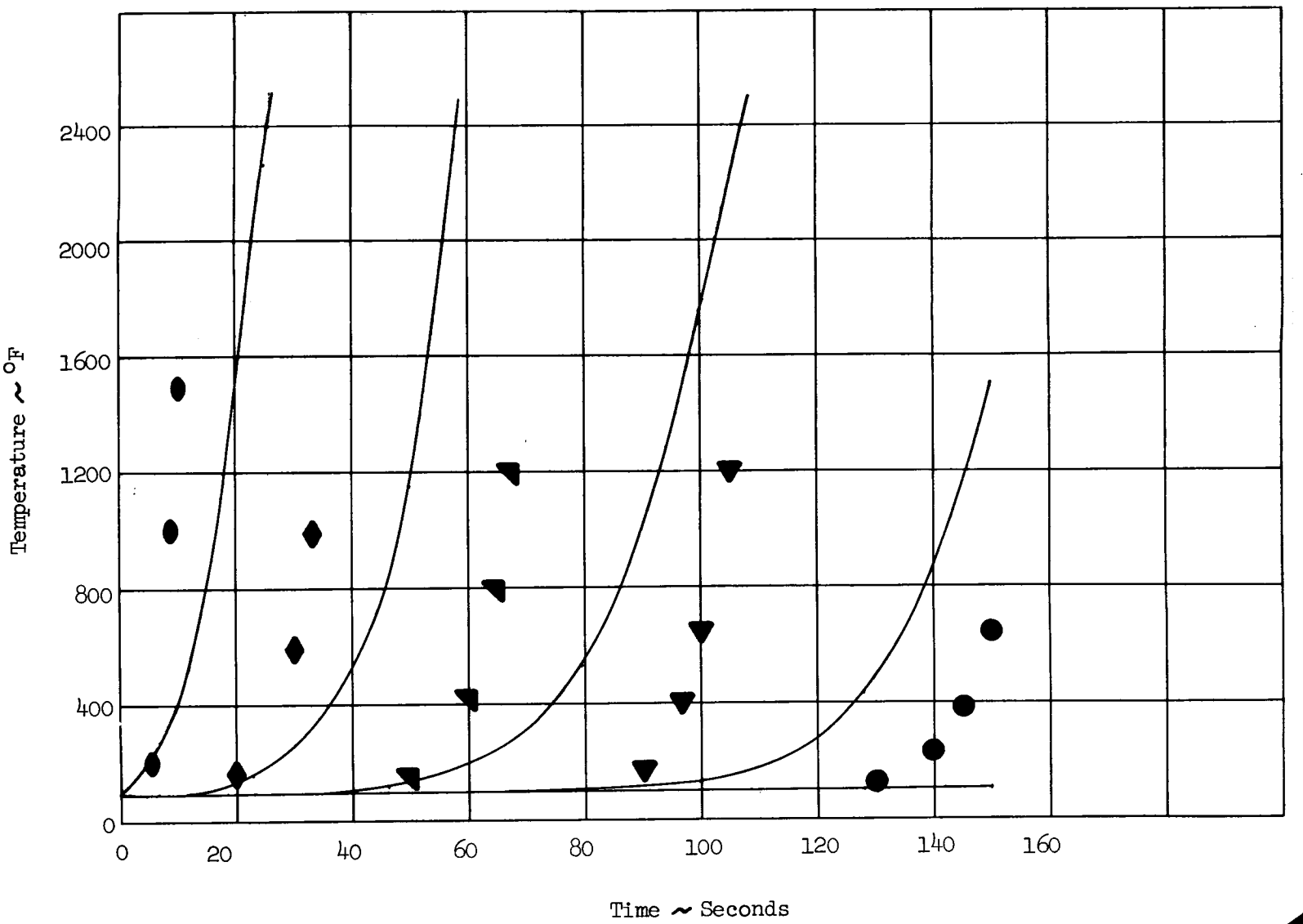

In presenting the predicted char depth histories it is necessary to define a "char depth" in terms of some fraction of the total allowable pyrolysis reaction. In the present case the char is arbitrarily defined to extend to the location at which the pyrolysis reaction is 20% complete. That is the char is taken to be that portion of the material for which the following inequality holds.

$$\left(\frac{\rho - \rho_c}{\rho_o - \rho_c}\right) \leq 0.8 \tag{237}$$

In evaluating this region ρ_o is taken as 33.0 lb/ft^3 and ρ_c is taken as 16.5 lb/ft^3. The location of this "char interface" is then obtained from the calculations by following the 29.5 lb/ft^3 isochore through the material as a function of time. Figure 63 shows the location of this point as a function of time for the conditions of Test Point 1. Since the 1000°F isotherm is sometimes taken as a measure of the char demarcation it is of interest to compare these two definitions. Figure 64 presents the temperature at the 29.5 lb/ft^3 isochore as a function of time for the conditions of Test Point 1. Also indicated on Figure 64 is the temperature history of the pyrolysis zone midpoint corresponding to the 24.75 lb/ft^3 isochore. As can be seen from the figure the 1000°F isotherm and 29.5 lb/ft^3 isochore agree quite well for this case.

The computational model employed for the calculations does not account separately for such quantities as combustion heating and mass transfer blocking since these effects are incorporated into a general boundary condition as given in Section 4.0. Physically these quantities are not separable but form a part of the overall coupled set of effects at the heated surface. In an effort to illustrate the magnitude of the several terms in a somewhat arbitrary fashion both the calculations and the test data have been examined in terms equation (238) which is a form of equation (208).

$$q_{OB} + q_{CO} - q_r = q_f + q_k \tag{238}$$

where

$$q_{OB} = \frac{q_c}{H_s}\left\{H_s - H_w\right\}\bar{\Phi} \tag{239}$$

$$q_r = \epsilon \sigma T_s^4 \tag{240}$$

FIGURE 63

TEST POINT 1

LOCATION OF THE 29.5 LB/FT^3 ISOCHORE

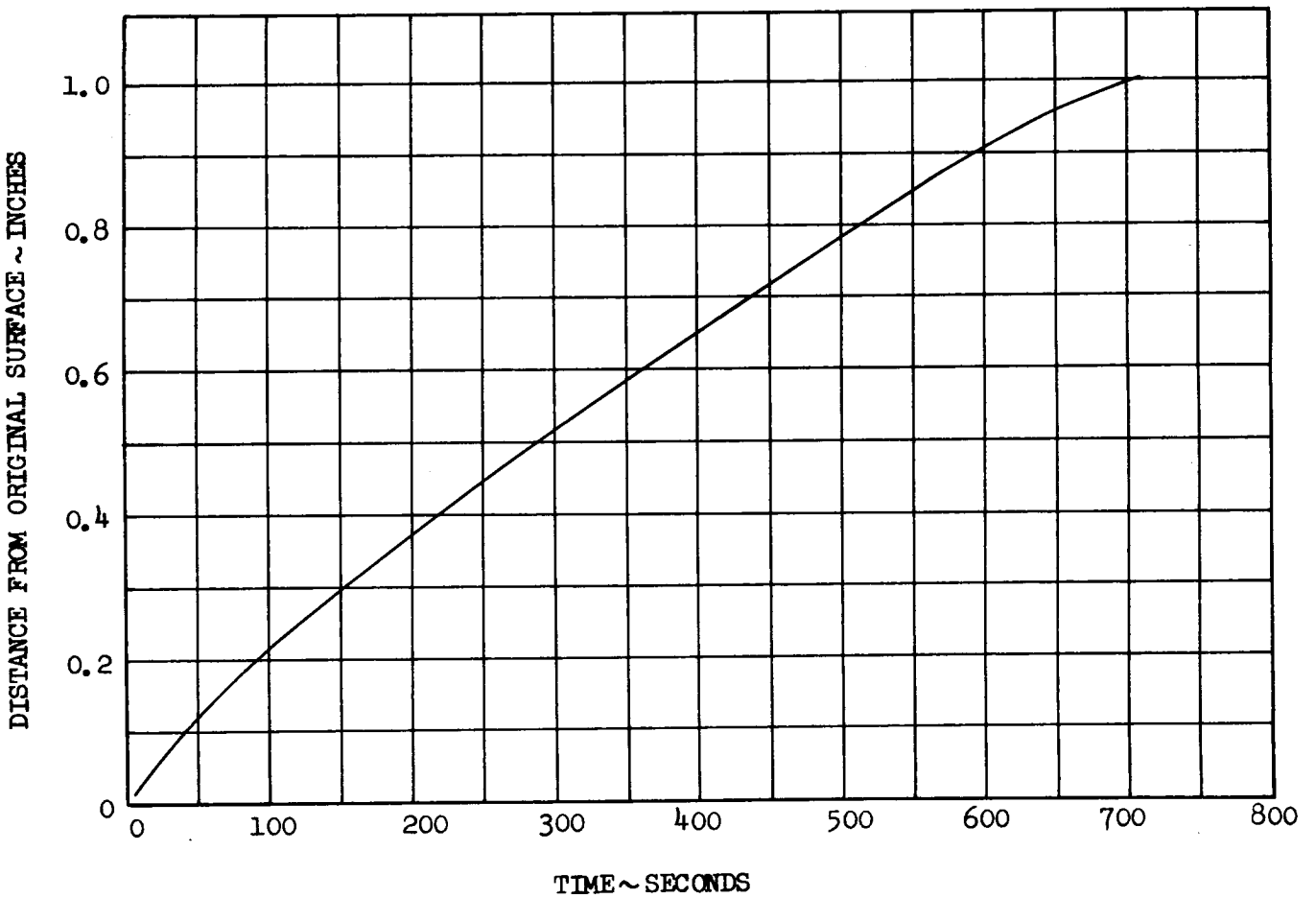

FIGURE 64

TEST POINT 1

ISOCHORE TEMPERATURE HISTORIES

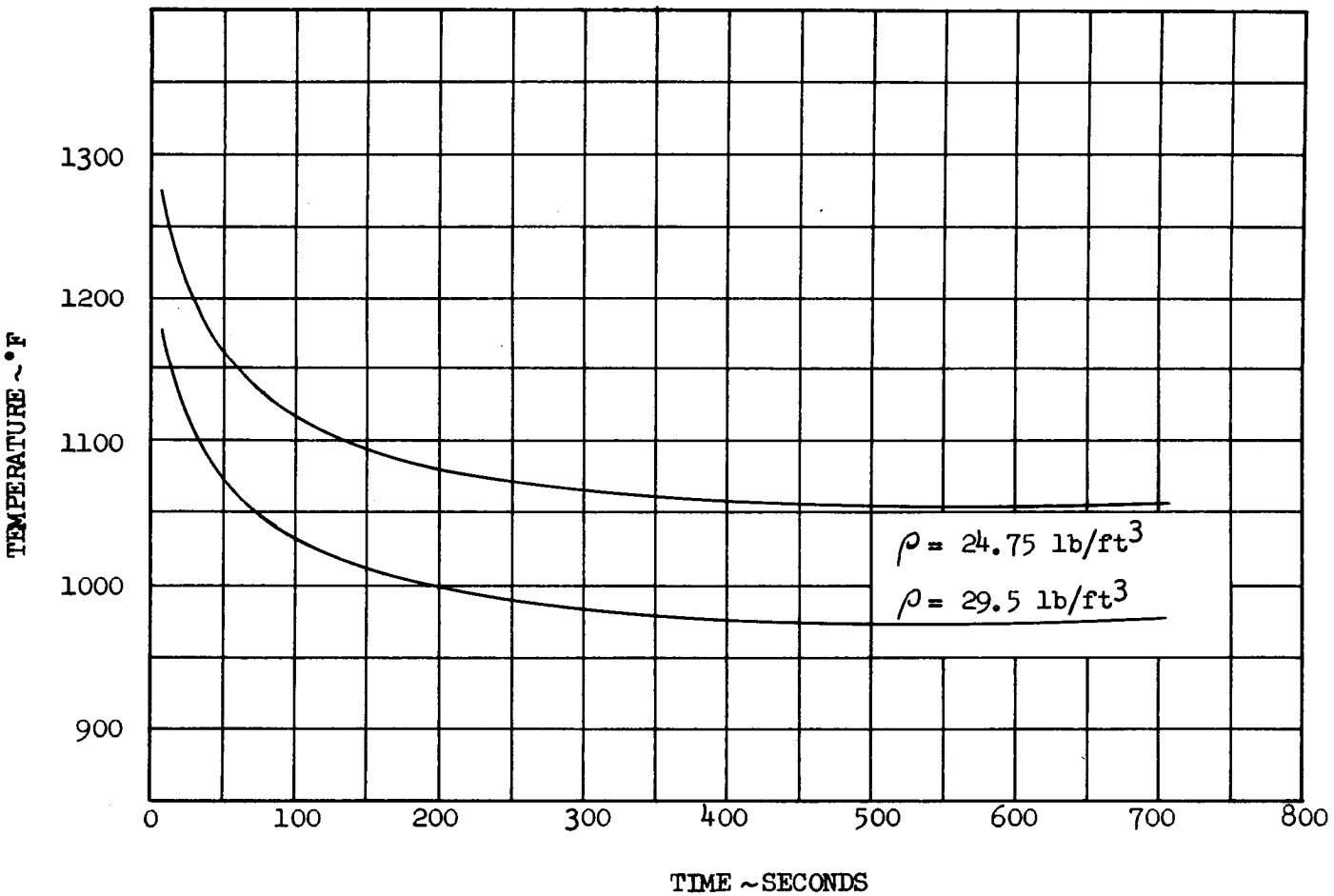

$$q_f = \rho_c H_v (\Delta s/\Delta t) \tag{241}$$

$$q_k = \rho_o \left(\frac{\Delta s}{\Delta t}\right)\left\{\left(\frac{\rho_o - \rho_c}{\rho_o}\right) C_g (T_s - 1000) + \left(\frac{\rho_c}{\rho_o}\right) C_{p_c} (T_s - 1000) + C_{p_o} (1000 - 70) + \left(\frac{\rho_o - \rho_c}{\rho_o}\right) \Delta H_c\right\} \tag{242}$$

$$\bar{\phi} = \exp\left\{-\bar{f}(1 + 0.618\,\bar{f})\right\} \tag{243}$$

$$\bar{f} = \frac{\rho_o \Delta s H_s \eta}{q_c \Delta t} \tag{244}$$

The quantity q_{OB} in equation (239) is the heat transfer rate to a wall at T_w corrected for the effects of mass transfer. The q_r of equation (240) is the rate of surface reradiation. The q_f of equation (241) is the rate of energy absorption due to surface material removal. The q_k of equation (242) is the rate at which energy enters the material by conduction. The quantity q_{CO} can in some sense be considered an energy input to the surface due to exothermic chemical reactions. This q_{CO} is actually a rather complex quantity within the framework of the model of Section 4.0 where it is given by equation (245)

$$q_{CO} = \frac{q_c w_e H_c}{H_s}\left\{1 - \left(\frac{\dot{S}_T}{\dot{S}_R}\right)^{1/N_r}\right\}\phi \tag{245}$$

The various terms appearing in equation (184) have been evaluated for several selected models both from the experimental data and from the transient numerical predictions. The steady state analysis of Section 3.6 has also been employed to evaluate the several terms. The results of these calculations appear in Table 10. It should be noted that the largest contributor to the values of q_{CO} is the radiation loss from the ablating surface. Since in the Plasmadyne tests this quantity is not measured directly as in the Model 500 tests any small error in the surface temperature results in large errors in the quantity q_{CO}. For example a

Table 10

ENERGY TRANSFER TERMS FOR SELECTED MODELS

Model	q_{OB} (BTU/ft^2-sec)	q_r (BTU/ft^2-sec)	q_f (BTU/ft^2-sec)	q_k (BTU/ft^2-sec)	q_{CO} (BTU/ft^2-sec)
PD157(1)	19.97	21.6	0.17	1.05	2.85
PD157(2)	18.40	17.10	0.56	4.13	3.39
PD157(3)	16.24	17.0	1.0	3.5	5.26
PD142(1)	52.13	113.7	2.56	23.28	87.41
PD142(2)	72.07	55.4	1.23	12.91	-2.53
PD142(3)	60.99	59.1	2.0	13.6	13.71
PD159(1)	91.43	174.4	3.72	37.71	124.41
PD159(2)	140.52	109.9	2.03	21.61	-6.98
PD159(3)	118.85	113.6	2.0	19.6	16.35
PD127(1)	31.42	54.4	1.86	14.08	38.91
PD127(2)	31.36	29.16	2.11	13.24	13.15
PD127(3)	28.10	29.3	2.0	13.2	16.40
PD131(1)	41.98	32.8	0.48	3.22	-5.48
PD131(2)	41.26	29.83	0.53	7.15	-3.75
PD131(3)	33.43	33.6	1.0	4.9	6.07
PD145(1)	48.29	90.6	6.36	15.36	64.04
PD145(2)	78.94	60.34	0.84	9.83	-7.93
PD145(3)	64.91	63.5	1.0	8.4	7.99
PD153(1)	115.31	121.2	4.16	38.42	48.46
PD153(2)	-	-	-	-	-
PD153(3)	113.84	105.6	4.0	32.7	28.46

Figures in parenthesis following the model number indicate the source of the data.

(1) Experimental
(2) Theoretical, Transient
(3) Theoretical, Steady-State

10% error in surface temperature introduces an error of 46% in q_r and an even larger error in q_{CO} since the quantity q_{OB} is also affected by this surface temperature error.

The comparison between theory and test as presented in this section is generally speaking not outstanding if all the experimental parameters are taken at their face value. A number of uncertainties in the test data tend to mitigate this lack of agreement somewhat however. In addition to those mentioned earlier one major potential contributor is the calorimeter size correction which has been applied to the measurements. Calorimeter measurements were made with a 5/8-inch diameter spherical calorimeter and the flux corrected to the model geometry by means of the factor 0.42 supplied by NASA/MSC. This factor was applied independently of test conditions. The theoretical value for this correction factor is appreciably larger than that employed and if correct would tend to improve the agreement between experiment and theory.

As mentioned earlier the observed surface temperatures appear higher than can be explained on any reasonable basis and therefore probably should not be given a great deal of weight.

In summary it is believed that although there is a lack of detailed agreement between the theoretical predictions and the Plasmadyne test results the model of Section 4.0 represents a good compromise with all of the available data. Considering the uncertainties in the data the model of Section 4.0 is felt to be the best available representation of the performance of the Apollo heat shield material for use in flight simulations.

6.0 Flight Simulations

The ultimate goal of any mathematical model of a thermal protection system is to provide an adequate numerical description of the performance of the system throughout the flight for which it is intended. The mathematical model described in Section 4.0 has been employed to examine several stations on the Apollo vehicle. The numerical simulation of the flight performance has been accomplished by means of the computer program described in Volume II of this report. The configuration and trajectory data employed in the calculations were supplied by NASA/MSC.

The trajectories supplied are designated as an undershoot (HR-1) and an overshoot (HL-1). Cold wall convective heat transfer rates and radiative heat transfer rates have been supplied for S/R = 0.9875. Figures 65, 66, 67 and 68 show the basic values of the cold wall convective heating, stagnation enthalpy, radiative heat transfer rate and stagnation pressure for the two trajectories considered. The composite structure considered in these calculations is shown schematically in Figure 69.

The model given in Section 4.0 is employed for the ablative material. The properties of the substructure materials are given as temperature independent and are listed in Table 11.

The inputs to the several body stations are obtained by using multipliers applied to the input parameters of Figures 65, 67 and 68. These multipliers were supplied by NASA/MSC and are shown in Table 12.

Table 11

Substructure Thermal Properties

Material Number*	k (BTU/ft-hr ^{o}R	C_p (BTU/lb ^{o}R	ρ (lb/ft^3)
2	9.71	0.11	479.
3	0.15	0.11	5.5
4	9.71	0.11	479.
5	0.0275	0.20	6.0
6	89.6	0.22	174.5
7	1.4	0.22	4.4
8	89.6	0.22	174.5

* Material numbers refer to the sequence in Figure 69.

FIGURE 65

Convective Flux Histories (S/R = 0.9875)

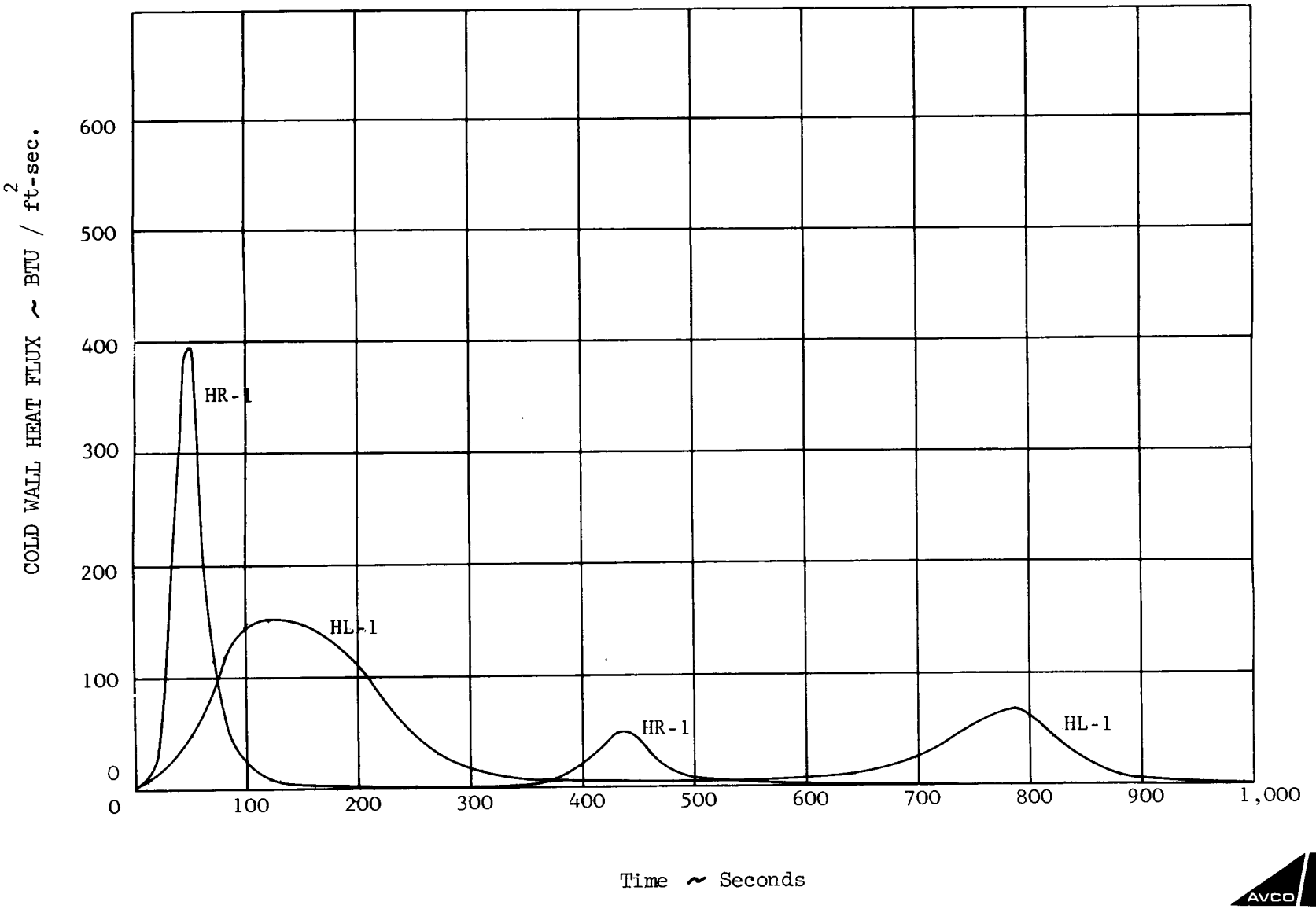

FIGURE 66

Stagnation Enthalpy Histories

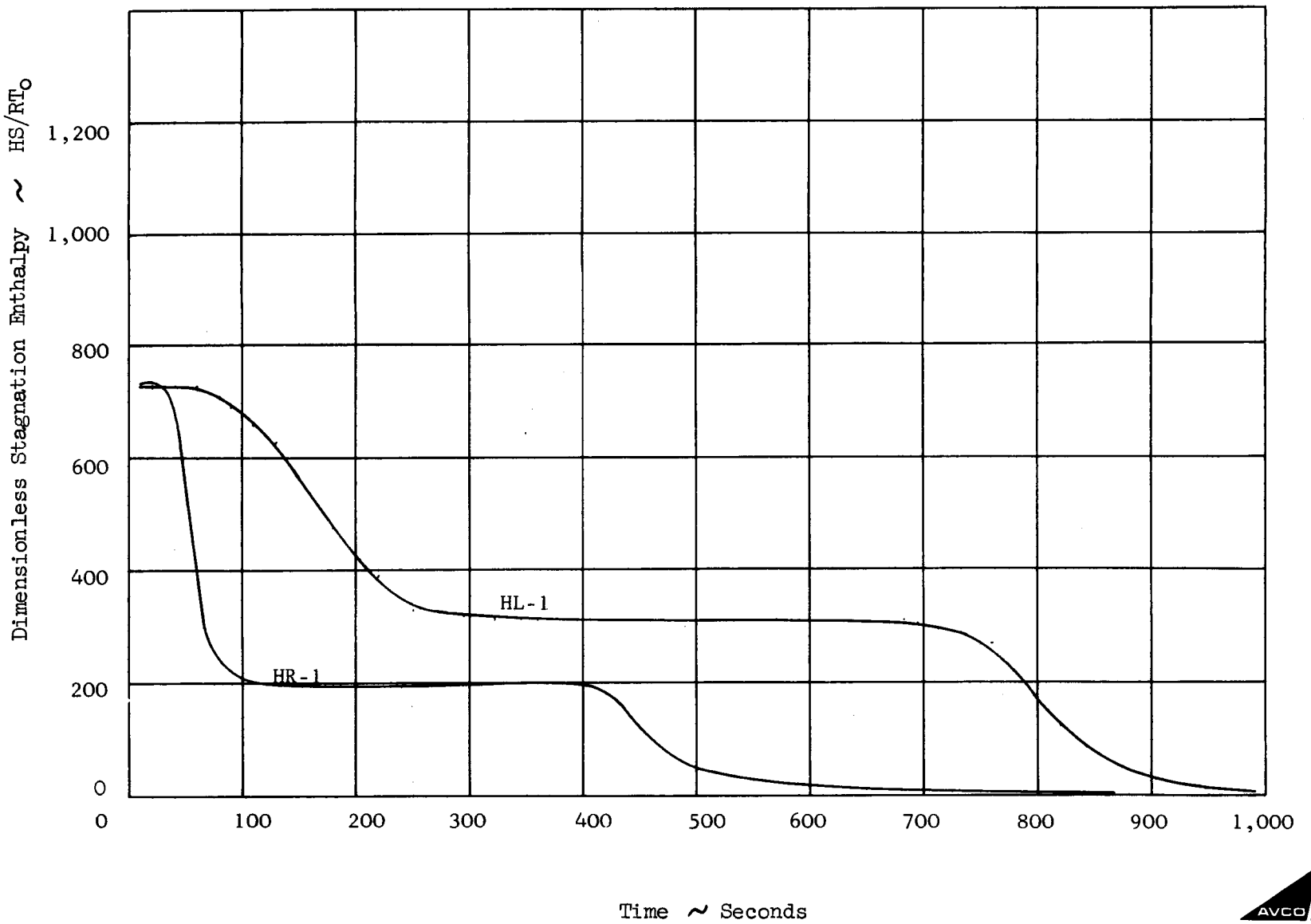

FIGURE 67

Radiant Flux Histories (S/R = 0.9875)

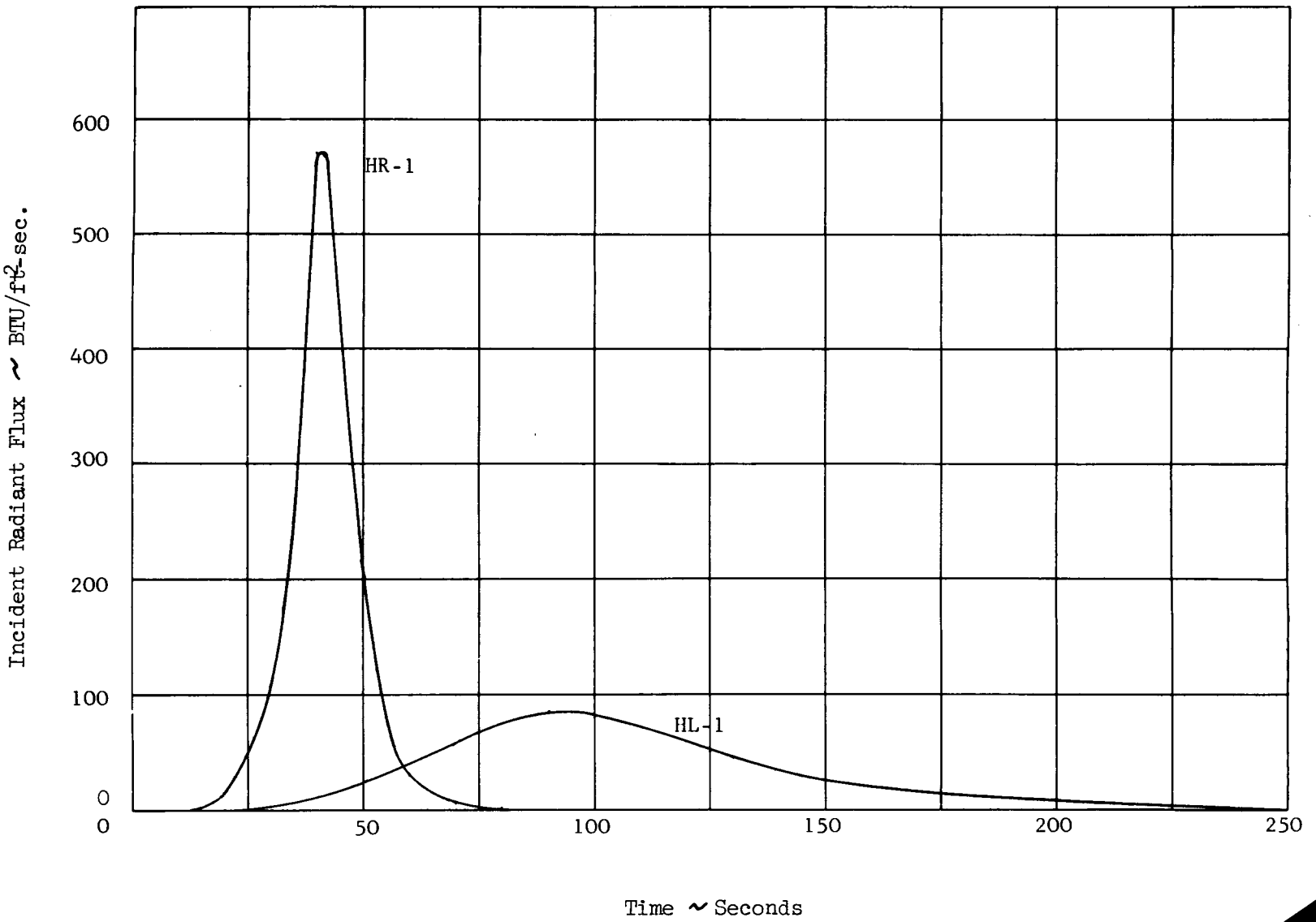

FIGURE 68

Stagnation Pressure Histories

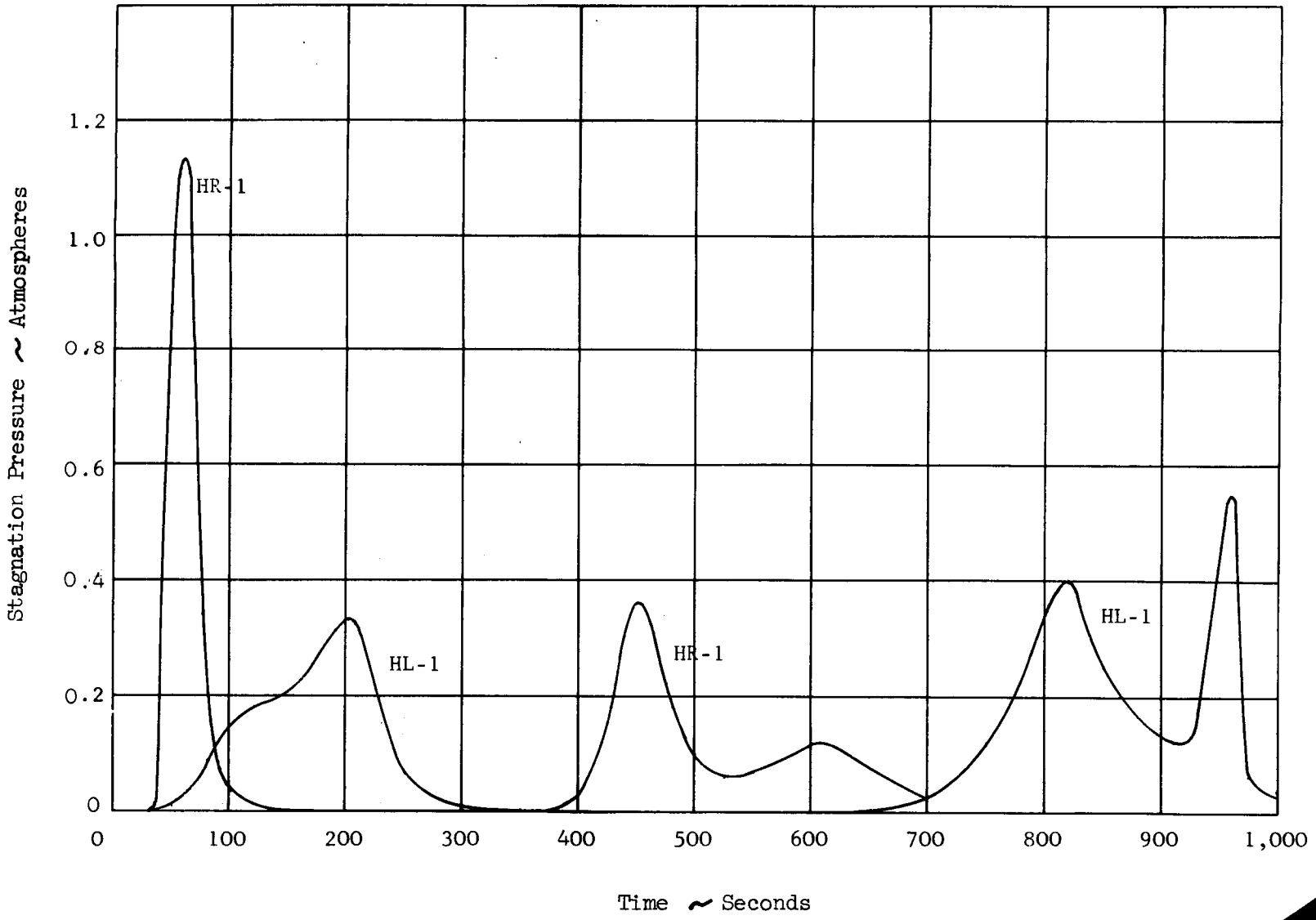

FIGURE 69

APOLLO COMPOSITE THERMAL PROTECTION SYSTEM AND STRUCTURE

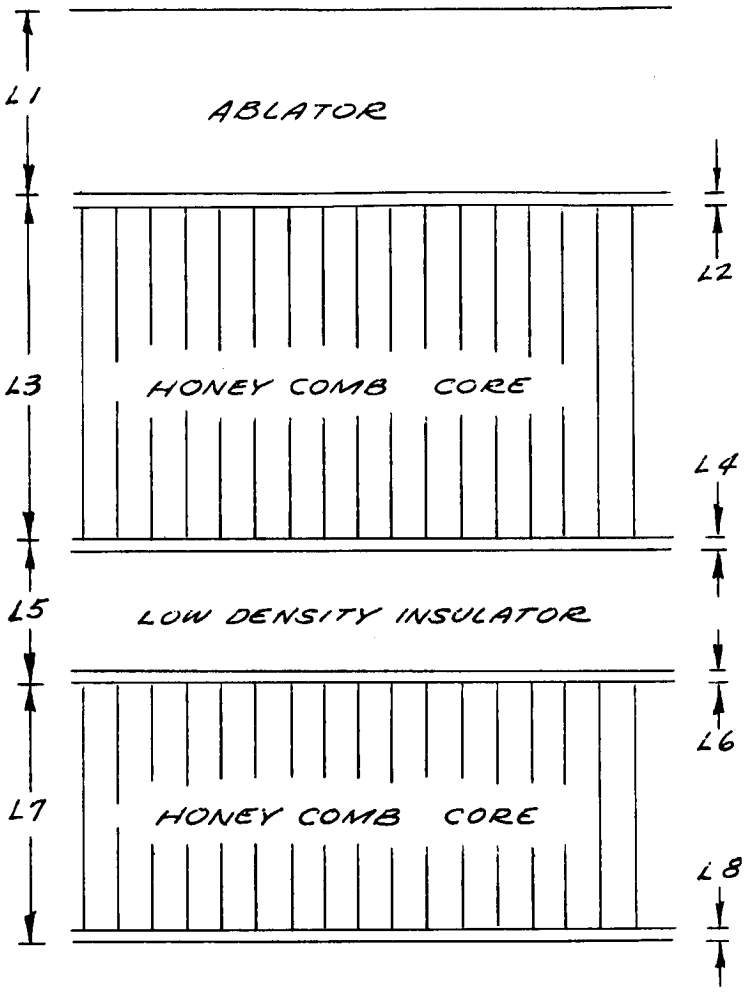

Body Station	L_1 inch	L_2 inch	L_3 inch	L_4 inch	L_5 inch	L_6 inch	L_7 inch	L_8 inch
S/R=0.0	1.79	0.008	2.00	0.008	0.80	0.016	1.50	0.016
+1.0	1.72	0.008	2.00	0.008	0.80	0.016	1.50	0.016
+1.6	0.79	0.008	0.5	0.008	1.50	0.010	0.50	0.010

Table 12

Input Parameter Multipliers

Body Station S/R	Convective Heating	Radiative Heating	Pressure
0.0	0.54	1.28	0.84
1.0	1.0	0.9	0.70
1.6	0.06	0.0	0.032

The program input requirements are described in Volume II of this report and will not be considered in such detail in this section. The input deck for running body location S/R=1.0 on trajectory HR-1 is reproduced as Table 13 together with brief descriptions of the tabular quantities. The non-tabular quantities are largely self explanitory or are considered in detail in Volume II.

Table 14 is a typical printout for this case. The various quantities appearing in the output are defined in Table 15 and in more detail in Volume II of this report.

6.1 Flight Simulation Results

As indicated in Section 5.0, the complete output of a simulation using the present model yields an extremely detailed numerical description of the thermal protection system throughout its history. Since a large number of quantities could be displayed as a product of these calculations only a few representative will be presented. Figures 70 and 71 show the calculated surface temperatures for the two trajectories and several body stations considered. Figures 72 through 75 show the time histories of the surface position as well as the locations of the 20.0 lb/ft^3 and 29.5 lb/ft^3 isochores. These two isochores correspond very nearly to 80% and 20% completion of the pyrolysis reaction and thus provide a measure of both the char thickness and of the thickness of the pyrolysis zone. No appreciable charring or surface recession is predicted to occur at S/R= 1.6.

Figures 76 and 77 show the envelope of maximum temperatures for the several cases considered. As is evident from the figures, there is very little temperature rise predicted at the bond line for any of the cases considered. Maximum bond line temperatures and total surface recession for the several cases are summarized in Table 16.

A product of the calculations is an estimate of the pressure distribution through the ablator as a function of time. In the case of the Apollo Material, the porosity is sufficiently large that only very small pressure differences are predicted to exist across the material using the modelof Section 4.0. Figure 78 shows the calculated total pressure difference across the heat shield material as a function of time for one of the cases. Figure 79 shows the pressure distribution through the ablator for several times during the flight.

TABLE 13

SAMPLE INPUT TO COMPUTER PROGRAM

(Numbers in parenthesis refer to notes at end of Table)

```
DATA* TABLE(1)=
DATA* 0.10E31,
DATA*  1060.0  1460.0                                                    (1)
DATA* 1.00E38,
DATA*
DATA*
DATA*
DATA* 0.30E31,
DATA* 1.00E25,
DATA*  0.0  0.2E-4  25.0  0.019  50.0  0.945  60.0  1.194  75.0
DATA* 0.373  100.0  0.0426  150.0  5.9E-4  200.0  0.34E-4  250.0  0.14E-4
DATA* 300.0  0.30E-4  350.0  3.96E-4  400.0  0.0285  425.0  0.151  450.0   (2)
DATA* 0.362  470.0  0.2556  475.0  0.222  500.0  0.102  525.0  0.060  550.0
DATA* 0.069  600.0  0.116  650.0  0.066  700.0  0.0244
DATA* 1.00E38,
DATA* 0.40E31,
DATA* 1.00E25,
DATA*  0.0  0.0  10.0  0.0  20.0  14.8  30.0  110.4  40.0  571.3
DATA* 50.0  210.7  60.0  31.4  70.0  5.9  80.0  1.7  90.0  0.8  140.0  0.0   (3)
DATA* 350.0  0.0  370.0  0.06  430.0  1.0  440.0  1.2  450.0  0.0
DATA* 1.00E38,
DATA* 0.50E31,
DATA* 1.00E25,
DATA*  0.0  2.4  10.0  8.5  20.0  39.5  30.0  145.5  40.0  321.1
DATA* 50.0  396.9  60.0  238.2  70.0  117.4  80.0  65.4  90.0  40.0  100.0
DATA* 25.8  120.0  10.8  140.0  4.2  160.0  1.9  180.0  1.0  250.0  0.4      (4)
DATA* 340.0  1.2  370.0  5.6  400.0  20.9  420.0  40.0  430.0  48.7  440.0
DATA* 50.5  460.0  30.3  480.0  13.6  500.0  7.3  550.0  3.5  600.0  1.8
DATA* 700.0  0.03
DATA* 1.00E38,
DATA* 0.60E31,
DATA* 1.00E25,
DATA*  0.0  35177.0  20.0  35271.0  40.0  34121.0  50.0  30259.0
DATA* 70.0  21136.0  90.0  18883.0  110.0  18391.0  130.0  18250.0  150.0   (5)
DATA* 18193.0  190.0  18117.0  250.0  18072.0  370.0  18234.0  380.0  18246.
DATA* 410.0  18002.0  430.0  16859.0  440.0  15592.0  480.0  9599.0  530.0
DATA* 7000.0  700.0  738.8
DATA* 1.00E38,
```

TABLE 13 (Continued)

```
DATA* 0.70E31,
DATA* 1.00E27,
DATA* 3.0,                                                    (6)
DATA* 1.00E38,
DATA* 0.80E31,
DATA* 1.00E27,
DATA* 2.0,                                                    (7)
DATA* 1.00E38,
DATA* 0.90E31,
DATA* 6.00E25,
DATA*  16.5  16.5  33.0  33.0                                 (8)
DATA* 1.00E38,
DATA* 1.10E31,
DATA* 4.00E25,
DATA*  0.0  33.0  650.0  33.0  700.0  31.35                   (9)
DATA* 1.00E38,
DATA* 1.20E31,
DATA* 4.00E25,
DATA*  0.0  31.35  1000.0  31.35  1100.0  31.19  1150.0  29.37
DATA* 1200.0  28.38  1250.0  24.42  1300.0  21.62  1350.0  19.80  1400.0
DATA* 18.65  1450.0  17.98  1500.0  17.32  1600.0  16.50        (10)
DATA* 1.00E38,
DATA* 1.30E31,
DATA* 1.00E27,
DATA* 1.0,                                                    (11)
DATA* 1.00E38,
DATA* 1.40E31,
DATA* 2.00E25,
DATA*  0.0  0.55  1000.0  0.66  2000.0  0.74  3000.0  0.79  4000.0
DATA* 0.83  8000.0  0.96                                      (12)
DATA* 1.00E38,
DATA* 1.50E31,
DATA* 1.00E27,
DATA* 6.0,                                                    (13)
DATA* 1.00E38,
```

TABLE 13 (Continued)

```
DATA* 1.60E31,
DATA* 1.00E27,
DATA* 5.0,                                                          (14)
DATA* 1.00E38,
DATA* 1.70E31,
DATA* 6.00E25,
DATA* 16.5 1.0 33.0 0.0                                             (15)
DATA* 1.00E38,
DATA* 1.80E31,
DATA* 6.00E25,
DATA* 16.5 1.0 33.0 0.0                                             (16)
DATA* 1.00E38,
DATA* 1.90E31,
DATA* 2.00E25,
DATA* 0.0 0.25 1000.0 0.32 2000.0 0.38 3000.0 0.41 4000.0           (17)
DATA* 0.43 6000.0 0.45
DATA* 1.00E38,
DATA* 2.00E31,
DATA* 2.00E25,
DATA* 0.0 0.20 1.0E4 2.40                                           (18)
DATA* 1.00E38,
DATA* 2.10E31,
DATA* 2.00E25,
DATA* 0.0 0.0473 1.0E4 0.2643                                       (19)
DATA* 1.00E38,
DATA* 2.20E31,
DATA* 6.00E26,
DATA* 0.0
DATA* 2.30E31,
DATA* 16.8
DATA* 2.40E31,                                                      (20)
DATA* 1.00E38,
DATA* 2.30E31,
DATA* 2.00E25,
DATA* 0.0 10.0 1200.0 10.0 3000.0 2.0
DATA* 4500.0 1.0
DATA* 1.00E38,
```

TABLE 13 (Continued)

```
DATA* 2.40E31,
DATA* 2.00E25,
DATA*  0.0  5.0  1000.0  2.0  2000.0  1.0                                    } (20)
DATA* 1.00E38,
DATA* 2.50E31,
DATA* 1.00E25,
DATA*  0.0  0.2E-4  25.0  5.1E-4  50.0  0.011  100.0  0.145
DATA* 150.0  0.204  175.0  0.271  200.0  0.338  250.0  0.0645  300.0          } (21)
DATA* 0.0119  350.0  17.7E-4  400.0  4.8E-4  500.0  1.86E-4  600.0  7.1E-4
DATA* 650.0  35.7E-4  700.0  0.024  750.0  0.116  820.0  0.400  850.0  0.250
DATA* 900.0  0.137  925.0  0.133  950.0  0.546  975.0  0.064  1000.0
DATA* 0.038  1450.0  1.0
DATA* 1.00E38,
DATA* 2.60E31,
DATA* 1.00E25,
DATA*  0.0  0.0  20.0  0.0  50.0  24.9  70.0  57.1  90.0  85.6               } (22)
DATA* 100.0  82.4  130.0  45.4  150.0  25.5  170.0  15.7  210.0  4.8  260.0
DATA* 2.0  350.0  0.0  630.0  0.0  740.0  1.8  800.0  1.9  830.0  0.0
DATA* 1.00E38,
DATA* 2.70E31,
DATA* 1.00E25,
DATA*  0.0  3.0  10.0  4.0  50.0  52.8  80.0  118.7  100.0  148.8
DATA* 120.0  152.3  150.0  149.5  180.0  157.5  220.0  84.1  270.0  30.6     } (23)
DATA* 310.0  15.8  350.0  8.9  410.0  4.7  480.0  3.5  580.0  5.1  640.0
DATA* 10.1  700.0  24.8  760.0  59.3  790.0  67.6  820.0  42.8  880.0
DATA* 8.2  940.0  2.5  1010.0  0.01  1066.0  0.05
DATA* 1.00E38,
DATA* 2.80E31,
DATA* 1.00E25,
DATA*  0.0  35165.0  70.0  35050.0  130.0  32500.0  190.0
DATA* 27570.0  250.0  23564.0  310.0  22985.0  370.0  22870.0  480.0        } (24)
DATA* 22827.0  680.0  22825.0  760.0  21375.0  820.0  14300.0  880.0
DATA* 8043.0  940.0  4240.0  1000.0  500.0  1066.0  287.0  1076.0  27.0
DATA* 1.00E38,
```

TABLE 13 (Continued)

```
DATA* 3.20E31,
DATA* 6.00E25,
DATA*  16.5  5.78E9  33.0  7.15E10                    (25)
DATA* 1.00E38,
DATA* 3.30E31,
DATA* 6.00E25,
DATA*  16.5  1.92E5  33.0  0.0                       (26)
DATA* 1.00E38,
DATA* 3.40E31,
DATA* 6.00E25,
DATA*  16.5  17.74  33.0  0.01                       (27)
DATA* 1.00E38,
DATA* 0.00000,
DATA* DATE  03.08 CASE  1.0  MEMO  2180.0
DATA** COMPUTATION AND PRINTING CONDITIONS                (28)
DATA*
DATA*
DATA* DELTAT  2.0              RHOLIM  15.0 PRINTC  1.0
DATA* FAREN  460.0
DATA*
DATA** INITIAL AND BOUNDARY CONDITIONS
DATA* TSTART  0.0                    TEMP  560.0 RHON  33.0 S  0.0
DATA* KINDQF(1)  1.0  6.0 PROBLE  1600.3
DATA** SURFACE HEATING ENVIRONMENT
DATA* P
DATA* 0.70E31,
DATA* HS
DATA* 0.80E31,
DATA* QF1
DATA* 0.40E31,
DATA* QMULF1  0.502 QF6
DATA* 0.50E31,
DATA* QMULF6  1.0 HWR  4.0
DATA* E1  -0.037
```

TABLE 13 (Continued)

```
DATA** SURFACE TERMS
DATA* E6  1.0 ALPHA  0.618 ETAS  0.4 ETAG1  0.8                RHOFRO
DATA* 0.90E31,
DATA* F1  1.0 HV1  581.0
DATA*
DATA* B3  1.7E4
DATA*                  HC  10000.0              ACHAR
DATA* 1.30E31,
DATA* RHC  16.5 CG1
DATA* 1.40E31,
DATA* DELH  500.0 KMULT
DATA* 1.50E31,
DATA* CMULT
DATA* 1.60E31,
DATA* NUM  8.0 MODEL  40.0E22
DATA* LENGTH(1)  1.72 NSUB(1)  -20.0 K(1)  1.0 RHO(1)
DATA* 0.90E31,
DATA* C(1)  1.0
DATA* LENGTH(2)  0.008 NSUB(2)  2.0 K(2)  9.71 RHO(2)  479.0 C(2)  0.11
DATA* LENGTH(3)  2.0 NSUB(3)  10.0 K(3)  0.15 RHO(3)  5.5 C(3)  0.11
DATA* LENGTH(4)  0.008 NSUB(4)  2.0 K(4)  9.71 RHO(4)  479.0 C(4)  0.11
DATA* LENGTH(5)  0.8 NSUB(5)  5.0 K(5)  0.0275 RHO(5)  6.0 C(5)  0.20
DATA* LENGTH(6)  0.016 NSUB(6)  2.0 K(6)  89.6 RHO(6)  174.5 C(6)  0.22
DATA* LENGTH(7)  1.50 NSUB(7)  8.0 K(7)  1.4 RHO(7)  4.4 C(7)  0.22
DATA* LENGTH(8)  0.016 NSUB(8)  2.0 K(8)  89.6 RHO(8)  174.5 C(8)  0.22
DATA* KV
DATA* 2.10E31,
DATA* KC  0.19 RHOK
DATA* 1.70E31,
DATA* CV
DATA* 2.00E31,
DATA* CC
DATA* 1.90E31,
```

TABLE 13 (Continued)

```
DATA* RHOC
DATA* 1.80E31,
DATA* GCBGM1  1.0 GCBGM2  1.0 GCBA1  1.0E7 GCBA2  3.26E5 GCBRO1  33.0
DATA* GCBRO2  33.0 GCBRR1
DATA* 1.10E31,
DATA* GCBRR2
DATA* 1.20E31,
DATA* GCBN1  1.0 GCBN2  2.0
DATA* GCBB1  1.2E4 GCBB2  2.140E4 TB1  0.0 TB2  0.0 TB3  0.0 TB4  5.901E-7
DATA* TB5
DATA* 0.60E31,
DATA* TB6  2.0 B8  0.0 P8  0.7 N888  1.0 H8
DATA* 0.30E31,
DATA*  GCBRR3  100.0
DATA*  DTMAX
DATA* 2.20E31,
DATA*  DTPRIN  10.0
DATA* RESUB 1.0
DATA* S8 1.0
DATA*                          TSTOP  1100.0 TB1  4.2
DATA* PP
DATA* 0.70E31,
DATA* PALPHA
DATA* 3.20E31,
DATA* PBETA
DATA* 3.30E31,
DATA* PRINTP  1.0
DATA*                          A3
DATA* 3.40E31,
DATA* EFRONT  0.667 TW  3.044
DATA* BETA5  9.1E8 BETA6  0.28 BETA7  1.61E5 TRMA  1.74E11 TRMB  1.632E5
```

TABLE 13 (Cont'd)

(1) Isotherm request
(2) Pressure-time for HR-1
(3) Radiative flux-time for HR-1
(4) Convective flux-time for HR-1
(5) Velocity-time for HR-1
(6) Function for pressure multiplier (RBG)
(7) Function to convert velocity to enthalpy (PTB)
(8) Density-char table
(9) ρ_{c1} - temperature table (GCB)
(10) ρ_{c2} -temperature table (GCB)
(11) Explicit function for pyrolysis kinetics (GCB)
(12) C_g - temperature table
(13) Thermal conductivity function (ZDB)
(14) Specific heat function (RSB)
(15) Multiplier in ZDB
(16) Multiplier in RSB
(17) C_{p_o} - temperature table
(18) C_{p_c} - temperature table
(19) k_o - temperature table
(20) Control for computational time increment
(21) Pressure-time for HL-1
(22) Radiative flux-time for HL-1
(23) Convective flux-time for HL-1
(24) Velocity-time for HL-1
(25) $\alpha(\rho)$ for internal pressure calculations
(26) $\beta(\rho)$ for internal pressure calculation
(27) Coefficient for rate controlled oxidation
(28) All Hollarith input quantities are defined in detail in Section 7 of Volume II

TABLE 14

Trajectory HR-1 S/R = 1.0

Typical Flight Simulation Output

NUMERICAL TIME STEP DETERMINED BY.....
E D E D E D E D E D

TIME	DELTAT	S	SQDT	L-S	Q23DR5	SUMQ	NETQ	SUMNETQ	HEATF	SUMHEAT
80.59055	1.809889	.15349	.001527	1.56651	52.9	1196.	74.9	12562.	9.3	1715.

NETQM	SUMQM	PHI	HW	HS	RHO-F-S	EARL	TOTMAS	RHO*SQDT	REGIME	CYCLE
39.42	6222.	.5327	25.248	241.34	1.	123.	1.38942	.00212	DIFFUSION	122

Q1&4&5	SQ145	FIORE2	QR	SUMQR	SRHOS	Q&XQM5	SUMQ&M
0.94	4746.	.9349	-29.73	-9123.	.2111	67.29	13048.16

NO.	TEMP	POSITION	NO.	TEMP	POSITION	NO.	TEMP	POSITION	NO.	TEMP	POSITION	NO.	TEMP	POSITION
1	2585.94	0.15349	12	100.77	0.74093	23	100.00	1.72377	34	100.00	3.73207	45	100.00	5.11457
2	2067.66	0.19265	13	100.01	0.81925	24	100.01	1.92811	35	100.00	3.73609	46	100.00	5.30209
3	1602.65	0.23181	14	100.00	0.90737	25	100.00	2.12855	36	100.00	3.89627	47	100.00	5.48959
4	1187.68	0.27098	15	100.00	1.01597	26	100.00	2.32390	37	100.00	4.05633	48	100.00	5.67709
5	765.18	0.31014	16	100.00	1.13256	27	100.00	2.52880	38	100.00	4.21639	49	100.01	5.86459
6	458.57	0.34930	17	100.00	1.25005	28	100.00	2.72890	39	100.00	4.37633	50	100.00	6.05209
7	265.73	0.38846	18	100.01	1.36753	29	100.00	2.92897	40	100.00	4.53644	51	100.00	6.18799
8	159.51	0.43742	19	100.00	1.48502	30	100.00	3.12833	41	100.00	4.54409	52	100.00	6.06809
9	113.02	0.50595	20	100.00	1.60251	31	100.00	3.32885	42	100.00	4.55203	37384	0.0	0.0
10	102.34	0.58428	21	100.00	1.72000	32	100.00	3.52930	43	100.00	4.73953	31872	0.0	0.0
11	100.40	0.66269	22	100.00	1.72400	33	100.00	3.72888	44	100.00	4.92703	******	0.0	0.0

NO.	RHO	MDOT	NO.	RHO	MDOT	NO.	RHO	MDOT	NO.	RHO	MDOT	NO.	RHO	MDOT
1	16.51	0.00361	6	31.35	0.00763	11	33.00	0.00000	16	33.00	0.00000	21	33.00	0.0
2	16.53	0.00361	7	31.81	0.00751	12	33.00	0.00000	17	33.00	0.00000	45	0.0	0.0
3	16.96	0.00357	8	32.99	0.00000	13	33.00	0.00000	18	33.00	0.00000	47	0.0	0.0
4	23.68	0.00237	9	33.00	0.00000	14	33.00	0.00000	19	33.00	0.00000	48	0.0	0.0
5	31.24	0.00063	10	33.00	0.00000	15	33.00	0.00000	20	33.00	0.00000	49	0.0	0.0

NO.	P	X	NO.	P	X	NO.	P	X	NO.	P	X	NO.	P	X
1	4.3310 02	0.15349	6	5.2110 02	0.34930	11	5.2790 02	0.66269	16	5.2790 02	1.13256	21	5.2790 02	1.72000
2	4.4930 02	0.19265	7	5.2630 02	0.38846	12	5.2790 02	0.74093	17	5.2790 02	1.25005	46	0.0	0.0
3	4.6690 02	0.23181	8	5.2790 02	0.43742	13	5.2790 02	0.81925	18	5.2790 02	1.36753	47	0.0	0.0
4	4.9130 02	0.27098	9	5.2790 02	0.50595	14	5.2790 02	0.90737	19	5.2790 02	1.48502	48	0.0	0.0
5	5.1270 02	0.31014	10	5.2790 02	0.58428	15	5.2790 02	1.01597	20	5.2790 02	1.60251	49	0.0	0.0

ISOTHERM= 600.00 DISTANCE 0.33124

ISOTHERM= 1000.00 DISTANCE 0.28837

TABLE 15

PRINTOUT NOMENCLATURE

NUMERICAL TIME STEP DETERMINED BY (EITHER) A,I,R,D,G,P,OR E, WHERE

A	DELTAT HAS BEEN DECREASED IN ATTEMPTING TO REACHED THE ABLATION TEMPERATURE
I	DELTAT HAS BEEN DECREASED DUE TO EITHER ABLATION THROUGH,AN INTERFACE OR IN ATTEMPTING TO ABLATE THE ENTIRE FIRST MATERIAL
R	DELTAT HAS BEEN DECREASED SINCE RHODOT (TIMES) DELTAT IS GREATER THAN RHOLIMIT
D	DELTAT IS THE INPUTED VALUE OF DTMAX WHICH IS THE LIMITING VALUE OF DELTAT
G	DELTAT CANNOT BE CHANGED DUE TO ONLY FAIR TO GOOD CONVERGENCE OF THE BOUNDARY CONDITIONS
P	DELTAT HAS BEEN DECREASED DUE TO POOR CONVERGENCE OF THE BOUNDARY CONDITIONS
E	DELTAT HAS BEEN INCREASED DUE TO EXCELLENT CONVERGENCE OF THE BOUNDARY CONDITIONS

OUTPUT CODE	UNITS	DISCRIPTION
TIME	SECONDS	PROBLEM TIME CORRESPONDING TO PRINTOUT
DELTAT	SECONDS	NUMERICAL TIME INCREMENT USED IN COMPUTING THE SOLUTION
S	INCHES	THICKNESS OF MATERIAL REMOVED
SDOT	IN/SEC	TOTAL SURFACE RECESSION RATE
L-S	INCHES	LENGTH OF REGION ONE REMAINING
Q2,3,6	BTU/FT**2-SEC	UNCORRECTED HEATING RATE I.E. (QF2 X QMULF2, QF3 X QMULF3 OR QFC X QMULF6 (E1)**E1 X (E2)**E2)
SUMQ	BTU/FT**2	TIME INTEGRATED VALUE OF Q2,3 OR 6
NETQ	BTU/FT**2-SEC	CORRECTED HEATING RATE (KINDQF 2,3,OR 6) WITHOUT MASS INJECTION (PHI)
SUMNETQ	BTU/FT**2	TIME INTEGRATED VALUE OF NETQ
HEATF	BTU/FT**2-SEC	NET SURFACE HEATING RATE K(DT/DX) AT X=S
TOHEAT	BTU/FT**2	TIME INTEGRATED VALUE OF HEATF
NETQM	BTU/FT**2-SEC	CORRECTED HEATING RATES (KINDQF2,3,OR 6) WITH MASS INJECTION (PHI)
SUMQM	BTU/FT**2	TIME INTEGRATED VALUE OF NETQM

TABLE 15 (Continued)

PHI		VALUE OF VARIABLE REDUCTION TERM PHI
HW		DIMENSIONLESS WALL ENTHALPY FOR SURFACE
HS		DIMENSIONLESS STAGNATION ENTHALPY
RHO-F-S	BTU/FT**2-SEC	RHOERO*RHOEMU X HEAT OF ABLATION RATE X SDOT
EABL	BTU/FT**2	TIME INTEGRATED VALUE OF RHO-F-S
QBACK	BTU/FT**2-SEC	REAR SURFACE HEATING RATE FOR KINDQB 1,3,AND 4. FOR KINDQB=3,PRINTOUT INCLUDES ONLY HBACK*TABACK
HEATR	BTU/FT**2-SEC	NET REAR HEATING RATE (K DT/DX) AT X=L
SUMR	BTU/FT**2	TIME INTEGRATED VALUE OF HEATR
TOTMAS	LB/FT**2	TIME INTEGRATED VALUE OF MDOT AT THE SURFACE
RHO X SDOT	LB/FT**2-SEC	MASS RATE OF ABLATION I.E.(RHOFRONT X RHOMULT X SDOT)
REGIME		FOR PROBLEM 1600.3 INDICATES TYPE OF SURFACE ABLATION, EITHER REACTION, TRANSITION, DIFFUSION OR SUBLIMATION
CYCLE		TOTAL COUNT OF MATRIX SOLUTION
Q1&4&5	BTU/FT**2-SEC	RATE OF HEATING FOR QF1 X QMULF1&HFRONT*TAFRONT&EFRONT X SIGMA X TEFRONT**4
SQ145	BTU/FT**2	TIME INTEGRATED VALUE OF Q1&4&5
E1ORE2		VALUE OF (E1)**E1 OR (E2)**E2 FOR KINDQF=6
QR	BTU/FT**2-SEC	SURFACE RADIATION LOSS
SUMQR	BTU/FT**2	TIME INTEGRATED VALUE OF QR
SRHOS	LB/FT**2	TIME INTEGRATED VALUE OF RHO*SDOT
SME*RHO	LB/FT**2-SEC	MASS RATE OF MECHANICAL EROSION FOR 1600.3
SUMSRS	LB/FT**2	TIME INTEGRATED VALUE OF SME*RHO
YDX	BTU/FT**2-SEC	SPACE INTEGRATED VALUE OF Y I.E.(SIDE HEATING)
YDXDT	BTU/FT**2	TIME INTEGRATED VALUE OF YDX
NO		NUMBER OF TEMPERATURE POINT, NO=1 AT X=S
TEMP	DEGREES	VALUE OF TEMPERATURE, EITHER RANKINE IF FAREN=0 OR FAHRENHEIT IF FAREN=460
POSITION	INCHES	LOCATION OF TEMPERATURE POINT FROM ORIGINAL SURFACE, X=0.0
Y	BTU/FT**3-SEC	AVERAGE VALUE IN EACH DELTAX INTERVAL AND DURING THE INTERVAL DELTAT, OF VOLUMETRIC, RADIATION, CONVECTIVE, AND AERO SIDE HEATING
RHO	LB/FT**3	AVERAGE VALUE IN EACH DELTAX INTERVAL OF THE CHAR DENSITY AT TIME OF PRINTOUT
MDOT	LB/FT**2-SEC	VALUE OF CHAR GAS FLOW RATE DURING THE INTERVAL DELTAT AT EACH X POSITION
P	LB/FT**2	AVERAGE VALUE IN EACH DELTAX INTERVAL OF PRESSURE AT TIME OF PRINTOUT
ISORHO		PRINTOUT OF DISTANCE,TEMPERATURE,AND AVERAGE TEMPERATURE IN REMAINDER OF FIRST MATERIAL FOR INPUTED VALUES OF ISORHO
FIXED DIST	INCHES	VALUE OF TEMPERATURE CORRESPONDING TO INPUTED VALUES OF FIXEDD
ISOTHERM	DEGREES	VALUE OF DISTANCE CORRESPONDING TO INPUTED VALUES OF ISOT
MAX-TEMP	DEGREES	MAXIMUM TEMPERATURE ACHIEVED DURING THE PROBLEM FOR THE X POSITIONS AT THE END OF THE PROBLEM

FIGURE 70

Surface Temperature Histories Trajectory HR-1

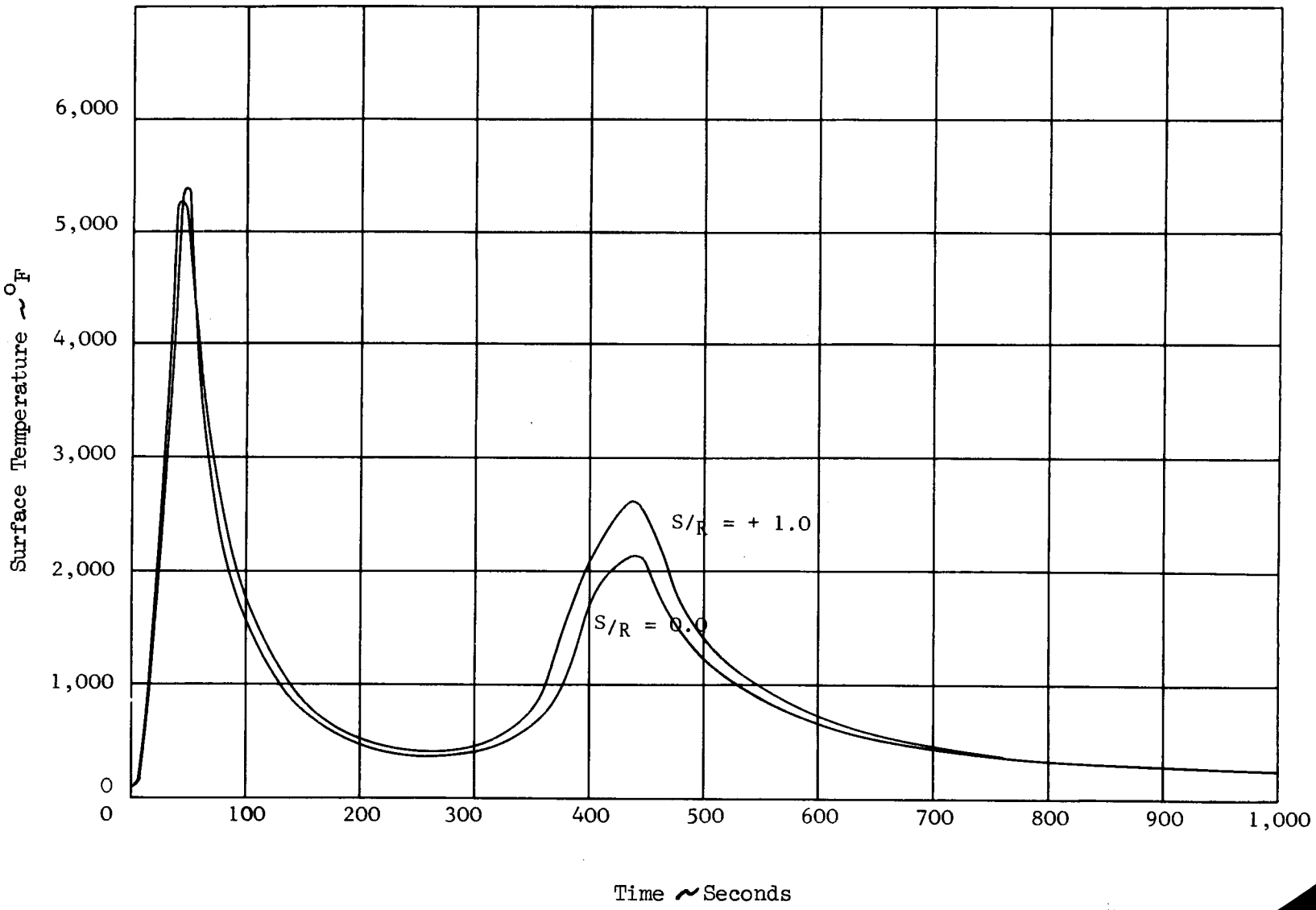

FIGURE 71

Surface Temperature Histories Trajectory HL-1

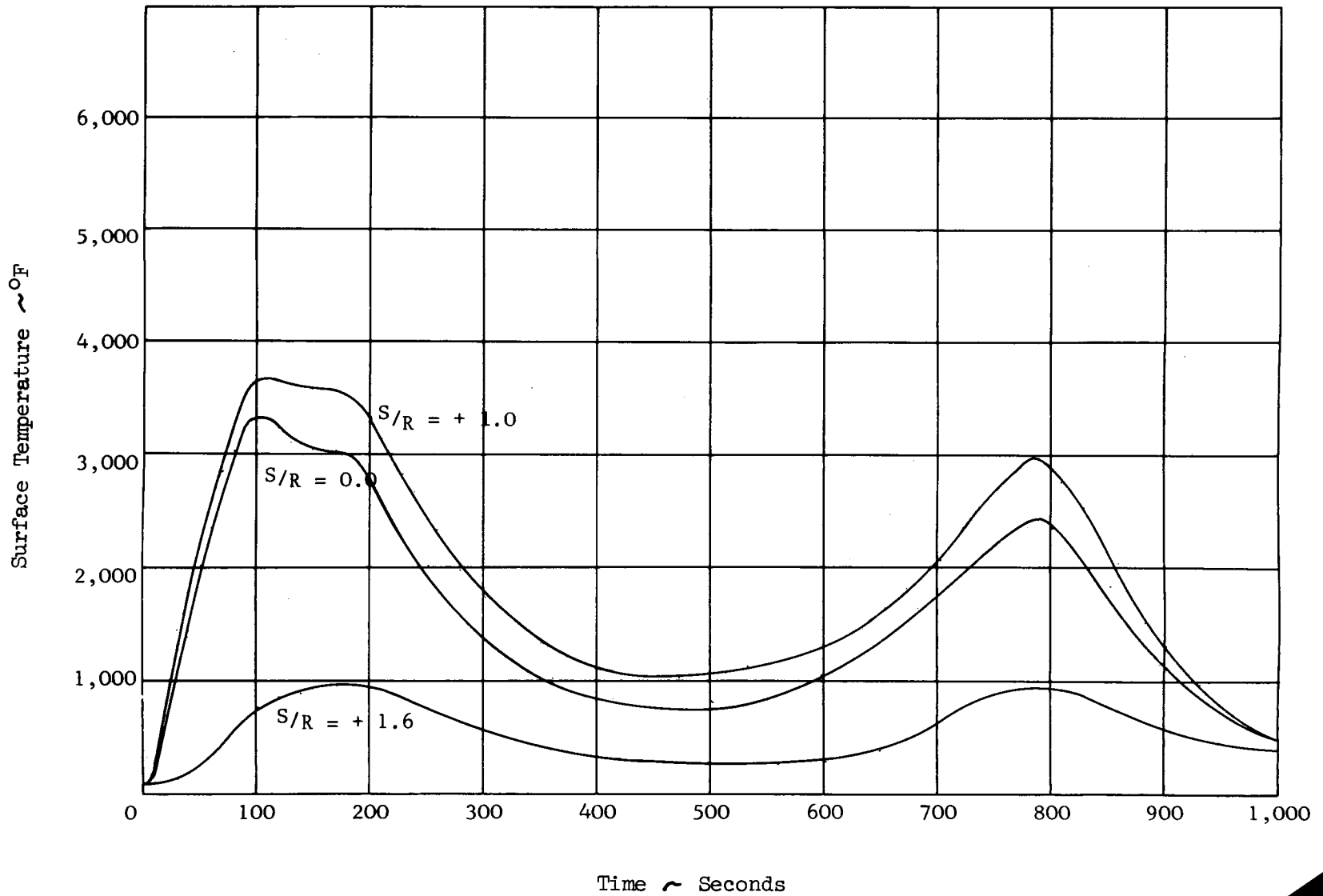

FIGURE 72

SURFACE POSITION AND ISOCHORE HISTORIES
TRAJECTORY HR-1 S/R = 0.0

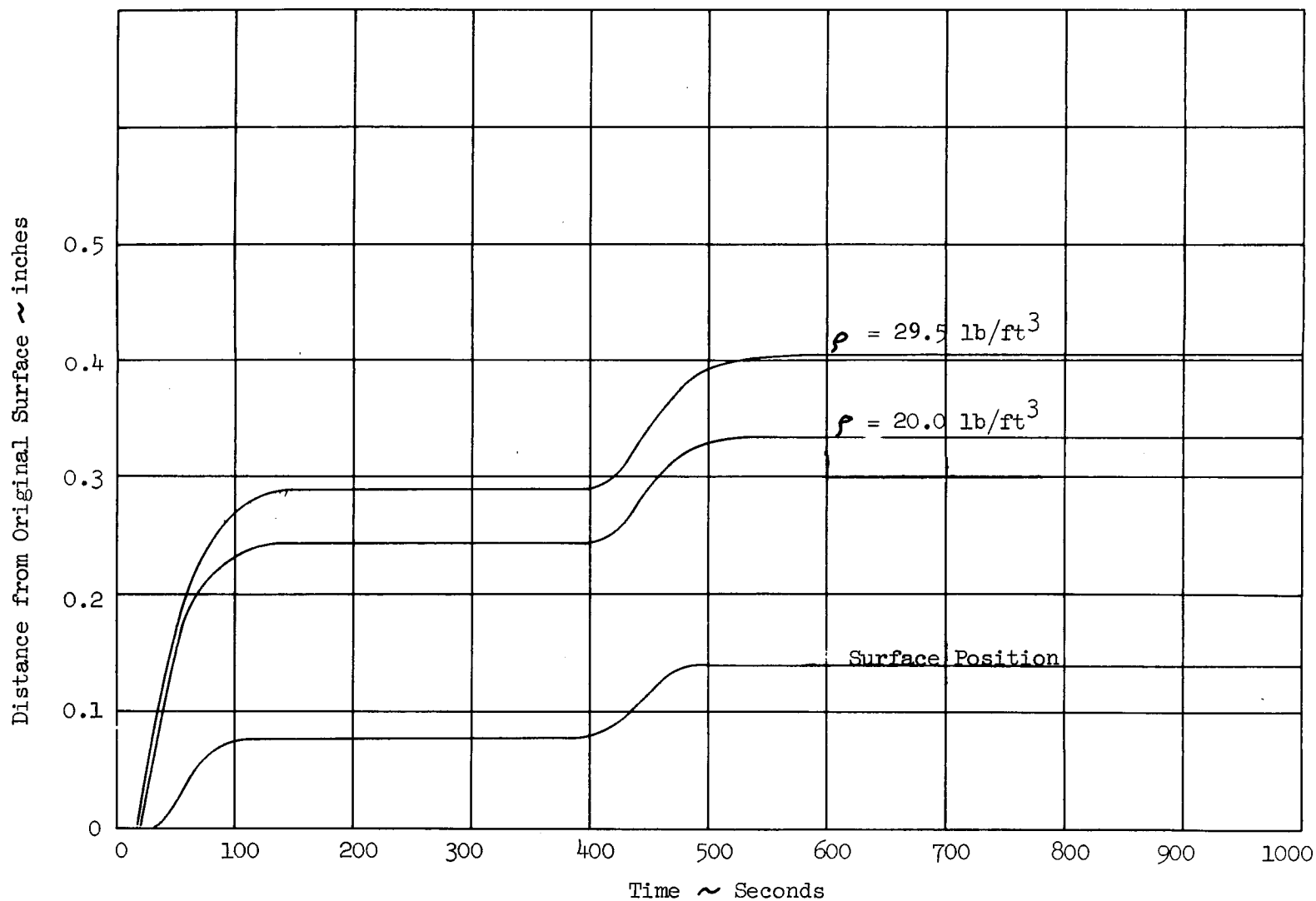

FIGURE 73

SURFACE POSITION AND ISOCHORE HISTORIES
TRAJECTORY HR-1 S/R = + 1.0

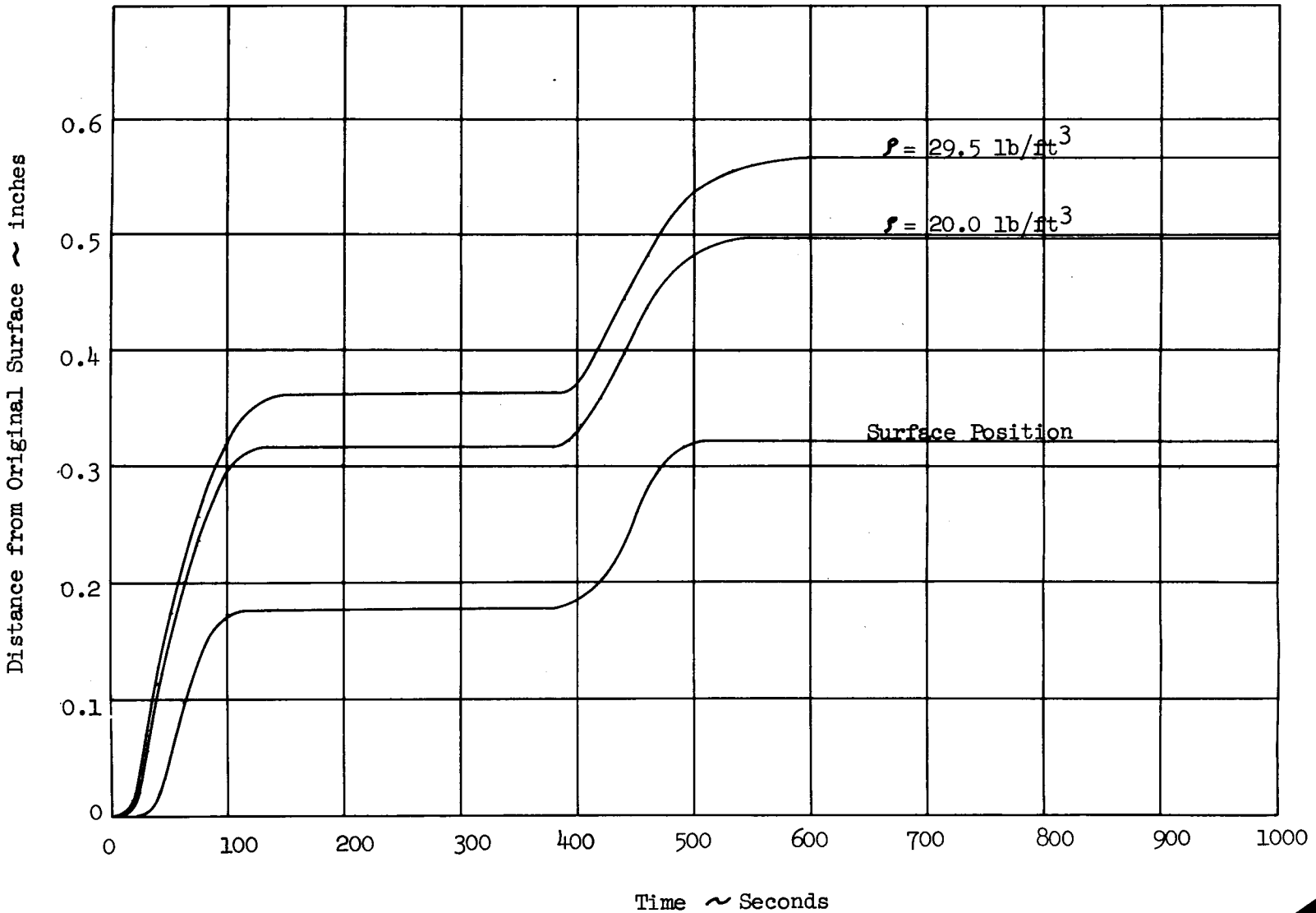

FIGURE 74

SURFACE POSITION AND ISOCHORE HISTORIES
TRAJECTORY HL-1 SR = 0.0

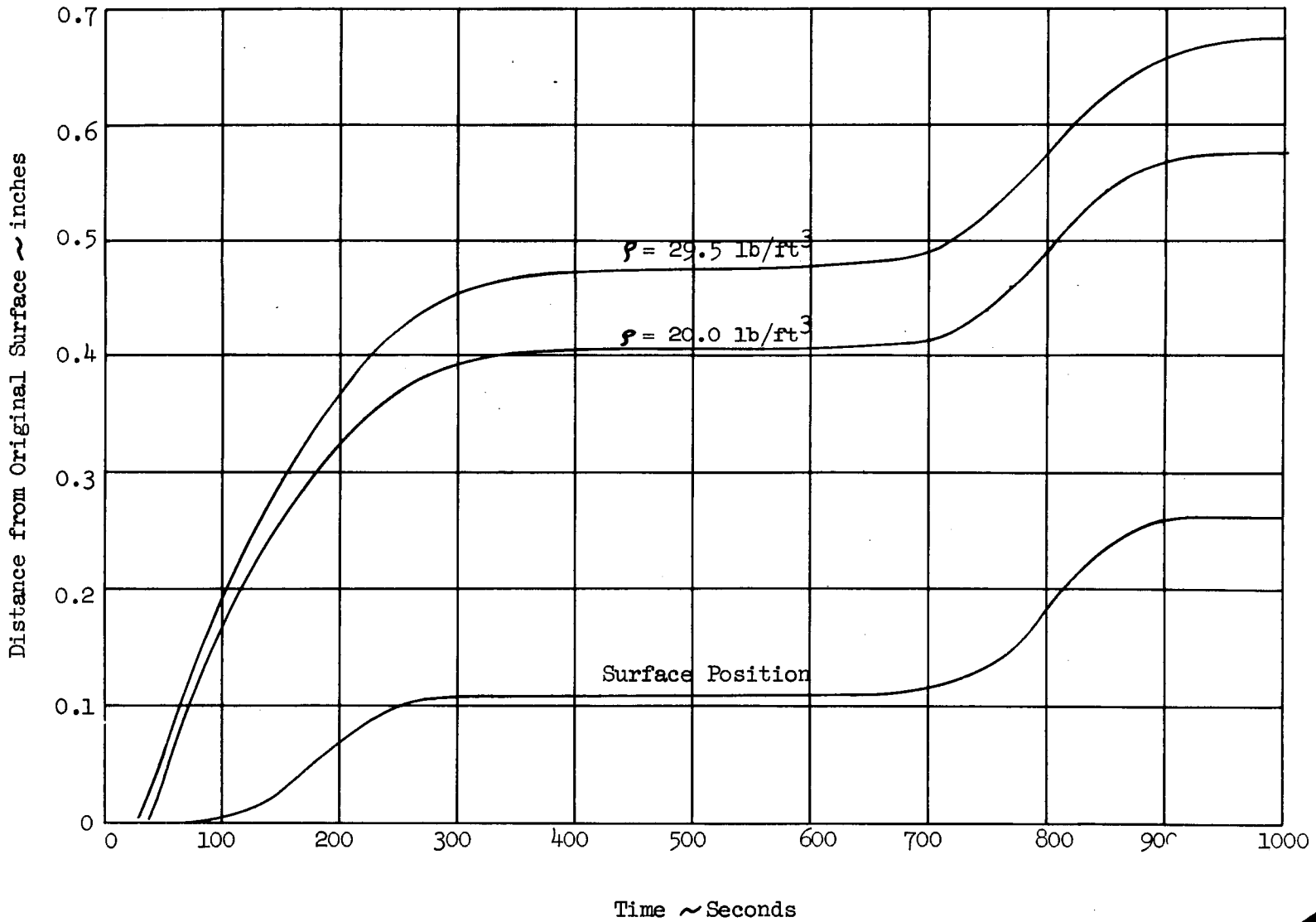

FIGURE 75

SURFACE POSITION AND ISOCHORE HISTORIES
TRAJECTORY HL-1 SR = + 1.0

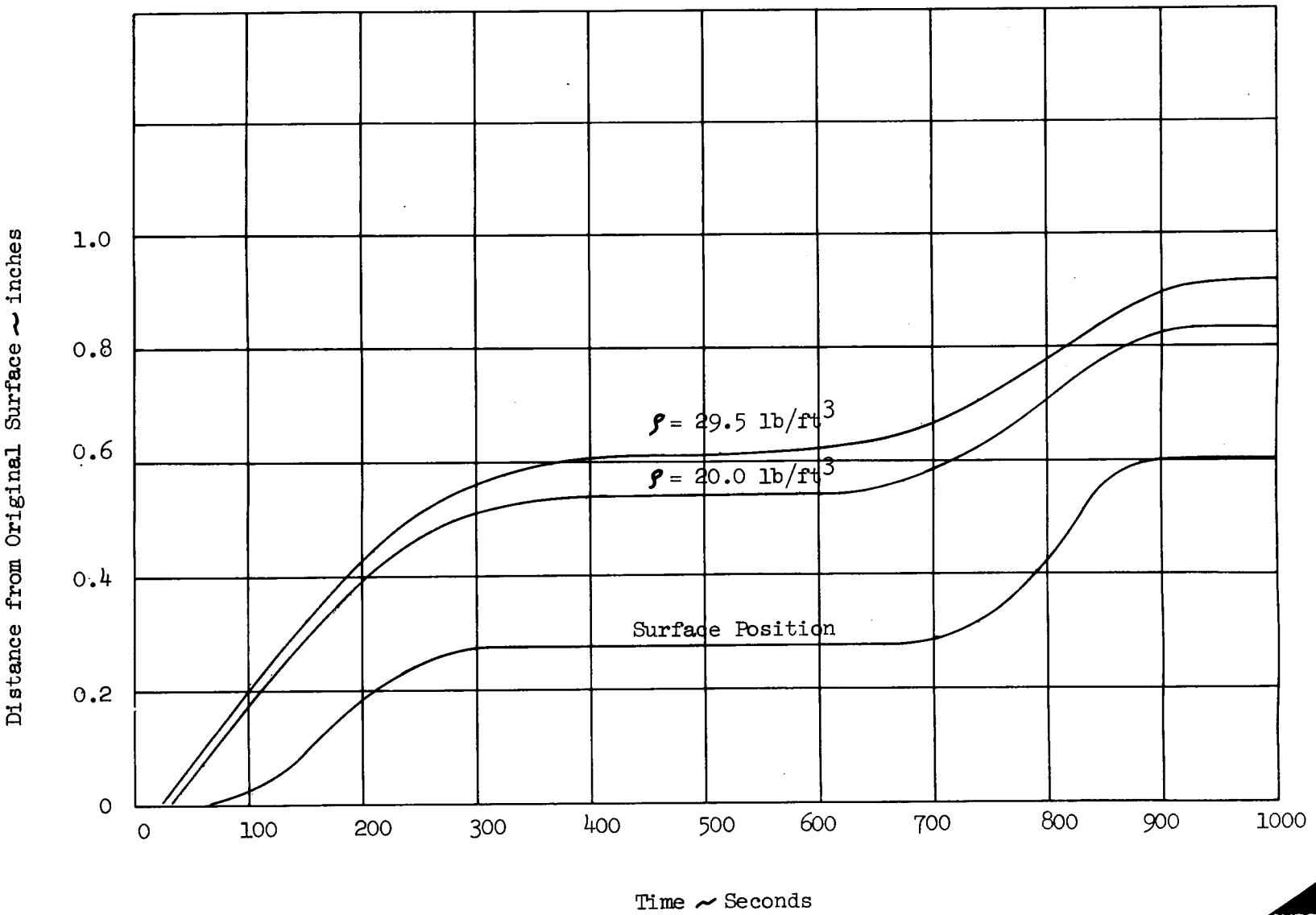

FIGURE 76

ENVELOPE OF MAXIMUM TEMPERATURES
TRAJECTORY HR-1

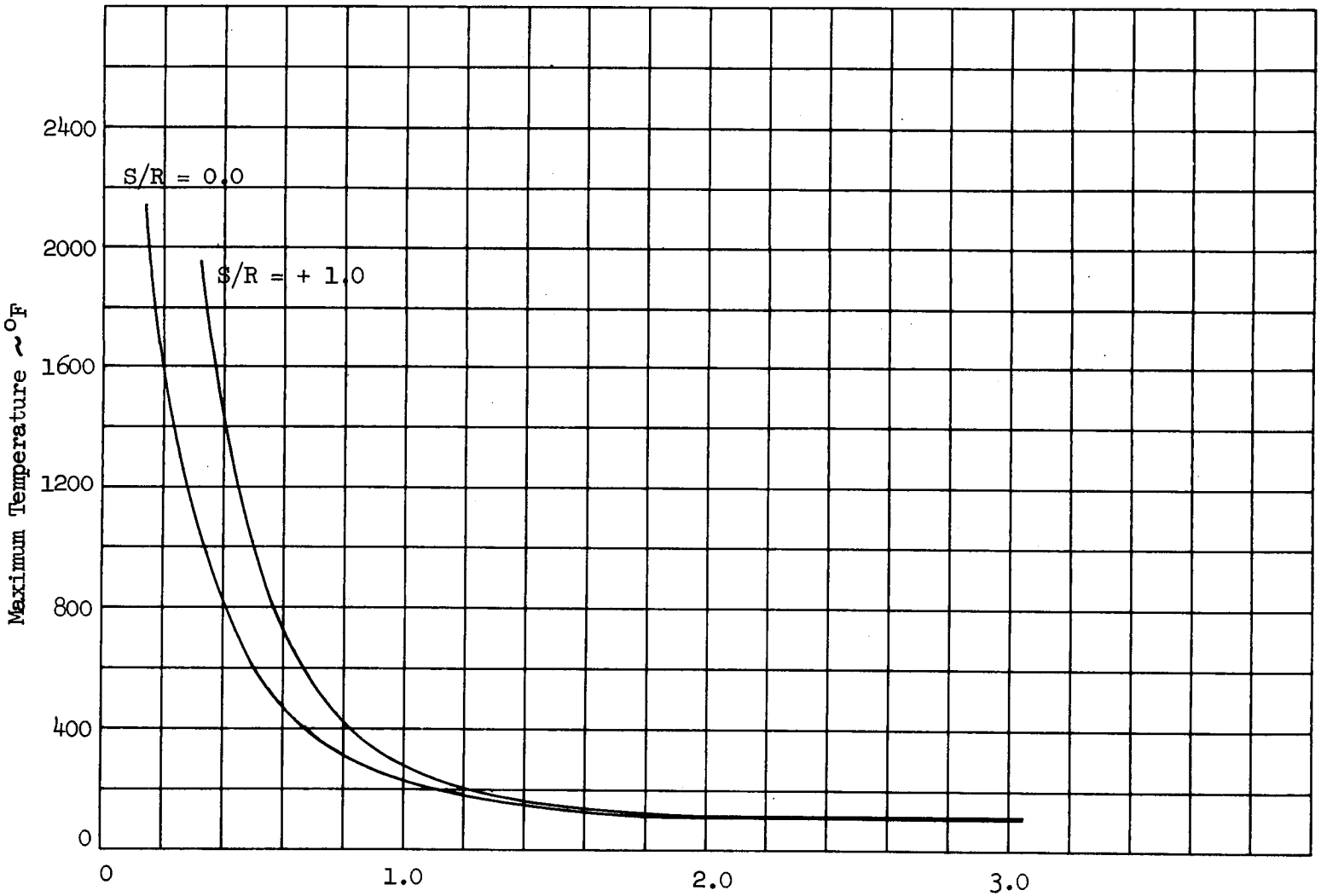

FIGURE 77

ENVELOPE OF MAXIMUM TEMPERATURES
TRAJECTORY HL-1

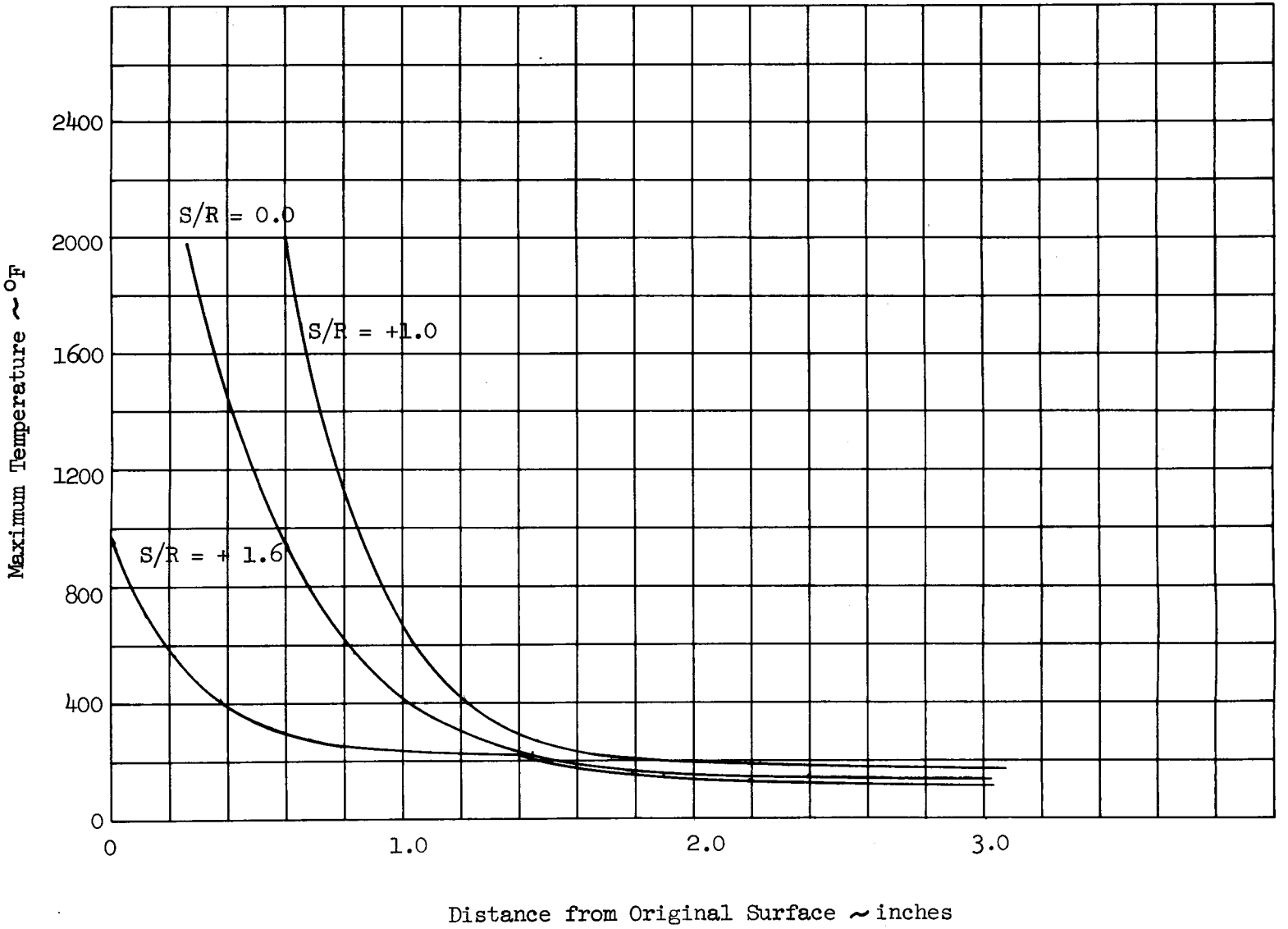

FIGURE 78

History of Pressure Drop Across the
Ablator Trajectory HL - 1 S/R = + 1.0

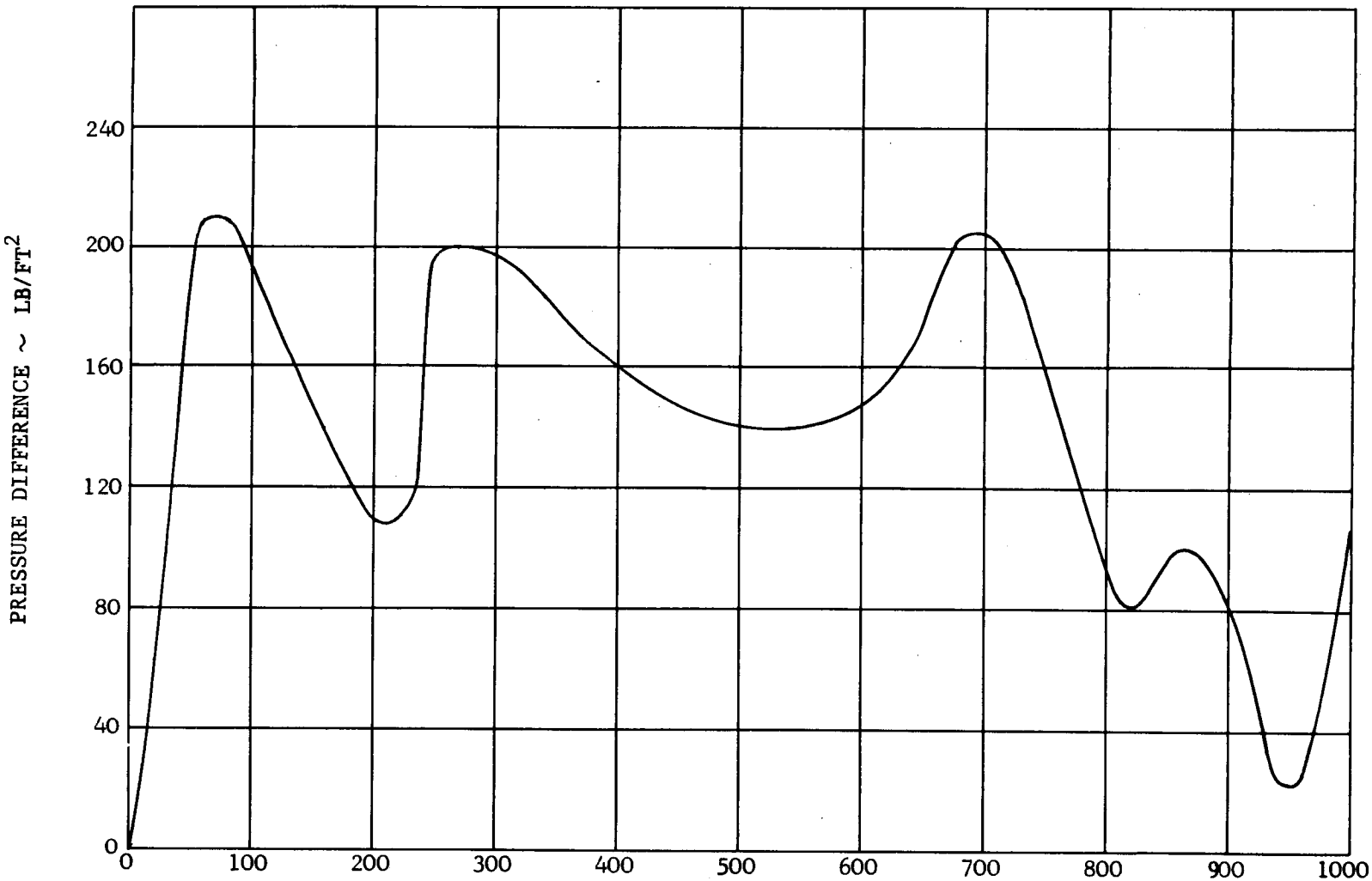

FIGURE 79

Typical Pressure Distributions
Trajectory HL-1 S/R - + 1.0

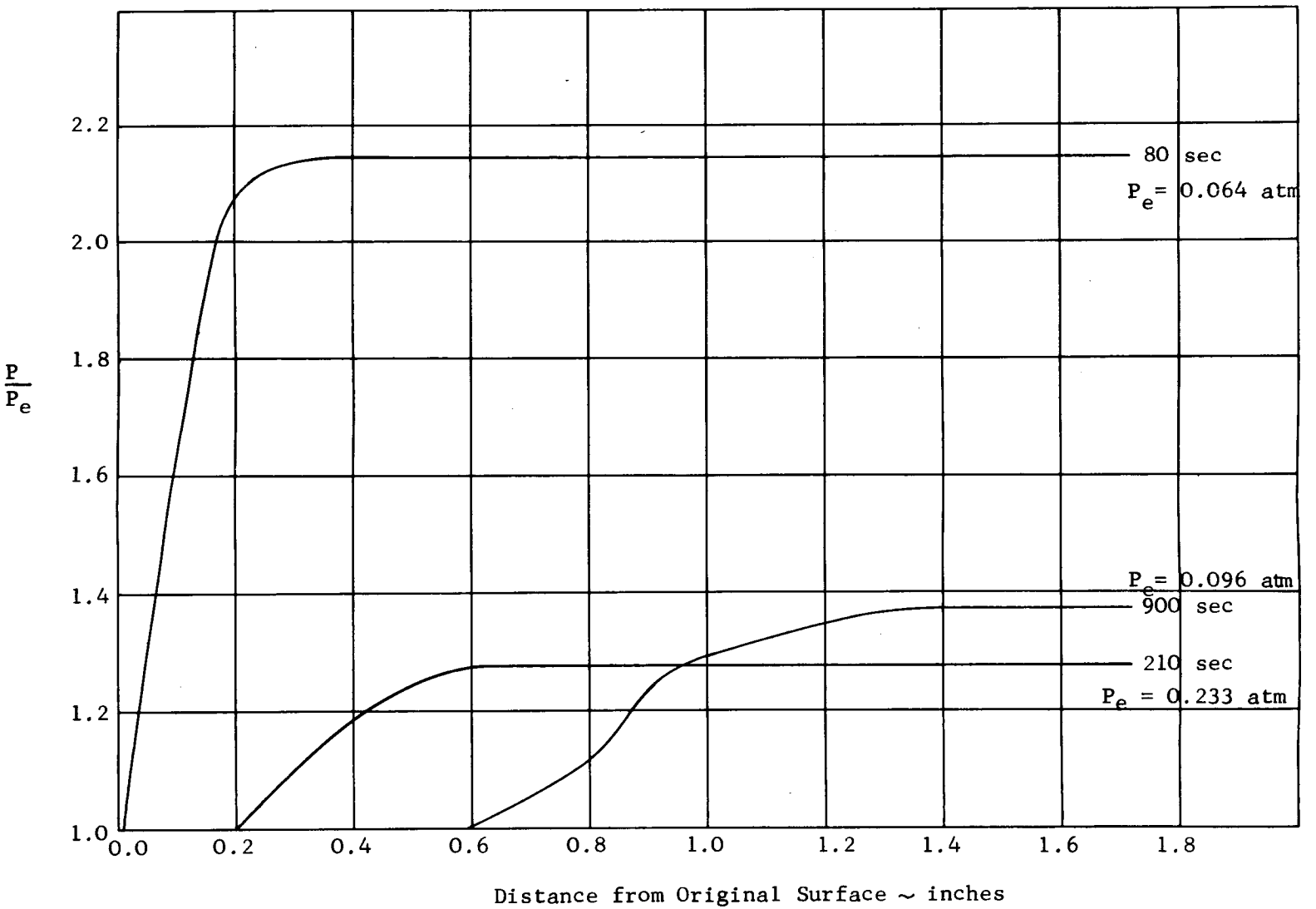

Table 16

Maximum Bond Temperatures and Total Surface Recession

(Initial Temperature = 100°F)

Body Station (S/R)	Trajectory	T_{BL} (max) °F	ΔS (inches)
0.0	HR-1	118.5	0.1413
	HL-1	162.0	0.2620
+1.0	HR-1	135.3	0.3223
	HL-1	212.1	0.6012
+1.6	HL-1	251.7	0.0

It is of interest to examine some of the components of the surface energy balance for a typical case as functions of time. Figure 80 shows a number of these components as functions of time for a typical re-entry case. The various energy components given are (1) the cold wall convective flux, q_c, corrected for the effects of wall temperature on heat transfer coefficient as described in Section 2.4, (2) the effective radiative input, $(1 - R_o)F_s$, (3) the conduction flux at the ablating surface, q_k, (4) the surface radiation loss, q_r, and (5) the net convective flux to the surface including the effects of combustion and mass transfer blocking. The remaining term in the surface energy balance as given by equation (222) is the energy associated with the surface motion, $\rho_s \dot{S} H_v$. In the present case the value of this term never exceeds 2.0 BTU/ft^2-sec and hence contributes very little to the overall energy balance.

FIGURE 80

Surface Energy Balance Components
Trajectory HL-1 S/R = + 1.0

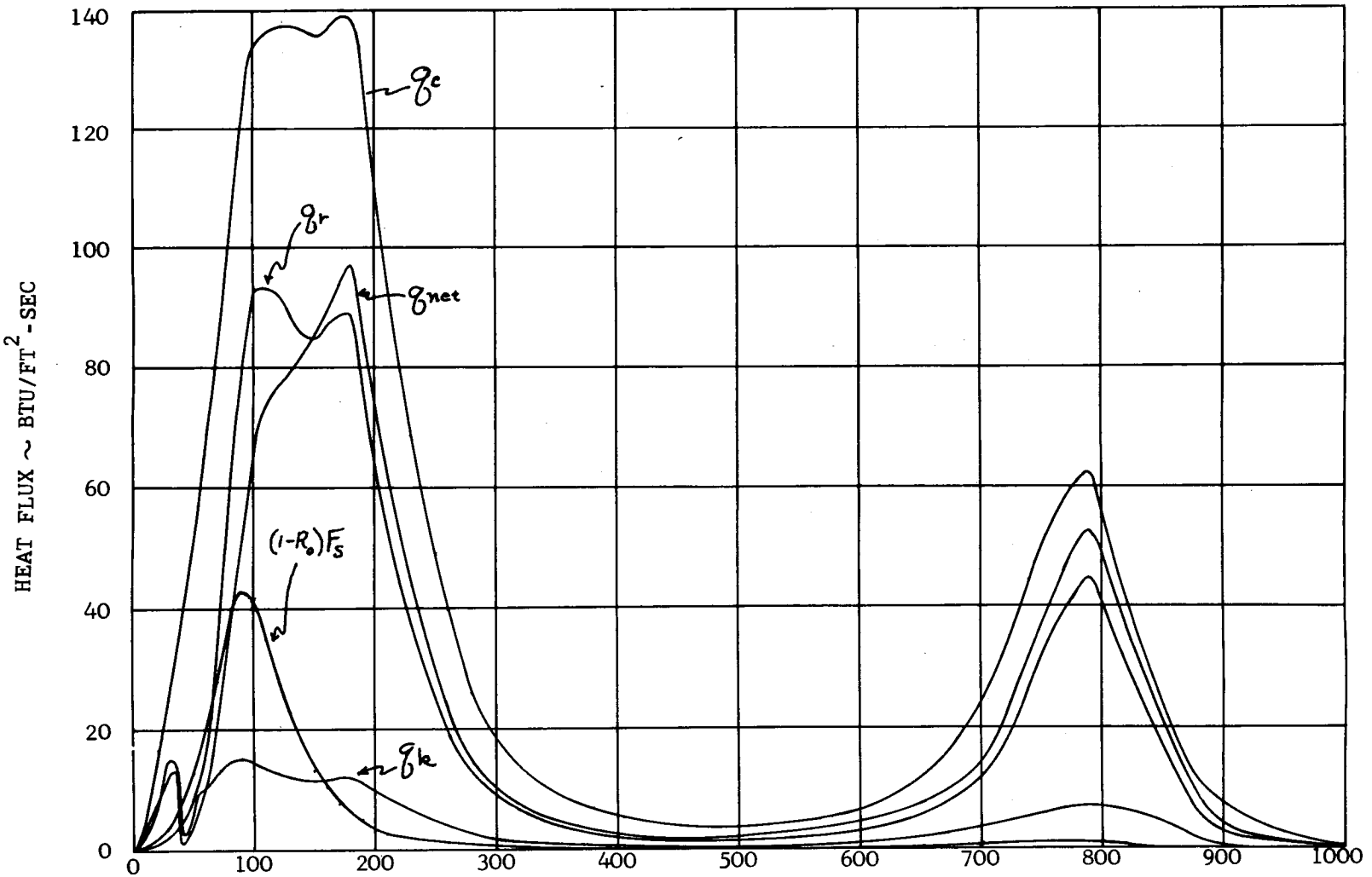

REFERENCES FOR VOLUME I

-1. Hurwicz, H., "Aerothermochemistry Studies in Ablation," presented at the Fifth AGARD Combustion and Propulsion Colloquium, Braunschweig, Germany, April 1962.

-2. Barriault, R. J., and J. Yos, "Analysis of the Ablation of Plastic Heat Shields that Form a Charred Surface Layer," ARS Journal 30 823, (1960).

-3. Scala, S. M., and L. M. Gilbert, "The Thermal Degradation of a Char Forming Plastic During Hypersonic Flight," presented at ARS Space Flight Report to the Nation, New York, October 1961, Paper No. 2100-61.

-4. Fay, J. A. and F. R. Riddell, "Theory of Stagnation Point Heat Transfer in Dissociated Air," Journal of the Aeronautical Sciences, Feb 1958.

-5. Hilsenrath, J., M. Klein and H. Woolley, "Tables of Thermodynamic Properties of Air Including Dissociation and Ionization from 1500°K to 15,000°K," AEDC-TR-59-20, Dec 1959.

-6. Hansen, C. F., "Approximations for the Thermodynamic and Transport Properties of High-Temperature Air," NACA TN 4150, March 1958.

-7. Eckert, E. R. G., "Engineering Relations for Heat Transfer and Friction in High Velocity Laminar and Turbulent Boundary Layer Flow Over Surfaces with Constant Pressure and Temperature," ASME Paper No. 55-A-31.

-8. Gross, J. F., J. P. Harnett, D. J. Masson and Carl Gazley, Jr., " A Review of Binary Laminar Boundary Layer Characteristics," Int. Journal of Heat and Mass Transfer, Vol 3, No. 3, pp 198-221 (1961).

-9. Dorrance, W. H. and F. J. Dore, "The Effects of Mass Transfer on Compressible Turbulent Boundary Layer Skin Friction and Heat Transfer," J. of the Aero. Sci., Vol 21, No. 6, June 1954.

-10. Rubesin, M. W., "An Analytical Estimation of the Effect of Transpiration Cooling on the Heat Transfer and Skin Friction Characteristics of a Compressible Turbulent Boundary Layer," NACA-TN-3341, 1954.

-11. Van Driest, E. R., "On Mass Transfer Near the Stagnation Point", RAND Symposium on Mass Transfer Cooling for Hypersonic Flight.

-12. JANAF -- Thermochemical Tables -- The Dow Chemical Company, 1960.

-13. Hochstim, A. R., "Theoretical Calculations of Thermodynamic Properties of Air," Fifth AGARD Combustion and Propulsion Colloquium, April 9, 1962.

-14. Scarborough, James B., Numerical Mathematical Analysis, 4th Edition, Johns Hopkins Press 1958.

-15. Green, L. and P. Duwez, "Fluid Flow Through Porous Metals", J. App. Mech. 18, 39, 1951

-16. Green, L. "Heat, Mass, and Momentum Transfer in Flow through Porous Media" presented at the ASME-AICHE Heat Transfer Conference, University Park, Pa. Aug. 11-15, 1957 ASME paper No. 57-HT-19

-17. Muskat, M. The Flow of Homogeneous Fluids Through Porous Media, J. W. Edwards, Inc. 1946.

APPENDIX I

Formulation of Radiant Heat Transfer Equations for Heat Shield Materials

Robert J. Spindler

1. Basic Principles

Consider an area element dA placed in a radiation field such that its normal is oriented in a direction specified by the unit vector $\vec{n}$. Let the radiation field be diffuse and non-isotropic, i.e., let energy be travelling in all possible directions and let there be different amounts flowing in each direction. In addition, let the radiant energy be distributed over a spectrum of frequencies. Let $dE_{\nu,\Omega}$ represent the energy in the frequency interval $d\nu$ centered at ν and contained in the solid angle increment $d\Omega$ (whose axis coincides with a unit vector $\vec{L}$), which flows across dA in time dt (see Figure 1):

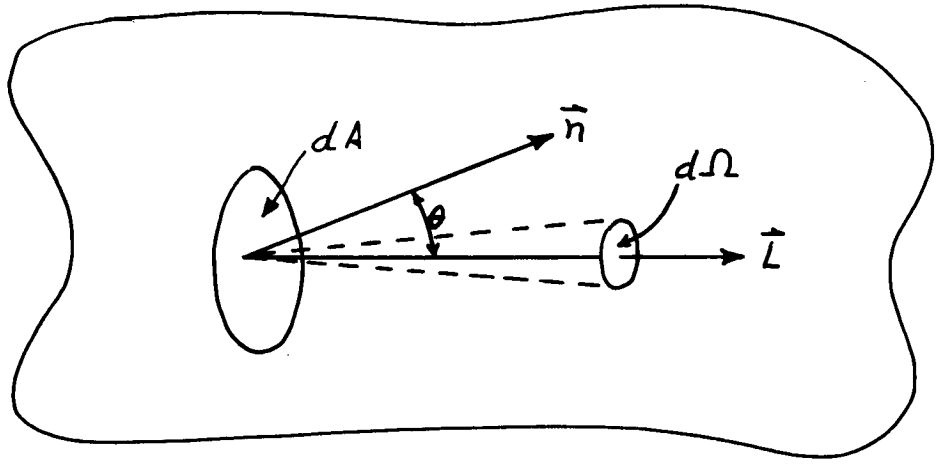

Figure 1. Illustration of Geometry of Radiation Field

The energy $dE_{\nu,\Omega}$ is proportional to $d\nu$, $d\Omega$, dt and the projection of dA in the direction of $\vec{L}$. The proportionality factor $i_{\nu,\Omega}$, is defined as the specific spectral intensity of the energy in the frequency and solid angle increments flowing across dA in this direction in time dt. Thus:

$$dE_{\nu,\Omega} = i_{\nu,\Omega}\, dA \cos\theta\, d\nu\, d\Omega\, dt \,, \tag{1}$$

where θ is the angle between $\vec{n}$ and $\vec{L}$. The dimensions of $i_{\nu,\Omega}$ are seen to be power per unit area per unit solid angle and frequency increments: (ergs/sec)/ cm^2 ster sec^{-1}.

Integration of (1) over a sphere of solid angles surrounding dA yields the net energy dE_ν in the frequency interval $d\nu$ centered on ν which crosses dA in time dt.

$$dE_\nu = dA\, d\nu\, dt \int_\Omega i_{\nu,\Omega} \cos\theta\, d\Omega \quad . \tag{2}$$

The integral in (2) is defined as a spectral distribution function, F_ν .

$$F_\nu = \int_\Omega i_{\nu,\Omega} \cos\theta\, d\Omega \quad . \tag{3}$$

With the aid of this function, the net energy in the frequency interval $d\nu$ crossing dA per unit time per unit area can be expressed as $F_\nu\, d\nu$:

$$F_\nu\, d\nu = \frac{dE_\nu}{dA\, dt} \quad . \tag{4}$$

The net flux of radiant energy (i.e., the net radiant heat flow) across dA is designated by F_o and is obtained by integrating F_ν over the spectrum of frequencies, ν_o to ν_f, containing this energy.

$$F_o = \int_{\nu_o}^{\nu_f} F_\nu\, d\nu \quad . \tag{5}$$

It is usually convenient to perform the integration in (3) in two parts, corresponding to the two hemispheres of solid angles on either side of dA. By constructing a hemisphere about dA and expressing an area element $d\sigma$ on this hemisphere in terms of the spherical coordinates r, θ and φ , it may be shown that:

$$d\Omega = \frac{d\sigma}{r^2} = \sin\theta\, d\theta\, d\varphi \quad . \tag{6}$$

Performing the integral in (3) over a complete sphere of solid angles yields the following expression for F_ν .

$$F_\nu = \int_{\varphi=0}^{2\pi} \int_{\theta=0}^{\pi/2} i_{\nu,\Omega} \cos\theta \sin\theta \, d\theta \, d\varphi + \int_{\varphi=0}^{2\pi} \int_{\theta=\pi/2}^{\pi} i_{\nu,\Omega} \cos\theta \sin\theta \, d\theta \, d\varphi \quad . \tag{7}$$

Rewriting, using the change of variables m = cos θ:

$$F_\nu = \int_{\varphi=0}^{2\pi} \int_{m=0}^{1} i_{\nu,\Omega} \, m \, dm \, d\varphi - \int_{\varphi=0}^{2\pi} \int_{m=0}^{-1} i_{\nu,\Omega} \, m \, dm \, d\varphi \quad . \tag{8}$$

If $i_{\nu,\Omega}$ is independent of Ω (isotropic), it follows that:

$$F_\nu = 2\pi i_\nu \left\{ \left[\frac{m^2}{2} \right]_0^1 - \left[\frac{m^2}{2} \right]_0^{-1} \right\} = 0 \quad , \tag{9}$$

i.e., the net transfer of energy across dA is zero. For such fields just as much power flows across dA in one hemisphere of solid angles as flows across it in the opposite hemisphere. The net radiant heat transfer in such a field is thereby zero. However, if the area element is not perfectly transparent, for example, if it is an opaque surface, a discontinuity is introduced into the radiation field which destroys the symmetry. The surface then absorbs energy incident on it from both hemispheres of solid angles and, if it has non-zero mass and specific heat, is heated accordingly. Thus, an opaque (or semi-opaque) material immersed in a radiation field will experience heating even if the field is isotropic. If the field is not isotropic there will be a net flow of energy across even a perfectly transparent surface, as shown by (8). In such situations, energy transport by radiation occurs in the material.

2. The Radiant Transfer Equation

In order to evaluate F_ν and F_o, $i_{\nu,\Omega}$ must be obtained as a function

of θ and φ from solutions to the radiant transfer equation. This equation is obtained by considering a volume element in an absorbing, scattering and emitting medium oriented in such a direction that the radiation in a particular solid angle element is normal to one face of the element. The excess of power outflow over the inflow in this direction is equated to the rate of change of energy of the element, yielding the desired relation. The power excess is the energy excess $\Delta E_{\nu,\Omega}$, divided by the time increment of the flow, dt.

The quantity $\Delta E_{\nu,\Omega}$ consists of four parts: (1) a part $\delta E^a_{\nu,\Omega}$, due to absorption losses, (2) a part $\delta E^e_{\nu,\Omega}$, due to emission contributions, (3) a part $\delta E^s_{\nu,\Omega}$, due to scattering out of the direction of the incident pencil of rays, and (4) a part $\delta E^*_{\nu,\Omega}$, due to scattering into the incident pencil, of energy travelling in other directions, by the material in the volume dAds. Thus:

$$\Delta E_{\nu,\Omega} = \delta E^a_{\nu,\Omega} + \delta E^e_{\nu,\Omega} + \delta E^s_{\nu,\Omega} + \delta E^*_{\nu,\Omega} \quad . \tag{10}$$

The quantity $\delta E^a_{\nu,\Omega}$ is proportional to the incident energy flowing in the ξ - direction, $E_{\nu,\Omega}(\xi)$, and to the differential path length $d\xi$, the proportionality factor α_ν being defined as the spectral absorption coefficient of the material.

$$\delta E^a_{\nu,\Omega} = -\alpha_\nu E_{\nu,\Omega}\, d\xi \quad . \tag{11}$$

The dimensions of α_ν are seen to be inverse length.

The quantity $\delta E^s_{\nu,\Omega}$ is similarly defined, the proportionality factor γ_ν being defined as the spectral scattering coefficient.

$$\delta E^s_{\nu,\Omega} = -\gamma_\nu E_{\nu,\Omega}\, d\xi \quad . \tag{12}$$

The dimensions of γ_ν are also inverse length.

The quantity $\delta E^e_{\nu,\Omega}$ is proportional to the volume $dA d\xi$ of the material element, the solid angle and frequency increments $d\Omega$ and $d\nu$, and the time increment dt. The proportionality factor $j_{\nu,\Omega}$ is defined as the spectral emission coefficient.

$$\delta E^e_{\nu,\Omega} = j_{\nu,\Omega}\, dA\, d\xi\, d\Omega\, d\nu\, dt \quad . \tag{13}$$

The dimensions of $j_{\nu,\Omega}$ are power per volume per unit solid angle and frequency increments.

The quantity $\delta E^*_{\nu,\Omega}$ represents the sum of all contributions to the energy flowing in the ξ-direction due to scattering into this direction by the material in dA dξ of energy travelling in other (ξ') directions. Let $E_{\nu,\Omega}(\xi')$ be the energy, in the frequency interval dν, contained in a solid angle increment dΩ whose axis lies in the ξ'-direction and forms the angle θ' with dA. The fraction of $E_{\nu,\Omega}(\xi')$ scattered in all direction in traversing the path length dξ/cos θ' through the volume dA dξ is:

$$\gamma_\nu E_{\nu,\Omega}(\xi')\, d\xi/\cos\theta' \quad .$$

The portion of this energy scattered into the solid angle increment dΩ whose axis is in the s-direction is $(1/4\pi)\, p(\xi,\xi')\, d\Omega$ times this, where $p(\xi,\xi')$ is a distribution function giving the angular dependence of the flow in the ξ-direction relative to the ξ'-direction. Thus, $\delta E^*_{\nu,\Omega}$ is the sum of these contributions over all solid angles.

$$\delta E^*_{\nu,\Omega} = \gamma_\nu \int_\Omega \frac{d\xi}{\cos\theta'} E_{\nu,\Omega}(\xi')\, p(\xi,\xi')\, \frac{d\Omega}{4\pi} \quad . \tag{14}$$

Combining (10-13), the following is obtained for $\Delta E_{\nu,\Omega}(\xi)$:

$$\Delta E_{\nu,\Omega}(\xi) = -(\alpha_\nu + \gamma_\nu) E_{\nu,\Omega} + j_{\nu,\Omega}\, dA\, d\xi\, d\Omega\, d\nu dt$$

$$+ \gamma_\nu\, d\xi \left[\int_\Omega \epsilon_{\nu,\Omega}(\xi')\, p(\xi,\xi') \frac{d\Omega}{4\pi\cos\theta'} \right] . \tag{15}$$

From the definition of the specific spectral intensity, the following relations can be written for $E_{\nu,\Omega}(\xi)$ and $E_{\nu,\Omega}(\xi')$:

$$E_{\nu,\Omega}(\xi) = i_{\nu,\Omega}(\xi) \cos\theta\, dA\, d\Omega\, d\nu dt \quad , \tag{a}$$

$$E_{\nu,\Omega}(\xi') = i_{\nu,\Omega}(\xi') \cos\theta\, dA\, d\Omega\, d\nu dt \quad . \tag{b}$$

(16)

Combining (10-16), remembering that cos $\theta = 1$, and choosing the magnitudes, $d\Omega = d\Omega'$ the radiant transfer equation is obtained by dividing (15) by dt, equating to $dE_{\nu,\Omega}/dt$, expressing $dE_{\nu,\Omega}/dt$ in terms of intensity and cancelling common terms. The result is the following.

$$\frac{di_{\nu,\Omega}}{d\xi} = -(\alpha_\nu + \gamma_\nu) i_{\nu,\Omega} + j_{\nu,\Omega} + \gamma_\nu \left[\int_\Omega i_{\nu,\Omega}(\xi') p(\xi,\xi') \frac{d\Omega}{4\pi} \right] . \qquad (17)$$

Equation (17) describes the change in intensity along a ray traversing an absorbing, scattering and emitting medium in a particular ξ -direction. Solution of this equation subject to appropriate boundary conditions gives $i_{\nu,\Omega}(\xi)$ at any point in the radiating medium.

For the special case of the volume elements of the material being in thermodynamic equilibrium, i.e., when thermal, chemical, radiative and mechanical equilibrium exist everywhere in the material, the emission coefficient is related to the absorption coefficient through the Planck intensity function $B_{\nu,\Omega}(T)$ and the refractive index n_ν of the medium, in accordance with Kirchoff's law.

$$j_{\nu,\Omega} = \alpha_\nu n_\nu^2 B_{\nu,\Omega}(T) , \qquad (18)$$

where:

$$B_{\nu,\Omega}(T) = \frac{2h\nu^3}{c^2} \frac{1}{(\exp \frac{h\nu}{kT}) - 1} . \qquad (19)$$

In (19), h, c and k are the Planck constant (erg sec), speed of light (cm/sec) and Boltzman constant (ergs/$^\circ$K), respectively. The absolute temperature in $^\circ$K is given by T.

If the material is not in thermodynamic equilibrium, due for example to the existence of temperature gradients, it is still possible to apply Kirchoff's law locally provided the volume elements are in radiative equilibrium, i.e. when the rate of depopulation of the various energy levels due to radiative transitions is equal to their rate of repopulation. Such a condition is known as local thermodynamic equilibrium. If this condition is satisfied everywhere in the medium, the radiant transfer equation (17) can be written as follows.

$$\frac{di_{\nu,\Omega}}{d\xi} = -(\alpha_\nu + \gamma_\nu) i_{\nu,\Omega} + \alpha_\nu n_\nu^2 B_{\nu,\Omega}(T) + \gamma_\nu \left[\int_\Omega i_{\nu,\Omega}(\xi') p(\xi,\xi') \frac{d\Omega}{4\pi} \right] . \qquad (20)$$

A more compact representation of equation (20) can be obtained by introducing the following abbreviations.

$$\left.\begin{aligned} K_\nu &\equiv (\alpha_\nu + \gamma_\nu) \quad , && \text{(a)} \\ \bar{\omega}_\nu &\equiv \frac{\gamma_\nu}{K_\nu} \quad , && \text{(b)} \\ i^*_{\nu,\Omega} &\equiv \int_\Omega i_{\nu,\Omega}(\xi')\, p(\xi,\xi')\, \frac{d\Omega}{4\pi} \quad . && \text{(c)} \end{aligned}\right\} \tag{21}$$

With the aid of these definitions, equation (20) may be written as follows.

$$\frac{di_{\nu,\Omega}}{d\xi} + K_\nu i_{\nu,\Omega} = J_{\nu,\Omega} \quad , \tag{22}$$

where:

$$J_{\nu,\Omega} = K_\nu \left[(1-\bar{\omega}_\nu)\, \eta_\nu^2\, B_{\nu,\Omega}(T) + \bar{\omega}_\nu\, i^*_{\nu,\Omega} \right] \quad . \tag{23}$$

If the parameter $\bar{\omega}_\nu$ is zero, scattering is entirely absent, and equation (22) reduces to the following:

$$\frac{di_{\nu,\Omega}}{d\xi} + \alpha_\nu i_{\nu,\Omega} = \alpha_\nu \eta_\nu^2 B_{\nu,\Omega}(T) \quad . \tag{24}$$

If $\bar{\omega}_\nu$ is unity, absorption is entirely absent, and equation (22) reduces to the following:

$$\frac{di_{\nu,\Omega}}{d\xi} + \gamma_\nu i_{\nu,\Omega} = \gamma_\nu i^*_{\nu,\Omega} \quad . \tag{25}$$

3. Application

Consider a semi-infinite layer of radiating material as shown in Figure 2. Let the surface and rear interfaces be located by y = s and y = L, respectively, where positive y is measured from the surface inward. Using the relation:

$$d\xi = dy/\cos\theta \quad , \tag{26}$$

equation (22) becomes:

$$\frac{d}{dy}\left(i_{\nu,\Omega}\cos\theta\right) + K_\nu i_{\nu,\Omega} = J_\nu \quad . \tag{27}$$

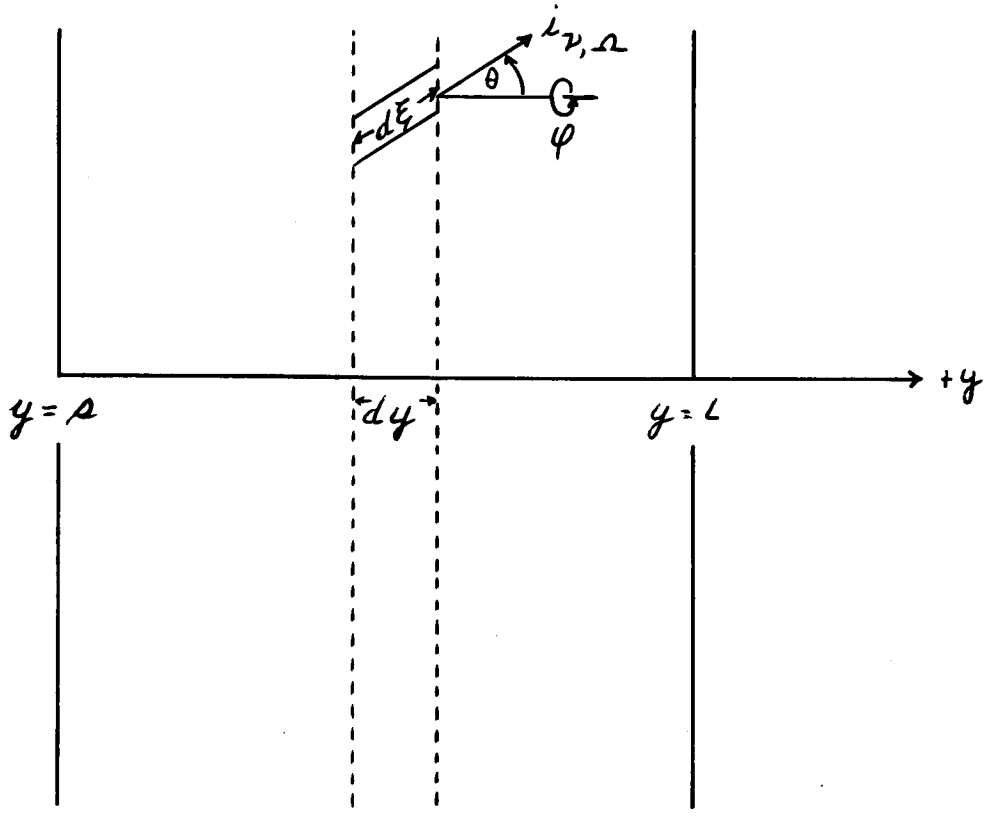

Figure 2. Illustration of Heat Shield Geometry

Multiplying (27) by $d\Omega$ and integrating over 4π steradians:

$$\frac{d}{dy}\int_\Omega i_{\nu,\Omega}\cos\theta\, d\Omega = -K_\nu\int_\Omega i_{\nu,\Omega}\, d\Omega + \int_\Omega J_\nu\, d\Omega \quad . \tag{28}$$

By equation (3), the left side of (28) is:

$$\frac{d}{dy}\int_\Omega i_{\nu,\Omega}\cos\theta\, d\Omega = \frac{d}{dy}F_\nu \quad . \tag{29}$$

Consider the first term on the right of (28). Using (6), this becomes:

$$K_\nu \int_\Omega i_{\nu,\Omega}\, d\Omega = K_\nu \int_{\varphi=0}^{2\pi} \int_{\theta=0}^{\pi/2} i_{\nu,\Omega} \sin\theta\, d\theta\, d\varphi + K_\nu \int_{\varphi=0}^{2\pi} \int_{\theta=\pi/2}^{\pi} i_{\nu,\Omega} \sin\theta\, d\theta\, d\varphi \quad . \tag{30}$$

Letting m = cos θ, (30) becomes:

$$K_\nu \int_\Omega i_{\nu,\Omega}\, d\Omega = K_\nu \int_{\varphi=0}^{2\pi} \int_{m=0}^{1} i_{\nu,\Omega}\, dm\, d\varphi - K_\nu \int_{\varphi=0}^{2\pi} \int_{m=0}^{-1} i_{\nu,\Omega}\, dm\, d\varphi \quad . \tag{31}$$

It is necessary to know the angular dependence of $i_{\nu,\Omega}$ before the integrations in (31) can be performed. This is not known a-priori, but for ease and convenience of calculation, the simplest possible non-isotropic distribution will be assumed. Thus, let $i_{\nu,\Omega}$ be assumed half-isotropic, i.e.:

$$\left.\begin{aligned} i_{\nu,\Omega} &= \text{constant}' = i_\nu' \quad (0 < \theta < \pi/2) \quad , \qquad \text{(a)} \\ i_{\nu,\Omega} &= \text{constant}'' = i_\nu'' \quad (\pi/2 < \theta < \pi) \quad , \qquad \text{(b)} \end{aligned}\right\} \tag{32}$$

for all values of φ. Thus:

$$K_\nu \int_\Omega i_{\nu,\Omega}\, d\Omega = K_\nu \left[2\pi \left(i_\nu' + i_\nu'' \right] \right] \quad . \tag{33}$$

Next, consider the second term on the right of (28). Using (23) this becomes:

$$\int_\Omega J_{\nu,\Omega}\, d\Omega = K_\nu (1-\bar{\omega}_\nu) n_\nu^2 \int_\Omega B_{\nu,\Omega}(T)\, d\Omega + K_\nu \bar{\omega}_\nu \int_\Omega i^*_{\nu,\Omega}\, d\Omega \quad . \tag{34}$$

Since the Planck intensity function is independent of Ω, the first term on the right of (34) becomes:

$$\kappa_\nu (1-\bar{\omega}_\nu) \eta_\nu^2 \int_\Omega B_{\nu,\Omega}(T)\, d\Omega = 4\pi (1-\bar{\omega}_\nu) \kappa_\nu \eta_\nu^2 B_\nu(T) \quad . \tag{35}$$

To evaluate the second term on the right of (34) it is necessary to know the angular dependence of $i^*_{\nu,\Omega}$. This is not known a-priori, but in order to make calculations possible it will be assumed that $i^*_{\nu,\Omega}$ is simply some fraction of $i_{\nu,\Omega}$. To keep the number of parameters to a minimum, it will be assumed that this fraction is simply $\bar{\omega}_\nu$. Thus:

$$i^*_{\nu,\Omega} = \bar{\omega}_\nu\, i_{\nu,\Omega} \quad . \tag{36}$$

By virtue of (32), $i^*_{\nu,\Omega}$ is also half-isotropic:

$$\left.\begin{aligned} i^*_{\nu,\Omega} &= \bar{\omega}_\nu\, i'_\nu \qquad (0 < \theta < \pi/2) \quad , \qquad \text{(a)} \\ i^*_{\nu,\Omega} &= \bar{\omega}_\nu\, i''_\nu \qquad (\pi/2 < \theta < \pi) \quad . \qquad \text{(b)} \end{aligned}\right\} \tag{37}$$

Using (37), the second term on the right of (34) becomes:

$$\kappa_\nu \bar{\omega}_\nu \int_\Omega i^*_{\nu,\Omega}\, d\Omega = \kappa_\nu \bar{\omega}_\nu^2 \left[2\pi (i'_\nu - i''_\nu)\right] \quad . \tag{38}$$

Combining equation (28), (29), (33), (35) and (38), the radiant transfer equation for the material becomes:

$$\frac{dF_\nu}{dy} = -\kappa_\nu \left[2\pi (i'_\nu + i''_\nu)\right] + 4\pi (1-\bar{\omega}_\nu) \kappa_\nu \eta_\nu^2 B_\nu(T) + \kappa_\nu \bar{\omega}_\nu^2 \left[2\pi (i'_\nu - i''_\nu)\right] \quad . \tag{39}$$

Combining equations (3) and (32), it may be shown that:

$$F_\nu = 2\pi \left[\tfrac{1}{2} (i'_\nu - i''_\nu)\right] \quad . \tag{40}$$

Thus:

$$K_\nu \bar{\omega}_\nu^2 \left[2\pi (i_\nu' - i_\nu'')\right] = 2 K_\nu \bar{\omega}_\nu^2 F_\nu \quad , \tag{41}$$

and therefore equation (39) may be written:

$$\frac{dF_\nu}{dy} - 2K_\nu \omega_\nu^2 F_\nu = - K_\nu I_\nu + 4\pi (1-\bar{\omega}_\nu) K_\nu n_\nu^2 B_\nu (T) \quad , \tag{42}$$

where:

$$I_\nu = 2\pi (i_\nu' + i_\nu'') \quad . \tag{43}$$

Equation (42) is one relation for the two quantities F_ν and I_ν. Another relation may be obtained by a similar procedure starting from equation (27). Multiplying (27) by $\cos\theta \, d\Omega$ and integrating over 4π steradians:

$$\frac{d}{dy} \int_\Omega i_{\nu,\Omega} \cos^2\theta \, d\Omega = - K_\nu \int_\Omega i_{\nu,\Omega} \cos\theta \, d\Omega + \int_\Omega J_\nu \cos\theta \, d\Omega . \tag{44}$$

Using equations (6) and (32), the left side of (44) becomes:

$$\frac{d}{dy} \int_\Omega i_{\nu,\Omega} \cos^2\theta \, d\Omega = \frac{d}{dy} \left\{ 2\pi i_\nu' \int_0^{\pi/2} \cos^2\theta \sin\theta \, d\theta + 2\pi i_\nu'' \int_{\pi/2}^{\pi} \cos^2\theta \sin\theta \, d\theta \right\} . \tag{45}$$

Let $m = \cos\theta$. Then (45) becomes:

$$\frac{d}{dy} \int_\Omega i_{\nu,\Omega} \cos^2\theta \, d\Omega = \frac{d}{dy} \left\{ 2\pi i_\nu' \int_0^1 m^2 \, dm + 2\pi i_\nu'' \int_{-1}^{0} m^2 \, dm \right\}$$

$$= \frac{1}{3} \frac{d}{dy} \left[2\pi (i_\nu' + i_\nu'')\right] .$$

Utilizing (43), this becomes:

$$\frac{d}{dy} \int_\Omega i_{\nu,\Omega} \cos^2\theta \, d\Omega = \frac{1}{3} \frac{dI_\nu}{dy} \quad . \tag{46}$$

From equation (3), the first term on the right of (44) can be written:

$$K_\nu \int_\Omega i_{\nu,\Omega} \cos\theta \, d\Omega = K_\nu F_\nu \quad . \tag{47}$$

The last term on the right of (44) may be written:

$$\int_\Omega J_\nu \cos\theta \, d\Omega = (1-\bar{\omega}_\nu) K_\nu \eta_\nu^2 B_\nu(T) \int_\Omega \cos\theta \, d\Omega + K_\nu \bar{\omega}_\nu \int_\Omega i^*_{\nu,\Omega} \cos\theta \, d\Omega \quad . \tag{48}$$

Using equation (6), the first term on the right side of (48) becomes:

$$(1-\bar{\omega}_\nu) K_\nu \eta_\nu^2 B_\nu(T) \int_\Omega \cos\theta \, d\Omega = 2\pi(1-\bar{\omega}_\nu) K_\nu \eta_\nu^2 B_\nu(T) \int_0^1 m \, dm + 2\pi(1-\bar{\omega}_\nu) K_\nu \eta_\nu^2 B_\nu(T) \int_0^{-1} m \, dm = 0 \quad . \tag{49}$$

Using (32) and (37), the second term on the right side of (48) becomes:

$$K_\nu \bar{\omega}_\nu \int_\Omega i_{\nu,\Omega} \cos\theta \, d\Omega = K_\nu \bar{\omega}_\nu \left\{ 2\pi \bar{\omega}_\nu i'_\nu \int_0^1 m \, dm + 2\pi \bar{\omega}_\nu i''_\nu \int_0^{-1} m \, dm \right\} = K_\nu \bar{\omega}_\nu^2 \left\{ 2\pi \left[\tfrac{1}{2} (i'_\nu - i''_\nu) \right] \right\} \quad .$$

By (40), this becomes:

$$K_\nu \bar{\omega}_\nu \int_\Omega i^*_{\nu,\Omega} \cos\theta \, d\Omega = K_\nu \bar{\omega}_\nu^2 F_\nu \quad . \tag{50}$$

Combining (46), (47), (49) and (50), equation (44) may be written:

$$\frac{dI_\nu}{dy} = -3 K_\nu (1 - \bar{\omega}_\nu^2) F_\nu \quad . \tag{51}$$

Equations (42) and (51) give two relations between I_ν and F_ν. The following relations are from equation (51):

$$2K_\nu \bar{\omega}_\nu^2 F_\nu = -\frac{2}{3}\frac{\bar{\omega}_\nu^2}{(1+\bar{\omega}_\nu^2)}\frac{dI_\nu}{dy}, \quad \text{(a)}$$

$$\frac{dF}{dy} = -\frac{1}{3(1+\bar{\omega}_\nu^2)}\frac{d}{dy}\left(\frac{1}{K_\nu}\frac{dI_\nu}{dy}\right). \quad \text{(b)} \qquad (52)$$

Substituting equation (52) into (42):

$$\frac{d}{dy}\left(\frac{1}{K_\nu}\frac{dI_\nu}{dy}\right) - 2\bar{\omega}_\nu^2\frac{dI_\nu}{dy} - 3(1+\bar{\omega}_\nu^2)K_\nu I_\nu = 12\pi(1-\bar{\omega}_\nu^2)(1+\bar{\omega}_\nu^2)\eta_\nu^2 K_\nu B_\nu(T) \qquad (53)$$

And, from (52a):

$$F_\nu = -\frac{1}{3(1+\bar{\omega}_\nu^2)}\left(\frac{1}{K_\nu}\frac{dI_\nu}{dy}\right). \qquad (54)$$

Solution of equation (53), subject to appropriate boundary conditions, yields I_ν as a function of y. Numerical differentiation of I_ν will then yield F_ν, as shown by equation (54). Integration of F_ν over all frequencies will then yield the net radiant heat flux as a function of y, as shown by equation (5). The derivative of this is the radiant heating term to be added to the heat equation.

4. Boundary Conditions

The following considerations lead to the boundary conditions appropriate to the problem. At the boundary y = s, the intensity $I_\nu(0)$ may be written:

$$I_\nu(0) = \int_\Omega i_{\nu,\Omega}(0)\, d\Omega, \qquad (55)$$

where $i_{\nu,\Omega}(0)$ is the specific spectral intensity of the rays at the surface. Let $i_\nu^+(\theta)$ and $i_\nu^-(\theta)$ represent the specific spectral intensities of rays reflected from and incident on the surface y = s from the interior of the material, respectively. Then:

$$I_\nu(0) = 2\pi\left\{\int_0^{\pi/2} i_\nu^+(\theta)\sin\theta\, d\theta + \int_{\pi/2}^{\pi} i_\nu^-(\theta)\sin\theta\, d\theta\right\}. \qquad (56)$$

By the law of reflection:

$$i_\nu^+(\theta) = R_\nu(\pi-\theta)\, i_\nu^-(\pi-\theta) \tag{57}$$

where $R_\nu(\pi - \theta)$ is the internal reflectivity of the surface. Combining (56) and (57), making the half-isotropic assumption of equation (32b) for i_ν^-, and assuming that the internal reflectivity is constant and numerically equal to the measurable external diffuse reflectivity R_ν^o for angles of incidence smaller than the critical angle θ_c, and is equal to unity for angles greater than θ_c, equation (56) becomes:

$$I_\nu(0) = 2\pi \left\{ \int_0^{\pi/2} i_\nu^-(\pi-\theta)\, R_\nu(\pi-\theta) \sin\theta\, d\theta + \int_{\pi/2}^{\pi} i_\nu^-(\theta) \sin\theta\, d\theta \right\},$$

$$= \left\{ R_\nu^o \int_0^{\theta_c} \sin\theta\, d\theta + \int_{\theta_c}^{\pi/2} \sin\theta\, d\theta + \int_{\pi/2}^{\pi} \sin\theta\, d\theta \right\} I_\nu''(0),$$

$$= \left[(1-\cos\theta_c) R_\nu^o + \cos\theta_c + 1 \right] I_\nu''(0),$$

$$\therefore \quad I_\nu(0) = (1+R_\nu^o)(1-\cos\theta_c)\, I_\nu''(0), \tag{58}$$

where:

$$I_\nu''(0) = 2\pi i_\nu'' . \tag{59}$$

Writing equation (58) in a form more convenient for the use which follows:

$$I_\nu''(0) = \frac{1}{(1+R_\nu^o)(1-\cos\theta_c)}\, I_\nu(0) . \tag{60}$$

The spectral distribution function evaluated at y = s is given by the following:

$$F_\nu(0) = \int_\Omega i_{\nu,\Omega} \cos\theta\, d\Omega . \tag{61}$$

Proceeding as was done in equation (55) to (58), $F_\nu(0)$ becomes:

$$F_\nu(0) = 2\pi \left\{ \int_0^{\pi/2} i_\nu^+(\theta) \cos\theta \sin\theta \, d\theta + \int_{\pi/2}^{\pi} i_\nu^-(\theta) \cos\theta \sin\theta \, d\theta \right\} ,$$

$$= 2\pi \left\{ \int_0^{\pi/2} i_\nu^-(\pi-\theta) R_\nu(\pi-\theta) \cos\theta \sin\theta \, d\theta + \int_{\pi/2}^{\pi} i_\nu^-(\theta) \cos\theta \sin\theta \, d\theta \right\} ,$$

$$= 2\pi \left\{ R_\nu^\circ \int_0^{\theta_c} \cos\theta \sin\theta \, d\theta + \int_{\theta_c}^{\pi/2} \cos\theta \sin\theta \, d\theta + \int_{\pi/2}^{\pi} \cos\theta \sin\theta \, d\theta \right\} i_\nu'' ,$$

$$= 2\pi \left\{ R_\nu^\circ \frac{1}{2}(1-\cos^2\theta_c) + \frac{1}{2}\cos^2\theta_c - \frac{1}{2} \right\} i_\nu''$$

$$\therefore \quad F_\nu(0) = -\frac{1}{2}(1-R_\nu^\circ)(1-\cos^2\theta_c) I_\nu''(0) \quad . \tag{62}$$

By combining (60) and (62), the necessary relation between $F_\nu(0)$ and $I_\nu(0)$ is obtained:

$$F_\nu(0) = -\frac{1}{2}\left(\frac{1-R_\nu^\circ}{1+R_\nu^\circ}\right)(1-\cos\theta_c) I_\nu(0) \quad . \tag{63}$$

The critical angle is defined as:

$$\theta_c = \sin^{-1}\left(\frac{1}{n_\nu}\right) \quad . \tag{64}$$

In the following discussion, it is assumed that n_ν can be calculated with sufficient accuracy from the Fresnel equations for normal incidence:

$$\left(\frac{n_\nu - 1}{n_\nu + 1}\right)^2 = R_\nu^\circ \quad . \tag{65}$$

Strictly speaking, the right side of (65) should be a normal reflectivity rather than a diffuse (hemispherical) reflectance, but this will be overlooked. Solving (65) for n_ν gives:

$$n_\nu = \left(\frac{1 + \sqrt{R_\nu^\circ}}{1 - \sqrt{R_\nu^\circ}} \right) \quad . \tag{66}$$

combining (64) and (66), the expression for θ_c becomes:

$$\theta_c = \sin^{-1} \left(\frac{1 - \sqrt{R_\nu^\circ}}{1 + \sqrt{R_\nu^\circ}} \right) \quad . \tag{67}$$

The square of n_ν will be needed in equation (53), thus:

$$n_\nu^2 = \left(\frac{1 + \sqrt{R_\nu^\circ}}{1 - \sqrt{R_\nu^\circ}} \right)^2 \quad . \tag{68}$$

A similar line of reasoning to that employed in equations (55) to (63) leads to the following boundary condition at y = L:

$$F_\nu(L) = +\frac{1}{2} \left(\frac{1 - R_\nu^L}{1 + R_\nu^L} \right) (1 - \cos \theta_c^L) I_\nu(L) \quad , \tag{69}$$

where R_ν^L is the internal reflectivity of the rear interface, and θ_c^L is the critical angle corresponding to this reflectivity:

$$\theta_c^L = \sin^{-1} \left(\frac{1 - \sqrt{R_\nu^L}}{1 + \sqrt{R_\nu^L}} \right) \quad . \tag{70}$$

By means of equation (54), the boundary conditions in (53) may be written as follows.

At y = s:

$$\left(\frac{dI_\nu}{dy} \right)_{y=s} = -\frac{3}{2} \left(\frac{1 - R_\nu^\circ}{1 + R_\nu^\circ} \right) (1 - \cos \theta_c)(1 + \bar{\omega}_\nu^2)(I_\nu)_{y=s} \quad . \tag{71}$$

At y = L:

$$\left(\frac{dI_\nu}{dy} \right)_{y=L} = +\frac{3}{2} \left(\frac{1 - R_\nu^L}{1 + R_\nu^L} \right) (1 - \cos \theta_c^L)(1 + \bar{\omega}_\nu^2)(I_\nu)_{y=L} \quad . \tag{72}$$

5. External Input

It will prove convenient to derive the expressions for the internal reflectivity of the material. This has really been done in the steps prior to equation (58), but is given again here. From the equation just before (58), the internal reflectivity is:

at y = s:

$$\bar{R}_\nu^{\,o} = R_\nu^{\,c} \int_0^{\theta_c} \sin\theta\, d\theta + \int_{\theta_c}^{\pi/2} \sin\theta\, d\theta \quad , \tag{73}$$

$$\therefore \bar{R}_\nu^{\,o} = R_\nu^{\,o} + (1 - R_\nu^{\,o}) \cos\theta_c \quad .$$

Similarly, at y = L:

$$\bar{R}_\nu^{\,L} = R_\nu^{\,L} + (1 - R_\nu^{\,L}) \cos\theta_c^{\,L} \quad . \tag{74}$$

The net radiant heat flux at point y due to an external radiant heat input whose spectral distribution function is F_ν^* may be calculated by writing the expressions for the net flux at this point on each "pass" as this energy experiences multiple internal reflections and summing. In the following derivation it will be convenient to drop clumsy and superflous subscripts. Thus, for purposes of this section:

$F_\nu^* = F^*$,

$R_\nu^o = R_o$,

$R_\nu^L = R_L$,

$\bar{R}_\nu^o = \rho_o$,

$\bar{R}_\nu^L = \rho_L$,

$a_\nu = a$,

$\int_s^L a_\nu\, dy = \tau_L$,

$\int_s^y a_\nu\, dy = \tau_y$,

$\int_y^L a_\nu\, dy = \tau_{yL}$.

Then, on the 1st pass, the net flux at point y due to the external input is $'F^*$:

$$'F^* = (1-R_o)F^* e^{-\tau_y} - (1-R_o)F^* \rho_L e^{-(\tau_L + \tau_{yL})} ,$$

on the 2nd pass:

$${}^2F^* = (1-R_o)F^* \rho_o \rho_L e^{-(2\tau_L + \tau_y)} - (1-R_o)F^* \rho_o \rho_L^2 e^{-(3\tau_L + \tau_{yL})} ,$$

and so forth. Summing up these contributions, the net radiant flux at point y due to the external input is:

$$F^*(1-R_o)\left\{\left[1 + \rho_o\rho_L e^{-2\tau_L} + \rho_o^2\rho_L^2 e^{-4\tau_L} + \ldots \text{etc.}\right]e^{-\tau_y} - \left[\rho_L e^{-\tau_L} + \rho_o\rho_L^2 e^{-3\tau_L} + \rho_o^2\rho_L^3 e^{-5\tau_L} + \ldots \text{etc.}\right]e^{-\tau_{yL}}\right\} .$$

Each of the series in the square brackets is a geometrical progression. Taking the sum of these progressions, one obtains the following:

$$F^*\left(\frac{1-R_o}{1-\rho_o\rho_L e^{-2\tau_L}}\right)\left(e^{-\tau_y} - \rho_L e^{-\tau_L}\right)e^{-\tau_{yL}} .$$

This expression must be added to equation (54) in order to include the effects of an external radiant heat load on the material.

6. Non-gray Assumptions

The simplest possible non-gray assumptions will be made regarding the frequency dependence of properties. It is assumed that, with the exception of k_ν, all properties (i.e., $\bar{\omega}_\nu$, n_ν, R^o_ν and R^L_ν) are independent of frequency. Furthermore, it is assumed that k_ν varies with frequency in a stepwise fashion, i.e., that k_ν may be represented by:

$$\begin{aligned}
K_\nu &= a_1 \qquad (\nu_o \le \nu < \nu_1) ,\\
K_\nu &= a_2 \qquad (\nu_1 \le \nu < \nu_2) ,\\
K_\nu &= a_3 \qquad (\nu_2 \le \nu < \nu_3) ,\\
&\vdots \qquad\qquad \vdots\\
K_\nu &= a_n \qquad (\nu_{n-1} \le \nu \le \nu_n) .
\end{aligned}$$

In order not to unduly tax the storage capacity of the computer, a maximum of 4 frequency intervals will be considered. The endpoints of these intervals must be specified in the input data. Then:

$$\left.\begin{aligned} \Delta\nu_1 &= (\nu_1 - \nu_0) \quad &\text{(a)}\\ \Delta\nu_2 &= (\nu_2 - \nu_1) \quad &\text{(b)}\\ \Delta\nu_3 &= (\nu_3 - \nu_2) \quad &\text{(c)}\\ \Delta\nu_4 &= (\nu_4 - \nu_3) \quad &\text{(d)} \end{aligned}\right\} \qquad (75)$$

It will prove convenient to use the following abbreviations in the remainder of the discussion.

$$\left.\begin{aligned} b &= 2\bar{\omega}^2 \quad &\text{(a)}\\ d &= 3(1+\bar{\omega}^2) \quad &\text{(b)}\\ f &= 12\pi(1-\bar{\omega})(1+\bar{\omega}^2)\left(\frac{1+\sqrt{R_0}}{1-\sqrt{R_0}}\right)^2 \quad &\text{(c)}\\ q_0 &= -\frac{1}{2}\left(\frac{1-R_0}{1+R_0}\right)(1-\cos\theta_0) \quad &\text{(d)}\\ q_L &= +\frac{1}{2}\left(\frac{1-R_L}{1+R_L}\right)(1-\cos\theta_L) \quad &\text{(e)}\\ \theta_0 &= \sin^{-1}\left(\frac{1-\sqrt{R_0}}{1+\sqrt{R_0}}\right) \quad &\text{(f)}\\ \theta_L &= \sin^{-1}\left(\frac{1-\sqrt{R_L}}{1+\sqrt{R_L}}\right) \quad &\text{(g)}\\ \rho_0 &= R_0 + (1-R_0)\cos\theta_0 \quad &\text{(h)}\\ \rho_L &= R_L + (1-R_L)\cos\theta_L \quad &\text{(i)} \end{aligned}\right\} \qquad (76)$$

and, for i = 1, 2, 3, 4:

$$\tau_i (L-s) = \int_s^L a_i \, dy \quad , \qquad \text{(a)}$$

$$\tau_i (y-s) = \int_s^y a_i \, dy \quad , \qquad \text{(b)} \qquad (77)$$

$$\tau_i (L-y) = \int_y^L a_i \, dy \quad , \qquad \text{(c)}$$

where a_i is the value of the attenuation coefficient in the ith frequency interval.

The value of the net radiant flux at point y in the material, due to both self-glowing and to an external radiant source is:

$$F_i (y) = -\frac{1}{d}\left(\frac{1}{a_i}\frac{dI_i}{dy}\right) + F_i^* \left(\frac{1-R_o}{1-\rho_o \rho_L e^{-2\tau(L-s)}}\right)\left(e^{-\tau(y-s)} - \rho_L e^{-\tau(L-s)}\right) e^{-\tau(L-y)} \quad , \qquad (78)$$

where I_i is obtained from solution of:

$$\frac{d}{dy}\left(\frac{1}{a_i}\frac{dI_i}{dy}\right) - b\frac{dI_i}{dy} - d a_i I_i = f a_i B_i \quad , \qquad (79)$$

$$B_i = C_1 \int_{\nu_{i-1}}^{\nu_i} \frac{\nu^3}{\left[\exp\left(\frac{C_2 \nu}{T}\right)\right] - 1} \, d\nu \quad , \qquad (80)$$

and the boundary conditions on (79) are:

$$\left(\frac{dI_i}{dy}\right)_{y=s} = -g_o \, d a_i \left(I_i\right)_{y=s} \quad , \qquad (81)$$

$$\left(\frac{dI_i}{dy}\right)_{y=L} = -g_L \, d a_i \left(I_i\right)_{y=L} \quad . \qquad (82)$$

The constants C_1 and C_2 in equation (8c) are the 1st and 2nd radiation constants.

APPENDIX II

STRUCTURAL CONSIDERATIONS

C. J. Martin

Introduction

Although the thermodynamics of charring ablators are well known and documented (see reference (1), for a representative listing), the mechanical response and possible mechanical spallation criteria have been almost neglected. Although numerous reasons can be advanced for this neglect, the reasons are probably among the following:

a) The fact that mechanical spallation does not arise in many of these materials.

b) The lack of an adequate mathemetical theory that is tractable and that describes the complex physical situation in the ablating material.

c) The order of magnitude difficulties that are introduced into the mathematics when one couples even the simplest type of elastic theory with the thermodynamics.

d) The lack of an adequately controllable experimental program to properly test any mechanical spallation criterion that is advanced as the result of such an analytical investigation.

e) The lack of adequate material properties, particularly at high temperatures.

Even in the face of these difficulties, some efforts have been made to include mechanical spallation in theoretical analyses.

In the open literature, the only existing effort that has attempted to consider a mechanical response (with the appropriate thermodynamics) and to advance a spall criterion is in the paper by Mathieu, reference (2), in 1964. In this paper, the mechanical response is given by the pressure of the exiting gases in the char layer and the mechanical response is called the mechanical normal stress defined to be the difference between the aerodynamic surface pressure and the internal gas pressure.

One of his spall criteria is that when this normal stress reaches a critical value, the char is ruptured and instantaneously removed. Since his model is one-dimensional, it is implied that a whole layer is cracked or "sliced" off.

The second criterion for removal takes into account the aerodynamic shear stress at the surface. The criterion is apparently empirically derived and says, essentially, that the char layer is sheared (instantaneously) when its thickness reaches a critical value.

Both of these criteria may be useful if it can be shown that other mechanical effects can be ignored completely. It should be borne in mind, however, that the critical char thickness criterion used in reference (2) was determined for a "nonablating" surface and the normal stress criterion of reference (2) completely neglects the thermo-mechanical component due to the forces in the solid part of the material. That is, the fact that the solid interacts with the gases is completely ignored and the tacit assumption is that the thermal stresses are small.

The use of ultimate stresses is a standard design criterion for failure of structures. However, it is a well known fact that while no one stress in a body may be at its utimate value, the correct combination of these same stresses can conceivably be enough to cause rupture or fracture. This is, of course, the notion of yield surfaces studied, for example, in metals by the theory of plasticity, reference (3), and for elastomeric materials by the theory of viscoelasticity, reference (4).

Other, and equally important, effects that must be included when considering spall criteria, are those of strain rate and temperature. T. R. Smith, reference (5), has investigated each of these effects numerously for rubbery materials, and has shown that increasing temperature lowers the ultimate stress level while increasing strain rate tends to raise the ultimate stress levels. Further, Lindsey et al, reference (4), have investigated these effects on the yield surfaces for various elastomers and have amply demonstrated that both effects change (appreciably) the size of yield surfaces.

Hence, it is felt that to advance an adequate theory to describe mechanical spallation, each of the above effects must be considered as important and each must be investigated to determine their influence on the present problem.

Three models are presented in the following sections. Each assumed that we are dealing with a porous elastic solid under the action of mechanical and thermal loadings. The theory underlying each is that of linear elasticity and the essential differences arise in the treatment of the gas pressure in the pores.

In the first model, we follow Biot's treatment, reference (6), and assume that the pores contain a viscous compressible fluid which obeys Poiseuille flow. This leads to six coupled equations of motion in the six displacements - those of the solid u,v,w, and those of the liquid U,V,W. The essential difference between Biot's model and ours lies in the derivation of the constitutive equations, in which we have added the effect of the transient temperature acting on the body. This model is derived in section 2 of this appendix.

The second model differs from the above in the aspect of the motion of the gaseous flow in the body. If we postulate that the gas flow obeys Darcy's Law, again, as Biot did in reference (7), we arrive at six coupled equations of motion in a slightly different form. This treatment differs from that of Biot in our derivation of the constitutive laws wherein we again account for the effects of temperature. This formulation is presented in section 3 of this appendix.

Realizing that the temperature distribution is obtained from an analysis such as that presented in the main body of this report, and does not include the effects of the interaction of the solid dilitation on the thermodynamics, i.e., the thermal problem is uncoupled from the mechanical one, we present in section 4 of this appendix, the linear elastic model that treats the gas pressure in the pores and the thermal distribution in the body as known functions of space and time. Since this model presupposes no particular set of constitutive laws for the pressure of the gas and since it has not been established definitely that the gas flow obeys any one flow law, it was felt that

as much useful information could be obtained from this model as from the above theories at this time.

Thus, attention has been focused on the model derived in section 4. We present in section 5 of this appendix in outline form, the elements of the numerical analysis used.

The test of a good theory is in a controllable system of laboratory experiments that duplicate certain aspects of the physical environment. However, it will become apparent, after reading the section dealing with the mathematical model, that before we can examine or even formulate a set of experiments to test a spall criterion, unusual testing techniques must be postulated and tests performed so that we can input realistic mechanical moduli into the numerical program of our mathematical model. That is, the extreme thermal and mechanical environment associated with the ablation process does not allow us to simply define mechanical moduli over a range of a few decades about room temperature. We must know each and every property as it varies with time and temperature. Thus, we conclude in section 6 of this appendix with a suggested minimum experimental program for measuring mechanical properties over the full range of temperatures and times.

2. Porous Solid and Poiseuille Flow

We consider a cartesian rectangular coordinate system in the body and designate the coordinate axes by x_i, i = 1,2,3. Using this notation we consider u,v, and w to be the displacement components of the solid part of our composite system in the directions x_1, x_2, and x_3 respectively.

In a similar manner we consider average fluid displacement components U, V and W and state that volume flow of the fluid is obtained by the product of the displacement and the average cross-sectional fluid area.

Strain displacement relations are obtained in the normal manner so that

$$e_{ij} = \frac{1}{2}\left(u_{ij} + u_{ji}\right), \quad i = 1,2,3 \tag{2.1}$$

For the strain in the fluid we consider the only pertinent quantity to be the dilitation ϵ where

$$\epsilon = \frac{\partial U}{\partial x_1} + \frac{\partial V}{\partial x_2} + \frac{\partial W}{\partial x_3} = U_{i,i} \qquad i = 1,2,3 \tag{2.2}$$

The stress tensor acting on the solid-fluid system is designated by

$$\tau_{ij} = \sigma_{ij} + \delta_{ij} S \tag{2.3}$$

where σ_{ij} is the stress components acting on the solid and S is proportional to the internal fluid pressure p so that

$$S = -\beta p \tag{2.4}$$

where β is the effective porosity of the system.

Biot next derives his stress-strain relations by means of the potential energy W of the unit volume. This, of course, leads to relations of the form

$$\sigma_{ij} = \frac{\partial W}{\partial e_{ij}} \quad , \quad S = \frac{\partial W}{\partial \epsilon} \qquad ij = 1, 2, 3 \tag{2.5}$$

However, because of the presence of the thermal field in the body, we consider the Helmholtz free energy function A and use the relations

$$\sigma_{ij} = \frac{\partial A}{\partial e_{ij}} \quad , \quad S = \frac{\partial A}{\partial \epsilon} \qquad ij = 1, 2, 3 \tag{2.6}$$

and strictly speaking

$$\mathcal{E} = -\frac{\partial A}{\partial T} \tag{2.7}$$

where $\mathcal{E}$ is the entropy of the system.

For a general anisotropic material A is a function of the six strains e_{ij}, the fluid dilitation ϵ, and the temperature T, so that

$$A = A(e_{ij}, \epsilon, T) \tag{2.8}$$

Assuming that at time t = 0, there are no stresses and strains and that $T = T_o$, we can expand A in a power series about this equilibrium position to obtain

$$A = A_o + a_{ij}e_{ij} + a_o\epsilon + a_1(T-T_o) + b_{ijk\ell}\, e_{ij}e_{k\ell} + a_2\epsilon^2 + a_3(T-T_o)^2 + C_{ij}e_{ij}\epsilon + d_{ij}e_{ij}(T-T_o) + a_4\epsilon(T-T_o) + \ldots \tag{2.9}$$

Substituting (2.9) into (2.6) yields

$$\sigma_{ij} = a_{ij} + b_{ijk\ell}\, e_{k\ell} + C_{ij}\epsilon + d_{ij}(T-T_o) + \ldots \tag{2.10}$$

$$S = a_o + 2a_2\epsilon + C_{ij}e_{ij} + a_4(T-T_o) + \ldots \tag{2.11}$$

Retaining only the linear terms in (2.10) and (2.11) and using the fact that

$$\sigma_{ij} = S = 0 \qquad \text{when} \quad e_{ij} = \epsilon = 0 \qquad \text{and } T = T_o \text{ we have}$$

$$\sigma_{ij} = b_{ijk\ell}\, e_{k\ell} + C_{ij}\,\epsilon + d_{ij}\,(T-T_o)$$

$$S = a_o + 2\,a_2\,\epsilon + C_{ij}e_{ij} + a_4(T-T_o)\ . \tag{2.12}$$

which is valid for a general anisotropic solid-fluid aggregate under the action of a temperature field.

To proceed further requires us to make certain assumptions about the nature of the elastic-solid. This means that the free energy function A is required to be form invariant under certain symmetry transformations of coordinates. Such symmetry transformation determine the relations between the various components of the tensors $b_{ijk\ell}$, the tensor c_{ij} and the tensor d_{ij}.

For example, we know, due to the symmetry of σ_{ij} and e_{ij} that

$$b_{ijk\ell} = b_{jik\ell} = b_{ij\ell k} = b_{k\ell ij}$$

$$C_{ij} = C_{ji} \qquad d_{ij} = d_{ji} \tag{2.13}$$

so that $b_{ijk\ell}$ has only 21 independent components while c_{ij} and d_{ij} have but 6 each.

Rather than derive the constitutive equations used in the various crystal classes, we simply list stress-strain laws for two types of elastic material - an orthotropic body and an isotropic body. For a full derivation the reader is referred to Green and Adkins, reference (9).

If the material is a rhombic system then the only non-zero components of the tensors in (2.13) are

$$\begin{pmatrix}\sigma_{11}\\ \sigma_{22}\\ \sigma_{33}\\ \sigma_{23}\\ \sigma_{13}\\ \sigma_{12}\end{pmatrix} = \begin{pmatrix} b_{1111} & b_{1122} & b_{1133} & 0 & 0 & 0\\ b_{1122} & b_{2222} & b_{2233} & 0 & 0 & 0\\ b_{1133} & b_{2233} & b_{3333} & 0 & 0 & 0\\ 0 & 0 & 0 & b_{2323} & 0 & 0\\ 0 & 0 & 0 & 0 & b_{1313} & 0\\ 0 & 0 & 0 & 0 & 0 & b_{1212}\end{pmatrix}\begin{pmatrix}e_{11}\\ e_{22}\\ e_{33}\\ e_{23}\\ e_{13}\\ e_{12}\end{pmatrix} + \epsilon\begin{pmatrix}C_{11}\\ C_{22}\\ C_{33}\\ 0\\ 0\\ 0\end{pmatrix} + (T-T_o)\begin{pmatrix}d_{11}\\ d_{22}\\ d_{33}\\ 0\\ 0\\ 0\end{pmatrix} \tag{2.14}$$

and

$$S = 2a_2\epsilon + C_{11}e_{11} + C_{22}e_{22} + C_{33}e_{33} + a_4 (T-T_o). \tag{2.15}$$

From (2.14) and (2.15), if one makes the assumption of isotropy, we find that

$$\begin{aligned} b_{2222} &= b_{3333} = b_{1111} \\ b_{2323} &= b_{1313} = b_{1212} = 1/2\,(b_{1111} - b_{1122}) \\ b_{2233} &= b_{1133} = b_{1122} \\ c_{33} &= c_{22} = c_{11} \\ d_{33} &= d_{22} = d_{11} \end{aligned} \tag{2.16}$$

For this last case, Biot defines

$$\begin{aligned} c_{11} &= Q, \\ b_{1111} - b_{1122} &= 2N \\ b_{1122} &= A \\ 2a_2 &= R \end{aligned}$$

so that

$$\begin{aligned} \sigma_{ij} &= 2Ne_{ij} + \delta_{ij}Ae + \delta_{ij}Q\epsilon + \delta_{ij}d_{11}(T-T_o) \\ S &= Qe + R\epsilon + a_4(T-T_o), \quad i,j = 1,2,3 \end{aligned} \tag{2.17}$$

in which we differ from his relations only in the inclusion of the constant terms multiplying the temperature.

We can eliminate d_{11} and a_4 in terms of thermal expansion terms by using the coefficient of volume expansion of the solid, defined by

$$\alpha_s = \left(\frac{\partial e}{\partial T}\right)_\sigma \tag{2.18}$$

and by defining a similar coefficient for the fluid

$$\alpha_f = \left(\frac{\partial \epsilon}{\partial T}\right)_S \tag{2.19}$$

Applying (2.18) and (2.19) to (2.17) gives

$$\sigma_{ij} = 2Ne_{ij} + \delta_{ij} Ae + \delta_{ij} Q\epsilon - \tfrac{1}{3}\delta_{ij}\left[(2N+3A)\alpha_s + 3Q\alpha_f\right](T-T_o)$$

$$S = Q\left[e - \alpha_s (T-T_o)\right] + R\left[\epsilon - \alpha_f (T-T_o)\right] \qquad (2.20)$$

Before going to the equations of motion, we mention that when we are at uniform temperature $T = T_o$, the coefficients in (2.20) are identical with those of Biot and may be determined experimentally as suggested by Biot.

Biot next derives equations of motion by means of Lagrange's equations. Since his derivation may be used unchanged for our problem we write down the six equations of motion directly. Thus we have

$$\sigma_{ij,j} = \frac{\partial^2}{\partial t^2}\left\{\rho_{11} u_i + \rho_{12} U_i\right\} \quad i,j = 1,2,3 \qquad (2.21)$$

and

$$S_i = \frac{\partial^2}{\partial t^2}\left(\rho_{12} u_i + \rho_{22} U_i\right) \quad i = 1,2,3 \qquad (2.22)$$

where Biot has introduced mass coefficients ρ_{11}, ρ_{12} and ρ_{22} which he calls "apparent masses". To relate these quantities to the mass of the aggregate, the mass of the solid, and the fluid, he shows that

$$\rho = \rho_{11} + 2\rho_{12} + \rho_{22} \qquad \text{(total mass of aggregate)}$$

$$(1-\beta)\rho_s = \rho_{11} + \rho_{12} \qquad \text{(mass of solid)}$$

$$\beta\rho_f = \rho_{12} + \rho_{22} \qquad \text{(mass of fluid).}$$

It is possible to formulate the entire system in terms of displacements by means of substituting (2.20) into (2.21) and (2.22). However, since this model will not be carried out any further we defer doing so at this time.

3. Porous Solid and Darcy's Law

The model described in this section differs from the above in the assumption that the fluid pressure is related to the fluid displacements by means of Darcy's Law. The theory presented here has been derived by Biot,

reference (7), and, as in section 2, is modified to include specific thermal effects.

To maintain as much of the notation of section 2 as is possible we make only the most essential changes where necessary.

We begin by defining a vector $\bar{w}$ which represents the flow of the fluid relative to the solid and is measured in terms of volume per unit area of the bulk material. The components of $\bar{w}$ are

$$w_i = \beta(U_i - u_i) \quad i = 1,2,3 \tag{3.1}$$

and by using (3.1) we denote the divergence of this vector by the variable $-\zeta$ so that

$$\zeta = -w_{i,i} \quad i = 1,2,3 \tag{3.2}$$

In the derivation of the stress-strain relations we use, instead of S, the pressure p so that the free energy function A is a function of e_{ij}, T and ζ. Instead of (2.6), then we have

$$\sigma_{ij} = \frac{\partial A}{\partial e_{ij}} \quad , \quad p = \frac{\partial A}{\partial \zeta} \tag{3.3}$$

Considering only the isotropic case, Biot then derives stress-strain laws, which in place of (2.20) are of the form

$$\begin{aligned} \sigma_{ij} &= 2\mu e_{ij} + \delta_{ij}\lambda_c e - \delta_{ij}\alpha M \zeta \\ &\quad - \tfrac{1}{3}\delta_{ij}\left[(2\mu + 3\lambda_c)\alpha_s - 3\alpha_f \alpha M\right](T - T_o) \\ p &= -\alpha M\left[e - \alpha_s (T - T_o)\right] + M\left[\zeta - \alpha_f (T - T_o)\right] \end{aligned} \tag{3.4}$$

where we have made the changes: $N \longrightarrow \mu$, $A \longrightarrow \lambda_c$, $Q \rightarrow -\alpha M$ and $R \rightarrow M$.

Darcy's Law, as used by Biot, may then be written as

$$-\frac{1}{\eta} p_{,i} = \kappa_{ij} \dot{w}_j \qquad i,j = 1,2,3 \tag{3.5}$$

where η is the viscosity of the fluid and the matrix r_{ij} is the flow resistivity matrix; its inverse

$$(k_{ij}) = (r_{ij})^{-1} \tag{3.6}$$

being usually called the permeability matrix. If (3.6) is used instead of (3.5), we have

$$\dot{w}_i = -\frac{1}{\eta} k_{ij} p_{,j} \qquad i,j = 1,2,3 \tag{3.7}$$

Finally, for an isotropic material, the matrix k_{ij}, reduces to

$$k_{ij} = k\,\delta_{ij}$$

so that (3.7) takes the form

$$\dot{w}_i = -\frac{k}{\eta} p_{,i} \tag{3.8}$$

In this case, k is called the coefficient of permeability.

We conclude this section with the equations of motion, derived by Biot and including the effects of dissipation in the equations of motion (2.21) and (2.22). Accomplished by means of Lagrange's equations, the derivation is not reproduced here but is merely stated in final form. Thus we obtain, using the notation of (2.20)

$$\begin{aligned} &2N e_{ij,j} + A e_{,i} + Q\epsilon_{,i} - \tfrac{1}{3}\left[(2N+3A)\alpha_s + 3Q\alpha_f\right] T_{,i} = \\ &\qquad \frac{\partial^2}{\partial t^2}\left(\rho_{11} u_i + \rho_{12} U_i\right) + \frac{\eta\beta^2}{k}\frac{\partial}{\partial t}\left(u_i - U_i\right) \end{aligned} \tag{3.9}$$

$$\begin{aligned} &Q\left[e_{,i} - \alpha_s T_{,i}\right] + R\left[\epsilon_{,i} - \alpha_f T_{,i}\right] = \\ &\qquad \frac{\partial^2}{\partial t^2}\left(\rho_{12} u_i + \rho_{22} U_i\right) - \frac{\eta\beta^2}{k}\frac{\partial}{\partial t}\left(u_i - U_i\right) \end{aligned} \qquad i,j = 1,2,3 \tag{3.10}$$

It should be noted if inertial terms can be neglected, equations (3.10) reduce essentially to Darcy's Law as stated in (3.8). Although other forms of (3.9) and (3.10) are available, we leave the theory in this form. Indeed, Biot carries the theory to the point where he can account for a completely anisotropic material.

4. Linear Elastic Model

If we do not consider the effects of fluid displacement and postulate that the pressure of the gas in the pores is a known transient pressure

distribution, then the above theory simplifies considerably.

The stress tensor in this case takes the form

$$\tau_{ij} = \sigma_{ij} - \beta p \delta_{ij} \tag{4.1}$$

where β is the porosity, p the gas pressure and σ_{ij} the stress components acting in the solid components of the body and related to the strains in the body by

$$\sigma_{ij} = 2\mu e_{ij} + \lambda \delta_{ij} e - (2\mu + 3\lambda)\alpha (T - T_0) \tag{4.2}$$

Here, μ λ are the ordinary Lamé components, α the coefficient of the thermal expansion and T the temperature in the body.

The strains are those defined in (2.1) with the additional assumption that there is no change in the z direction. Thus, under the plane strain assumption,

$$e_z = e_{xz} = e_{yz} = 0 \tag{4.3}$$

As a consequence of (4.3), equations (4.1) and (4.2) become

$$\begin{aligned}
\tau_x &= (2\mu + \lambda)e_x + \lambda e_y - (2\mu + 3\lambda)\alpha(T - T_0) - \beta p \\
\tau_y &= \lambda e_x + 2(\mu + \lambda)e_y - (2\mu + 3\lambda)\alpha(T - T_0) - \beta p \\
\tau_z &= \nu(\sigma_x + \sigma_y) - E\alpha(T - T_0) - \beta p \\
\tau_{xy} &= 2\mu e_{xy} \\
\tau_{xz} &= \tau_{yz} = 0
\end{aligned} \tag{4.4}$$

where E and ν are respectively Young's modulus and Poisson's ratio. We next postulate that the material parameters vary only with y and t and are constant in the x direction. Then

$$\begin{aligned}
&\mu = \mu(y,t), \quad \lambda = \lambda(y,t), \quad \alpha = \alpha(y,t) \\
&E = E(y,t), \quad \nu = \nu(y,t), \quad \beta = \beta(y,t)
\end{aligned} \tag{4.5}$$

The equations of motion simplify from (2.21) to

$$\tau_{x,x} + \tau_{xy,y} = \frac{\partial}{\partial t}\left(\rho \frac{\partial u}{\partial t}\right)$$

$$\tau_{xy,x} + \tau_{y,y} = \frac{\partial}{\partial t}\left(\rho \frac{\partial v}{\partial t}\right) \tag{4.6}$$

where ρ is the total mass of the aggregate and as such, $\rho = \rho(y,t)$, by assumption.

Certain assumptions must now be made about the state of the body at time $t = 0$. For our purpose, we shall consider the temperature to be uniform, so that $T = T_o$, and we shall further assume that the properties, expressed by (4.5), are those evaluated at $t = 0$ and $T = T_o$. Thus,

$$\mu = \mu_c(y,0), \quad \lambda = \lambda_o(y,0), \quad \alpha = \alpha_c(y,0)$$
$$\beta = \beta_c(y,0), \quad E = E_c(y,0), \quad \nu = \nu_o(y,0) \tag{4.7}$$

As initial conditions for the equations of motion, (4.6), we shall assume that

$$\begin{aligned} u(x,y,o) &= 0 \\ v(x,y,o) &= 0 \\ \partial u/\partial t\,(x,y,o) &= 0 \\ \partial v/\partial t\,(x,y,o) &= 0. \end{aligned} \tag{4.8}$$

As boundary conditions for our problem, we choose to load the face $y = H$ with stresses $P_1(x,t)$, $P_2(x,t)$ so that

$$\tau_{xy}(x,H,t) = P_1(x,t)$$
$$\tau_y(x,H,t) = P_2(x,t) \tag{4.9}$$

while at the face $y = 0$, we rigidly attach the body to a wall,

$$u(x,o,t) = v(x,o,t) = 0 \tag{4.10}$$

Finally, we consider the body to have length L in the x direction, and postulate no displacement and no shear on these two boundaries. Then

$$u(o,y,t) = u(L,y,t) = 0$$
$$\tau_{xy}(o,y,t) = \tau_{xy}(L,y,t) = 0 \tag{4.11}$$

The problem as now posed is complete. To solve the system, we eliminate the stresses that appear in (4.6), (4.9) and (4.11) by means of (4.4). In this way we need to solve for the displacements u(x,y,t) and v(x,y,t) only. Then, by means of (4.4) we can obtain the rest of our information.

However, we do not solve this system as it stands. Instead, we make one further assumption. This assumption involves the character of the applied loads $P_1(x,t)$, $P_2(x,t)$ in (4.9) and states that their variation in the x direction is piecewise smooth with only finite jumps over the interval $0 \leq x \leq L$. Imposing this condition on (4.9), we postulate that (4.9) can be replaced by

$$\tau_{xy}(x,H,t) = P_1(x,t) = \sum_{n=0}^{\infty} P_{1n}(t) \sin \frac{n\pi x}{L}$$

$$\tau_y(x,H,t) = P_2(x,t) = \sum_{n=0}^{\infty} P_{2N}(t) \cos \frac{n\pi x}{L} \qquad (4.12)$$

If we use (4.12) in place of (4.9), then we examine our system for solutions u(x,y,t), v(x,y,t) in the form

$$u(x,y,t) = \sum_{n=0}^{\infty} U_n(y,t) \sin \frac{n\pi x}{L}$$

$$v(x,y,t) = \sum_{n=0}^{\infty} V_n(y,t) \cos \frac{n\pi x}{L}$$

$$T(x,y,t) - T_0 = \sum_{n=0}^{\infty} T_n(y,t) \cos \frac{n\pi x}{L} \qquad (4.13)$$

$$p(x,y,t) = \sum_{n=0}^{\infty} P_n(y,t) \cos \frac{n\pi x}{L}$$

Substituting (4.13) into (4.4), (4.6), (4.8)-(4.11), we arrive at the system of equations which form the basis of our numerical program. These are listed below.

$$\tau_x(x,y,t) = \sum_{n=0}^{\infty} \tau_x^{(n)}(y,t) \cos \frac{n\pi x}{L}$$

$$\tau_y(x,y,t) = \sum_{n=0}^{\infty} \tau_y^{(n)}(y,t) \cos \frac{n\pi x}{L}$$

$$\tau_{xy}(x,y,t) = \sum_{n=0}^{\infty} \tau_{xy}^{(n)}(y,t) \sin \frac{n\pi x}{L} \qquad (4.14)$$

$$\tau_z(x,y,t) = \sum_{n=0}^{\infty} \tau_z^{(n)}(y,t) \cos \frac{n\pi x}{L}$$

where

$$\tau_x^{(n)}(y,t) = (2\mu+\lambda)\frac{n\pi}{L}U_n + \lambda V_n' - (2\mu+3\lambda)\alpha T_n - \beta p_n$$

$$\tau_y^{(n)}(y,t) = (2\mu+\lambda)V_n' + \lambda\frac{n\pi}{L}U_n - 2\mu+3\lambda)\alpha T_n - \beta p_n \qquad (4.15)$$

$$\tau_{xy}^{(n)}(y,t) = \mu\left[U_n' - \frac{n\pi}{L}V_n\right]$$

$$\tau_z^{(n)}(y,t) = \nu\left[\tau_x^{(n)} + \tau_y^{(n)}\right] - E\alpha T_n - (1-2\nu)\beta p_n$$

The problem to be solved for U_n and V_n is then given by

$$(\mu U')' - (2\mu+\lambda)\frac{n^2\pi^2}{L^2}U_n - (\rho\dot{U}_n)^{\cdot} - \frac{n\pi}{L}\left[(\mu+\lambda)V' + \mu' V_n\right]$$

$$= -\frac{n\pi}{L}\left[(2\mu+3\lambda)\alpha T_n + \beta p_n\right]$$

$$\frac{n\pi}{L}\left[(\mu+\lambda)U_n' + \lambda' U_n\right] + \left[(2\mu+\lambda)V_n'\right]' - \frac{n^2\pi^2}{L^2}\mu V_n - (\rho\dot{V}_n)^{\cdot} \qquad (4.16)$$

$$= \left[(2\mu+3\lambda)\alpha T_n + \beta p_n\right]'$$

where

$$(\quad)' \equiv \frac{\partial}{\partial y}(\quad)\ ,\ (\dot{}) \equiv \frac{\partial}{\partial t}(\quad) \text{ and } n = 0,1,2\ldots$$

The initial and boundary conditions are

$$U_n(y,0) = V_n(y,0) = \dot{U}_n(y,0) = \dot{V}_n(y,0) = 0$$

$$U_n(0,t) = V_n(0,t) = 0$$

$$\mu\left[U_n' - \frac{n\pi}{L}V_n\right] = P_{1n}(t) \text{ at } Y = H \qquad (4.17)$$

$$(2\mu+\lambda)V_n' + \lambda\frac{n\pi}{L}U_n = (2\mu+3\lambda)\alpha T_n + \beta p_n + P_{2n} \text{ at } y = H$$

$$n = 0, 1, 2, \ldots$$

We note that (4.11) are identically satisfied. Equations (4.16), (4.17) represent the final system upon which the numerical program has been based. In the next section we present the numerical analysis used to prepare the system for programming.

Before passing on to the numerical analysis, we mention an important aspect of this whole program, i.e., a spallation criterion.

At this stage, we feel that we cannot advance any adequate spallation criteria. To do so would require knowledge of all of the stresses, strains, velocities etc. and would require a judgement as to which of these is most important. Since we have not as yet run, in our program, any actual flight or reentry environment cases, any statement about spallation would be pure guessing at this time. Suffice it to say that we shall examine, for a candidate spallation criterion, the following quantities:

1) Velocity components: $\dot{u}$, $\dot{v}$

2) Acceleration components: $\ddot{u}$, $\ddot{v}$

3) Strain components: e_x, e_y, e_{xy}

4) Strain rates: $\dot{e}_x$, $\dot{e}_y$, $\dot{e}_{xy}$

5) Stress components: τ_x, τ_y, τ_z, τ_{xy}

Once we have these quantities, it is possible to compute, additionally, the principal stresses, the maximum shearing stress, the maximum normal stresses, and any information needed.

We then proceed to analyze these components as possible spall criteria. Particular attention will be focused on strain rates, principle normal stresses and the maximum shearing stress. For a particular material, these stresses will be checked against yield surfaces which will need to be found experimentally. As noted in the introduction, such yield surfaces are strain-rate and temperature dependent and for this search for a mechanical spall criterion to be successful, complete experimental information is deemed important.

5. Numerical Procedure

It has been shown in the last section that the basic system of equations to be solved are equations (4.16) and (4.17). These must be solved for as many values of n = 0,1,2..., as needed in the Fourier Series (4.13) and (4.14).

We now define

$$(2\mu + 3\lambda)\alpha T_n + f p_n = D(t,y)$$

$$\frac{n\pi}{L} = \omega_n \qquad (5.1)$$

and, upon suppressing the subscript n, we may write equations (4.16)-(4.17) in the following simplified manner:

$$(\mu u')' - \omega^2 M u - \omega A v' - \omega \mu' v - (\rho \dot{u})^{\cdot} = -\omega D \tag{5.2}$$

$$(M v')' - \omega^2 \mu v + \omega A u' + \omega \lambda' u - (\rho \dot{v})^{\cdot} = D' \tag{5.3}$$

in which

$$M = 2\mu + \lambda, \qquad A = \mu + \lambda \tag{5.4}$$

Moreover,

$$u = v = \dot{u} = \dot{v} = o \qquad \text{at } (o,y) \tag{5.5}$$

$$u = v = o \qquad \text{at } (t,o) \tag{5.6}$$

$$(u' - \omega v) = P_1(t) \qquad \text{at } (t,L) \tag{5.7}$$

$$M v' + \omega \lambda u = D + P_2(t) \text{ at } (t,L) \tag{5.8}$$

To solve the system (5.2)-(5.8) we use an implicit difference scheme, to be described below. This scheme is known to be stable when the material properties are constant. Not much is known about its behavior for variable properties.

We introduce a mesh of points in the open rectangle $0 \leq y \leq L$, $0 \leq t \leq \infty$. The general point is denoted by (n,j) n = 0,1,2,....., j = 1,2,..., J - 1, J, J being some fixed number. The values of u(t,y) and v(t,y) are approximated by u(n,j) and v(n,j), respectively. The space and time increments are variable.

We now replace first and second space as well as time derivatives of u,v, and tabular input functions in (5.2), (5.3) by standard central differences. The implicit difference scheme specifies that the terms involving time derivatives be replaced by central differences in time about the point (n,j), whereas all other terms in (5.2), (5.3) be replaced by a weighted average of spatial central differences about the points (n-1,j), (n,j) and (n+1,j), which are multiplied by the (constant) weighting factors θ_1, θ_2, θ_3, respectively, and added. The sum of θ_1, θ_2 and θ_3 is equal to unity.

The boundary conditions (5.6) present no difficulties. For the conditions (5.7) and (5.8) we employ higher order backward differences for the derivatives at the points (n, L). No weighting is used here, since the weighted terms cancel out.

The first two conditions of (5.5), again, present no difficulties. To express the first condition in different form, we write, letting Δ_t be the first time increment,

$$u(1,j) = u(0,j) + \Delta_t \dot{u}(0,j) + \tfrac{1}{2}\Delta_t^2 \ddot{u}(0,j), \quad j = 1,2,\ldots,J-1. \tag{5.9}$$

Using (5.9), (5.5) and (5.2) we reach

$$u(1,j) = \frac{\omega}{2\rho(1,j)} \Delta_t^2 D(1,j), \quad j = 1,2,\ldots,J-1. \tag{5.10}$$

An analogous procedure yields

$$v(1,j) = -\frac{1}{2\rho(1,j)} \Delta_t^2 D'(1,j), \quad j = 1,2,\ldots,J-1. \tag{5.11}$$

The right hand sides of (5.10), (5.11) were actually weighted at times $t = 0$ and $t = 1$. For the values of $u(1, J)$ and $v(1,J)$ we evaluate the expressions obtained from (5.7) and (5.8) at $t = 1$.

We thus have the explicit values of u and v at the points $(0,j)$ ($u \equiv v \equiv 0$) and $(1,j)$, for all j.

In terms of these values we can find $u(2,j)$ and $v(2,j)$, and, generally, once we know $u(n,j)$, $u(n-1,j)$, $v(n,j)$ and $v(n-1,j)$, we can find the values of $u(n+1,j)$ and $u(n+1,j)$ and $u(n+1,j)$ for all j.

Since no derivatives higher than the second appear in (5.2), (5.3) the resulting algebraic system of the difference equations appears as follows:

$$\begin{bmatrix} B_1 & A_1 & & & & & \\ C_2 & B_2 & A_2 & & & & \\ & C_3 & B_3 & A_3 & & & \\ & & \cdot & \cdot & \cdot & & \\ & & & C_{J-1} & B_{J-1} & A_{J-1} & \\ & & & \hat{C}_J & \hat{B}_J & \hat{A}_J & \end{bmatrix}_n \begin{bmatrix} X_1 \\ X_2 \\ X_3 \\ \cdot \\ X_{J-1} \\ A_J \end{bmatrix}_{n+1} = \begin{bmatrix} F_1 \\ F_2 \\ F_3 \\ \cdot \\ F_{J-1} \\ F_J \end{bmatrix}_n \tag{5.12}$$

The coefficient matrix is of order J x J, each of its elements A_j, B_j, C_j being a 2 x 2 matrix whose entries are functions of the material properties, the non-homogeneous terms in (5.2), (5.3) and the space and time increments. Each X_j $(n+1)$ equals the vector whose components are the unknown values $u(n+1, j)$, $v(n+1,j)$. F_j depends entirely upon material properties, non-homogeneous

terms, space and time increments and the known values of u and v at (n,j) and (n-1,j).

The last row of the coefficient matrix in (5.12) contains 3 elements due to the higher order backward difference used at y = L (j = J). We may eliminate X_{J-2} between the Jth and (J-1)st equation in (5.2) to obtain an equation containing only X_{J-1} and X_J. Carrying out this procedure we obtain a coefficient matrix which is tri-diagonal, and the system is of the form

$$\begin{bmatrix} B_1 & A_1 & & & & \\ C_2 & B_2 & A_2 & & & \\ & C_3 & B_3 & A_3 & & \\ & & \cdot & \cdot & \cdot & \\ & & & C_{J-1} & B_{J-1} & A_{J-1} \\ & & & & C_J & B_J \end{bmatrix}_n \begin{bmatrix} X_1 \\ X_2 \\ X_3 \\ \cdot \\ X_{J-1} \\ X_J \end{bmatrix}_{n+1} = \begin{bmatrix} F_1 \\ F_2 \\ F_3 \\ \cdot \\ F_{J-1} \\ F_J \end{bmatrix}_n \tag{5.13}$$

To solve this system we use Potter's method. This consists of defining the following quantities:

$$\mathbf{Z}_j(n) = \left[B_j(n) - C_j(n)\ \mathbf{Z}_{j-1}(n)\ A_{j-1}(n)\right]^{-1} \tag{5.14}$$

$$q_j(n) = F_j(n) - C_j(n)\ \mathbf{Z}_{j-1}(n)\ q_{j-1}(n) \tag{5.15}$$

where $n = 1,2,\ldots, j = 1,2,\ldots,J$, and where we define

$$C_1(n) = A_J(n) = \begin{bmatrix} 0 & 0 \\ 0 & 0 \end{bmatrix} \tag{5.16}$$

Equation (5.13) - (5.16) now imply

$$X_j(n+1) = \mathbf{Z}_j(n) q_j(n) - \mathbf{Z}_j(n)\ A_j(n)\ X_{j+1}(n+1), \tag{5.17}$$

for n = 1,2,.....

We know the values of X_j (0) and X_j (1) from the initial condition. For the values of X_j (2), X_j (3),....., we use (5.17) by using n = 1,2,... .

Indeed, letting j = J, J-1, J-2, ..., 2, 1, in (5.17), we easily obtain $X_J(n+1)$, $X_{J-1}(n+1)$, ..., $X_2(n+1)$, $X_1(n+1)$. This completes the description of Potter's methods.

Once we have obtained u and v by the methods just described, we can get all other pertinent quantities from the equations presented in the previous section.

6. Experimental Program

As already expressed in section 4 of this appendix, we require that the following mechanical moduli be given as functions of time and temperature:

1) μ - shear modulus

2) K - bulk modulus

3) E - uniaxial tension modulus

4) ν - Poisson's ratio

5) α - Coefficient of linear thermal expansion

In addition to the above, ultimate tensile, compressive and shear stresses must be found and yield surfaces constructed for variable strain-rate and temperatures. Finally, some efforts should be made to measure tensile and shear properties of the char in the ablation environment, i.e., while the material is actually ablating.

Before detailing a proposed test program it is well known that a number of tests have been performed to determine the uniaxial tension modulus versus temperature over a limited range (to approximately 250°F). In addition, the shear modulus has been studied over approximately the same range. However, no data have been recorded of the variation of E or μ with time as well as temperature. Further, due to the inherent scatter attributed to manufacturing methods, etc., it is deemed necessary to conduct all required tests for this program from the same batch of material, thereby eliminating unknown factors from the resultant test data.

The tests to be described below should be performed on virgin material as well as charred ablated samples. The charred samples should be used in an attempt to characterize the mechanical behavior of the char layer as influenced by temperature and time but should primarily be used to measure the ultimate properties as these are influenced by temperature.

In this connection, it is felt necessary to attempt to measure these ultimate properties of the char layer in the OVERS (or similar) test facility to see if heating rates and ablation temperatures change drastically the shear strength obtained at room and higher temperatures.

A. Tests to be Performed

Material moduli to be found are: E, ν, μ, K, and α. The analytical effort has been written in such a manner that it can use either E, ν, and α or μ, K and α. Each must be known as functions of time and temperature. Standard test equipment is available to determine each of these moduli at temperatures to approximately 1000°F and for varying strain rates. Which set of quantities should be used depends entirely on the credibility of the measurements.

1) Measuring E, ν and α

a) Standard tension tests (uniaxial) and compression tests should be performed on the virgin material and recorded versus time in 50°F increments between room temperature (R.T.) and 1000°F. Five (5) strain rates between dead loading and 6000 in/in/min should be employed on 2" gage length specimens at each temperature should be run.

Lateral contraction versus longitudinal extension (for Poisson's ratio) measured concurrently.

b) Standard thermal expansion tests to measure α should be performed on a minimum of 8 samples in two orthogonal directions.

2) Measuring μ and K

a) Standard torsion tests to measure μ should be performed on the virgin material in 50°F increments between R.T. and 1000°F. At least five (5) tests at each temperature should be run.

b) A bulk compression apparatus to measure K has been assembled at AVCO. Tests should be performed at a minimum of nine temperatures and ten tests at each temperature.

At the present time, as far as is known, the limit of standard test capability is at 1000°F. Even though this is well below ablation environment temperatures, trends should be well established if the above tests are performed.

3) Tests on the Charred Material

It is felt that the char is a brittle material and unaffected by temperature and strain rate. However, to show this we should have estimates of its mechanical properties as well.

a) In standard test apparatus, we recommend that test #1 and #2 (above) be performed at several strain rates and at least three temperatures between R.T. and 1000°F for mechanical properties as well as ultimate properties.

b) Because the above tests may prove to be very difficult to perform due to its brittleness (at least at R.T.), a box shear apparatus should be constructed and box shear tests performed to determine (at least) the ultimate shear strength of the char layer at nine test temperatures. Several tests at each temperature should be carried out.

c) If the above tests (a) and (b) can be performed this would give an indication of the trend of the char mechanical moduli with temperature. It is then recommended that the OVERS (or similar) test facility be used to study the effect of temperature and heating rate on the ultimate shear strength of the char layer as the sample is ablating. For this purpose a ceramic collar should be constructed to fit around the sample from which should be hung dead weights equivalent in magnitude to the ultimate shear strength measured at the lower temperatures of b) above. By this means, a crude estimate of the effects of heating rate and temperature on this property can be measured. At least two tests for each value of ultimate shear strength found in b).

4) Yield Surfaces and Spallation Criteria

As indicated in the introduction to this appendix and subsequently in the text, failure of the ablator will most likely come about as a result of some principle stress or combination of stresses lying on a yield surface for a particular strain rate and temperature. To actually state that if a stress exceeds to many psi, etc. failure will occur, requires that the yield surfaces (or failure envelopes) must be known at each temperature and time. Rather than go into great detail about these studies, especially since the analytical model has not yet even been programmed, we refer the reader to the remarkable work of Lindsey et al, reference (4), called "The Triaxial Failure of Viscoelastic Materials" in which they report an abundance of material dealing with this subject.

REFERENCES FOR APPENDIX II

1. H. Hurwicz, Aerothermochemistry Studies in Ablation, Fifth AGARD Combustion and Propulsion Colloquium, Brunswick, Germany, April 9-13, 1962.

2. R. D. Mathieu, Mechanical Spallation of Charring Ablators in Hyperthermal Environments, AIAA Journal, 2, p. 1621, 1964.

3. R. Hill, The Mathematical Theory of Plasticity, Oxford U. Press, New York 1950.

4. G. H. Lindsey, et al, The Triaxial Tension Failure of Viscoelastic Materials, Aerosapce Research Laboratories, Office of Aerospace Research, USAF, ARL 63-152, September 1963.

5. T. R. Smith, Stress-Strain-Time-Temperature Relationships for Polymers, ASTM Special Technical Pub., No. 325, p. 60-89, 1962.

6. M. A. Biot, Theory of Propagation of Elastic Waves in a Fluid-Saturated Porous Solid, Part 1: Low-Frequency Range, J. of Acoust. Soc. Amer., 28, pp 169-178, Mar. 1956.

7. M. A. Biot, Mechanics of Deformation and Acoustic Propagation in Porous Media, J. Appl. Phys., 33, No. 4, p. 1482-1498, April 1962.

8. T. R. Munson and R. J. Spindler, Transient Thermal Behavior of Decomposing Materials, Part 1: General Theory and Application to Convective Heating, Avco/RAD-TR-61-10, May 3, 1961.

9. A. E. Green and J. E. Adkins, Large Elastic Deformations, Oxford, Clarendon Press, 1960.

DISTRIBUTION LIST

Addressee	No. Copies
National Aeronautics and Space Administration Manned Spacecraft Center Structures and Mechanics Division, ES3 Thermo-Structures Branch Attention: Mr. Don Curry	30 plus 1 repro
National Aeronautics and Space Administration Manned Spacecraft Center General Research Procurement Branch, BG721 Attention: Mr. Tom Mancuso	1
National Aeronautics and Space Administration Manned Spacecraft Center Technical Information Division Documentation Section, BF33 Attention: Miss Retha Shirkey	4
Air Force Systems Command Air Force Materials Laboratory Plastics and Composits Branch Nonmetallic Materials Division Wright-Patterson Air Force Base Ohio, 45433 Attention: H. S. Schwartz, Chief	1
National Aeronautics and Space Administration Manned Spacecraft Center Technology Utilization Officer Attention: Mr. John T. Wheeler	1
Research Library - Wilmington	3
Research Library - Lowell	1
Reports Distribution Center - Wilmington	60